



A University of Sussex PhD thesis

Available online via Sussex Research Online:

<http://sro.sussex.ac.uk/>

This thesis is protected by copyright which belongs to the author.

This thesis cannot be reproduced or quoted extensively from without first obtaining permission in writing from the Author

The content must not be changed in any way or sold commercially in any format or medium without the formal permission of the Author

When referring to this work, full bibliographic details including the author, title, awarding institution and date of the thesis must be given

Please visit Sussex Research Online for more information and further details

**The Role Of The Mammalian INO80
In Maintaining Genome Stability**

Hanan Eid A Alatwi

Thesis submitted for the degree of Doctor of Philosophy

University of Sussex

January 2017

Acknowledgments

I would like to express my deep appreciation and gratitude to my supervisor, Professor Jessica Downs, for her continuing guidance, encouragement and support. Prof. Downs, it was such an honour knowing and working with you, and I will never forget how your words ‘I have faith in you’ greatly boosted my confidence and made the impossible possible in the research. I am also truly indebted and thankful for my co-supervisor, Prof. Penny Jeggo for her generous support and guidance. I would like also to thank all the people in the Downs lab; it was a great pleasure to work with such a welcoming and lively group.

I owe sincere and earnest gratitude to my mother and my siblings for their love, support, and dedication in helping me. This thesis in all honesty owes much to them and without their encouragement, I would not have been able to overcome these difficult four years. Also, I would like to offer my heartfelt thanks to my best friends for all the good and fun times we shared, which made my journey towards the PhD degree smooth, enjoyable, and gainful.

Finally, with all the warmth of my love, I would like to dedicate this work to the person who has always inspired me and taught me that life without knowledge, ambition, and dignity is not a life. Each letter and idea in this thesis is owed to the soul of my father, Eid Abushail Alatwi. Dad you were always in my thoughts during this journey; you are deeply and painfully missed every day.

Publications

Alatwi, H.E., Downs, J.A. (2015). Removal of H2A.Z by INO80 promotes homologous recombination. *EMBO rep* 16, 986–994.

López-Perrote, A., **Alatwi, H.E.**, Torreira, E., Ismail, A., Ayora, S., Downs, J.A., Llorca, O. (2014). Structure of Yin Yang 1 Oligomers that Cooperate with RuvBL1-RuvBL2 ATPases. *J. Biol. Chem.* jbc.M114.567040.

University of Sussex

Hanan Eid A Alatwi

Doctor of Philosophy in Biochemistry

The Role Of The Mammalian INO80 In Maintaining Genome Stability

Summary

Linear DNA is packaged into higher-order structures termed chromatin, in which the majority of DNA sequences are structurally inaccessible and functionally inactive. Hence, chromatin must exist in a dynamic state to govern the accessibility of the DNA to various regulatory factors that control nuclear processes, such as transcription, DNA replication, and DNA repair. Accessibility in turn is mediated by post-translational modifications, histone variants, histone chaperones, and ATP-dependent chromatin remodelling complexes. In particular, these complexes, such as the multi-subunit INO80 complex, are characterized by their ability to utilise ATP hydrolysis to alter histone-DNA contact by the sliding, eviction, or exchange of histones or nucleosomes. Since its identification in 1999, many INO80 subunits have been purified and structurally characterized. Here, we structurally and biochemically characterized the recently identified human INO80 YY1 subunit and demonstrated a role for YY1 together with RUVBL2, another INO80 subunit, in promoting DNA repair by homologous recombination (HR). Consequential to its chromatin-remodelling activity, INO80 plays multiple roles in cellular metabolism including DNA repair and chromosomal stability. Although evidence from yeast and mammals has indicated the involvement of INO80 in HR repair, the exact mechanism affected by INO80 therein remained unclear. Through a combination of live cell imaging and *in vivo* techniques, we revealed that in human cells the histone variant H2AZ is rapidly removed from damaged chromatin by INO80. Furthermore, we found that INO80 together with the histone chaperone, ANP32E, promotes HR by removing H2AZ from damaged chromatin. Finally, we verified that INO80 is required for the maintenance of chromosomal stability and that loss of INO80 in CIN+ tumour cells induced cell death. Therefore, INO80 may serve as a therapeutic target for the selective elimination of CIN+ tumour cells.

Table of contents

Chapter 1.	16
Introduction	16
1.1 General introduction to chromatin and its structure	17
1.2 Chromatin organization	20
1.2.1 DNA sequence-based nucleosome preferences	20
1.2.2 Post-translational histone modifications (PTMs)	21
1.2.3 Histone variants	26
1.2.4 Histone chaperones.....	33
1.2.5 ATP-dependent chromatin remodellers.....	36
1.3 DSB repair in mammals: an overview	48
1.3.1 DNA breaks.....	48
1.3.2 DSB repair pathway choice	49
1.3.3 DSB repair pathways	50
1.3.4 Chromatin response to DSBs.....	59
1.3.5 DSB repair in regions of heterochromatin	61
1.3.6 Role of INO80 in DNA repair.....	63
1.3.7 H2AZ: A critical histone variant involved in DNA repair	67
1.4 Chromosome instability	69
1.4.1 Chromosome segregation in mitosis in human cells: an overview.....	69
1.4.2 Centromere structure.....	70
1.4.3 The role of INO80 in chromosomal stability	72
1.5 Thesis objectives	74
Chapter 2.	76
Material and Methods	76
2.1 Cell lines and culturing conditions	77
2.2 Irradiation (IR)	77
2.3 Small interfering RNA (siRNA) knockdown conditions	78
2.4 Immunofluorescence for HR analysis	79
2.5 Western blotting (WB)	80
2.6 Sister chromatid exchange (SCE) assay	81
2.7 Bimolecular fluorescence complementation assay (BiFC)	82
2.7.1 Cloning	82
2.7.2 BiFC assay	86
2.7.3 Laser microirradiation used for tracking BiFC foci	86
2.8 Laser microirradiation used for tracking protein dynamics at sites of damaged chromatin	87
2.9 Resection assay	88
2.10 Analysis of micronuclei and abnormal mitosis	88
2.11 Analysis of aneuploidy	88
2.12 Cell viability assay	89
Chapter 3.	90
Biochemical characterization of YY1 and its role in homologous recombination	90
3.1 Introduction	91
3.2 Results	95
3.2.1 YY1 forms multimers <i>in vitro</i> and <i>in vivo</i>	95
3.2.2 Characterization of YY1 structure.....	99

3.2.3	YY1 binds ssDNA, dsDNA, and HJs <i>in vitro</i> , which is enhanced by the RUVBL1-RUVBL2 complex.....	102
3.2.4	YY1 functions together with RUVBL2 to promote RAD51 filament formation, likely as subunits of the INO80 complex; this function is enhanced by the ATPase activity of RUVBL2.....	105
3.2.5	YY1 and RUVBL2 might have a late function during HR	111
3.2.6	YY1 and RUVBL2 might not represent the homologous complex of the bacterial branch-migration enzyme RuvA.....	114
3.3	Discussion.....	119
3.3.1	Human YY1 is a multimeric protein	119
3.3.2	YY1 association with RUVBL1-RUVBL2 enhances its ability to bind several types of DNA.....	121
3.3.3	YY1 co-operates with RUVBL2 to promote HR	123
3.3.4	Lack of <i>in vivo</i> evidence for homogeneity between YY1, a human subunit of the INO80 complex, and RuvA, a bacterial subunit of the branch-migration enzyme	126
Chapter 4.	128
Removal of H2AZ by INO80 promotes homologous recombination	128	
4.1	Introduction.....	129
4.2	Results.....	131
4.2.1	H2AZ dynamics at sites of damaged chromatin.....	131
4.2.2	RUVBL2, a subunit of INO80, accumulates at the sites of damaged chromatin	135
4.2.3	H2AZ is a barrier for resection	137
4.2.4	Cells lacking SRCAP exhibit a resection defect.....	140
4.2.5	INO80 has a mild effect on resection	142
4.2.6	Depletion of H2AZ rescues the RAD51 foci formation defect.....	143
4.2.7	ANP32E works together with INO80 to remove H2AZ from chromatin.....	146
4.2.8	INO80 and ANP32E are required for efficient repair by HR.....	150
4.3	Discussion.....	152
4.3.1	H2AZ removal from damaged chromatin in human cells is dependent on INO80	154
4.3.2	INO80 has a moderate role in resection.....	156
4.3.3	INO80 promotes RAD51 foci formation by removing H2AZ at DSB sites.....	158
4.3.4	INO80 work co-operatively with ANP32E to promote HR by removing H2AZ from damaged chromatin.....	159
4.3.5	Efficient HR requires the removal of H2AZ by INO80 and ANP32E.....	160
Chapter 5.	162
Role of INO80 in chromosomal stability	162	
5.1	Introduction.....	163
5.2	Results.....	165
5.2.1	Depletion of INO80 results in an increase in the number of micronuclei (MN) in CIN+ cells.....	165
5.2.2	Depletion of INO80 causes a defect in structural CIN rather than numerical CIN in U2OS cells.....	167
5.2.3	Loss of INO80 causes cell death in CIN+ cells	170
5.2.4	RKO cells are sensitive to the loss of INO80	174
5.3	Discussion.....	176
5.3.1	INO80 is likely to be required for chromosomal stability	176
5.3.2	INO80 constitutes a proposed therapeutic target for CIN+ tumours	178
Chapter 6.	181

Discussion	181
References	187
Appendix	220

List of figures & tables

Figure 1. 1 Diagram demonstrating the classification of chromatin remodellers...37	37
Table 1. 1 Subunits of the INO80 complex in yeast and humans.....38	38
Figure 1. 2 Schematic diagram showing the domain organization of the catalytic subunit, INO80, of the human INO80 complex.39	39
Figure 1. 3 A model for eukaryotic Holliday junction resolution based on the bacterial RuvA/RuvB complex.....40	40
Figure 1. 4 The proposed embryonic structure of the INO80 complex. Adapted from (Tosi et al., 2013).....42	42
Table 1. 2 The dependency between INO80 subunits in yeast (Tosi et al., 2013)...42	42
Figure 1. 5 The NHEJ repair pathway.....52	52
Figure 1. 6 The homologous recombination repair pathway.....56	56
Figure 1. 7 The Alt-NHEJ repair pathway.58	58
Table 2. 1 siRNA oligos used in this project.....79	79
Table 2. 2 Primary antibodies used in this project.....80	80
Table 2. 3 Secondary antibodies used in this project.81	81
Table 2. 4 Plasmids and components used for cloning.....82	82
Table 2. 5 Oligonucleotides used for cloning.....83	83
Table 2. 6 Plasmids used in laser microirradiation experiments for tracking protein dynamics at sites of damaged chromatin.....87	87
Figure 3. 1 YY1 multimerises <i>in vitro</i>96	96
Figure 3. 2 YY1 <i>in vivo</i> mutimerisation.....98	98
Figure 3. 3 Structure of human YY1 (complex A).....99	99
Figure 3. 4 YY1 multimerises in larger complexes through the association of YY1 dimers.....101	101
Figure 3. 5 YY1 binding to DNA and RUVBL1-RUVBL2 <i>in vitro</i>104	104
Figure 3. 6 INO80 is required for RAD51 foci formation.....109	109
Figure 3. 7 RUVBL2 ATPase activity is required for promoting RAD51 foci formation.....110	110
Figure 3. 8 Loss of YY1 and/or RUVBL2 causes a defect in SCE number.....113	113
Figure 3. 9 YY1 mutimerisation <i>in vivo</i> after exposure to 5Gy γ -IR.....115	115
Figure 3. 10 Lack of YY1-BiFC foci co-localization with γ H2AX foci.....116	116
Figure 3. 11 Laser micro-irradiation treatment of U2OS cells co-transfected with YY1-VN and YY1-VC. The red line indicates the laser path.116	116
Figure 3. 12 <i>In vivo</i> association between YY1 and RUVBL2 was not detected.118	118
Figure 3. 13 Comparison between the structure of YY1 complex A and tetrameric RuvA.....121	121
Figure 4. 1 H2AZ dynamics at sites of damaged chromatin.....133	133

Figure 4. 2 H2B dynamics at sites of damaged chromatin.	134
Figure 4. 3 RUVBL2 accumulation at sites of damaged chromatin.....	136
Figure 4. 4 H2AZ acts as a barrier for resection.....	139
Figure 4. 5 Cells lacking SRCAP exhibit a resection defect.....	141
Figure 4. 6 Cells depleted for INO80 exhibit a mild defect in resection.	142
Figure 4. 7 INO80-depleted cells exhibit significant defects in RAD51 foci number that can be rescued by H2AZ depletion.	144
Figure 4. 8 SRCAP depletion causes a reduction in the number of RAD51 foci.	145
Figure 4. 9 INO80 and ANP32E work together to promote RAD51 foci formation following irradiation and their deficit can be rescued by H2AZ depletion. ...	149
Figure 4. 10 Depletion of H2AZ rescues the SCE defect in cells depleted of INO80 or ANP32E.	151
Figure 4. 11 Diagram illustrating the status of HR in four models.	153
Figure 5. 1 Depletion of INO80 results in an increase in the number of micronuclei in CIN+ cells.....	166
Figure 5. 2 Depletion of INO80 causes a defect in structural CIN in U2OS cells. ...	168
Figure 5. 3 Depletion of INO80 does not affect the number of chromosomes in U2OS cells.....	169
Figure 5. 4 Loss of INO80 causes cells lethality in CIN+ cells.....	173
Figure 5. 5 RKO is sensitive to INO80 loss.....	175

List of abbreviations

53BP1	p53 binding protein 1
Å	Angstrom
AAA+	ATPases associated with diverse cellular activities
Ac	Acetylated
Alt-NHEJ	Alternative non homologous end joining
ANP32E	Acidic nuclear phosphoprotein 32 family member E
APC	Anaphase promoting complex
ARP5	Actin-related protein 5 homolog
ARP8	Actin-related protein 8 homolog
ASF1	Anti-silencing function 1
ATM	Ataxia-telangiectasia mutated
ATP	Adenosine triphosphate
BAF180	Polybromo 1
BAH	Bromo-adjacent homology
BAP1	BRCA1-associated protein-1
BCCIP	BRAC2/CDKN1A interacting protein
BER	Base excision repair
BiFC	Bimolecular fluorescence complementation
BLM	Bloom syndrome RecQ like helicase
bp	Base pair
BRCA1	Breast cancer associated protein 1
BRCA2	Breast cancer 2, early onset
BRCT	BRCA1 C terminus
BRD	Bromodomain
BrdU	bromodeoxyuridine
BRG1	Brahma related gene 1
C-terminus	Carboxyl terminus
CBP	CREB Binding Protein
Cdc20	Cell division cycle protein 20
CDK	Cyclin-dependent kinase
CENP-A	Centromere protein A

CENP-F	Centromere protein F
CENP-H	Centromere protein H
CENP-I	Centromere protein I
CHD	Chromodomain helicase DNA
CHD1L	Chromodomain helicase DNA binding protein 1 like
ChIP	Chromatin immunoprecipitation
Chk1	Checkpoint kinase 1
CIN	Chromosomal instability
CIN+	Chromosomal instability positive cells
CIN-	Chromosomal instability negative cells
CPT	Camptothecin
CTD	C-terminal domain
CtIP	CTBP-interacting protein
DAPI	4',6-diamidino-2-phenylindole
DNA	Deoxyribonucleic acid
DNA-PK	DNA dependent protein kinase
DNA-PKcs	DNA dependent protein kinase catalytic subunit
DNA2	DNA replication helicase/nuclease 2
DSB	Double strand break
dsDNA	Double strand DNA
EGFP	Enhanced green fluorescent protein
EM	Electron microscopy
EXO1	Exonuclease 1
FHA	Forkhead-associated
FRET	Fluorescence resonance energy transfer assay
G/Gly	Glycine
GA	Glutaraldehyde
GFP	Green fluorescent protein
Glu	Glutamate
Gy	Gray
h	Hour
HAT	Histone acetyltransferase
HC	Heterochromatin

HDAC	Histone deacetylase
HFD	Histone fold domain
HIR	Histone regulator
His	Histidine
HJ	Holliday junction
HP1	Heterochromatin protein 1
HR	Homologous recombination
HSA	Helicase-SANT domain
HU	hydroxyurea
IES	Ino eighty subunit
ING2	Inhibitor of growth family member 2
INO80	Inositol 80 chromatin remodeller
IP	Immune-precipitation
IR	Ionising radiation
K/Lys	Lysine
KAP1	KRAB-associated protein 1
Kb	Kilo base pairs
KDa	kilodalton
LRR	leucine-rich repeat
MAD2	Mitotic arrest deficient 2
Mb	Mega base pairs
MCRS1	Microspherule Protein 1
MDa	Megadalton
Me	Methylated
MEF	Mouse embryonic fibroblast
min/m	Minute
ml	Millilitre
mM	Millimolar
mm	Millimetre
MMC	Mitomycin C
MMR	Mismatch repair
MMS	Methyl methanesulfonate
MN	Micronuclei

MOF	Males absent on the first, a histone acetyltransferase
MRE11	Meiotic recombination 11
MRN	MRE11 RAD50 and NBS1 complex
mRNA	Messenger RNA
N-terminus	Amino-terminus
NBS1	Nijmegen breakage syndrome 1
nCIN	Numerical chromosomal instability
NER	Nucleotide excision repair
NFR	Nucleosome-free region
NFRKB	Nuclear factor related To KappaB binding protein
NHEJ	Non homologous end joining
Nhp10	Non-histone protein 10
NLS	Nuclear localization signal
nm	Nanometre
NS	Not significant
NTD	N-terminal domain
ORF	Open reading frames
PARP1	Poly (ADP-ribose) polymerase 1
PBAF	Polybromo-associated BAF
PCNA	Proliferating Cell Nuclear Antigen
PHD	Plant homeo domain
PI3K	Phosphatidylinositol 3-kinase
Pol θ	Polymerase θ
PP2A	Phosphatase 2A
PRC1	Polycomb repressive complex 1
PRR	Post-replication repair
PTIP	BRCT domain-containing protein interacts with Pax2
PTM	Post-translational histone modification
R/Arg	Arginine
R2TP	Rvb1-Rvb2-Tah1-Pih1 complex
RBAP46	RB binding protein 46, chromatin remodelling factor
RBAP48	RB binding protein 48, chromatin remodelling factor
RCT	Random conical tilt method

Rif1	Replication timing regulatory factor 1
RING1B	Ring finger protein 2 (RNF2)
RNF168	Ring finger protein 168
RNF8	Ring finger protein 8
RPA	Replication protein A
RT	Room temperature
RUVBL1	RuvB Like AAA+ ATPase 1
RUVBL2	RuvB Like AAA+ ATPase 2
s	Second
S/Ser	Serine
SA1, 2	Stromal antigen 1, 2
SCE	Sister chromatin exchange
sCIN	Structural chromosomal instability
SD	Standard deviation
SDS-PAGE	Sodium dodecyl sulphate-polyacrylamide gel electrophoresis
SEC	Size exclusion chromatography
shRNA	Short hairpin RNA
siRNA	Small interfering RNA
SMARCAL1	SWI/SNF related, matrix associated, actin dependent regulator of chromatin, subfamily A like 1
SMC1	Structural maintenance of chromosomes protein 1
SMC3	Structural maintenance of chromosomes protein 3
SRCAP	Snf2-related CREBBP activator protein
ssDNA	Single stranded DNA
SWI/SNF	SWItch/Sucrose non-fermentable chromatin remodelling complex
SWR1	SWi2/snf2-related complex 1 (yeast)
T/Thr	Threonine
TDRD3	Tudor domain containing 3 protein
TFIIB	Transcription factor IIB
TFIID	Transcription factor IID
TIP60	Tat interacting protein, 60kDa

TRRAP	Transformation/transcription domain-associated protein
TSS	Transcription start site
UCHL5	Ubiquitin carboxyl-terminal hydrolase isozyme L5
UV	Ultraviolet
V(D)J	Variable (V), Diversity (D) and Joining (J) genes
v/v	Volume per unit volume
VC	C-terminal non-fluorescent fragments of the Venus protein
VN	N-terminal non-fluorescent fragments of the Venus protein
w/v	Weight per unit volume
WT	Wild type
XLF	XRCC4-like factor
XRCC3	X-ray repair complementing defective repair in chinese hamster cells 3
XRCC4	X-ray repair complementing defective repair in chinese hamster cells 4
Y/Tyr	Tyrosine
YY1	Ying Yang 1
ZFN	Zinc finger nucleases
γ H2AX	Phosphorylated H2AX
μ g	Microgram
μ l	Microliter
μ M	Micromolar
μ m	Micrometre

Chapter 1.

Introduction

1.1 General introduction to chromatin and its structure

Within the nucleus, 2 meters of linear DNA are packaged into a higher-order structure termed chromatin. Chromatin consists of negatively charged DNA wound around positively charged protein complexes called nucleosomes, which allow the DNA to overcome the electrostatic repulsion that would occur if it were coiled around itself. In addition to serving the vital function of fitting long linear DNA molecules into the nucleus, chromatin also protects the DNA and plays important roles in mitosis, meiosis, gene expression, and DNA replication (Maeshima et al., 2014).

The core unit of chromatin is the nucleosome, which consists of 146 base pairs of DNA wrapped tightly, in approximately 1.65 superhelical turns, around a histone octamer, composed of two H2A-H2B dimers and an (H3-H4)₂ tetramer. The core histones display a highly conserved structure, the histone fold, in which three alpha helices ($\alpha 1$, $\alpha 2$, and $\alpha 3$) are connected with two short loops (L1 and L2). Each histone has a flexible tail that extends from the surface of the nucleosome and contains sites that can undergo covalent modification. These histone tails play vital roles in chromatin function. Histones H3 and H4 only have N-terminal tails, whereas histones H2A and H2B also have C-terminal tails. Histones H3 and H4 are among the most conserved proteins in eukaryotes. H2A and H2B are also conserved; however, they exhibit considerable species-specific variation, especially in their tails (Luger, 2001; Lewin et al., 2011). Nucleosomes are thought to be assembled in two steps: 1) the core (H3-H4)₂ tetramer is first connected through a strong 4-helix bundle (4-HB) between the two H3 molecules and deposited into DNA to form a tetrasome, which includes one turn of DNA wrapped around the centre of the H3-H4 tetramer; 2) the two H2A-H2B dimers associate with the tetramer via interaction between the C-terminal docking domain of

H2A with H3 and H4 to form the final octamer, while the L1 loops from each H2A molecule interact to stabilize the association of the two H2A-H2B molecules within the nucleosome, and the remaining DNA wraps around the octamer. (Luger, 2001; Lewin et al., 2011, Billon & Cote, 2012; Dennehey & Tayler, 2014). The mechanism of disassembly is a reversal of the assembly process, starting with unwrapping of the DNA and the loss of the H2A-H2B dimer, followed by disassociation of the H3-H4 tetramer from the DNA (Dennehey & Tayler, 2014).

The nucleosome, which provides the first level of organized structure of nuclear DNA, compacts the naked DNA by almost 6-fold, generating a 10 nm fibre that has been likened to “beads on a string” (Olins & Olins, 1974). The second level of chromatin organization consists of the interaction of the linker histone, H1, with the 10 nm fibre, and compacts the chromatin by approximately 40-fold to form a 30 nm fibre. Formation of this structure is also facilitated by the histone tails via internucleosomal interactions; for example, the N-terminal tail of the core histone H4 interacts with the acidic patch on the surface of H2A-H2B dimers in the adjacent nucleosome (Luger et al., 2012; Price & D’Andrea, 2013). This structure is thought to be the primary form of chromatin in both interphase and mitotic chromosomes. The higher-order structures beyond the 30 nm fibre, culminating in chromosome loops, remain poorly understood; however, 60–300 nm fibres, termed chromonema, have been observed by light and electron microscopy (Luger, 2001, Maeshima et al., 2014).

Packaged DNA can be categorized as either euchromatin or heterochromatin, depending on the density of staining observed during the cell cycle (Heitz, 1928; Huisinga et al., 2006). Heterochromatin reflects highly condensed genomic areas that are poor in genes and rich in repetitive sequences (e.g., centromeric and pericentromeric repeats and

telomeric regions), as well as transcriptionally silent DNA, such as the inactive X chromosome in female mammals (Wilson et al., 1990) and the mating-type locus in yeast (Lorentz et al., 1992). By contrast, euchromatin consists of less condensed areas, which are gene-rich and transcriptionally active (Huisinga et al., 2006).

1.2 Chromatin organization

When in a highly compacted state, the majority of DNA sequences are structurally inaccessible and functionally inactive. Hence, chromatin must exist in a dynamic state that can be relaxed to a greater or lesser extent, to govern the accessibility of the DNA to various enzymes and regulatory factors and control nuclear processes, such as transcription, and DNA recombination, replication, and repair. Accessibility is regulated by a variety of factors including the preferences of nucleosomes for some DNA sequences, post-translational modifications, histone variants, histone chaperones, and ATP-chromatin-remodelling factors (Chambers & Downs, 2012; Seeber et al., 2013; Chen & Shen, 2010; Price & D'Andrea, 2013; Conaway & Conaway, 2009). The following sections consist of a detailed discussion of these factors.

1.2.1 DNA sequence-based nucleosome preferences

It was previously widely believed that nucleosomes package genomic DNA in a nonspecific manner; however, high-resolution genome-wide analyses demonstrated that nucleosomes occupy the genome in favoured positions. This preferential mechanism is vitally important for modelling the chromatin structure in regions containing genes and for the regulation of their expression. In yeast, gene promoters include nucleosome-free regions (NFRs) upstream of the transcription start site (TSS), consisting entirely of poly (dA:dT) tracts, which inhibit nucleosome formation. The inhibition stems from the intrinsic stiffness of the tracts, which means that wrapping them around the histone octamer is energetically unfavourable; hence, it is possible that the depletion of nucleosomes at promoters depends on the length, number, and homopolymeric nature of these poly (dA:dT) tracts (Radman-Livaja & Rando, 2010; Struhl & Segal, 2013).

By contrast, nucleosomes immediately flanking NFRs, known as -1 and +1 nucleosomes, are preferable positions for nucleosomes and are enriched in TA dinucleotides. Typically, nucleosome formation favours DNA sequences with flexible dinucleotides (AA, TT, or TA) with a periodic repeat every 10 bp, which facilitates the bending of DNA around the nucleosomes. Linker DNA shows a strong preference towards inflexible sequences, including poly (dA:dT) tracts, and therefore it favours exclusion of nucleosomes (Radman-Livaja & Rando, 2010; Struhl & Segal, 2013).

In mammals, the same phenomena occur; however, the position of the +1 nucleosome relative to the TSS differs between organisms, suggesting variation in the mechanisms of transcription regulation (Radman-Livaja & Rando, 2010).

1.2.2 Post-translational histone modifications (PTMs)

Post-translational histone modifications (PTMs) are covalent modifications that mainly affect the flexible unstructured tails of histones. All histones can be post-translationally modified at many residues by, for example, methylation, acetylation, phosphorylation, ubiquitination, sumoylation, and ADP-ribosylation. PTMs can directly affect chromatin structure by altering histone-DNA and histone-histone chemical interactions. In addition, histone PTMs have vital functions in creating binding sites for non-histone proteins and facilitating their recruitment, due to their ability to act as scaffolds for numerous effector proteins, known as “readers”. Remarkably, the majority of histone PTMs are reversible. Cells contain enzymes to both add and remove these PTMs (known as “writers” and “erasers”, respectively), hence the accessibility to a specific genomic site and the recruitment of regulatory factors (non-histone proteins) are firmly controlled by PTMs. Consequently, cellular mechanisms, such as gene transcription, and DNA recombination, replication, and repair are mediated by histone PTMs

(Kouzarides, 2007; Musselman et al., 2012; Venkatesh & Workman, 2015). Notably, misregulation or complete loss of several histone PTMs is implicated in a number of human diseases, including cancer, the neurological disorder Sotos syndrome, and Wolf-Hirschhorn syndrome (Bhaumik et al., 2007).

The specificity of PTMs is regulated by the specificity of modifying enzymes for their target sites on particular histones. Many modified sites are subjected to a single PTM; however, others are subjected to multiple PTMs (e.g., H3K9 is either acetylated or methylated depending on the particular conditions). Moreover, modification of one site in a histone tail might lead to a subsequent effect, such as inhibition or activation, on another site. This led Strahl and Allis (2000) to propose the histone code hypothesis, in which the combined impact of multiple PTMs on one or several modified sites can determine a unique subsequent function. In the following sections, I consider the most well characterized PTMs (methylation, acetylation, and phosphorylation) and their roles in transcription and replication; other PTMs and their roles in DNA double-strand break (DSB) repair will be introduced later.

1.2.2.1 Methylation

Methylation usually occurs on the lysine and arginine residues of histone tails. Lysine can be mono-, di-, and tri-methylated, while arginine is subject to mono-methylation, or symmetrical or asymmetrical di-methylation. Methylation does not affect the net charge of nucleosomes, instead the size and hydrophobic state of the modified residue are altered. Lysine can be methylated on various canonical sites, including K4, K9, K26, K27, K36, and K79 on histone H3; K20 on histone H4; and K26 on histone H1. Reader domains that can specifically recognize methyl lysine have been reported, including chromodomain, double chromodomain (DCD), chromobarrel, tandem Tudor domain

(TTD), Tudor, ATRX-DNMT3-DNMT3L (ADD), ankyrin, bromo-adjacent homology (BAH), malignant brain tumour (MBT), plant homeodomain (PHD), Pro-Trp-Trp-Pro (PWWP), WD40, and zinc finger CW (zf-CW). These readers usually bind through an aromatic cage, which is moulded from two or four residues. The size of the aromatic cage and the precise composition of residues identify the specificity towards mono-, di-, or tri-methylated states (Musselman et al., 2012).

Many of the functions of methylated lysine have been well described in the context of gene transcription regulation. Globally, methylation of histone H3 Lys4 (H3K4me) is considered a mark for gene activation (Schneider et al., 2004). Mono-methylation of this residue (H3K4me1) is a marker of active enhancer elements, and is recognized by the chromobarrel domain of Tip60 acetyltransferase, enabling estrogen-induced transcription (Jeong et al., 2011). Similarly, the binding of TAF3, a subunit of the basal transcription complex, TFIID, to H3K4me3 via its PHD domain is a mark of transcriptionally active regions (Vermeulen et al., 2007), while the binding of H3K4me3 to ING2, a subunit of the mSin3a histone deacetylase complex, results in gene repression (Shi et al., 2006). Importantly, a conserved enrichment of tri-methylated lysine has been reported in the 5' regions of actively transcribed genes (Schneider et al., 2004).

In addition, methylation of lysine is associated with DNA replication, as the recruitment of ORC1, a subunit of the origin of replication complex that mediates pre-DNA replication licensing, is facilitated by H4K20me, through a direct interaction with its BAH domain (Kuo et al., 2012). Moreover, two methylation sites, H3K27 and H3K9, are implicated in the formation of heterochromatin and gene silencing. H3K27me1 and H3K9me3 are enriched in pericentromeric heterochromatin, while H3K27me3 and

H3K9me2 co-localize in inactive regions of euchromatin. The recruitment of polycomb and heterochromatin protein 1 (HP1) proteins, which are involved in the formation and spreading of heterochromatin, is mediated by H3K27me and H3K9me, respectively, via direct interaction with the chromodomains of these proteins (Fischle et al., 2003; Min et al., 2003; Bannister et al., 2001; Fischle et al., 2005).

Arginine can be methylated on several canonical residues, including R2, R8, R17, and R26 of histone H3; R3 of histone H4; and R11 and R29 of histone H2A (Musselman et al., 2012). Although more studies are required to investigate the significance of the methylation of arginine, one good example of the functional consequences of this modification is the recruitment of the transcriptional activator TDRD3, which is mediated by the recognition of asymmetrically di-methylated histone H3 R17 and asymmetrically di-methylated histone H4 R3 (H3R17me2a and H4R3me2a) by the Tudor domain of TDRD3, promoting gene expression (Yang et al., 2010).

1.2.2.2 Acetylation

Acetylation also occurs on lysine residues and neutralizes the positive charge on the NH₃ of this amino acid. Lysine can be acetylated on several canonical sites, including K4, K9, K14, K18, K23, K27, K36, and K56 of H3; K5, K8, K12, K16, K20, and K91 of H4; K5 and K9 of H2A; and K5, K12, K15, K16, K20, and K120 of H2B. Acetyl lysine reader domains have been identified, including the bromodomain, double PHD finger (DPF), and double pleckstrin homology (PH) domain (Musselman et al., 2012).

Acetylation of lysine is associated with a dynamic chromatin state and with a more open conformation, as a result of weakening of the interaction of the histone with negatively charged DNA. For a long time, this was thought to be the only purpose of acetylation; however, this modification has been found to be widely linked to gene transcription.

The recruitment of proteins of the BRD family of transcription regulators is mediated by acetylation via their bromodomains (Filippakopoulos et al., 2012). In addition, H3K14ac is essential for activating and regulating the *DPF3b* and *MOZ* genes via its binding to their DPF domains (Zeng et al., 2010; Qiu et al., 2012). Similarly, the recruitment of BRG1, a catalytic subunit of the SWI/SNF complex, at DSBs is mediated by the recognition of H3ac (at K9, K14, K18, and K23) by its bromodomain (Lee et al., 2010).

1.2.2.3 Phosphorylation

Phosphorylation can occur on the hydroxyl groups of serine and threonine residues, and results in the introduction of a negatively charged group; hence, phosphorylation is widely thought to be involved in the compaction of chromatin. Histones can be phosphorylated at T3, T6, S10, T11, S28, and T45 of H3; S1 of H4; S1 and T120 of H2A; S139 of human histone variant H2AX; and S14 of H2B (Kouzarides, 2007; Musselman et al., 2012). Phosphorylation can also occur at Y57 of H2A mediated by casein kinase 2 (Basnet et al., 2014).

A well-studied reader domain recruited to phosphorylated histones is the tandem BRCT domain that can specifically recognize and bind to the S139 of histone H2AX in mammals (Stucki et al., 2005; Lou et al., 2006). Phosphorylated H2AX (γ H2AX) is widely considered to be a DSB marker and plays an important role in DSB repair; it will be discussed in more detail later in this chapter. In addition, phosphorylation plays a vital role in chromosome condensation and segregation in mitosis, as the phosphorylation of H3S10, mediated by Aurora B kinase, is necessary for disassociation of HP1 from chromosomes during mitosis, and acts in this process by inhibiting the interaction between the chromodomain of HP1 and H3K9me (Hirota et

al., 2005).

1.2.3 Histone variants

Histone variants are non-allelic variants that differ from the core histones (H2A, H2B, H3, and H4) in sequence. The variation can be as little as a single amino acid or as extensive as an alternative tail sequence, and can affect the interaction between DNA and nucleosomes or interactions within nucleosomes, resulting in changes in the level of chromatin compaction. The expression of histone variants is independent of replication and can occur throughout the cell cycle, unlike canonical histone expression, which is restricted to the S phase (i.e., it is DNA replication-dependent). Moreover, the deposition mechanism of these variants is also different, in that it generally requires specific factors, such as histone chaperones or chromatin remodellers. These differences reflect an alteration in the function of histone variants relative to their canonical counterparts. Variants have been identified for all core histones, except histone H4. For instance, H3.3 and CENP-A are variants of canonical H3, and H2AX, H2AZ, macro H2A, and H2ABBD are variants of canonical H2A (Sarma & Reinberg, 2005; Henikoff & Ahmad, 2005; Talbert & Henikoff, 2010). In the next sections, I focus on some universal histone variants, including CENP-A and H2AZ, while H2AX will be discussed later.

1.2.3.1 CENP-A

CENP-A (also known as Cse4 in yeast) is an H3 variant unique to centromeres; it has approximately 50–60% homology with canonical H3 in the histone fold domain (HFD) and there is no conservation in the N-terminal tail relative to the core H3 protein or among species (Talbert & Henikoff, 2010; Verdaasdonk & Bloom, 2011). CENP-A is essential for recruitment of kinetochore proteins to the centromere (Howman et al.,

2000). Interestingly, yeast Cse4 can substitute for human CENP-A, indicating that the two proteins build similar nucleosome structures, regardless of the divergence of their sequences (Wieland et al., 2004). CATD, a CENP-A centromere-targeting domain within the HFD, which is critical for centromere function, facilitates the interaction of CENP-A with other factors (Black et al., 2007), such as suppressor of chromosome missegregation 3 (Scm3) in yeast (Zhou et al., 2011). In addition, tetramers of CENP-A-H4 are more rigid than those of the canonical H3-H4 tetramer, which is important for the maintenance of centromere structure that is required for efficient chromosome segregation (Verdaasdonk & Bloom, 2011).

The timing of CENP-A loading into centromeres during the cell cycle varies among species. It is loaded in anaphase and G1 in higher eukaryotes (e.g., humans and *Drosophila melanogaster*), in S–G2 in yeast, and in late G2 in plants (Verdaasdonk & Bloom, 2011). Various proteins have been identified from different studies in either human or yeast as involved in facilitating the loading of CENP-A (Fujita et al., 2007; Foltz et al., 2009; Verdaasdonk & Bloom, 2011), leading to a model in which licensing and loading are distinguished. In humans, this begins with recruitment of MIS18, CENP-H, CENP-I, RBAP46, and RBAP48 (Fujita et al., 2007), followed by the recruitment of loading proteins, such as KNL2 and HJURP (a human homolog of yeast Scm3) (Foltz et al., 2009). The histone chaperone, CAF1 (chromatin assembly factor 1), and HIR (a histone regulator) are associated with the disassembly of CENP-A from centromeric chromatin, and with preventing extra-centromeric incorporation of CENP-A in *Saccharomyces cerevisiae* (Rosa et al., 2011).

1.2.3.2 H2AZ

H2AZ is a highly conserved histone variant that shares 60% sequence identity with the canonical histone H2A across eukaryotes (Zlatanova & Thakar, 2008). H2AZ is essential in flies (Clarkson et al., 1999) and H2AZ knockout mice exhibit an embryonic lethal phenotype (Faast et al., 2001); however, H2AZ-deleted yeast strains exhibit slow growth rather than lethality. Mutant yeast strains also suffer from chromosomal instability (Carr et al., 1994), transcriptional defects (in both gene silencing and activation of transcription) (Meneghini et al., 2003), and genotoxic and environmental stress (i.e., formamide sensitivity at 28°C and lethality at 37°C) (Jackson & Gorovsky, 2000). H2AZ is also involved in DNA replication and DNA repair (Downs et al., 2004; Xu et al., 2012). Moreover, overexpression of H2AZ has been observed in many patients with cancer, including breast cancer, particularly during metastasis, (Zucchi et al., 2004; Svtelis et al., 2010) and sporadic colorectal cancer, more specifically in microsatellite instability (MIN) cell lines, which exhibit a phenotype linked to a defect in the mismatch DNA repair pathway (Dunican et al., 2002). Taken together, this evidence suggests a key role for H2AZ in faithful maintenance of the genome.

Although H2AZ shares 60% sequence similarity with canonical H2A, their crystal structures reveal several differences between them, which may be sufficient to alter the function of H2AZ (Suto et al., 2000). First, the equivalent of the docking domain of the core H2A histone is altered in H2AZ, which is important for interaction with H3-H4. Importantly, the alteration of Glu104 in H2A to Gly106 in H2AZ leads to the loss of three hydrogen bonds, which destabilizes the interaction with the H3-H4 tetramer. Second, the existence of His112, which can bind a metal ion, on the surface of H2AZ-containing nucleosomes offers a distinctive surface for protein interactions. Third, H2AZ has an extended acidic patch, which provides a unique binding domain and

interacts with DNA, the linker histone H1, and the N-terminal tail of histone H4. Fourth and finally, the L1 loop is altered in H2AZ, which may reflect an alteration of the stability within the nucleosome, as this loop is important for H2A/H2A self-interaction. Taken together, these modifications in the structure of H2AZ suggest a destabilization of H2AZ-containing nucleosomes; however, contradicting data has emerged from different laboratories about the ability of H2AZ to create, or be associated with, a less stable chromatin environment. In 2001, Abbott and colleagues characterized the ionic-strength dependence of reconstituted H2A- and H2AZ-containing nucleosomes from recombinant human histones by analytical ultracentrifugation. The sedimentation coefficients of these particles demonstrated a significant destabilization of H2AZ-containing nucleosomes, compared with those containing H2A. The authors attributed this to the loose binding of the H2AZ-H2B dimer to the nucleosome (Abbott et al., 2001). In agreement with this, another study in yeast showed that nucleosomal H2AZ is unstable and vulnerable to loss under increased salt conditions, compared with the canonical histones H2A and H3 (Zhang et al., 2005). By contrast, an analysis of salt-dependent stability by fluorescence resonance energy transfer (FRET) demonstrated that H2AZ-containing nucleosomes are stabilized compared with core nucleosomes, due to the association with the H3-H4 tetramer (Park et al., 2004). However, it was recognized recently that the destabilizing effect of H2AZ is dependent on, first, pre-existing PTMs on other histones or PTMs on H2AZ itself, and, second, the presence of histone variants such as H3.3 (Billon & Cote, 2012; Zlatanova & Thakar, 2008). Further, nucleosomes containing H2AZ can have two copies of the H2AZ-H2B dimer (termed homotypic nucleosome, ZZ), or one copy each of H2AZ-H2B and the core dimer, H2A-H2B (termed heterotypic nucleosome, AZ), with a relative distribution of these forms in yeast chromatin of 35% and 65%, respectively (Luk et al., 2010). One can predict that

nucleosomes containing homotypic dimers are less stable than the heterotypic nucleosomes; however, more research is required to confirm such a prediction.

In addition, H2AZ can undergo alternative post-translational modification, compared with the major H2A histone. Human H2AZ is acetylated on K4, K7, K11, and K13 (Boyne et al., 2006). Prior acetylation of the core histones H4 and H2A by TIP60 is required to enable H2AZ to be incorporated into nucleosomes by the chromatin remodeller, SWR1/p400 (Altaf et al., 2009; Xu et al., 2012). Chromatin immunoprecipitation (ChIP) data from the Bystricky laboratory indicate that TIP48, a subunit of TIP60, promotes H2AZ acetylation, as depletion of TIP48 by small interfering (si)RNA results in a reduction in the level of acetylated H2AZ at the TSS and enhancer of *CCND1* compared with controls (Dalvai et al., 2013).

Interestingly, acetylation of H2AZ in mouse is dynamic throughout embryonic developmental stages, with preferential accumulation in euchromatin. Acetylated H2AZ was detected in pre-implantation blastomeres, while no acetylation was observed at the two-cell embryonic stage, a major genome activation stage. However, acetylation of H2AZ was detected at all subsequent stages investigated, including 4-, 8-, and 16-cell embryos, as well as the blastocyst (Bošković et al., 2012). These data suggest that H2AZ may be associated with diverse gene expression events at distinct embryonic stages.

H2AZ lysines can also be mono-methylated at the K4 and K7 residues in the N-terminal tail by the methyltransferase SETD6 (Binda et al., 2013), and H2AZ can undergo mono-ubiquitination on residues K121, K120, and K125 of its C-terminus, mediated by RING1B, a subunit of polycomb repressive complex 1 (PRC1) (Sarcinella et al., 2007). Notably, mono-ubiquitinated H2AZ localizes to the heterochromatin of the human

female inactive X chromosome (IMR90 cells) (Sarcinella et al., 2007), and is widely used as a transcriptional silencing mark (Sevilla & Binda, 2014).

The unique features of H2AZ differentiate the function of this variant from that of the canonical histone, facilitating the regulation of various biological processes, including transcription, heterochromatin maintenance, DNA repair, and chromosome segregation (the latter two processes are discussed in later sections). H2AZ is involved in transcription; in yeast, H2AZ is found at all promoters as part of two nucleosomes flanking the NFR, which contains the TSS (Raisner et al., 2005). It is involved in both activation and repression of transcription, and evidence from an experiment, in which the transcriptomes in wild-type and H2AZ-deleted strains were characterized, identified 214 genes that were activated by H2AZ and another 107 that were repressed (Meneghini et al., 2003). The majority of studies in yeast report an inverse correlation between H2AZ enrichment at promoters and transcription activity (Raisner et al., 2005; Li et al., 2005; Zhang et al., 2005; Millar et al., 2006). ChIP and microarray analyses found a correlation between the acetylation state of H2AZ and transcription activity, demonstrating that H2AZ associates preferentially with the promoters of repressed genes, whereas the acetylation of H2AZ at K14 was found to be enriched at the promoters of active genes (Millar et al., 2006). In humans, similar to yeast, H2AZ is enriched at promoters both upstream and downstream of TSSs and the level of its enrichment correlates with gene activity (Barski et al., 2007).

Separate from its role in transcription, evidence published from several laboratories indicates the association of H2AZ with the formation of higher-order chromatin structure. The Tremethick group demonstrated the importance of the extended acidic patch in H2AZ that associates with the N-terminus of H4 on the adjacent nucleosome,

using a condensed array structure, and found that a larger acidic patch has a higher affinity for the H4 tail than core H2A, due to stronger electrostatic interactions, leading to a more compact nucleosome structure (Fan et al., 2004). In addition, they found that HP1a preferentially binds to highly folded chromatin fibres containing H2AZ, rather than those containing H2A (Fan et al., 2004). Moreover, the presence of H2AZ in satellite repeats in pericentric heterochromatin (Greaves et al., 2007) supports the assertion that H2AZ has a function in chromatin condensation. Overall, it is highly likely that H2AZ governs accessibility to chromatin by, 1) stabilizing nucleosomes and creating more compact chromatin, and 2) opening this condensed chromatin, when required, through the virtue of its ability to be modified by PTMs, and possibly more specifically through acetylation.

H2AZ is expressed throughout the cell cycle and is highly dynamic; it can be incorporated into chromatin and then removed in a function-dependent manner (Papamichos-Chronakis et al., 2011). Several studies in yeast demonstrate that H2AZ can be deposited into chromatin via exchange of H2A-H2B with H2AZ-H2B by SWR1 (Krogan et al., 2003; Kobor et al., 2004; Mizuguchi et al., 2004), and in mammals via either the SWR1 homolog SRCAP (Ruhl et al., 2006) or P400, a subunit of the TRRAP/TIP60 complex (Xu et al., 2012). However, the reverse mechanism (i.e., removal of H2AZ and re-incorporation of canonical H2A into chromatin) is still under study, especially in mammals. Very recently, biochemical studies identified ANP32E, an H2AZ chaperone that can specifically remove H2AZ from chromatin (Obri et al., 2014; Mao et al., 2014). In yeast, INO80 controls the removal of H2AZ (Papamichos-Chronakis et al., 2011).

1.2.4 Histone chaperones

Histone chaperones were initially described as a “nucleoplasmin”, referring to the ability of these proteins to prevent histone-DNA aggregation at physiological salt concentrations, and stimulate nucleosome assembly *in vitro* (Laskey et al., 1978; Earnshaw et al., 1980). Today, the term histone chaperones refers to a large number of proteins that can bind to histones and are involved in accomplishing one or more of the following functions: transfer of newly synthesized histones from the cytoplasm to the nucleus, facilitation of histone PTMs by presentation of histones to histone-modifying enzymes, storage of free histones in the cell, deposit of histones onto DNA, and removal of histones from the nucleosome (Dennehey & Tyler, 2014; Gurard-Levin et al., 2014). Histone chaperones can be classified into H2A-H2B and H3-H4 chaperones, depending on their binding specificity. In addition, unique histone chaperones may exist for each histone variant. The activity of histone chaperones can be replication-dependent, where they are associated with chromatin assembly during DNA synthesis, or replication-independent, where they function outside of periods of DNA synthesis, for example, during transcription. Histone chaperones vary in their structure, which makes it challenging to identify them; however, the majority of chaperones contain an acidic patch, which may facilitate their interaction with histones, since the latter are positively charged (Dennehey & Tyler, 2014). Here, I will only describe the ANP32E histone chaperone in detail, as it features strongly in the work described in this thesis.

1.2.4.1 ANP32E, an H2AZ histone chaperone

ANP32E belongs to the ANP32 family, consisting of 32 evolutionarily conserved proteins, which is part of the leucine-rich repeat (LRR) superfamily. The ANP32 family is characterized by an N-terminal domain containing a LRR region, which varies from

between two to four repeats, and a C-terminal acidic tail, rich in aspartic and glutamic acids. Similar aspartic/glutamic acid-rich domains are present in tubulin and many other histone chaperone proteins. Members of this family are associated with modulation of cell signal transduction and control of gene expression (Matilla & Radrizzani, 2005). ANP32E is a protein with a molecular weight of approximately 30.7 KDa, which was first identified in *Xenopus laevis* oocytes by stimulating its phosphorylation in nuclear localization signal (NLS)-dependent manner (Kurihara et al., 1996). In addition, ANP32E spatially co-localizes with the catalytic subunit of phosphatase 2A (PP2A) and inhibits its activity (Matilla & Radrizzani, 2005). High levels of ANP32E expression were observed in mouse thymus, peripheral blood leukocytes, colon, small intestine, prostate, spleen, skeletal muscle, liver, and kidney (Matilla & Radrizzani, 2005).

ANP32E was recently identified as a histone chaperone that can specifically remove H2AZ from chromatin in human cells (Obri et al., 2014; Mao et al., 2014). Both studies carried out immune-affinity purification of H2AZ and canonical H2A and identified ANP32E as a major interaction partner of H2AZ. The Hamiche group reported ANP32E as a member of the p400/TIP60 complex, based on mass spectrometry data, in which the p400/TIP60 complex and some of its subunits, including RUVBL1 and RUVBL2, were identified in both H2AZ and ANP32E purified complexes (Obri et al., 2014). Furthermore, pull-down and immune-precipitation (IP) experiments demonstrated that the specificity of the interaction of ANP32E with H2AZ is determined by its C-terminal acidic region, as interruption or deletion of this domain completely abolished the interaction with H2AZ (Obri et al., 2014; Mao et al., 2014). A crystal structure of the H2AZ-ANP32E complex revealed that ANP32E recognizes H2AZ through particular residues (T103 and I104) in the α C helix of H2AZ. Interestingly, these residues are conserved in H2A; the H2A glycine residue, G98, is the

only difference between H2AZ and H2A that has been found to be key for the specific interaction of ANP32E with H2AZ rather than H2A. Insertion of glycine in the H2AZ interaction motif completely abrogates its interaction with ANP32E (Obri et al., 2014; Mao et al., 2014). Remarkably, the crystal structure also revealed that the interaction between H2AZ and ANP32E via the H2AZ α C helix impeded the interaction between H2AZ and H3-H4 (Obri et al., 2014; Mao et al., 2014). Moreover, the Zhou group demonstrated that ANP32E prevents the aggregation of DNA with H2AZ-H2B, but not that between DNA and H2A-H2B (Mao et al., 2014). Finally, an *in vitro* experiment that mimicked the natural state of nucleosomes revealed that ANP32E is involved in removal, rather than deposition, of H2AZ. In this experiment, H2A- and H2AZ-containing nucleosomes were assembled on a 256 bp 5S DNA, immobilized on magnetic beads, and incubated with recombinant ANP32E, and the purified complexes were analysed by SDS-PAGE and immunoblotting, and detected with either anti-H2A or anti-H2AZ. The results revealed that H2AZ was disassociated from nucleosomes, as a large amount of unbound H2AZ was detected after incubation with ANP32E (Obri et al., 2014; Mao et al., 2014). Together, the results of all of these various *in vitro* experiments confirm the function of ANP32E as a specific histone chaperone for the removal of H2AZ.

This function of ANP32E in specific removal of H2AZ has also been addressed by cell culture experiments. Genome-wide comparative ChIP-seq analyses of both mouse embryonic fibroblasts (MEFs) (Obri et al., 2014) and human HeLa cells (Mao et al., 2014) revealed that depletion of ANP32E results in an increase of H2AZ accumulation at TSS regions. In addition, the absence of ANP32E in MEFs results in incorporation of H2AZ into enhancer and insulator sequences, which are usually H2AZ-free regions (Obri et al., 2014). Also, overexpression of ANP32E in HeLa cells results in a

significant decrease of H2AZ accumulation at +1 nucleosomes, whereas ANP32E knockdown leads to an increase in the occupancy of H2AZ at +1 nucleosomes (Mao et al., 2014). Moreover, recent data from the Downs and Price laboratories demonstrate that ANP32E is required for removal of H2AZ from DSBs, and that failure to remove H2AZ leads to defective DSB repair pathways (Alatwi & Downs, 2015; Gursoy-Yuzugullu et al., 2015). However, the fact that H2AZ knockout is embryonically lethal in mice, while ANP32E knockout does not result in such a phenotype (Obri et al., 2014), suggests that there may be a partner molecule that also has a role in removal of H2AZ from chromatin. Notably, a recent work from our laboratory demonstrated that this is indeed the case, and that ANP32E works cooperatively with INO80, a chromatin remodeler, to remove H2AZ from chromatin at DSBs (Alatwi & Downs, 2015); these results will be presented in chapter 4.

1.2.5 ATP-dependent chromatin remodellers

ATP-dependent chromatin-remodelling complexes are characterized by their ability to use ATP hydrolysis to alter histone-DNA contacts. All of these proteins share a similar ATPase domain and use ATPase-derived energy to remove the nucleosomal barriers that can prevent various proteins from binding to DNA. This function can be exerted by sliding, evicting, or exchanging histones or nucleosomes (Chambers & Downs, 2012; Seeber et al., 2013; Chen & Shen, 2010; Price & D'Andrea, 2013; Clapier & Cairns, 2009; Conaway & Conaway, 2009).

Although all chromatin remodellers share a conserved ATPase domain, each also has a unique flanking domain, leading to the classification of these proteins into four families:

1) SWI/SNF family proteins, which contain a bromodomain that can bind acetylated histone tails; 2) the ISWI family, which has SANT and SLIDE domains that can bind

unmodified histone tails and DNA; 3) CHD-remodelling proteins, which have a tandem chromodomain that associates with methylated histones; and 4) the INO80 complex, which has an insert in the middle of the ATPase domain (Clapier & Cairns, 2009; Seeber et al., 2013). However, Flaus et al. (2006) provided a new classification system for these remodellers, based on sequence similarities in the helicase-like region. In that scheme, chromatin remodellers are classified into six major families: Snf2-like, Swr1-like, SMARCAL1, Rad54-like, Rad5/16-like, and ERCC6/SSO1653-like. These can be further categorized into 24 subfamilies (Figure 1.1). Here, I discuss the INO80 complex, which was a fundamental target of this project.

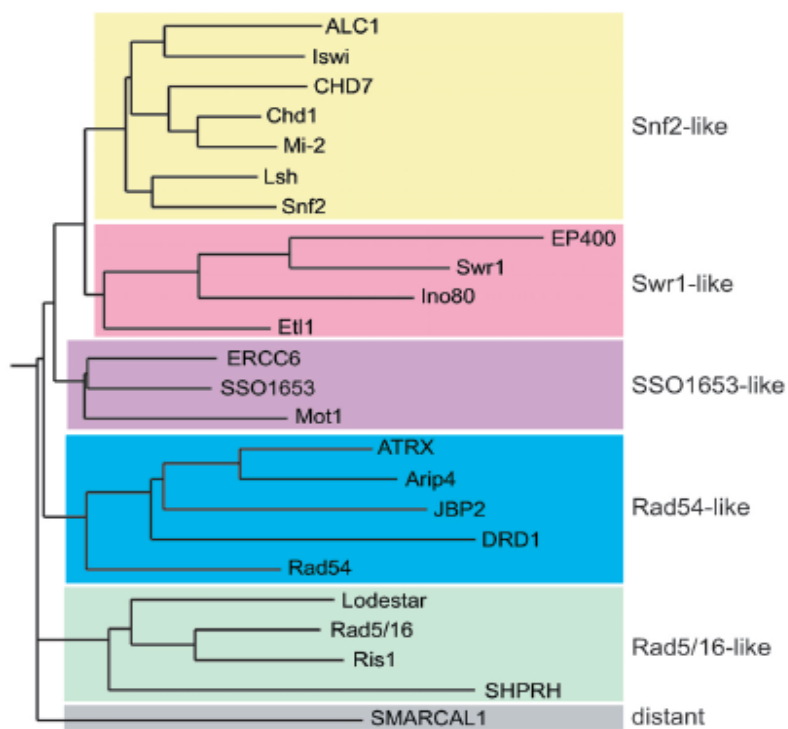


Figure 1. 1 Diagram demonstrating the classification of chromatin remodellers.

Adapted from (Flaus et al., 2006).

1.2.5.1 INO80: an overview

1.2.5.1.1 Structure and subunits

INO80 is a chromatin-remodelling complex of the Swr1-like family that was first identified in *S. cerevisiae* (Ebbert et al., 1999), but is conserved in multicellular eukaryotes. Some of its 15 subunits are common to both yeast and metazoan complexes. The yeast subunits identified to date are Ino80, Rvb1, Rvb2, Arp4, Arp5, Arp8, Act1 (actin), Ies2, Ies6, Ies1, Ies3–5, Taf14 (Anc1), and Nhp10; the human complex shares the first eight subunits and also contains the mammal-specific subunits Amida, INO80E, NFRKB, MCRS1, INO80D, UCHL5, and YY1 (Table 1.1) (Seeber et al., 2013).

Yeast INO80	Human INO80
Ino80	INO80
Rvb1	RUVBL1/TIP49a
Rvb2	RUVBL2/TIP49b
Arp4	BAF53a (INO80K)
Arp5	ARP5
Arp8	ARP8
Ies2	IES2/PAPA-1
Ies6	IES6/C18orf37
Act1 (actin)	
Taf14/Anc1	
Ies1	
Ies3	
Ies4	
Ies5	
Nhp10	
	INO80D (FLJ20309)
	NFRKB
	MCRS1
	Amida (TCF3)
	YY1
	INO80E (FLJ90652/CCDC95)
	UCHL5 (UCH37)

Table 1.1 Subunits of the INO80 complex in yeast and humans.

The catalytic subunit of the INO80 complex, INO80, has an ATPase domain that contains a characteristic internal spacer region (Figure 1.2). This conserved region is essential for the recruitment of the majority of the evolutionarily conserved subunits IES2, IES6, and ARP5 and the AAA+ ATPase subunits RUVBL1 and RUVBL2 (Chen et al., 2011). INO80 also contains a helicase-SANT (HSA) domain, which is important for recruitment of YY1, ARP4, and ARP8, as deletion of this domain from human INO80 resulted in loss of these subunits (Chen et al., 2011). Finally, recruitment of the metazoan-specific subunits (i.e., Amida, INO80E, INO80D, NFRKB, UCHL5, and MCRS1) is dependent on the N-terminal region of human INO80, since deletion of this region led to the loss of these subunits from the complex. By contrast, deletion of the C-terminus did not cause any loss of INO80 complex subunits (Chen et al., 2011).

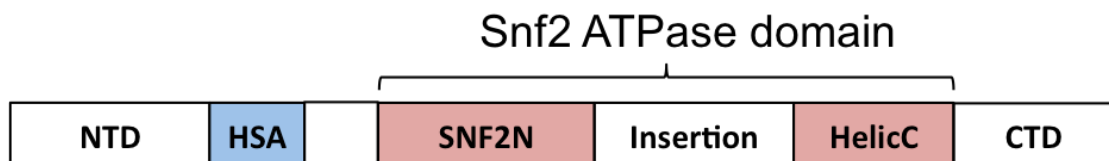


Figure 1. 2 Schematic diagram showing the domain organization of the catalytic subunit, INO80, of the human INO80 complex.

The SNF2N ATPase domain contains an insertion in the middle. NTD, N-terminal domain; HSA, helicase-SANT domain; CTD, C-terminal domain. Adapted from (Chen et al., 2011).

The conservation of this complex among widely divergent organisms suggests that it plays an important role in one or more essential processes. For example, deletion of INO80 in yeast results in either lethal or sick strains (Chambers & Downs, 2012), and causes early embryonic lethality in mouse (Min et al., 2013). The mammalian INO80 complex contains RUVBL1 and RUVBL2, AAA+ proteins homologous to the bacterial helicase RuvB (Lopez-Perrote et al., 2012), a subunit of the Holliday junction branch-migration complex (Mayanagi et al., 2008; Fujiwara et al., 2008). YY1 was first

identified as a subunit of human INO80 in 2007 (Wu et al., 2007). Previously, it was well known as a transcription factor; however, biochemical analysis by Wu et al. demonstrated *in vitro* interactions between YY1 and the INO80 subunits INO80, BAF53a, and RUVBL1 and 2, indicating that YY1 is also a component of the INO80 complex. YY1 binds Holliday junctions (HJs) *in vitro* and interacts with RUVBL1 and RUVBL2, homologs of RuvB, suggesting that YY1 may be the mammalian ortholog of bacterial RuvA (Wu et al., 2007). In bacteria, RuvA forms an octamer (a pair of tetramers) that specifically binds Holliday junction DNA and target RuvB to the junction, where it forms two hexameric rings on either side of the RuvA octamer. Together, the two proteins form a complex that facilitates ATP-dependent branch migration of the junction (Figure 1.3) (Mayanagi et al., 2008). Two actin-related proteins (Arps), Arp5 and Arp8, are unique to INO80, whereas Arp4 is also found in the NuA4 histone acetyltransferase (HAT). Association of these unique Arps requires the presence of the Ruv proteins (Chambers & Downs, 2012).

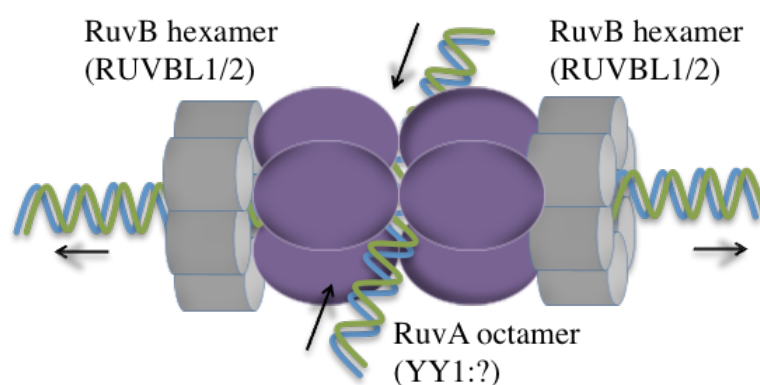


Figure 1.3 A model for eukaryotic Holliday junction resolution based on the bacterial RuvA/RuvB complex.

RuvB is the bacterial homolog of mammalian RUVBL1 and RUVBL2, which form two hexamers flanking the octamer of RuvA, the putative YY1 homolog. The resultant complex binds to Holliday junction DNA and facilitates branch migration.

Since INO80 was identified as an ATPase-dependent chromatin remodeller (Ebbert et al., 1999), many of its subunits have been purified and structurally characterized, including RUVBL1/2 (Gorynia et al., 2011; Lopez-Perrote et al., 2012), actin (Vorobiev et al., 2003), Arp4, and Arp8 (Fenn et al., 2011; Gerhold et al., 2012). However, possibly due to its enormous size (1.3 MDa), the overall structure of INO80 was only determined very recently in *S. cerevisiae* (Tosi et al., 2013). A combination of a hybrid structural approach, three-dimensional and cryo-electron microscopy, mass spectrometry, and chemical crosslinking revealed the “embryonic” structure of the INO80 complex (Figure 1.4). This study revealed many aspects of the dependency and crosslinking between the subunits of INO80, and knowledge of these features could impact our understanding of the functions of the subunits. For example, the study found that association of Ies6 with the complex is dependent on the presence of Arp5, both of which are conserved in humans (see Table 1.2 for the other subunits). This helped to determine the exact part of the complex occupied by each subunit and to build up the “embryonic” structure, which consists of head (Rvb1/2), neck (Ies2 and Arp5), body (Nhp10, Ies1, Ies3, and Ies5), and foot (Act1, Arp4 Arp8, Ies4, and Taf14) regions (Figure 1.4) Both head and neck subunits crosslink to the INO80 ATPase, the body domain subunits crosslink to the N-terminus of INO80 (the metazoan subunits), and the foot subunits crosslink to the HSA domain region (Tosi et al., 2013).

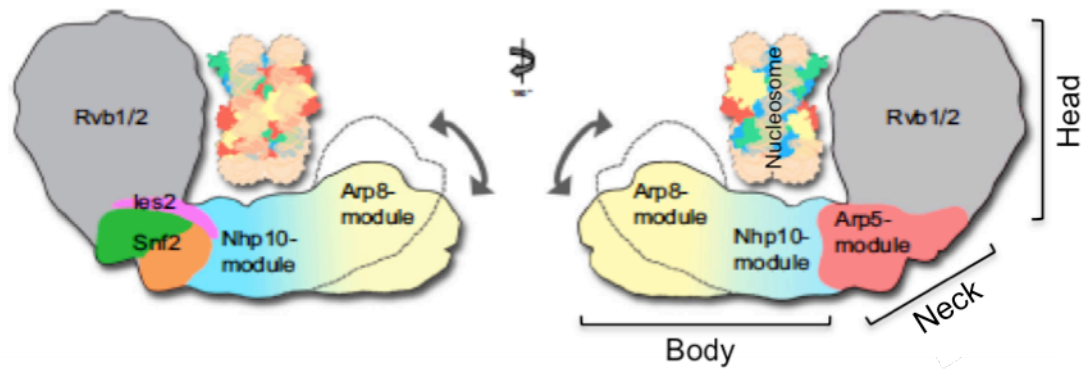


Figure 1. 4 The proposed embryonic structure of the INO80 complex. Adapted from (Tosi et al., 2013).

	WT	Δ arp5	Δ arp8	Δ nhp10	
Ino80	
Rvb1/2	
Ies2	
Arp8	.	.	X	.	
Arp4	.	.	X	.	
Act	.	.	x	.	
Taf14	.	.	x	.	
Ies4	.	.	X	.	
Arp5	.	X	.	.	
Ies6	.	X	.	.	
Nhp10	.	.	.	X	
Ies1	.	.	.	X	
Ies3	.	.	.	X	
Ies5	.	.	.	X	
sum	15	13	12	11	

Table 1. 2 The dependency between INO80 subunits in yeast (Tosi et al., 2013).

1.2.5.1.2 Remodelling activity

There are multiple lines of *in vitro* evidence in the literature to support the idea that INO80 is an ATPase-dependent chromatin remodeller. Biochemical analysis demonstrated that INO80 can bind DNA and exert a 3'→5' helicase activity. The directional helicase activity was revealed by the ability of INO80 to bind 24 mer oligonucleotides (3'→5') rather than 32 mer oligonucleotides (5'→3') *in vitro* (Shen et al., 2000). That study and others revealed that DNA binding by INO80 is ATPase-

dependent (Shen et al., 2000; Shen et al., 2003; Udugama et al., 2011). Biochemical evidence for the *in vitro* chromatin-remodelling activity of INO80 was obtained by incubating the INO80 complex and ATP with a reconstructed chromatin template and monitoring its accessibility to the *Bam*HI restriction enzyme. Addition of INO80 resulted in elevated cleavage, indicating increased accessibility of the restriction site (Shen et al., 2000).

Moreover, the ability of INO80 to alter nucleosome spacing was demonstrated *in vitro* by the combination of a nucleosome-sliding assay and high-resolution site-directed mapping. These techniques were used to demonstrate that INO80 can space nucleosomes almost 30 bp apart, with a preference for di- and tri-nucleosomes (Udugama et al., 2011). Another study revealed that this activity is dependent on the ATPase and HSA domains of INO80 and their recruited subunits (Chen et al., 2011). In this study, a sliding assay was performed on a purified FLAG-INO80 complex (WT) or manipulated INO80 complexes (i.e., with an N-terminal deletion (Δ N), a C-terminal deletion (Δ C), Δ NC, Δ N, and HAS deletion, or ATPase mutants) in the presence of reconstructed nucleosomes positioned near the end of the DNA strand. In all cases, nucleosomes slid towards the middle of the DNA, except where an INO80 mutant form with either an ATPase mutation or HAS deletion was used, which led to complete abolition of sliding activity (Chen et al., 2011).

Further, a recent study in yeast demonstrated that INO80 has histone-exchange activity towards the H2AZ histone variant (i.e., removal of H2AZ and incorporation of H2A) (Papamichos-Chronakis et al., 2011). A mononucleosome ChIP-chip analysis determined an increase in H2AZ enrichment in *ino80* Δ , compared with wild-type, strains. The same study also revealed that the dynamic alteration of H2AZ content in

nucleosomes linked to transcription states is regulated by INO80. The *KAR4* locus, a cell cycle-dependent gene that is highly expressed during G1 and repressed in G2 phase, was analysed. H2AZ is normally enriched at the repressed *KAR4* promoter during G2 and depleted during activation in G1. Depletion of INO80 resulted in maintenance of an equal level of H2AZ distribution during the repressed and active states, indicating that H2AZ cannot be removed in the absence of INO80 (Papamichos-Chronakis et al., 2011). Importantly, the study showed that INO80 is required for removal of unacetylated H2AZ, as failure to remove unacetylated H2AZ (in *ino80* Δ strains that express mutant H2AZ that cannot be acetylated) resulted in sensitivity to replication stress and DNA damage-inducing drugs. Further, expression of an acetylated H2AZ mimic in *ino80* Δ strains rescued the phenotypes associated with INO80 depletion (i.e., slow growth, and defects in DNA replication and damage repair) (Papamichos-Chronakis et al., 2011).

Finally, the embryonic structure of yeast INO80 and the identification of all crosslinks between INO80 subunits and nucleosomes led to a speculative model that could explain how INO80 participates in the spacing of nucleosomes. Briefly, Tosi et al. hypothesized that INO80 can form a flexible cradle, in between its head, neck, and body regions, that can accommodate and embrace the nucleosome. It is envisaged that nucleosomal DNA binds to the head, neck, and body, while the flexible foot region attaches to histones at both sides of the nucleosome (Figure 1.4). The authors also suggested that the large conformational change in INO80 might facilitate the open nucleosome conformation, in which H2A-H2B dimers are moderately disassociated from the H3-H4 tetramer, and that this could enable the histone-exchange activity of the INO80 complex (Tosi et al., 2013).

1.2.5.1.3 In vivo functions of INO80

As a consequence of its chromatin-remodelling activity, INO80 also plays multiple roles in cellular metabolism. Initially, INO80 was identified as a transcriptional regulator that governs the expression of genes such as *INO1*, *PHO5*, and *Ty1* (Ebbert et al., 1999). Strikingly, the Δ *ino80* mutation in yeast alters the expression of 1156 genes by at least 1.5-fold relative to the wild-type strain (Van Attikum et al., 2004). A more recent study, carried out under environmental stress conditions (e.g., heat and ionic stress), revealed that adverse conditions increased the recruitment of INO80 to open reading frames (ORFs), suggesting that the complex plays a direct role in the transcription of stress-response genes (Klopf et al., 2009). In human HeLa cells lacking INO80, ARP8, IES6, and IES2 subunits of the INO80 complex, gene expression profile analysis revealed that 251 genes were regulated by INO80, including 149 down-regulated, and 102 up-regulated, genes (Cao et al., 2015).

In addition, INO80 influences DNA replication by promoting recovery of stalled replication forks; in the absence of yeast INO80, recovery is delayed (Shimada et al., 2008). In mammals, INO80 is recruited to replication forks via direct interaction with BRCA1-associated protein-1 (BAP1), a tumour suppressor and nuclear de-ubiquitinating enzyme, through its HAS domain; depletion of BAP1 abolishes INO80 recruitment. Recruitment of BAP1-INO80 is mediated by interaction between BAP1 and ubiquitinated H2A; the latter is ubiquitinated by RING1B (also called RNF2). Inhibition of H2A ubiquitination by RING1B depletion abolished the recruitment of BAP1 and INO80 to replication forks (Lee et al., 2014). INO80 is required for stabilization of stalled replication forks, since INO80-deficient cells exhibit a reduction in replication elongation (Vassileva et al., 2014; Lee et al., 2014), an increase in replication origin usage during S phase, hypersensitivity to hydroxyurea (HU), and

hyperactivity of Chk1 signalling (S phase checkpoint), and around half of replication forks failed to restart after release from replication stress (Vassileva et al., 2014). Further, human INO80 regulates ubiquitination of proliferating cell nuclear antigen (PCNA), a DNA polymerase sliding clamp involved in DNA synthesis and repair, which is essential for post-replication repair (PRR). Defects in PRR increase the amount of DSBs mediated by phosphorylation of the C-terminal of INO80 at either S1512 or S1516 during DNA replication (Kato et al., 2012). The results of these studies clearly demonstrate the involvement of INO80 in DNA replication.

Although the potential role of INO80 in regulating the cell cycle in response to its function in DNA damage (Papamichos-Chronakis et al., 2006; Morrison et al., 2007; Seeber et al., 2013) or replication (Vassileva et al., 2014), by either delaying or arresting the cell cycle, has been referred to, the exact mechanism regulating such a process remains elusive. However, a very recent study reported for the first time a direct association of INO80 with the cell cycle via negative regulation of p21^{Waf1/Cip1}, a universal inhibitor of cyclin kinases that controls the cell cycle by regulating the active state of cyclin-dependent kinases (CDKs) (Cao et al., 2015). Cell flow cytometry analysis demonstrated a delay in progression from G2/M to G1 in the absence of INO80 compared to the control, suggesting a role for INO80 in cell cycle regulation. The authors then carried out gene expression profile analysis, demonstrating that among the genes most up- and down-regulated by INO80 were those related to the cell cycle. After siRNA knockdown of INO80 in HeLa cells, the mRNA levels of cyclin C (*CCNC*), BRAC2/CDKN1A interacting protein (*BCCIP*), and MAD2 mitotic arrest deficient like 1 (*MAD2L1*) were decreased, whereas increases in the expression of cyclinG1 (*CCNG1*), cyclin-dependent kinase 2 (*CDK2*), cyclin-dependent kinase 6 (*CDK6*), and *p21* were observed. Together with the observed high expression of p21 protein in

INO80 or ARP8 knocked-down cells, these results indicate negative regulation of p21 by INO80 (Cao et al., 2015). Further, INO80 was found to co-localize with the activated p53 tumour suppressor at 2.2 and 1.0 kb upstream of the p21 TSS. The recruitment of INO80 at this site is mediated by p53, evidenced by the low enrichment of INO80 at the p21 TSS in p53^{-/-} HCT116 cells (Cao et al., 2015). This study clearly demonstrates the involvement of INO80 in the cell cycle through negative regulation of p21 expression, which suggests direct involvement of INO80 in cancer aetiology.

Finally, and crucially, INO80 regulates DNA repair and chromosome segregation, which also implicates the complex in the development of cancer. In the following sections, a thorough dissection of the role of INO80 in DNA repair and chromosomal stability will be provided.

1.3 DSB repair in mammals: an overview

DSBs are among the most toxic DNA lesions; a single unrepaired lesion can lead to chromosomal rearrangements and genomic instability. Since tens of thousands of DNA breaks occur every day in each human body, it is essential to understand the mechanisms of their repair (Krejci et al., 2012). Here, I will briefly discuss the factors that influence the choice of repair mechanism, followed by an overview of repair pathways and a thorough discussion of the roles of the chromatin remodeller, INO80, and the histone variant, H2AZ, in DSB repair.

1.3.1 DNA breaks

Single- or double-strand breaks in DNA can be generated endogenously, e.g., by replication fork collapse or reactive oxygen species produced as a byproduct of cellular metabolism, or exogenously, e.g., by ionizing radiation (IR), UV light, or chemotherapy. When lesions occur in only one strand of the DNA molecule, they can be excised and the missing segment can be replaced by copying the sequence information from the intact DNA strand. By this mechanism, the vast majority of DNA lesions generated by internal (e.g., reactive oxygen species) or external (e.g., UV light and some chemical mutagens) sources are repaired by pathways including base excision repair (BER), nucleotide excision repair (NER), and mismatch repair (MMR). However, more complex damage, where two or more lesions (base and/or sugar damage) are induced to the double-stranded DNA molecule either opposite to each other or within a few nucleotides, can be induced by IR, in the form of either X-rays or gamma rays (γ -IR). DSBs cannot be repaired by restoration of the sequence from the complementary strand, as information is missing from both strands; therefore, more advanced pathways

of repair are required to generate the missing copy and repair the damage (Iliakis et al., 2015).

1.3.2 DSB repair pathway choice

DSB repair can be carried out by homologous recombination (HR), which occurs in late S and G2 phases of the cell cycle, non-homologous end joining (NHEJ), which is active throughout the cell cycle (Chapman et al., 2012; Murray et al., 2012), or by a backup pathway, alternative-NHEJ (Alt-NHEJ) (Windhofer et al., 2007). Although it remains unclear how the cell decides which repair pathway to use in each case, in-depth work from the Jeggo laboratory suggests that several factors significantly influence the choice of pathway. These include the following: 1) the position of the cell in the cell cycle; 2) the status of resection initiation; 3) the complexity of the DNA lesion; and 4) chromatin structure at the site of damage (Shibata et al., 2011). The same group previously demonstrated that DSBs within regions of heterochromatin are repaired preferentially by HR in the G2 phase (Beucher et al., 2009).

A fascinating model for the competition between NHEJ and HR to repair DSBs was proposed by the Jeggo group (Shibata et al., 2011). In that model, a first attempt to repair the damage is made by NHEJ by rapid binding of DNA-PK and KU to DSB ends, followed by prompt and efficient DSB repair. However, if the two ends cannot rapidly rejoin, either due to the presence of a complex DSB or compact chromatin that first needs to be relaxed, the repair will be performed by HR. If, for any reason (e.g., loss of CtIP), resection cannot be initiated, then a second attempt will be made by NHEJ. However, if the resection was initiated successfully, or perhaps an extensive resection was achieved, repair will commit to HR. This model was based on the observation that, in CtIP-depleted cells, resection was abolished, while cells repaired DSBs rapidly and

efficiently by NHEJ, whereas, blocking HR after the initiation of resection, by depleting BRCA2, prevented repair by either HR or NHEJ, probably due to the excess of resected ssDNA (Shipata et al., 2011). This model explains the crucial role of lesion resection state in pathway choice.

Other factors that have a basic influence on either the initiation or progress of resection should be taken into account, including cell cycle phase and the balance between 53BP1 and BRCA1. Resection occurs in a cell cycle-dependent manner with CDK phosphorylation of several substrates, including CtIP and EXO1, during S and G2 phases (Mimitou & Symington, 2011); more details will be provided later in this chapter. The resection process can be blocked by the prevention of CtIP binding to DNA ends by 53BP1, promoting repair by NHEJ. Hence, 53BP1 function is a barrier to resection when it is phosphorylated by ATM, promoting the recruitment of Rif1 and PTIP, which stimulates further recruitment of the downstream nuclease, Artemis. Depletion of either 53BP1 or Rif1 results in extensive resection and inhibition of repair by NHEJ (Ceccaldi et al., 2016); however, BRCA1 promotes HR repair through direct interaction with phosphorylated CtIP to initiate resection, which is required for efficient resection (Yun & Hiom, 2009).

1.3.3 DSB repair pathways

1.3.3.1 NHEJ

Around 80% of DSBs induced by IR are repaired by NHEJ, which does not require a homologous template (Beucher et al., 2009; Riballo et al., 2004). In this pathway, the Ku heterodimer (Ku70/Ku80) binds to broken DNA ends, thereby preventing resection (Mimori & Hardin, 1986). Ku forms a ring that encircles double-stranded DNA, translocates along the DNA, and recruits the catalytic subunit of DNA-dependent

protein kinase (DNA-PKcs) (Gottlieb & Jackson, 1993). PKcs facilitates Ku binding to the DNA end ligation complex, consisting of ligase IV, XRCC4, and XLF. Ligation is performed through a series of interactions, starting with that of Ku with the BRCT domain of ligase IV, which interacts with XRCC4 via two BRCT domains in the C-terminus of ligase IV (Costantini et al., 2007). The resulting complex then interacts with XLF, facilitating tethering of the DSB ends (Ahnesorg et al., 2006). Consequently, the DNA ligase complex is able to ligate the broken ends and repair the lesion; however, when incompatible ends are present, an extra step is required before ligation can occur. In such cases, the Artemis endonuclease is activated by autophosphorylation, mediated by DNA-PKcs. Activated Artemis cleaves the hairpin structures formed at DNA ends to remove the damaged or mismatched nucleotides (Ma et al., 2002; Schlissel, 2002).

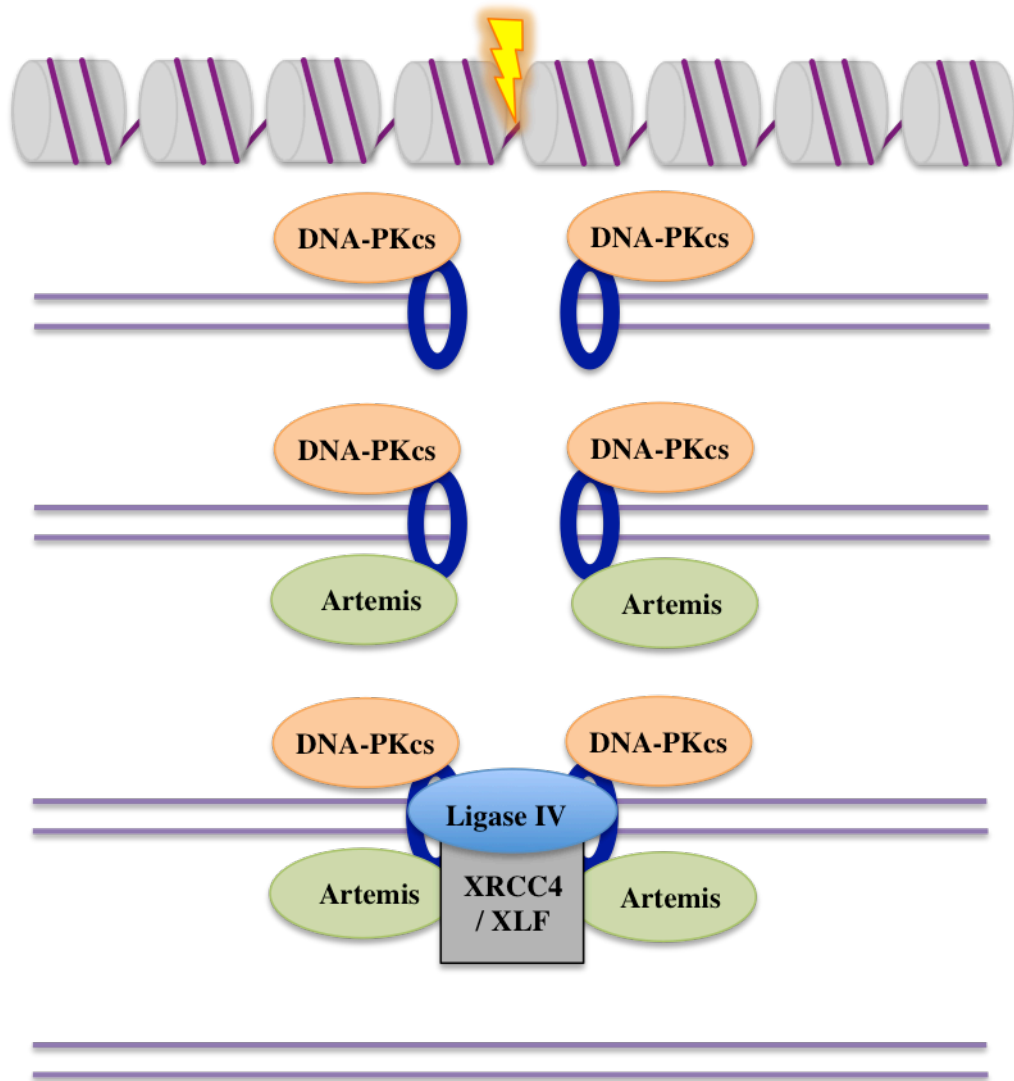


Figure 1. 5 The NHEJ repair pathway.

In response to DSBs, the Ku70/80 heterodimer (blue rings) binds to the broken DNA ends. This promotes the recruitment of DNA-PKcs, which bind to the broken DNA ends and activate Artemis. Activated Artemis processes the broken DNA ends and can cause loss of genetic information. Ultimately, Ligase IV, XRCC4, and XLF ligate the broken DNA ends together.

1.3.3.2 HR

HR is a complex pathway of DSB repair in which a homologous sequence on a sister chromatid is used as a repair template. The Jeggo laboratory showed that around 20% of DSBs induced by IR (γ -rays or X-rays) in G2 phase are repaired by HR (Beucher et al., 2009). HR is critical for repair of several kinds of damage, including collapsed replication forks and chromosome breaks, and deficiencies in HR are thought to be responsible for a subset of breast, ovarian, and other cancers (Roy et al., 2012).

The HR pathway involves a cascade of signals that recruit repair factors, eventually resulting in repair of the lesion. Repair is initiated by the recruitment of the MRN complex, which contains the MRE11, RAD50, and NBS1 proteins, to the damage site. At the site of the lesion, MRN activates the protein kinase, ATM (Lavin, 2008). Activation of ATM is associated with stimulation of the repair checkpoints controlled by p53 and Chk2, as well as recruitment of repair proteins, such as BRCA1 and 53BP1 (Jackson & Baetke, 2009; Kennedy & D'Andrea, 2006). Activation of ATM also results in phosphorylation of histone H2AX at serine 139 near the C-terminus. This creates a docking site for the BRCT domain of the MDC1 protein. Phosphorylated H2AX (γ H2AX) forms foci in response to irradiation within minutes; these foci are widely used as DSB markers (Lou et al., 2006). Recruitment of MDC1 to DSBs forms a binding site for subsequent recruitment of the MRN and ATM complex, resulting in the creation of a γ H2AX domain that spreads along the chromatin for hundreds of kilobases around the DSB (Figure 1.5) (Rogakou et al., 1998; Xu et al., 2012; Price & D'Andrea, 2013). MDC1 also facilitates the later recruitment of two E3 ubiquitin ligases, RNF8 and RNF168, which ubiquitinate the chromatin and promote recruitment of BRCA1 and 53BP1. It remains unclear how cells decide to undergo repair via HR; as noted above, this decision could be affected by several factors (Shibata et al., 2011).

HR is initiated by a resection step in which the 5' overhangs are degraded to yield single-stranded DNA (ssDNA) with a 3' overhang "tail". This is a complicated process involving several helicases, endonucleases, and other proteins. Once this step is initiated, the cell is committed to repair the damage by HR, and may block KU binding (Shibata et al., 2011). Initiation of resection is thought to be regulated by the MRN-CtIP complex. When DSBs occur during S or G2 phases, CtIP is activated through an interaction with either CDK (via phosphorylation on T847) (Huertas & Jackson, 2009) or ATM (via phosphorylation on S664/745) (Shibata et al., 2011). Phosphorylated CtIP is then recruited to the damage site via direct interaction with the FHA domain in the N-terminus of NBS1, a component of the MRN complex (Mimitou & Symington, 2009; Mimitou & Symington, 2011). Subsequently, resection proceeds through two steps, in which the active MRN-CtIP complex binds to the 5' DNA ends and resects or removes approximately 50–100 nucleotides, resulting in the formation of short 3' ssDNA tails. The second step then occurs rapidly, to recruit EXO1 and BLM-DNA2, which bind to the 5' DNA ends and perform an extensive resection, yielding long 3' ssDNA tracts. The long ssDNA tracts activate DNA damage checkpoints and ensure fidelity of repair by preventing repair with short repeats. These tracts vary in length from a few hundred nucleotides to tens of kilobases, depending on the availability and location of the homologous templates and the speed of the repair (Figure 1.6) (Chung et al., 2010; Mimitou & Symington, 2011).

Once the long ssDNA overhangs are generated, they are quickly coated by replication protein A (RPA), which stabilizes them, protects them from degradation, and prevents them from forming secondary structures (Fanning et al., 2006). This step is followed by the replacement of RPA with RAD51, resulting in the formation of a RAD51 filament. The incorporation of RAD51 is thought to be regulated by BRCA2, a repair protein

implicated in breast cancer, because defects in this protein completely abolish RAD51 filament formation (Liu et al., 2010). RAD51 monomers bind to the eight BRC repeats on BRCA2, which promotes their binding to ssDNA in a one-to-one binding fashion (Filippo et al., 2008; Ceccaldi et al., 2016). The RAD51 filament is involved in the search for the homologous sister chromatid, by a mechanism that remains poorly understood. Once the homologous template is found, the RAD51 filament invades the homologous strand, and the missing sequence is copied. Finally, Holliday junction resolution takes place, resulting in the separation of the newly generated strands in which the damage has been repaired (Figure 1.6) (Krejci et al., 2012).

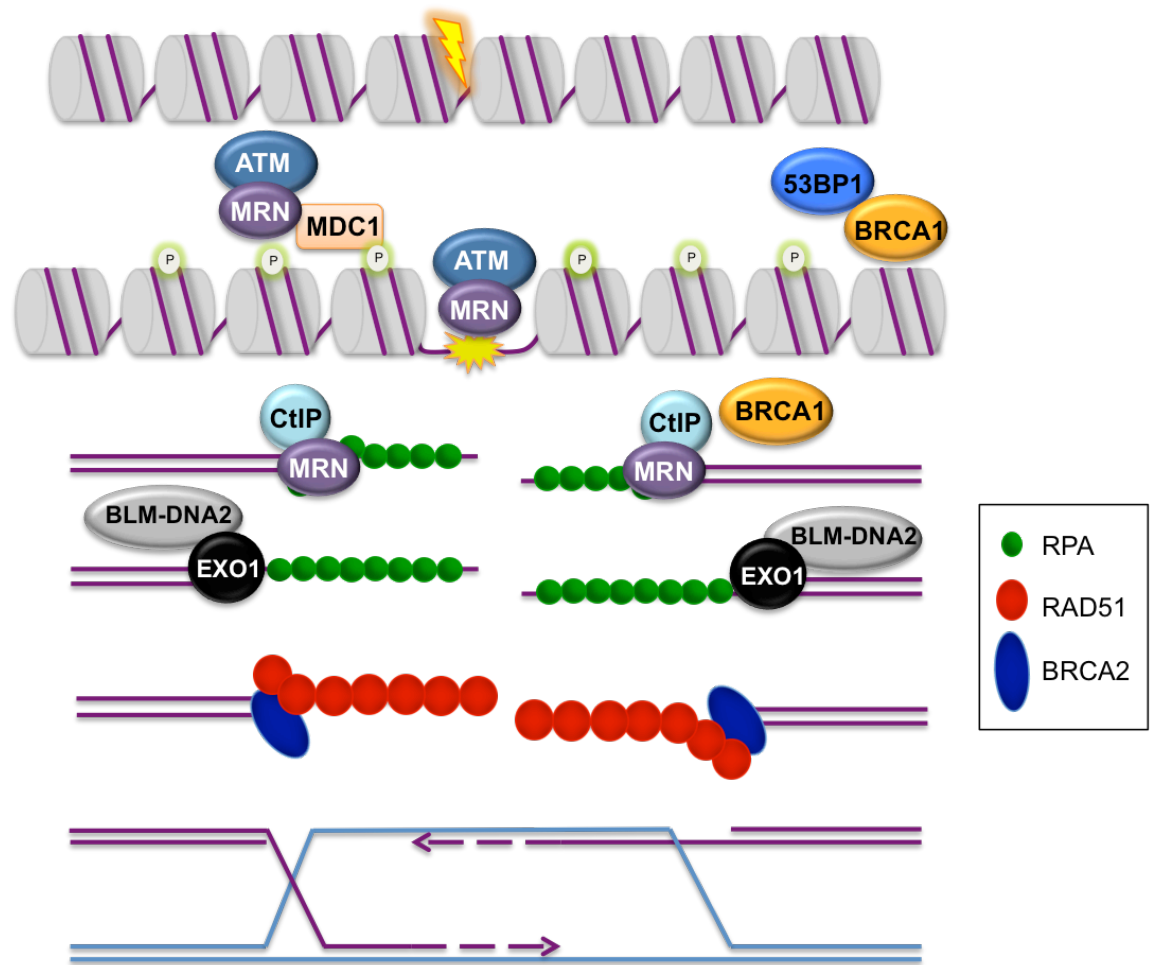


Figure 1. 6 The homologous recombination repair pathway.

Once DSBs are induced, MRN is recruited to the site of damage and activates ATM. Activation of ATM leads to H2AX phosphorylation and further recruitment of MDC1, 53BP1, and BRCA1. Next, MRN-CtIP binds to the 5' end of the DNA, resulting in the production of a short 3' ssDNA that is directly coated by RPA. Extensive resection is then achieved by EXO1 and BLM-DNA2, resulting in a long 3' ssDNA coated with RPA. Next, BRCA2 is recruited and facilitates the replacement of RPA with RAD51, resulting in the formation of the RAD51 filament, which is involved in the search for the homologous sister chromatid from which the missing sequence is copied, allowing repair of the damage.

1.3.3.3 Alt-NHEJ

Alt-NHEJ was originally described as a backup mechanism for the NHEJ pathway for end joining of chromosomal DSBs during V(D)J recombination, due to its error-prone outcomes and its novel detection in the absence of NHEJ. However, the current dominant hypothesis is that this pathway functions primarily in the presence of both HR and NHEJ (Caccaldi et al., 2016). Alt-NHEJ is an error-prone mechanism that generates chromosomal translocations and mutagenic rearrangements. Although this pathway is recognized, its detailed mechanism remains ambiguous. Alt-NHEJ can proceed when Poly (ADP-ribose) polymerase 1 (PARP1) is recruited to DSBs. A short end resection is formed that facilitates recruitment of other proteins, including DNA ligase I and III, XRCC1, and polymerase θ (Pol θ), resulting in annealing at microhomologies (Iliakis et al., 2015; Caccaldi et al., 2016).

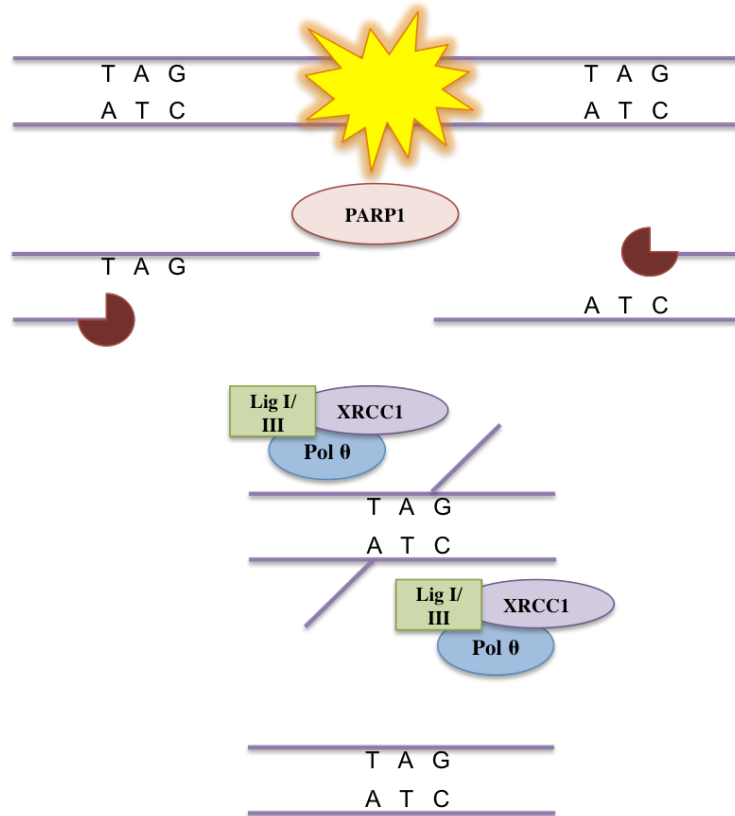


Figure 1. 7 The Alt-NHEJ repair pathway.

Alt-NHEJ is mediated by the recruitment of PARP1 to DSBs. Resection of short DNA sequences can occur to expose microhomology regions (the example illustrated here is TAG). These are eventually annealed by Lig I/III, XRCC1, and Pol θ . Thus, this pathway is error prone as a result of excessive DNA deletion.

1.3.4 Chromatin response to DSBs

The occurrence of DSBs within the highly compact organization of chromatin structure presents a challenge for the DSB repair machinery to detect and access the damaged area and to repair it. The “access-repair-restore” model was proposed in 1991, and highlights the need for initial reorganization of the chromatin, followed by repair of the damage, and finally restoration of the local chromatin after the repair is completed (Smerdon, 1991). This involves highly complex chromatin modifications, achieved by a collection of histone variants, PTMs, histone chaperones, and remodelling factors, some of which are responsible for chromatin relaxation, while others play roles in recruiting repair factors and promoting the repair. Herein, I will focus on some of the very early events that lead to relaxation and opening of the chromatin for repair.

Although phosphorylation of H2AX by ATM is one of the most frequent PTMs that lead to activation of the DNA damage response, this step is dependent on upstream chromatin decondensation. Bakkenist et al. (2003) demonstrated that altering chromatin and chromosome structure in the absence of DSBs, by exposing cells to hypotonic conditions, chloroquine or a histone deacetylase inhibitor, led to a rapid induction of phosphorylated ATM, as determined by western blot and immunofluorescence analyses. However, using the same treatment after exposure of cells to IR (2 Gy) enhances the amount of phosphorylated ATM, suggesting that activation of ATM requires an upstream change in chromatin structure (Bakkenist et al., 2003). In addition, another group monitored the local expansion of chromatin upon induction of DSBs by laser-microirradiation in WT, H2AX^{-/-}, and ATM^{-/-} MEFs expressing GFP-tagged H2B. The similarity in expansion (approximately 30%) observed upon DNA damage in WT MEFs

and those depleted of H2AX or ATM suggested that chromatin is decompacted after induction of DSBs, independently of ATM and H2AX (Kruhlak et al., 2006).

Acetylation is a key factor in the opening of chromatin at DSBs. As mentioned previously, lysine acetylation promotes the formation of relaxed chromatin structures by neutralizing the negative charge on lysines, and therefore decreasing both histone-DNA and histone-histone interactions within nucleosomes (Musselman et al., 2012). At DSBs, histones H2AX and H4 are acetylated by the TIP60 HAT and acetylation spreads for hundreds of kilobases away from the DSB (Downs et al., 2004; Murr et al., 2006). CBP and p300 HATs can also acetylate H2AX at K36 (Jiang et al., 2010); H3 at K18; and H4 at K5, K8, K12, and K16, at DSBs (Ogiwara et al., 2011). Moreover, another HAT, MOF (also called KAT8), facilitates H4 acetylation at K16 (Li et al., 2010). Depletion of MOF by siRNA results in a 20 minute delay of γ H2AX formation after treatment with IR (Sharma et al., 2010). This suggests that H4 acetylation may be an upstream event that facilitates the formation of γ H2AX. As mentioned previously, the N-terminal tail of the core histone H4 interacts with the acidic patch on the surface of H2A-H2B dimers of adjacent nucleosomes (Luger et al., 2012). Disruption of this interaction by acetylation of H4 at K16 inhibits the formation of 30 nm fibres and results in chromatin relaxation (Shogren-Knaak et al., 2006); therefore, it has been suggested that an additional increase in H4 and H2A acetylation may promote further relaxation at DSBs (Kruhlak et al., 2006; Price & D'Andrea, 2013). However, it was shown recently that H4 acetylation by TIP60 requires incorporation of H2AZ at DSBs (Xu et al., 2012); this will be discussed further later in this section.

Other PTMs are also associated with an early response to DSBs, including poly(ADP-ribosylation) and ubiquitylation. Poly(ADP-ribosylation) is facilitated by poly(ADP-

ribose) polymerases (PARPs), which add multiple ADP-ribose moieties to form a poly(ADP-ribose) (PAR) chain. This is one of the earliest PTMs detected at DNA damage sites. Poly(ADP-ribosyl)ation functions together with NHEJ to facilitate the recruitment of repair factors such as XRCC1. Poly(ADP-ribosyl)ation is also likely to be associated with chromatin relaxation to enable repair because it is involved in the recruitment of chromatin-remodelling factors including CHD1L (also called ALC1) (Smeenk & Attikum, 2013). Ubiquitylation involves the attachment of ubiquitin (a highly conserved 76-amino acid protein) to lysine residues at the C-terminus of the target protein. Ubiquitin is adenylated by an E1 ubiquitin ligase in an ATP-dependent manner. The adenylated ubiquitin is transferred to an E2 ubiquitin ligase, which in turn binds to an E3 ubiquitin ligase to facilitate the ligation of ubiquitin to the target protein (Smeenk & Attikum, 2013). In response to DSBs, the E3 ubiquitin ligase RNF8 is recruited to DSBs through an interaction with phosphorylated MDC1 via its FHA domain, which facilitates Ubc13 (an E2 ligase)-mediated polyubiquitination of the H1 linker histone at K63. This in turn signals the recruitment of RNF168 (an E3 ligase), which promotes ubiquitination of histone H2A at K13 and K15. These ubiquitylation events serve as a platform to recruit various repair proteins including 53PB1 and BRCA1 (Smeenk & Attikum, 2013; Smeenk & Mailand, 2016).

1.3.5 DSB repair in regions of heterochromatin

In mammals, heterochromatin (HC) is characterized by enrichment of histone methylation marks (most typically H3K9me3 at constitutive HC, while H3K27me3 marks facultative), low levels of histone acetylation, in addition to the presence of HP1, KAP1, histone deacetylases (HDACs), and histone methyltransferases, which are required for its maintenance (Saksouk et al., 2015). HC is a barrier to DSB repair, and

slow repair at regions of HC has been reported (Boucher et al., 2009; Shibata et al., 2011). Also, as mentioned above, in the G2 phase of the cell cycle, DSBs at HC induced by IR are predominantly repaired by HR. This was determined based on the co-localization of RPA foci, which are specific markers of HR, and H3K9me3/H4K20me3, which are markers of HC (Kakaroukas et al., 2013). Notably, HR can also function at euchromatin when NHEJ is inhibited by depletion of the key factor, DNA-PK (Shibata et al., 2011). Ideally, NHEJ will repair DSBs in G2 rapidly and efficiently; however, if prompt repair cannot occur, resection will be initiated to allow for slow repair by HR (Shibata et al., 2011; Kakaroukas et al., 2013). At HC DSBs, KAP1 and HP1 are phosphorylated by ATM. This leads to the release of CHD3 (an ATP-remodeller with affinity for methylated histones) from HC, resulting in the relaxation of the compact chromatin (Price & D'Andrea, 2013). 53BP1 also plays important and opposing role at HC DSBs induced by IR in G2. In general, 53BP1 acts as a barrier to resection and directs repair towards NHEJ; however, under these specific circumstances (i.e., HC DSBs induced by IR at G2), this protein acts to promote HR. This is evidenced by the outcomes of knockdown of 53BP1, which results in an increase in chromosome breaks and a decrease in RPA foci, RAD51 foci, and sister chromatid exchanges, similar to the phenotype observed as a result of ATM inhibition, which is rescued by depleting KAP1. This, together with the fact that co-depletion of KAP1 and 53BP1 restores the defect in HR caused by depletion of BRCA1, led the authors to propose a model postulating an essential role for 53BP1 in HC DSB repair. In the model, the barrier of 53BP1 at HC DSB ends is overcome by BRCA1, perhaps by repositioning its binding away from the DNA molecule ends to allow resection, while retention of 53BP1 at the chromatin tethers activated ATM and subsequent robust KAP1 phosphorylation leads to the promotion of HC relaxation (Kakaroukas et al., 2013).

1.3.6 Role of INO80 in DNA repair

Yeast cells lacking Ino80 are hypersensitive to factors that induce DNA damage, for example, hydroxyurea (HU), methyl methanesulfonate (MMS), ultraviolet (UV) light, and IR, suggesting the involvement of INO80 in DNA repair (Shen et al., 2000). A ChIP study in yeast provided physical evidence for the recruitment of several INO80 subunits to DSBs; Ino80, Arp5, and Arp8 can be detected at DSBs within 30 minutes of damage induction (Van Attikum et al., 2004). In yeast, INO80 is recruited to DSBs via a direct interaction with γ H2AX, mediated by the Nhp10, Ies3, and Arp4 subunits (Downs et al., 2004; Van Attikum et al., 2004; Morrison et al., 2004). In mammals, however, the recruitment of INO80 to DSBs is independent of γ H2AX, but sensitive to loss of ARP8, suggesting that ARP8 mediates the initial recruitment of INO80. In support of this idea, recruitment of INO80 to sites of laser-induced DNA damage is not defective in H2AX^{-/-} MEFs, but recruitment is abolished in ARP8-deficient human cells (Kashiwaba et al., 2010). Additionally, immunofluorescence and chromatin fractionation data from cells defective in ARP5 reveal a severe reduction in the accumulation of γ H2AX following DSB induction, suggesting a direct interaction between ARP5 and γ H2AX that could facilitate the spread of H2AX phosphorylation into the chromatin around DSBs (Kitayama et al., 2009). By contrast, the other subunits of INO80 do not appear to be involved in similar interactions with γ H2AX, or in the process of INO80 recruitment (Kashiwaba et al., 2010).

Recently, Gospodinov et al. (2011) showed that INO80 mediates 5'→3' resection of DSB ends, as revealed by labelling of ssDNA with bromodeoxyuridine (BrdU) and simultaneous immunofluorescence detection of BrdU and foci of RPA, a protein that coats ssDNA. Depletion of ARP8 and the absence of INO80 have similar effects on

RPA foci (Gospodinov et al., 2011). Consistent with this finding, a recent study in mice revealed that INO80 depletion leads to a decrease in formation of both RPA32 and BrdU foci (Min et al., 2013). Biochemical studies reveal that RUVBL2 (TIP49b) and its yeast homolog, Rvb2, act as 3'→5' DNA helicases at 3' ssDNA overhangs of at least 30 nucleotides in length, suggesting the potential involvement of RUVBL (TIP49) in the resection step of HR (Papin et al., 2010). A recent study from the Jackson laboratory found that depletion of the INO80 complex or its subunits, YY1 or RUVBL1, results in a mild defect in resection upon treatment with Camptothecin, reflected by a reduction in the intensity of BrdU staining (ssDNA) rather than a reduced number of foci (Nishi et al., 2014). Further, the study showed a novel role for NFRKB, a subunit of human INO80, in regulating resection in a mechanism regulated by ubiquitin carboxyl-terminal hydrolase L5 (UCHL5), another subunit of human INO80, also known as UCH37. Briefly, depletion of UCHL5 resulted in a significant reduction (by almost half) of NFRKB expression, suggesting that UCHL5 stabilizes and protects NFRKB from degradation, perhaps via its ubiquitylation activity. A similar phenotype resulted from either individual or combined depletion of UCHL5 and YY1, observed as a reduction in HR efficiency, RPA intensity, RAD51 foci formation, and IR resistance, together with a reduction in the recruitment of EXO1, but not CtIP. This suggests that ubiquitination and degradation of NFRKB, which is regulated by UCHL5, is a key factor that controls the extensive resection during HR (Nishi et al., 2014). Another group also reported a mild defect in resection, manifested as a slight reduction in the percentage of cells with RPA foci, in a stable INO80 knockout cell line (Dong et al., 2014). These multiple lines of evidences suggest that the INO80 complex is involved in resection; however, the exact roles played by INO80 in this process remain unknown.

The literature does not provide clear evidence that INO80 is involved in regulating the

formation or accumulation of RAD51 foci. Gospodinov et al. (2009) showed that, in mammalian cells lacking RUVBL (TIP49), accumulation of RAD51 foci in response to irradiation decreased 2-fold relative to the control; however, because this subunit belongs to multiple chromatin-remodelling complexes (INO80, TRRAP-TIP60, and SRCAP), it was necessary to determine which RUVBL-containing complex mediates this effect on RAD51 foci. The authors treated the cells with sodium butyrate, a histone deacetylase inhibitor, resulting in hyperacetylation and relaxation of chromatin. As a result, RAD51 foci were completely restored, and the authors therefore attributed the activity of RUVBL to its association with TRRAP-TIP60, a HAT, rather than INO80. Subsequently, however, the same authors (Gospodinov et al., 2011) reported that absence of the INO80 subunit causes a severe reduction in the recruitment of 53BP1, a DNA repair protein, but has no concomitant effect on formation of RAD51 foci. This discrepancy raises questions and suggests that further studies are required to understand the role of INO80 in DNA repair (see discussion in chapter 3). However, in haploid yeast, in which the homologous donor chromosome is absent, lack of Arp8 results in defective RAD51 recruitment, whereas in the presence of the homologous donor (i.e., when DSBs are repairable) no defect in RAD51 accumulation is observed (Tsukuda et al., 2009). These conflicting observations suggest that RAD51 might be regulated indirectly by INO80; however, additional studies will be required to test this idea.

Defects in INO80, RUVBL, or YY1 cause UV hypersensitivity in both mouse (Wu et al., 2007) and human (Park et al., 2010) cells, and the recruitment of INO80 to DSBs induced by laser-microirradiation in human cells (Kashiwaba et al., 2010) clearly reflects its association with DNA repair in mammals. Consistent with these observations, a GFP reporter system revealed a severe defect in HR repair efficiency

(approximately 8-fold decreased relative to control cells) caused by the absence of either INO80 or YY1 (Wu et al., 2007). Therefore, it is clear that loss of INO80 results in a failure of DSB repair, at least to some extent.

How, then, does INO80 promote DNA repair in mammalian cells? One possible answer is that INO80 regulates the expression of genes that are involved in repair. An analysis of published microarray data and an immunoprecipitation study revealed that expression of RAD54B and XRCC3, both of which are implicated in DSB repair, is repressed by depletion of INO80 in human cells (Park et al., 2010). However, the fact that INO80 is recruited to DSBs weakens this model. An alternative possibility is that INO80 acts as a chromatin remodeller to regulate the removal, exchange, and spacing of histones near DSBs, thereby opening the damage site and providing access to factors involved in repair. A conclusive demonstration of such an effect remains elusive; future efforts should address this issue in mammalian cells, with support from data obtained in yeast. A ChIP study shows that enrichment of histones H2B and H3 at DSBs is reduced in INO80-depleted cells; this observation was interpreted as a reflection of eviction activity at break sites (Tsukuda et al., 2005). The ability of the INO80 subunits, YY1 and RUVBL1/2, to bind Holliday junctions *in vitro*, together with the involvement of the complex in resection, supports a possible role for the INO80 complex as a chromatin remodeller acting to reorganize the chromatin, particularly in these two steps of DSB repair, which require further modifications (Jeggo & Downs, 2014).

INO80 was previously linked to H2AZ, a variant of H2A, in the context of its role as a transcriptional regulator. Moreover, H2AZ was recently shown to be critical for HR repair in mammals (Xu et al., 2012), providing potential insight into the possible function of INO80 at DSBs; this issue will be addressed in detail later in this chapter.

Importantly, these models are not mutually exclusive, and it is very likely that both functions of INO80 are involved in DSB repair. Investigation of INO80 function during HR in response to DSBs is one of the major targets for this thesis, and further published data relating to this role will be provided in chapters 3 and 4 (Lopez-Perrote et al., 2014; Alatwi & Downs, 2015).

1.3.7 H2AZ: A critical histone variant involved in DNA repair

Evidence from CHIP experiments in yeast (Kalocsay et al., 2009) and mammals (Xu et al., 2012) demonstrates the physical enrichment of H2AZ at DSBs. A report from the Price laboratory describes the extensive characterization of the role of H2AZ in DNA repair in human cells (Xu et al., 2012). In that study, the authors confirmed the exchange of H2AZ at DSBs by CHIP, taking advantage of the zinc finger nucleases (p84-ZFN and p230-ZFN). Remarkably, H2AZ accumulated at DSBs within 4 h, similar to γ H2AX, but with a lower level of enrichment. H2AZ exhibited the ability to spread around DSBs for approximately 10–50 kb along the chromatin, also similar to the behaviour of γ H2AX. In addition, the study revealed a new role for P400 in the exchange of H2AZ with the canonical H2A histone at DSBs; either inactivation or deletion of P400 caused a significant reduction (approximately 2-fold) in H2AZ enrichment at DSBs. Moreover, Xu et al. (2012) showed that the incorporation of H2AZ at DSBs is important for acetylation, based on similar defects in enrichment of acetylated histone H4, in the absence of H2AZ, P400, or TIP60. Immunofluorescence analysis of H2AZ-depleted cells revealed a severe reduction, if not complete abolition, of ubiquitination (FK2 foci) and BRCA1 foci formation. However, ATM activation, H2AX phosphorylation, and recruitment of MDC1, 53BP1, and CtIP were not impacted by the absence of H2AZ. Together, these data suggest that H2AZ depletion may

negatively impact HR. To test this idea, the authors used a GFP HR reporter system that revealed a moderate reduction in the level of HR compared with that of the control in H2AZ-depleted cells.

Surprisingly, the NHEJ pathway was also defective in H2AZ-depleted cells. Therefore, additional experiments were performed to assess resection and KU70/80, critical factors in HR and NHEJ, respectively (Xu et al., 2012). In yeast, it was reported that H2AZ deletion caused a delay in resection, observed as a lag in RPA recruitment to DSBs, which was monitored by a ChIP assay for Rfa1, a RPA subunit (Kalocsy et al., 2009). Unexpectedly, in human cells resection was defective, as an increase in RPA and BrdU foci was observed, whereas KU70/80 was lost. However, inhibition of ssDNA formation in H2AZ-depleted cells by silencing of CtIP rescued the reduction of KU70/80 as well as the defect in NHEJ. These results led the authors to argue that, when both HR and NHEJ are defective, cells must activate a backup repair pathway. As cells lacking KU70 could repair DSBs via the Alt-NHEJ pathway, a process requiring CtIP rather than KU70/80, the authors speculated that, in the absence of H2AZ, cells repair DSB via Alt-NHEJ. This model was confirmed by observation of Alt-NHEJ in cells lacking H2AZ, using a GFP-Alt-NHEJ reporter system (Xu et al., 2012). Together, these lines of evidence emphasize the importance of the role of H2AZ at DSBs; however, little is known about the mechanism of H2AZ exchange at DSBs in mammals, and this thesis reveals for the first time a role for INO80 in regulating the removal of H2AZ at DSBs in human cells (Alatwi & Downs, 2015); more details will be provided in chapter 4.

1.4 Chromosome instability

Chromosomal instability (CIN) is a type of genomic instability that has been observed in many solid tumours and various haematological malignancies, and is strongly associated with several types of cancer, including breast, lung, and colon cancer. CIN refers to a dynamic state, where cells continuously gain or lose whole chromosomes or parts of chromosomes. Tumours may exhibit one of two types of CIN: numerical CIN (nCIN), caused by loss or gain of whole chromosomes at a higher rate than normal cells, and structural CIN (sCIN), caused by an increased rate of structurally abnormal chromosomes (McGranahan et al., 2012). The main cause for nCIN is chromosome missegregation, while sCIN can result from aberrant DNA repair pathways, telomere dysfunction, and chromosomal fragile sites, with a phenotype of gain or loss of chromosome fragments, deletion, amplification, and translocation of DNA (McGranahan et al., 2012). In this section, I will provide an overview of mitotic chromosome segregation and centromere structure, as a key factor in the maintenance of proper segregation, and a summary of the known roles of INO80 in chromosomal stability.

1.4.1 Chromosome segregation in mitosis in human cells: an overview

During interphase, cells undergo growth phase (G1 phase), DNA replication (S phase), and another growth phase (G2 phase), before preparing to enter mitosis. Mitosis consists of five sub-phases: prophase, prometaphase, metaphase, anaphase, and telophase. Upon entry to mitosis (prophase), chromosomes condense and centromeres form to facilitate the recruitment of kinetochore proteins and centrosomes to form the two poles of the mitotic spindle (Verdaasdonk & Bloom, 2011; Cheeseman & Desai, 2008; Sullivan & Morgan, 2007). Moreover, and importantly, cohesin is released from

chromatin except in the centromeric region, which is protected by shogoshin 1, to allow proper segregation (Losada, 2014). Cohesin is a ring complex consisting of SMC1, SMC3, RAD21, and either SA1 or SA2, required for sister chromatid cohesion. During prometaphase, the nuclear envelope breaks down and kinetochores attach to spindle microtubules. In metaphase, all chromosomes undergo bi-oriented attachment to the spindle; inappropriate attachment or mono-oriented attachment causes an arrest in metaphase. Once all chromosomes are properly attached, tension is generated, resulting in activation of Cdc20, which binds to APC to form the APC-Cdc20 complex. APC-Cdc20 degrades securin, leading to activation of separase. Active separase will cleave centromeric cohesin and facilitate sister chromatid separation during anaphase. Finally, during telophase, chromatids decondense and the nuclear envelope re-forms, resulting in two daughter cells, each of which has an exact copy of the duplicated genome (Verdaasdonk & Bloom, 2011; Cheeseman & Desai, 2008; Sullivan & Morgan, 2007).

1.4.2 Centromere structure

The centromere is a unique region of mitotic chromosomes that is essential in linking sister chromatids and serves as a loading platform to assemble the kinetochore, a special structure that forms on both sides of the centromere to facilitate attachment to spindle microtubules. In addition, cohesin and condensin (a multi-subunit complex essential for the structure and function of chromosomes) are enriched at centromeres, serving to generate tension and facilitate chromosome segregation (Verdaasdonk & Bloom, 2011; Bloom, 2014).

The centromere itself is constructed of a defined sequence that varies in length among species. For example, simple eukaryotes, such as budding yeast, have a centromere consisting of 125 bp, while human centromeres can be up to 5 Mb in length and contain

between 1 and 4 Mb of 171 bp alpha satellite repeats, known as a regional centromere. Despite this, it is widely believed that the unique chromatin structure of centromeres is the main determinant of their function, rather than their specific sequence (Verdaasdonk & Bloom, 2011; Bloom, 2014).

What is special about chromatin at centromeres? Chromatin can be categorized into two regions at centromeres: centromeric and pericentric. Centromeric chromatin is identified by the deposition of the histone variant CENP-A (see 1.2.3.1) and enrichment of H3K4me₂, which is associated with euchromatin (Verdaasdonk & Bloom, 2011; Bloom, 2014). Depletion of H3K4me₂ results in a lack of HJURP, a complex that deposits CENP-A into chromatin, and abolishes CENP-A deposition at centromeres (Bergmann et al., 2011). By contrast, pericentric chromatin, which flanks the centromeric region, is enriched in H3K9me₂, H3K9me₃, and H4K20me₃, and is associated with heterochromatin (Verdaasdonk & Bloom, 2011; Bloom, 2014). These PTMs are important for recruiting cohesin, maintaining pericentric structure, and accurate segregation (Verdaasdonk & Bloom, 2011). By contrast, loss of H4K20me₃ is a hallmark of human cancer and can result in aberrant centromere function and a consequent increase in the level of aneuploidy (Fraga et al., 2005; Verdaasdonk & Bloom, 2011).

Histone variant H2AZ is enriched in centromeric and pericentric chromatin in both humans and mouse. Interestingly, CENP-A-containing nucleosomes contain H2A, while H2AZ is associated with H3K4me₂-containing nucleosomes and to a lesser extent with H3K9me₃ (Greaves et al., 2007). H2AZ-containing nucleosomes function as a boundary between euchromatin and heterochromatin (Meneghini et al., 2003). A study in fission yeast showed that loss of H2AZ results in loss of silencing at centromeres and

defects in chromosome segregation. They found that H2AZ functions in silencing centromeres via regulation of the expression of CENP-C, a centromere protein required for centromere silencing. Overexpression of CENP-C rescues the defect caused by H2AZ depletion (Hou et al., 2010). Recently, it was revealed that incorporation of H2AZ in pericentric chromatin is regulated by the heterochromatin state at this region, since alteration of the state of pericentric heterochromatin, using either SUV39h double-null MEFs that lack H3K9me3, or inhibition of methylation by treatment of NIH3T3 fibroblasts with 5'-aza 2'-deoxycytidine, leads to enrichment of H2AZ at pericentric heterochromatin. Further, the state of pericentric heterochromatin influences the centric chromatin state by altering the level of CENP-A (Boyarchuk et al., 2014).

1.4.3 The role of INO80 in chromosomal stability

The first indication that the INO80 complex plays a role in chromosome segregation came from the Downs laboratory (Chambers et al., 2012). Their study showed that the absence of either Ies6 or Ino80 leads to a defect in chromosome segregation; the authors attributed this phenotype to an alteration in pericentric chromatin (i.e., chromatin flanking the centromeres) rather than changes to centromeric nucleosomes themselves. Furthermore, the study revealed that H2AZ enrichment in pericentric chromatin is altered in strains lacking Ies6 and Ino80, and that overexpression of H2AZ accelerates development of polyploidy, whereas down-regulation of H2AZ prevents it. The authors ultimately attributed these alterations to misincorporation of H2AZ, and concluded that the INO80 complex is involved in the maintenance of genome stability.

In support of this idea, a mammalian study from the Shi laboratory also showed that loss of YY1 (an INO80 subunit) causes polyploidy and chromosomal abnormalities, including chromosome and chromatid breaks, and triradial or quadriradial chromosomes

(Wu et al., 2007). These authors investigated the potential causes of this phenotype by performing FACS analysis on cells exposed to UV-C radiation to monitor defects in cell cycle progression. Since no defect was observed during the G1/S and G2/M checkpoints, the phenotype was attributed to a direct function of YY1 in DNA repair. Further, a recent study reported an up-regulation of premature separation of sister chromatids, with an increase in chromosome breaks in metaphase, caused by down-regulation of INO80 in the CH12-F3 cells, a lymphoma cell line (Kracker et al., 2015).

Finally, as mentioned previously, INO80 is a negative regulator of p21, which is a potent CDK inhibitor that regulates the G2/M cell cycle phase (Cao et al., 2015). The same study showed that INO80 also regulates other M phase checkpoint proteins, including MAD2L1 (See 1.2.5.1 for more details). Further, silencing of INO80, using siRNA in a p53^{+/+} HCT116 cell line, resulted in an increase of cells with large nuclei, most of which showed high expression of p21. Remarkably, depletion of INO80 using siRNA also resulted in a significant increase in the number of cells with more than two centrosomes per nucleus, aberrant cytokinesis, and multipolar spindle formation (Cao et al., 2015). These multiple lines of evidence indicate that INO80 plays fundamental roles in chromosome stability. How this type of chromatin remodeller is associated with this pathway remains elusive; it may be through negative regulation of p21 expression, or alternatively as a result of a more direct role in mediating kinetochore attachments, for example. Determination of the answer to this question was established as one of the aims of this thesis.

1.5 Thesis objectives

This thesis aimed to investigate and identify the roles of the mammalian INO80 complex across three major areas.

First, work from the Shi laboratory has identified that YY1 functions as a subunit of the human ATPase chromatin remodelling complex INO80. Furthermore, they showed that YY1 is able to bind HJs *in vitro* and interact with the RuvB homologs RUVBL1 and RUVBL2, suggesting that YY1 might represent the mammalian ortholog of bacterial RuvA (Wu et al., 2007). Therefore, the major aims for Chapter 3 were to investigate whether human YY1 exhibits a similar structure to bacterial RuvA, forms multimers *in vivo*, and/or has the ability to function together with RUVBL1/2 *in vivo* to promote HR.

Second, evidence from yeast (Downs et al., 2004; Morrison et al., 2004; Van Attikum et al., 2004) and mammals (Gospodinov et al., 2008, 2011; Kashiwaba et al., 2010) has confirmed the involvement of INO80 in HR repair, although the exact mechanism impacted by INO80 in this repair pathway has remained unclear. Yeast INO80 regulates the removal of H2AZ from chromatin (Papamichos-Chronakis et al., 2011) and evidence from human cells has indicated the critical role of H2AZ incorporation in DSB repair (Xu et al., 2012). Hence, the experiments in Chapter 4 aimed to test whether INO80 promotes HR via a pathway that involves the removal of H2AZ from damaged chromatin.

Finally, a study on yeast from our laboratory revealed a new role for INO80 in chromosome segregation via a pathway that regulates H2AZ enrichment within centromeric structures (Chambers et al., 2012). Chromosomal instability represents a

hallmark for most advanced cancer such as colon, lung, and cervical tumours (Tanaka & Hirota, 2016; McGranahan et al., 2012). Thus, the aims of Chapter 5 were to highlight the role of mammalian INO80 in maintaining chromosomal stability and to test the suitability of INO80 as a therapeutic target for CIN+ tumour cells.

Chapter 2.

Material and Methods

2.1 Cell lines and culturing conditions

The cell lines used in this study were as follows:

- 1BR-hTERT: Immortalised human fibroblasts
- A549: Human lung adenocarcinoma epithelial cell line
- HeLa: Human cervical cancer cell line
- U2OS: Human osteosarcoma cell line (CIN+)
- RKO: Human colorectal carcinoma cell line (CIN-)
- DLD1: Human colorectal adenocarcinoma cell line (CIN-)
- HT-29: Human colorectal adenocarcinoma cell line (CIN+)
- NCIH747: Human colorectal adenocarcinoma cell line (CIN+)

A549, HeLa, and RKO cell lines were complemented with MEM Complete medium comprised of minimum essential medium (MEM) (Gibco) supplemented with 10% foetal bovine serum (Gibco) and 1% penicillin and streptomycin (Gibco). 1BR-hTERT, U2OS, and HT-29 cells were cultured in Dulbecco's MEM (Gibco) and DLD1 and NCIH747 cell lines were cultured in PRMI (Gibco) containing 15% foetal bovine serum and 1% penicillin/streptomycin. All cells were incubated at 37°C in a humidified 95% air and 5% CO₂ atmosphere.

2.2 Irradiation (IR)

Cells were irradiated by exposure to a ¹³⁷Cs source at a dose rate of 1 Gy/9 s. For G2 phase experiments, 4 µM aphidicolin (Sigma-Aldrich; A4487) was added to prevent S-phase cells from progressing into G2.

2.3 Small interfering RNA (siRNA) knockdown conditions

siRNA-mediated knockdown was performed using:

1) HiPerFect Transfection Reagent (Qiagen) for the experiments described in Chapters 3 and 4, using the following transfection conditions:

Per 4×10^5 cells in 4 ml media, the following reaction mixture was assembled and then added to suspended cells following a 10 min incubation at room temperature (RT):

- 20 μ M siRNA from 50 mM stock siRNA solutions
- 12 μ l Hiperfect transfection reagent
- 200 μ l OptiMEM (Gibco).

The cells were then grown for 24 h and another round of transfection was carried out.

The cells were then grown for an additional 48 h prior to IR.

2) Lipofectamine RNAiMAX Transfection Reagent (Invitrogen) for the experiments described in Chapter 5, using the following transfection conditions:

Per 4×10^5 cells in 4 ml media, the following reaction mixture was assembled and added to suspended cells following a 10 min incubation at room temperature (RT):

- 20 μ M siRNA from 50 mM stock siRNA solutions
- 2.5 μ l Lipofectamine RNAiMAX Transfection Reagent
- 500 μ l OptiMEM.

Table 2.1 siRNA oligos used in this project.

siRNA	Supplier	Sequence
INO80	Dharmacon	SMARTpool siRNA
INO80	Origene	SMARTpool siRNA
YY1	Dharmacon	SMARTpool siRNA
RUVBL2 (TIP49b)	Dharmacon	SMARTpool siRNA
BRCA2	Dharmacon	SMARTpool siRNA
H2AZ	Dharmacon	SMARTpool siRNA
ANP32E	Dharmacon	5'-CGGCUUCCCAGCUUAAAUA-3'
SRCAP	Dharmacon	SMARTpool siRNA

2.4 Immunofluorescence for HR analysis

Cells plated on cover slips were fixed for 10 min with 4% paraformaldehyde (PFA) in phosphate buffered saline (PBS) (v/v) (Electron Microscopy Sciences; 15710), and permeabilised for 1 min with 0.2 % Triton X-100 in PBS. For RPA or Rad51 foci, pre-extraction was achieved by incubating the cells with 0.2 % Triton X-100 in PBS for 0.5–1 min prior to PFA fixation, during which process the non-chromatin bound protein would be removed allowing for clear visualization of the remaining protein. Then, cells were washed with PBS and incubated with primary antibody diluted in 2% (w/v) bovine serum albumin (BSA) in PBS for 1 h at RT. Cells were then washed three times and incubated with secondary antibody (diluted in 2% (w/v) BSA in PBS) for 30 min at RT in the dark. Slides were mounted using VECTASHIELD+DAPI (Vector Laboratories Ltd.) and visualized using a Nikon e400 microscope for counting; for imaging, an Applied Precision® DeltaVision® RT Olympus IX70 deconvolution microscope and softWoRx® Suite software were used. In each sample a minimum of 25 cells was scored blindly; error bars represent the SD error between three independent

experiments.

2.5 Western blotting (WB)

Cells were lysed by resuspension in Laemmli buffer and sonicated using a Diagenode Bioruptor sonicating waterbath for 2 cycles using pulses of 30 s on and 30 s off. Samples were then electrophoresed and immobilized on nitrocellulose membranes. The membranes were blocked with 5% milk (Marvel milk powder in Tris-buffered saline with 0.1% Tween 20 (TBST) buffer) for 1 h at RT. Primary antibodies were then added to the membrane at the appropriate dilution in 5% milk and incubated overnight at 4°C. The membranes were then washed 3 times with TBST buffer and incubated with the secondary antibody for 1 h at RT. Pierce® ECL Western Blotting Substrate was used for the chemiluminescent detection of secondary antibodies; blots were exposed to chemiluminescence-sensitive film in the dark room and the films were developed.

Table 2.2 Primary antibodies used in this project.

Antibody	Supplier	Catalogue No.	Concentration
γH2AX	Millipore	05-636	1:800
RPA	Millipore	NA18	1:100
RAD51	Santa Cruz Biotechnology	SC_8349	1:200
CENP-F	Abcam	ab5	1:1000
CENP-A	Abcam	ab13939	1:100
INO80	Abcam	ab118787	1:2000
INO80	Bethyl	A303-371A	1:2000
YY1	Santa Cruz Biotechnology	H-414	1:1000
RUVBL2	Abcam	ab36569	1:5000
H2AZ	Cell Signaling Technology	2718S	1:1000

ANP32E	Sigma-Aldrich	SAB2100124	1:1000
Ku80	Abcam	ab33242	1:1000
KAP-1	Abcam	ab22553	1:1000
Tubulin	Abcam	ab7750	1:10000

Table 2. 3 Secondary antibodies used in this project.

Antibody	Supplier	Catalogue No.	Concentration
FITC	Sigma Aldrich	F0257	1:100
CY3	Sigma Aldrich	C2306	1:200
AlexFluor 488	Invitrogen	A21206	1:400
AlexFluor 555	Invitrogen	A21422	1:400
Goat Anti-Rabbit HRP	Dako	P0449	1:2000
Rabbit Anti-Mouse HRP	Dako	P044801-2	1:2000
Rabbit Anti-goat HRP	Dako	P0449	1:2000

2.6 Sister chromatid exchange (SCE) assay

HeLa cells (2×10^5 cells) were double transfected with siRNA oligos. At 24 h following transfection, the cultures were grown for two cell cycles (approximately 48 h) in the presence of 15 μ M BrdU (Sigma-Aldrich). Cells were treated with 100 μ g mitomycin C (Sigma-Aldrich) for the last 16 h of the 48 h culture period. Colcemid (Sigma-Aldrich) was added at a final concentration of 0.1 μ g/ml 2 h before harvesting cells. The harvested cells were swelled in 60 mM KCl for 15 min at RT and then fixed with methanol/glacial acetic acid (3:1). Next, the fixed cell suspension was dropped onto glass slides and air-dried overnight. Slides were then stained with 10 μ g/ml Hoescht 33258 (Sigma-Aldrich) for 20 min, UV-irradiated (355 nm) for 1 h, heated at 60°C for 1

h, and stained with Giemsa (1:20 diluted in dH₂O; Sigma-Aldrich: 32884) for a maximum of 5 min. Slides were then rinsed, air-dried overnight, and mounted with Eukitt quick-hardening mounting medium (Sigma-Aldrich). Slides were visualized using a Zeiss light microscope and Simple-PCI software. SCEs were scored in a minimum of 1000 chromosomes; error bars represent the SD error between three independent experiments.

2.7 Bimolecular fluorescence complementation assay (BiFC)

2.7.1 Cloning

2.7.1.1 Plasmids and constructs

The pBiFC plasmid was provided by Dr. Chang-Deng Hu (Addgene). The coding region of the human *YY1* gene was amplified from *YY1* cDNA and cloned into the BiFC plasmids to generate YY1_VN and YY1_VC. Similarly, the coding region of the human *RUVBL2* gene was amplified from *RUVBL2* cDNA and cloned into pBiFC_VC to generate RUVBL2_VC.

Table 2.4 Plasmids and components used for cloning.

Plasmid	Source	Description
pBiFC_VN	Addgene; 22010 (pBiFC_VN173)	Mammalian expression vector encoding the N-terminal region of fluorescent protein Venus, CMV promoter, <i>AMP</i> ^R
pBiFC_VC	Addgene; 22011 (pBiFC_VC155)	Mammalian expression vector encoding the C-terminal region of fluorescent protein Venus, CMV promoter, <i>AMP</i> ^R
<i>YY1</i> cDNA	Source BioScience	Human full length cDNA
<i>RUVBL2</i> cDNA	Origene; NM_006666	Human cDNA open reading frame (ORF) clone
YY1_VN	Generated for this	Mammalian expression vector encoding

	study	the <i>YY1</i> gene and the N-terminal region of fluorescent protein Venus, CMV promoter, <i>AMP</i> ^R
YY1_VC	Generated for this study	Mammalian expression vector encoding the <i>YY1</i> gene and the C-terminal region of fluorescent protein Venus, CMV promoter, <i>AMP</i> ^R
RUVBL2_VC	Generated for this study	Mammalian expression vector encoding the <i>RUVBL2</i> gene and the C-terminal region of fluorescent protein Venus, CMV promoter, <i>AMP</i> ^R

Table 2. 5 Oligonucleotides used for cloning.

Oligo no.	Name	Sequence (5' to 3')	Application
1688	YY1-VN_F	CGATGAATTCAATGG CCTCGGGCGACACCCT	Forward primer for cloning <i>YY1</i> into pBiFC_VN using the EcoR1 site
1689	YY1-VN_R	CTTCAGATCTATCTGG TTGTTTTTGGCCTTAG	Reverse primer for cloning <i>YY1</i> into pBiFC_VN using the BglII site
1690	YY1-VC155_F	CGATGAATTCGGATG GCCTCGGGCGACACC CT	Forward primer for cloning <i>YY1</i> into pBiFC_VC using the EcoR1 site
1691	YY1-VC_R	TCTAAGATCTCCTGGT TGTTTTTGGCCTTAG	Reverse primer for cloning <i>YY1</i> into pBiFC_VC using the BglII site
1692	RUVBL2-VC_F	CGATGAATTCGGATG GCAACCGTTACAGCC ACA	Forward primer for cloning <i>RUVBL2</i> into pBiFC_VC using the EcoR1 site
1693	RUVBL2-VC_R	TCTACTCGAGATGGA GGTGTCCATGGTCTCG	Reverse primer for cloning <i>RUVBL2</i> into pBiFC_VC using the XhoI site

1694	RUVBL2_F _CH	AAGATCTCCAAGCTG GGCCGCTCCTTCACAC	Forward primer to check the sequence of the <i>RUVBL2</i> cDNA that was inserted in pBiFC_VC, located after the first 600 bp of the ORF
------	-----------------	-------------------------------------	---

2.7.1.2 PCR

PCR-based DNA amplification was used for the amplification of the coding region of the *YY1* and *RUVBL2* genes and for verification of their integration. PCR was performed by using the KOD Hot Start DNA polymerase kit (Novagen) following manufacturer protocol. Amplified DNA products were purified using the QIAquick PCR Purification Kit (Qiagen) following manufacturer protocol.

2.7.1.3 Restriction Digestion

To generate YY1_VN and YY1_VC, sequential restriction digests of DNA were carried out in 10 µl reaction volumes using 8 µl DNA, 0.5 µl BglIII restriction enzyme (New England Biolabs), and 1 µl of the appropriate NE Buffer. The reaction tubes were incubated overnight at 37°C. Next, 0.5 µl EcoR1 restriction enzyme (New England Biolabs) was added to the reaction followed by incubation for 3 h at 37°C. However, to generate RUVBL2_VC, double restriction digestion of the DNA was performed utilizing both of the relevant restriction enzymes simultaneously; the reaction tubes were incubated overnight at 37°C.

2.7.1.4 DNA ligation

Ligation of DNA fragments into the appropriately digested plasmids was performed using T4 DNA Ligase (New England Biolabs) by mixing the following in 1.5 ml Eppendorf tubes: 25 ng vector DNA, 75 ng insert DNA, 1 µl ligase buffer, 1 µl T4 DNA ligase, and H₂O to a total volume of 10 µl; the reaction tubes were then incubated

overnight at RT. Insert DNA and linearized plasmid DNA were mixed in a ratio of 3 insert: 1 vector, according to the following equation:

$$\frac{\text{insert size} \times 3 \times 25 \text{ ng (amount of vector used)}}{\text{vector size}}$$

2.7.1.5 Transformation of bacteria with the ligated plasmids

For each ligation reaction, 50 µl competent cells (XL1 blue) were added. The mixtures were incubated on ice for 40 min, subjected to heat-shock at 42°C for 1 min, then immediately placed back on ice for 2 min. Next, 500 µl Luria-Bertani (LB) broth media free of antibiotic was added to each reaction tube followed by incubation for 30 min in a 30°C shaker incubator. The tubes were then spun at 13,000 rpm for 1 min, the supernatant was discarded, and the pelleted bacteria were plated on LB agar plates containing the appropriate antibiotic (Ampicillin, 100 µg/ml; Sigma). The plates were incubated overnight at 37°C. Individual colonies were picked and grown in 2 ml LB medium containing the appropriate antibiotic overnight in a 30°C shaker incubator. DNA was extracted using QIAprep Spin Miniprep or Maxiprep kits (Qiagen) as described in the manufacturer protocol.

2.7.1.6 Agarose gel electrophoresis

Agarose gel electrophoresis was used to separate DNA fragments by size. DNA samples containing 1× loading buffer (1 part loading dye, 5 parts 30% glycerol) in a volume of 12 µl were loaded onto a 1% agarose gel (1× TAE (40 mM Tris·acetate, 2 mM Na₂EDTA·2H₂O, pH 8.5) and 3 µl ethidium bromide). In addition, 12 µl of an appropriate ladder (New England Biolabs) was loaded in a separate lane. Following separation based on charge (80 V, room temperature), the DNA fragments were

visualised using a UV light imager and cut out of the gel using a clean scalpel. DNA was extracted from the agarose gel using a QIAquick Gel Extraction Kit (Qiagen) following manufacturer protocol.

2.7.2 BiFC assay

For the BiFC assay, 1.5×10^5 U2OS cells were plated on a coverslip and co-transfected with 0.25 μg VN- and VC-driven plasmids using the NanoJuice Transfection Reagent Kit (Novagen). At 24 h post transfection, cells were irradiated with 5 Gy γ -IR, fixed with 3% (w/v) PFA, permeabilised with 0.5% Triton X-100 in PBS for approximately 30 min, and mounted using VECTASHIELD+DAPI. Slides were analysed and imaged using an Applied Precision® Delta Vision® RT Olympus IX70 deconvolution microscope.

2.7.3 Laser microirradiation used for tracking BiFC foci

To track BiFC foci, 2×10^5 U2OS cells were plated onto 35-mm glass-bottom dishes (MatTek) and co-transfected with YY1_VN and YY1_VC constructs using a NanoJuice Transfection Reagent Kit. The cells were allowed to express the constructs for 24 h and were then incubated with 10 $\mu\text{g}/\text{ml}$ Hoechst 33285 for 1 h at 37°C prior to IR. BiFC positive cells were irradiated with a v405 laser line (20% power/2000 repetition) through a 60 \times objective using a Spinning Disc confocal microscope and Slidebook 5.5 software. Images were captured at 10 s intervals following laser damage for a total time of 2 min.

2.8 Laser microirradiation used for tracking protein dynamics at sites of damaged chromatin

Exponentially growing human U2OS cells were plated onto 35-mm glass-bottom dishes and transfected with pTGFP-H2AZ, pEGFP-RUVBL2 (Origene), or pEGFP-H2B using NanoJuice according to the manufacturer's protocol. The cells were allowed to express the construct for 24 h and were then incubated with 10 $\mu\text{g/ml}$ Hoechst 3458 for 30 min at 37°C prior to irradiation. The microscope system used was an Intelligent Imaging Innovations spinning disk confocal microscope with a Yokogawa CSU-X1 spinning disk device on an Olympus IX-71 confocal microscope. GFP positive cells were irradiated with a 405 nm ultraviolet laser set at power of 7:1000 for either H2AZ or H2B and at 30:1000 for RUVBL2 and channelled through a 60 \times objective. Images were captured at 10 s intervals following laser damage for a total time of 5 min for H2AZ and H2B and 30 min for RUVBL2. The generated images were acquired using a Photometrics Evolve 512 \times 512 EMCCD camera using Slidebook 6 software. In protein recruitment experiments, signal intensity was quantified along the laser path using Slidebook 6 software in a minimum of 10 cells; error bars represent the SD between three independent experiments.

Table 2. 6 Plasmids used in laser microirradiation experiments for tracking protein dynamics at sites of damaged chromatin.

Plasmid	Source	Description
pTGFP-H2AZ	Origene	Mammalian expression vector, <i>TGFP</i> under the control of the CMV promoter, <i>AMP^R</i>
pEGFP-RUVBL2	Origene	Mammalian expression vector, <i>EGFP</i> under the control of the CMV promoter, <i>AMP^R</i>
pEGFP-H2B	Hocheggerlab's laboratory	Mammalian expression vector, <i>EGFP</i> under the control of the CMV promoter, <i>AMP^R</i>

2.9 Resection assay

Cells were treated for 1 h with 1 mM camptothecin (Sigma-Aldrich) and left to recover for 1 h. Recovered cells were then stained, and γ H2AX positive cells were scored as described previously (section 2.4) for a minimum of 100 cells per experiment.

2.10 Analysis of micronuclei and abnormal mitosis

Prior to observation, 2×10^5 cells were double-transfected with siRNA oligos, plated on cover slips, and left to grow for 24 h. Transfection cultures were then fixed for 10 min with 4% PFA in PBS (v/v). Slides were mounted with VECTASHIELD+DAPI and visualized using an EVOS® FL microscope (AMG) for counting. A minimum of 1000 cells was scored blindly; error bars represent the SD error between two independent experiments. Images were obtained using an Applied Precision® Delta Vision® RT Olympus IX70 deconvolution microscope with softWoRx® Suite software.

2.11 Analysis of aneuploidy

For aneuploidy assessment, 2×10^5 cells were double transfected with siRNA oligos, plated on cover slips, and left to grow for 24 h. Transfection cultures were then fixed for 10 min with 4% PFA in PBS (v/v). Cells were washed with PBS and incubated with primary antibody diluted in 2% (w/v) BSA in PBS for 1 h at RT. Cells were then washed three times and incubated with secondary antibody (diluted in 2% (w/v) BSA in PBS) for 30 min at RT in the dark. Slides were mounted with VECTASHIELD+DAPI. A minimum of 30 anaphase cells were imaged using an Applied Precision® Delta Vision® RT Olympus IX70 deconvolution microscope with softWoRx® Suite software. Deconvoluted images were then analysed using ImageJ Software and the numbers of

CENP-A foci were scored in all images; error bars represent the SD error between two independent experiments.

2.12 Cell viability assay

Viability assays were carried out in 96-well plates. Cells were counted and triplicate-seeded in a total volume of 100 μ l medium. Cell densities were optimized as follows: U2OS: 3000 cells/well, HT29: 2000 cells/well, NCIH747: 5000 cells/well, DLD1: 2000 cells/well, and RKO: 4000 cells/well. Cells were incubated with 20 μ l CellTiter-Blue reagent (Promega) for 1–3 hours before being read depending on the required time point. Fluorescence was measured using a microplate reader (Promega). Data represent a relative mean to the readout of the first time point (24 h) from three independent experiments.

Chapter 3.

Biochemical characterization of YY1
and its role in homologous
recombination

3.1 Introduction

YY1 (Ying Yang 1) represents a ubiquitous zinc-finger transcription factor belonging to the Polycomb Group protein family, which comprise a collection of homeobox gene regulators that are associated with haematopoiesis and cell cycle regulation. Human YY1 is a 414-amino acid protein with an estimated molecular weight of 44 KDa. The C-terminus of YY1 contains four C₂H₂-type zinc-finger motifs that characterize its transcriptional function as an activator or repressor. These motifs are vital for interaction with DNA as well as for protein-protein interaction (Houbaviy et al., 1996). However, the N-terminus is thought to be involved in transcriptional activation only; furthermore, it is followed by a glycine-rich domain and 11 consecutive histidine residues, the functions of which remain elusive. YY1 controls a range of cellular and viral genes through its ability to either activate or repress their expression; this transcriptional role has been extensively studied and reviewed elsewhere (Gordon et al., 2005). Moreover, YY1 has been shown to be implicated in replication, embryogenesis, and cell growth, differentiation, and proliferation. Overexpression of YY1 in a range of cancer cells including; prostate, cervical, colorectal, ovarian, and breast cancers has further suggested its utility as a prognostic marker (Gordon et al., 2006).

Previously, work from the Shi laboratory has identified that YY1 also functions as a subunit of the human ATPase chromatin remodelling complex INO80 (Wu et al., 2007). Therein, a double-tag experiment was performed to purify the Flag-HA-YY1 complex from HeLa cells, after which the proteins co-purified with the YY1 complex were identified by tandem mass spectrometry. This process identified seven subunits of the INO80 complex including INO80, RUVBL1, RUVBL2, ARP4, ARP5, ARP8, and β -actin, as well as DNA-PKcs and KU86, components required for non-homologous end

joining repair, within the YY1 complex. The association of these factors with the complexes was then confirmed by western blotting and glycerol-gradient sedimentation, which failed to identify the KU86 component. In addition, YY1 was found to physically interact with the N-terminal and the middle segment of INO80, and interactions were identified with RUVBL1, RUVBL2, and ARP4 as well. Notably, glycerol-gradient sedimentation for the YY1 protein showed multiple bands with different molecular weights, suggesting the ability of YY1 to form multimers *in vitro*. Moreover, Wu et al. (2007) also demonstrated an association of the YY1-INO80 complex in homologous recombination (HR) repair as indicated by a decrease of approximately 13-fold in HR efficiency of I-SceI-induced double strand breaks (DSBs) in short hairpin (sh)YY1 and/or shINO80 treated HR-293T and HT1080-1885 cell lines. Further *in vitro* evidence was provided by using a gel-shift assay to show the ability of YY1 to bind Holliday junctions (HJ), whereas CtIP (used as a control owing to its ability to bind ssDNA) and RUVBL1/2 failed to bind HJ *in vitro* (Wu et al., 2007).

RUVBL1 and RUVBL2 are ATPases associated with diverse cellular activities (AAA+) proteins that exhibit 45% identity and 65% similarity in their sequence and are homologous to the bacterial helicase RuvB (Lopez-Perrote et al., 2012). RuvB is a subunit of the HJ branch-migration complex, which together with RuvA and RuvC provides the energy for the resolution of HJs (Mayanagi et al., 2008; Fujiwara et al., 2008, Lopez-Perrote et al., 2012). All AAA+ proteins contain highly conserved motifs termed Walker A and Walker B that are responsible for ATPase activity and usually form a hexameric ring structure (Nano & Houry, 2013). The structures of human RUVBL1 and RUVBL2 have been determined and were found to form a dodecamer consisting of two heterohexameric rings, with alternating subunits in each ring, that

bound back-to-back via their internal DII domain (Figure 1.3) (Lopez-Perrote et al., 2012). In addition, RUVBL1 and RUVBL2 have the ability to bind dsDNA and ssDNA as well (Matias et al., 2006). Notably, the binding domain for ssDNA, which comprises the N-terminal $\alpha\beta\alpha$ subdomain of the AAA+ domain, is similar to the ssDNA binding domain of replication protein A (RPA) (Matias et al., 2006). RUVBL1 and RUVBL2 are essential subunits of several complexes including INO80, SWR1, TIP60, PI3K (which regulates the activity of phosphatidylinositol 3-kinase), and R2TP (associated with the biogenesis of small nucleolar ribonucleoproteins (snoRNPs)) (Nano & Houry, 2013) and are thus associated with a variety of cellular functions including transcription, DNA repair, telomere assembly, mitotic spindle assembly, and cancer (Nano & Houry, 2013).

The ability of YY1 to bind HJs *in vitro* and interact with the RuvB homologs RUVBL1 and RUVBL2 suggests that YY1 might represent the mammalian ortholog of bacterial RuvA (Wu et al., 2007). In bacteria, RuvA forms an octamer (a pair of tetramers) that specifically binds HJ DNA and targets RuvB to the junction, where it forms two hexameric rings on either side of the RuvA octamer. Together, the two proteins form a complex that facilitates ATP-dependent branch migration of the junction (Figure 1.3) (Mayanagi et al., 2008). However, several related questions remain unanswered; i.e., whether human YY1 exhibits a similar structure to bacterial RuvA, forms multimers *in vivo*, and/or has the ability to function together with RUVBL1/2 *in vivo* to promote HR. To address these issues, we established a collaboration with the Llorca laboratory (López-Perrote et al., 2014), wherein they characterised the structure of YY1 for the first time and examined the ability of YY1 to bind multi-types of DNA. In turn, I tested

the ability of YY1 to form multimers *in vivo* and examined the role of YY1 during HR (López-Perrote et al., 2014).

3.2 Results

3.2.1 YY1 forms multimers *in vitro* and *in vivo*

As was mentioned above, it has been reported that YY1 can form multimers *in vitro* (Wu et al., 2007). To confirm this ability of the protein, our collaborator expressed a His-tagged YY1 in bacteria and then purified the full-length His-YY1. The purified complex was then subjected to oligomerisation analysis, in which the His-YY1 was first cross-linked for 30 minutes using a glutaraldehyde (GA) reagent and then analysed by sodium dodecyl sulphate-polyacrylamide gel electrophoresis (SDS-PAGE) and western blotting with an anti-YY1 antibody. As can be seen in Figure 3.1, only monomeric His-YY1 was detected in the control (i.e., His-YY1 without GA cross-linking); however, four cross-linked bands with different molecular weights were detected together with the monomer YY1 in the sample incubated with GA, confirming the ability of YY1 to form multimers *in vitro* (López-Perrote et al., 2014). Notably, this study also demonstrated that His-YY1 behaved as oligomers in size exclusion chromatography (SEC, a technique used widely to purify proteins depending on their sizes). Furthermore, it was found that His-YY1 migrated as two distinct molecules, termed complex A (approximately 100–150 kDa) and complex B (approximately 200–300 kDa) (López-Perrote et al., 2014).

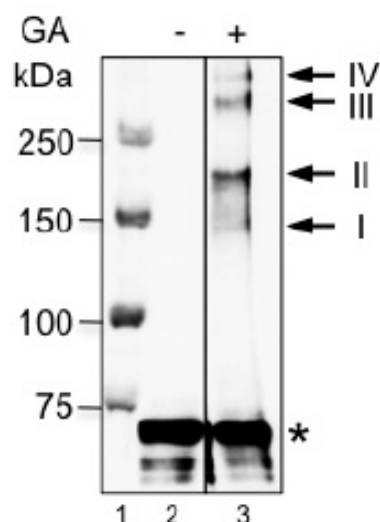


Figure 3. 1 YY1 multimerises *in vitro*.

Western blot with an anti-YY1 antibody of His-YY1 after crosslinking with glutaraldehyde (GA); lane 1, molecular weight standards (Bio-Rad); lane 2, control without GA; lane 3, 30 minutes of incubation with GA. The His-YY1 monomer migrates as a 70 kDa protein in SDS-PAGE (labelled as *). Crosslinked bands, with relative molecular weights of multiples of the YY1 monomer, are labelled with arrows (from López-Perrote et al., 2014).

Next, I attempted to determine whether the oligomerisation of YY1 also occurs *in vivo*.

To this end, I used the bimolecular fluorescence complementation (BiFC) assay, which allows the ready observation of *in vivo* interactions between adjacent proteins. When the assay is successful, interaction is detected as a fluorescent signal (Figure 3.2A); however, in some cases even bona fide interactions cannot be detected using this method, either because the proteins are separated by a large distance or because their conformations or orientations prevent fluorescence complementation (Shyu et al., 2008; Kerppola, 2008). For this procedure, I cloned the coding region of YY1 into each of the BiFC constructs, i.e., vectors containing N- and C-terminal non-fluorescent fragments of the Venus protein (VN and VC, respectively) to detect YY1 self-interaction *in vivo*. These constructs were transiently co-transfected into U2OS cells, which were incubated for 24 h to allow expression. Prior to observation, the cells were permeabilised and

fixed (see method 2.7.2). As controls, cells were co-transfected with 1) YY1-VN and empty vector VC, 2) YY1-VC and empty VN, or 3) the two empty vectors, VN and VC.

Notably, we were able to detect large fluorescent foci in cells transfected with the two plasmids containing the YY1 coding region, whereas a pan-nuclear fluorescence with no foci was present in the controls (Figure 3.2B). This observation demonstrated that YY1 forms a multimer *in vivo*.

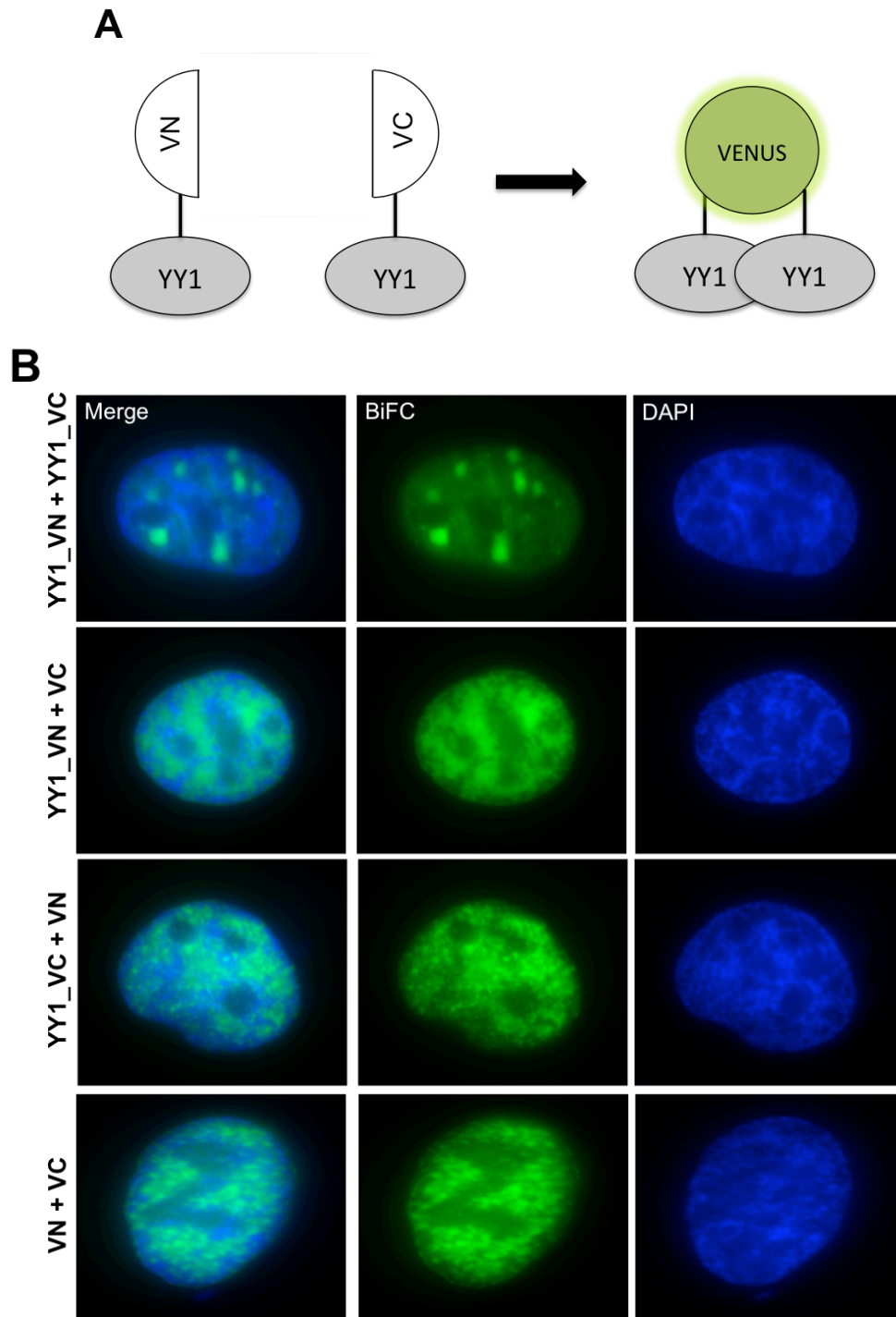


Figure 3. 2 YY1 *in vivo* mutimerisation.

(A) Scheme of the expression constructs used in BiFC experiments. The coding sequence of YY1 was fused to either the N-terminal (YY1-VN) or C-terminal (YY1-VC) domain of Venus. (B) U2OS cells transiently co-transfected with plasmids expressing the fusions in A were analysed by fluorescence microscopy. Co-transfection of YY1-VN with VC or YY1-VC with VN displayed no difference in pan-nuclear fluorescence compared with cells co-transfected with the empty vectors (VC and VN). Only cells co-transfected with both YY1 fusion constructs (YY1-VN and YY1-VC) exhibited distinct foci present in the nuclei.

3.2.2 Characterization of YY1 structure

As little is known regarding the structure of the human YY1, our collaborator utilised high-resolution electron microscopy (EM) to further characterise the purified His-YY1 complex A. This revealed a square-shaped molecule with a low-density region at its centre (Figure 3.3A) (López-Perrote et al., 2014). Additionally, the two-dimensional averages of the His-YY1 complex showed the existence of 2 or 4 identical YY1 subunits (Figure 3.3A). Furthermore, they were able to demonstrate the three-dimensional structure of the human YY1 by analysing 16,362 images obtained by EM through image processing methods and the *ab initio* random conical tilt (RCT) method. This revealed that the human YY1 protein was composed of two regions: the top region “head” comprised a compact square-shaped region and the bottom region “arms” was slightly elongated (Figure 3.3B) (López-Perrote et al., 2014).

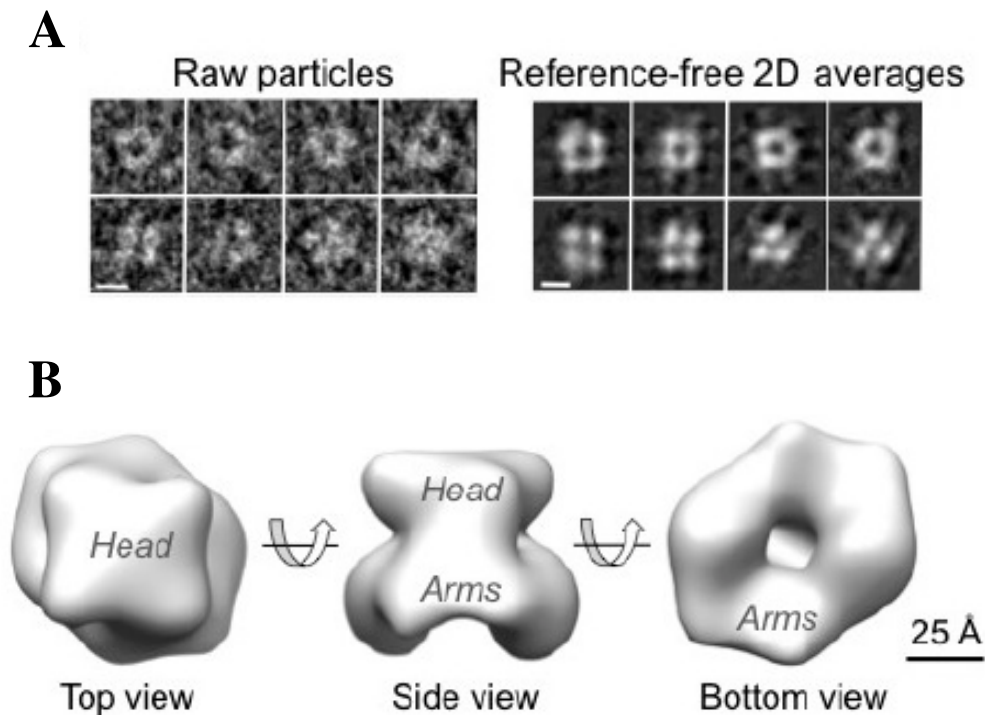


Figure 3. 3 Structure of human YY1 (complex A).

(A) Single molecule images and 2D reference-free averages of complex A of His-YY1 show a typical square shape. Scale bar represents 5 nm. (B) 3D structure of the YY1 dimer. Scale bar represents 25 Å (from López-Perrote et al., 2014).

Next, our collaborator attempted to characterise complex B of the YY1. To this end, they purified a more stable YY1 tagged to Strep-II on the N-terminus, which prevents YY1 aggregation. Then, the purified oligomeric form of Strep-II-YY1 was stabilized by a GraFix method in a glycerol/GA gradient. Oligomerisation of this complex was confirmed by high-resolution EM as for His-YY1 (complex A) (Figure 3.4A & B) (López-Perrote et al., 2014). This revealed an elongated structure of approximately 100 Å in length, approximately double in size compared to complex A, which was also re-purified from Strep-II-YY1 and processed using the same method to confirm its previously observed structure (Figure 3.4A & B). This led to the conjecture that YY1 dimers might associate in two different ways to form large oligomeric complexes (Figure 3.4C).

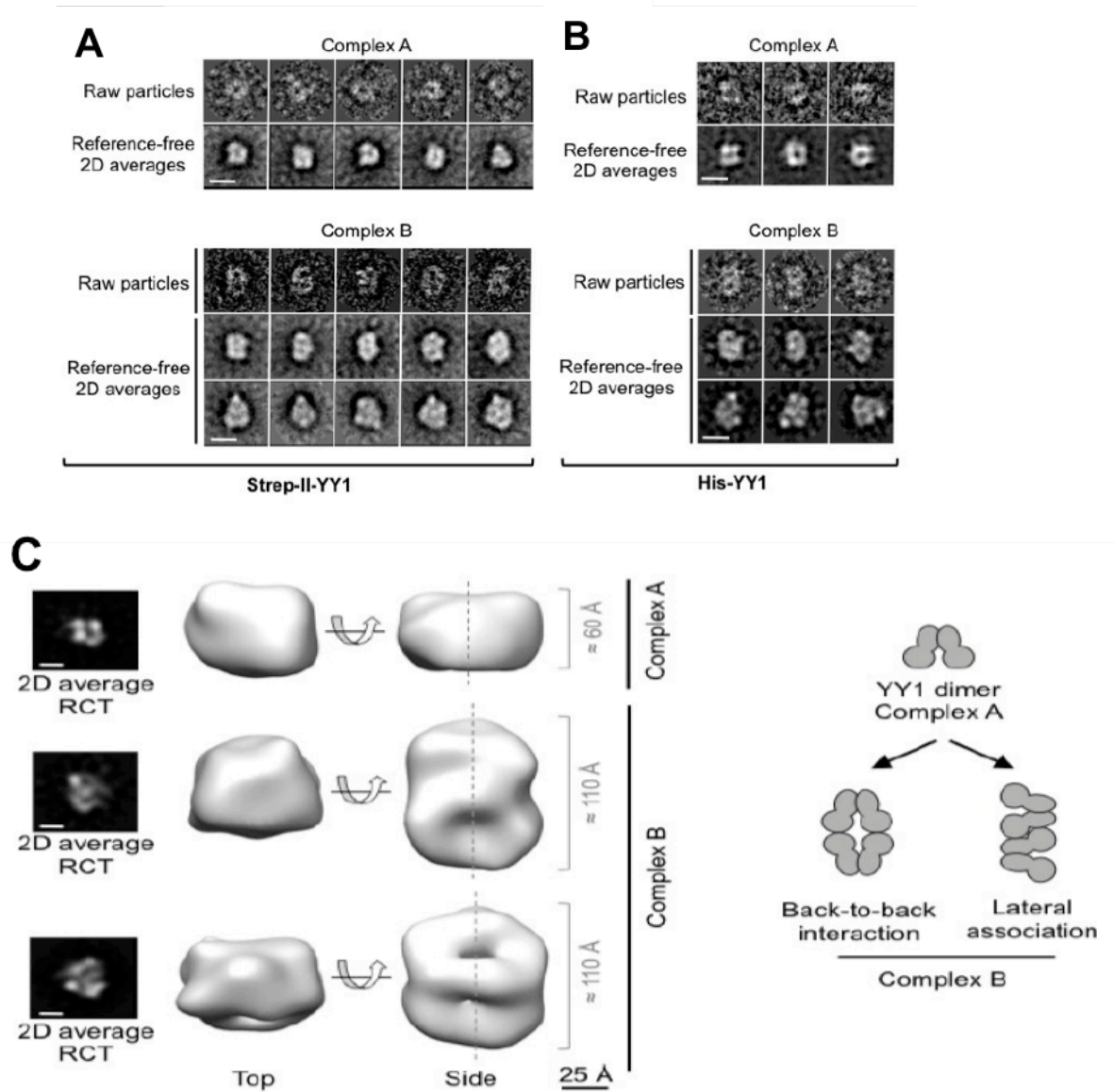


Figure 3.4 YY1 multimerises in larger complexes through the association of YY1 dimers.

Raw molecule images and 2D reference-free averages of (A) Strep-II-YY1 and (B) His-YY1 (complex A & B). (C) Left panel: representative RCT structures obtained from images and averages of Strep-II-YY1 (complex A & B). Scale bar represents 25 Å. Right panel: hypothetical models for YY1 association. Two potential ways of association of YY1 dimers into larger oligomers, based on the 2D averages and the RCT structures of complexes A and B, are proposed (from López-Perrote et al., 2014).

3.2.3 YY1 binds ssDNA, dsDNA, and HJs *in vitro*, which is enhanced by the RUVBL1-RUVBL2 complex

The C-terminal region of YY1 contains C₂H₂ type zinc finger motifs that characterize its function as a transcription factor and are capable of binding a consensus DNA sequence [5'-(C/g/a)(G/t)(C/t/a)CATN(T/a)(T/g/c)-3'] found at the promoter of genes (Houbaviy et al., 1996), as shown by Wu et al. using DNA substrates containing the consensus sequence (Wu et al., 2007). Our collaborator further disclosed the capability of the oligomeric form of human YY1 to bind different types of DNA substrates that include or exclude the consensus sequence (López-Perrote et al., 2014). To this end, they used the purified oligomeric form of YY1; i.e., complex B of Strep-II-YY1, to test its capability to bind DNA *in vitro* in an electrophoretic mobility shift assay (EMSA) by incubating the Strep-II-YY1 complex with different types of DNA substrate: HJ, dsDNA without the consensus sequence, dsDNA with the consensus sequence, and ssDNA (Figure 3.5A). The shifted bands observed in this assay indicated that oligomeric YY1 could bind HJ, ssDNA and dsDNA regardless of its specificity for consensus sequence binding (Figure 3.5A).

Our collaborator further confirmed that human YY1 was able to bind RUVBL1 and RUVBL2 *in vitro*, as previously demonstrated (Wu et al., 2007). More specifically, pulldown data confirmed that oligomeric YY1 could bind RUVBL1 whereas it failed to bind RUVBL2. In addition, it was shown that YY1 could bind the whole complex, i.e., RUVBL1-RUVBL2, that had been expressed and purified using the same method as for purifying His-YY1 (Figure 3.5B) (López-Perrote et al., 2014). This result suggests that YY1 binds the RUVBL1-RUVBL2 complex through a direct interaction with

RUVBL1.

Notably, Our collaborator was also able to demonstrate that the presence of the RUVBL1-RUVBL2 complex enhanced the ability of oligomeric YY1 to bind HJ and dsDNA (Figure 3.5C & D) as well as ssDNA (López-Perrote et al., 2014). This was performed using the EMSA technique by incubating Strep-II-YY1 and His-RUVBL1-RUVBL2 with HJ and dsDNA substrates, which resulted in shifted bands of greater intensity (Figure 3.5C & D) compared to those observed when YY1 alone was incubated with the DNA substrates (Figure 3.5A) (López-Perrote et al., 2014).

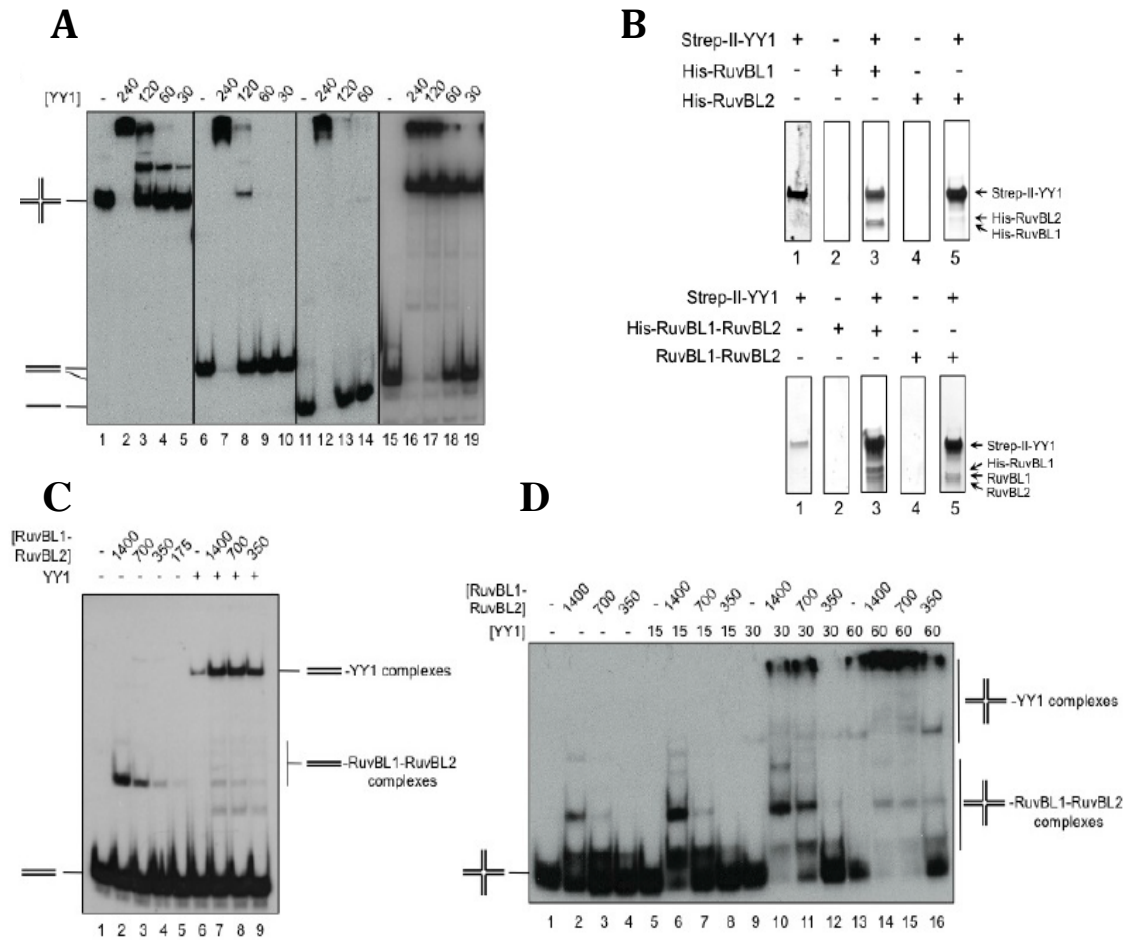


Figure 3. 5 YY1 binding to DNA and RUVBL1-RUVBL2 *in vitro*.

(A) EMSA assay showing binding of Strep-II-YY1 to several DNA substrates: HJ (lanes 1–5), dsDNA non-consensus sequence (lanes 6–10), 80-nt ssDNA (lanes 11–14), and dsDNA consensus sequence (lanes 15–19). The binding reaction consisted of 0.3 nM DNA mixed with different concentrations of YY1 (nM) as shown above the lanes. (B) Pulldown experiment showing the interaction between Strep-II-YY1 and His-RUVBL1, His-RUVBL2, His-RUVBL1-RUVBL2, or RUVBL1-RUVBL2. (C) EMSA assay showing that RuvBL1-RuvBL2 enhances the binding of YY1 to the dsDNA consensus sequence; the reactions contain decreasing concentrations of His-RUVBL1-RUVBL2 (as shown in nM) and 15 nM Strep-II-YY1. (D) EMSA assay showing that RuvBL1-RuvBL2 enhances the binding of YY1 to HJ; protein concentrations used are shown at the top of each lane (nM) (from López-Perrote et al., 2014).

3.2.4 YY1 functions together with RUVBL2 to promote RAD51

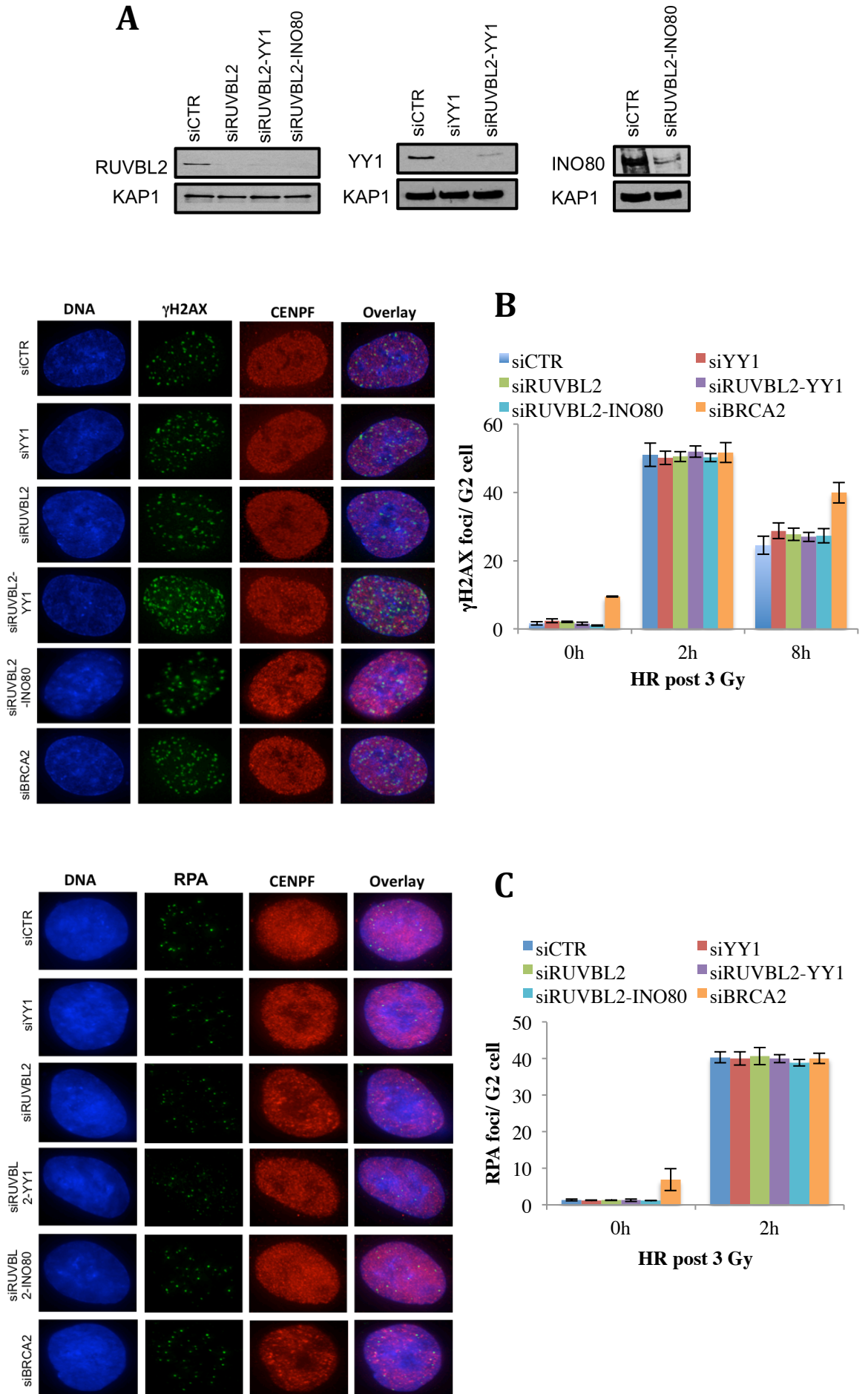
filament formation, likely as subunits of the INO80 complex; this function is enhanced by the ATPase activity of RUVBL2

YY1 was previously identified as a subunit of the human INO80 complex and its absence and/or that of INO80 led to a decrease in the HR efficiency of I-SceI-induced DSBs (approximately 13-fold) (Wu et al., 2007). However, the precise mechanism by which it functions in HR remained unclear, although it has been suggested that it might bind HJ and promote branch migration. The finding by our collaborator that the RUVBL1-RUVBL2 complex enhanced the ability of YY1 to bind dsDNA, ssDNA, and HJ *in vitro* (López-Perrote et al., 2014) urged us to further investigate its role during HR. To this end, we monitored HR in A549 cells and used siRNA to silence a group of genes (Figure 3.6A). These cells were exposed to 3 Gy γ -irradiation (IR) to induce DSBs and then fixed at 0 (i.e., before damage), 2, or 8 h. Next, I stained for γ H2AX, RPA, and RAD51 to determine whether the absence of the aforementioned subunits resulted in damage sensitivity (by monitoring γ H2AX foci) and to determine whether the cells exhibited defects in resection (by monitoring RPA foci) or RAD51 filament formation (by monitoring RAD51 foci) (Figure 3.6B–D). HR is restricted to S and G2 phases; however, because 20% of DSBs are repaired via HR in G2 phase and, more specifically, most of the breaks that occur in heterochromatin areas are repaired by HR in G2 (Shibata et al., 2011), I stained for CENP-F to mark G2 cells and only counted cells that were CENP-F-positive (Figure 3.6B–D). In addition, to ensure that only cells in G2 at the time of IR were analysed, I added aphidicolin to cells prior to IR to arrest S-phase cells and prevent them from progressing to G2 (Shibata et al., 2011; Beucher et al., 2009).

These experiments demonstrated that depletion of any of the tested proteins *per se* did not cause damage to dsDNA, as reflected by the absence of γ H2AX foci prior to IR. Furthermore, at 2 h, all siRNA-treated cells exhibited similar phenotypes as the control, indicating that the damage induced by IR was not affected by YY1, RUVBL2, or INO80 depletion. Furthermore, the reduction in γ H2AX foci at 8 h post IR suggested that G2 cells had undergone repair and that no additive defect was caused by the absence of YY1, RUVBL2, or INO80. In contrast, BRCA2-depleted cells were unable to repair the damage as efficiently as the other cells (Figure 3.6B). Similarly, no defect was observed in resection, as reflected by the comparable numbers of RPA foci in cells depleted for YY1, RUVBL2, INO80, or BRCA2 and control cells (Figure 3.6C).

Notably, the number of RAD51 foci was reduced by approximately 2-fold in YY1 and RUVBL2 depleted-cells compared to controls, although the defect in BRCA2-depleted cells was much more severe (Figure 3.6D). This suggested that these two factors might function in promoting or stabilizing RAD51 foci during HR. Next, to test whether YY1 and RUVBL2 worked together during HR, we co-depleted these proteins, as further defects might be expected if the two proteins function in different pathways to promote HR. However, the co-depletion of YY1 and RUVBL2 resulted in no additive defect on the number of RAD51 foci as compared to that observed following their individual depletion. This suggested that YY1 functions co-operatively with RUVBL2 to promote HR, likely by stimulating or stabilizing the formation of RAD51 filaments. It has been shown that co-depletion of YY1 and INO80 resulted in a similar defect on the HR efficiency to that observed following the absence of either individually (decrease of approximately 13-fold) (Wu et al., 2007). Here, I co-depleted RUVBL2 and individual subunits of the human INO80 complex to determine whether this function is specific to

the YY1-RUVBL1-RUVBL2 complex as a distinct mechanism or if it represents a subsequent function resulting from the roles of these proteins as subunits of the INO80 complex. As previously, an additional defect in the number of RAD51 foci would be predicted if the two complexes were working in separate pathways to promote HR. However, cells co-depleted for RUVBL2 and INO80 showed similar defects in RAD51 foci to that observed in the absence of YY1 and/or RUVBL2, suggesting that YY1 and RUVBL2 function during HR as part of the INO80 complex.



D

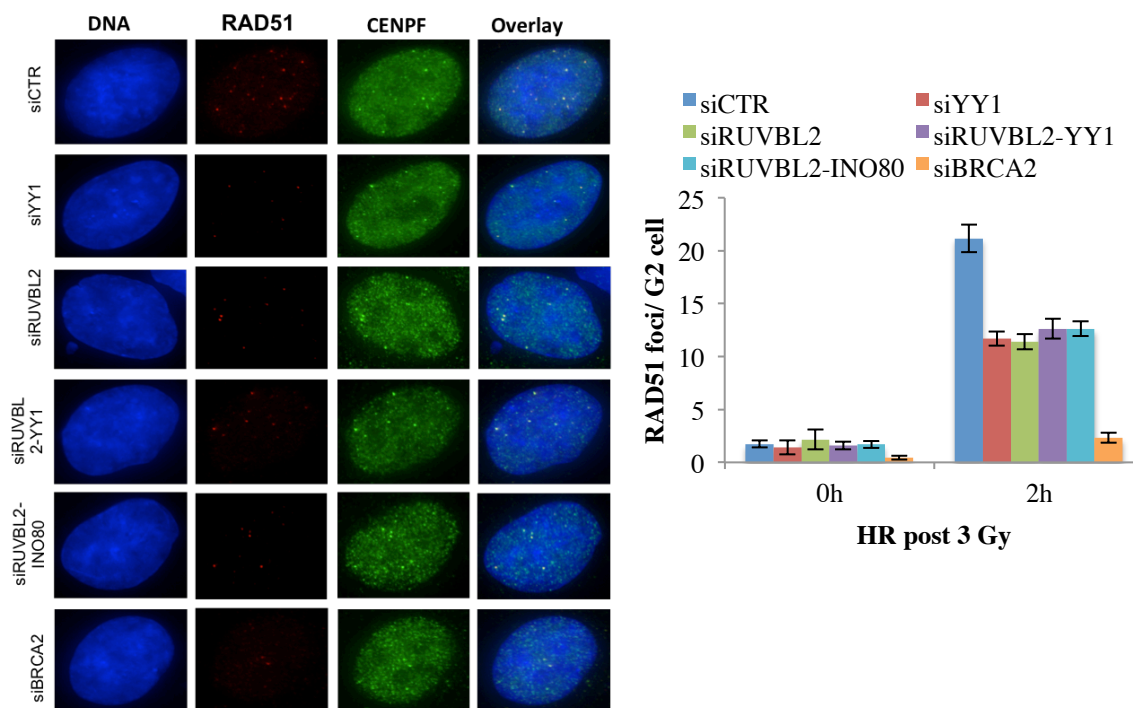


Figure 3. 6 INO80 is required for RAD51 foci formation.

(A) Western blot showing the efficiency of RUVBL2, YY1, and INO80, knockdown; KAP-1 is used as a loading control. Immunofluorescence images of G2 nuclei (A549 cells), showing the number of γ H2AX (B), RPA (C), or RAD51 (D) foci in control (siCTR) and knocked down cells at 2h post exposure to 3 Gy of γ -IR; right panel: number of foci per G2 cell either before exposure to 3 Gy of γ -IR (0 h) or at 2 (B-D) and 8 h (B) after damage. Average number of foci per G2 cell were quantified and presented as the means of 3 independent experiments; error bars represent \pm SD.

Next, to determine whether the ATPase activity of the RUVBL1/2 is required for RAD51 foci formation after IR exposure, a point mutation within the Walker A motif of RUVBL2 was utilized by (Amani Ismail, 2014) that impairs ATP binding but does not disrupt protein folding. An siRNA-resistant GFP-tagged RUVBL2 expression construct was generated within which the K83A point mutation was introduced. Then, U2OS cells were transfected with siRUVBL2, both siRUVBL2 and wild-type GFP-RUVBL2, or both siRUVBL2 and mutant GFP-RUVBL2-K83A. The transfected cells were then irradiated, fixed, and the RAD51 foci were counted as described. We found that inhibition of RUVBL2 ATPase activity yielded a decrease in the number of RAD51 foci in siRUVBL2-cells transfected with the mutant GFP-RUVBL2-K83A similar to that caused by depletion of RUVBL2 (siRUVBL2 alone); however, transfection of RUVBL2 depleted-cells with the wild-type construct rescued the defect in RAD51 foci formation to the level of the control (Figure 3.7). This clearly showed that the ATPase activity of RUVBL2 is required to promote RAD51 foci formation during HR.

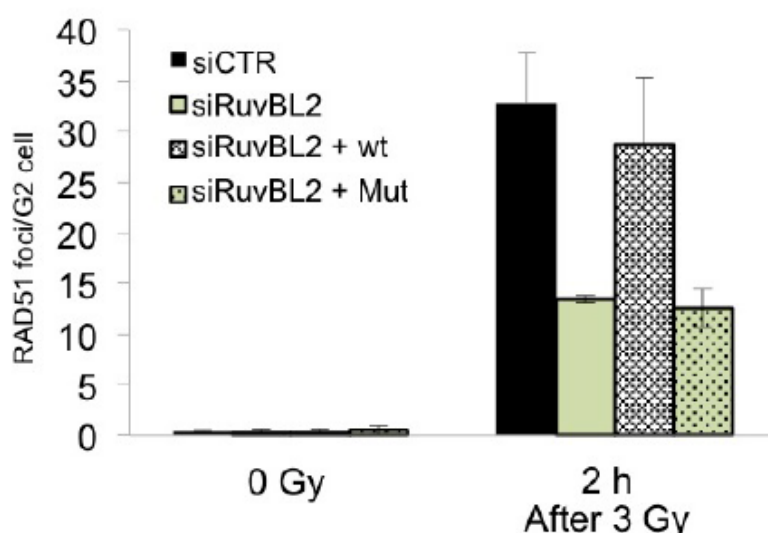


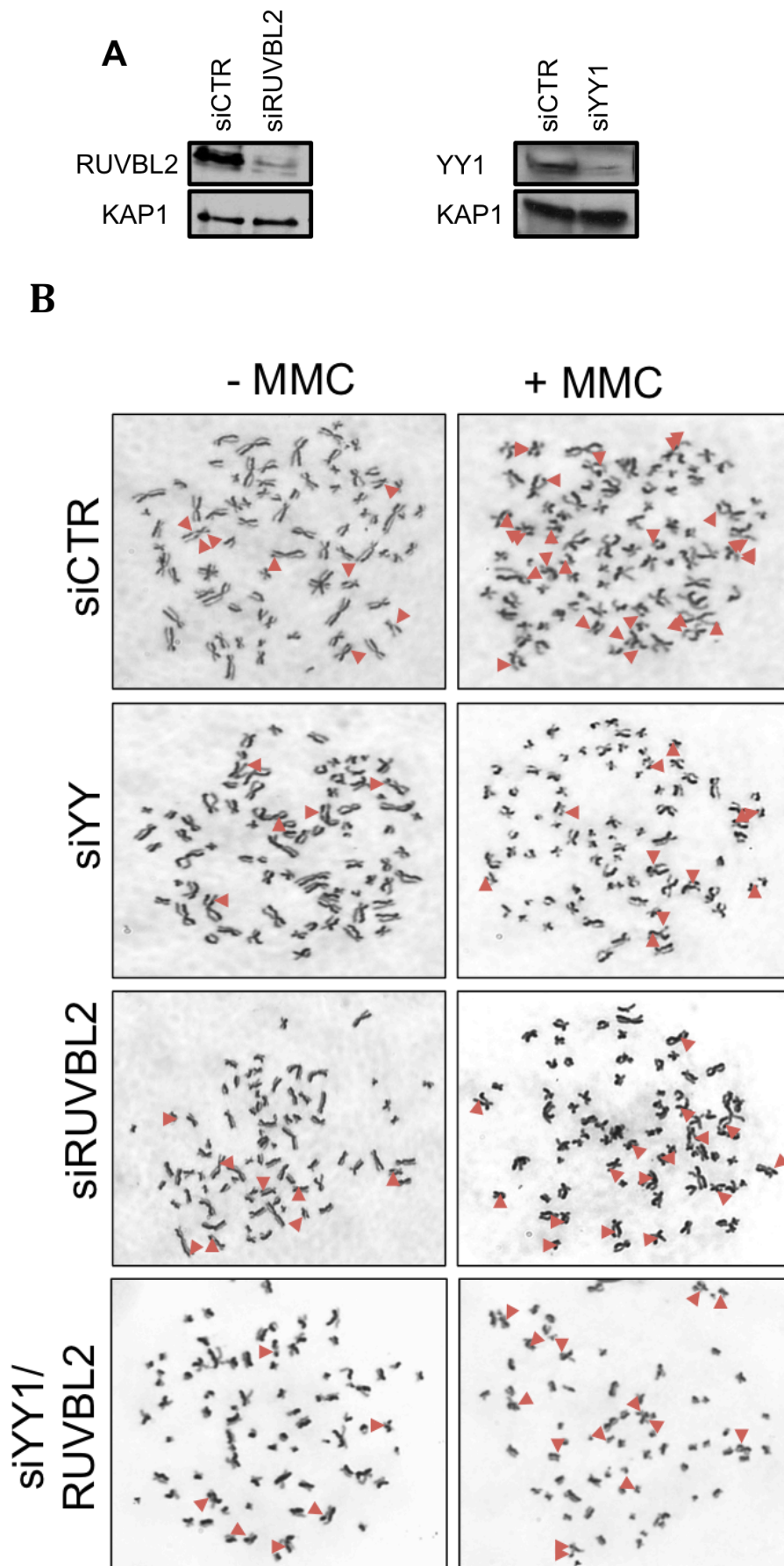
Figure 3. 7 RUVBL2 ATPase activity is required for promoting RAD51 foci formation.

U2OS cells transfected with siRNA directed against RuvBL2 and either GFP, GFP-RuvBL2, or GFP-RuvBL2-K83A. Average RAD51 foci per GFP positive G2 cell was quantified and presented as the means of 3 experiments; error bars represent \pm SD (Amani Ismail, (from López-Perrote et al., 2014)).

3.2.5 YY1 and RUVBL2 might have a late function during HR

To investigate the possibility that the observed HR defect phenotypes (Figure 3.6) reflect the roles of the YY1 and RUVBL2 proteins as subunits of the INO80 complex rather than as branch-migration enzymes, we carried out sister chromatid exchange assays (SCE) on HeLa cells depleted of YY1, RUVBL2, or both YY1 and RUVBL2, with the supposition that if the proteins act as a branch-migration enzyme, simultaneous depletion should result in an additive phenotype. Specifically, the SCE assay allowed us to monitor defects in the final outcome of HR by counting the number of exchanges between sister chromatids. Here, I induced DSBs in HeLa cells by using mitomycin C (MMC) rather than IR to confirm that the observed defects in RAD51 foci were not specific to DSBs induced by IR in G2 cells. In this experiment, BrdU-labelled HeLa cells were incubated with MMC for 16 h, colcemid was added to arrest cells in mitosis, and then the mitotic cells were harvested. To observe SCE, chromosomes were spread and stained.

Notably, if the YY1 and RUVBL2 have a distinct function during this late step in HR, a more severe defect in the number of SCEs would be expected than that observed in RAD51 foci. However, although depletion of YY1 and RUVBL2 resulted in a decrease of the number of SCEs compared to the control, this defect was similar to that previously observed in the formation of RAD51 foci. This result suggested that the defect in RAD51 might be passed on to the next stage of HR and therefore could not be recovered. Similarly, the co-depletion of YY1 and RUVBL2 caused no additive defect in the number of SCEs to that observed in RUVBL2 or YY1 depletion, suggesting that these two proteins function in the same pathway to promote repair by HR (Figure 3.8).



C

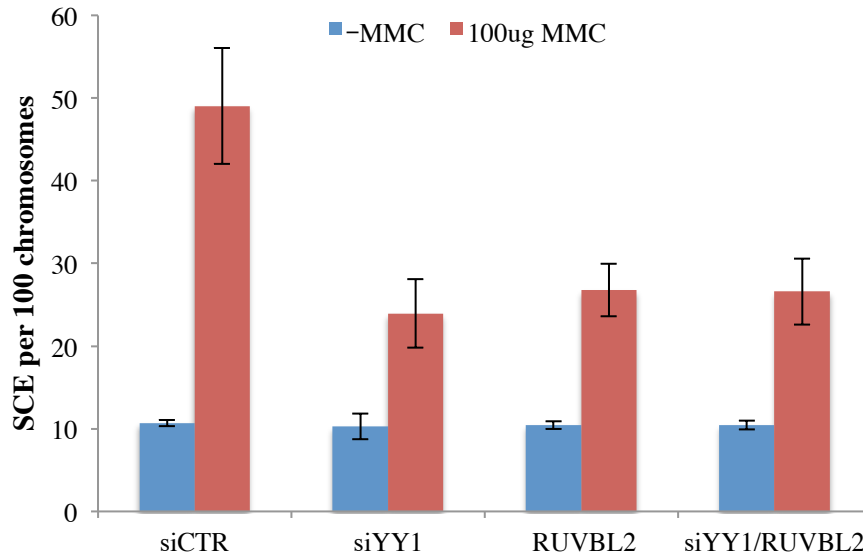


Figure 3. 8 Loss of YY1 and/or RUVBL2 causes a defect in SCE number.

(A) Western blot data showing the efficiency of RUVBL2 and YY1 knockdown; KAP-1 is used as a control. (B) Representative images of mitotic spreads in either MMC treated or untreated HeLa cells; chromosomes were labelled with BrdU and stained with Giemsa allowing visualisation of the exchange between sister chromatids. (C) Number of SCEs per 100 chromosomes were quantified and presented as the mean of 3 independent experiments; error bars represent \pm SD

3.2.6 YY1 and RUVBL2 might not represent the homologous complex of the bacterial branch-migration enzyme RuvA

The *in vitro* data by our collaborator showed that YY1 is able to bind dsDNA and HJ and interacts with the RUVBL1-RUVBL2 complex (López-Perrote et al., 2014), suggesting that YY1 might represent the human homolog of bacterial RuvA. However, our current *in vivo* results suggest that YY1 functions together with RUVBL2 to promote RAD51 foci formation during HR as part of their function within the INO80 complex. To resolve this dilemma, I investigated whether YY1 behaves as an oligomer in response to its role in HR. For this, I performed a BiFC experiment as previously described (see 3.2.1); U2OS cells transfected with the given plasmid (Figure 3.9) were then irradiated with 5 Gy γ -IR to induce DSBs (Figure 3.9). However, similar foci were observed in the damaged cells (Figure 3.9) as had been observed in non-irradiated cells (i.e., undamaged cells; Figure 3.2B). This result suggested that YY1 although exists as a multimer *in vivo*, this multimerisation is not related to its function in HR.

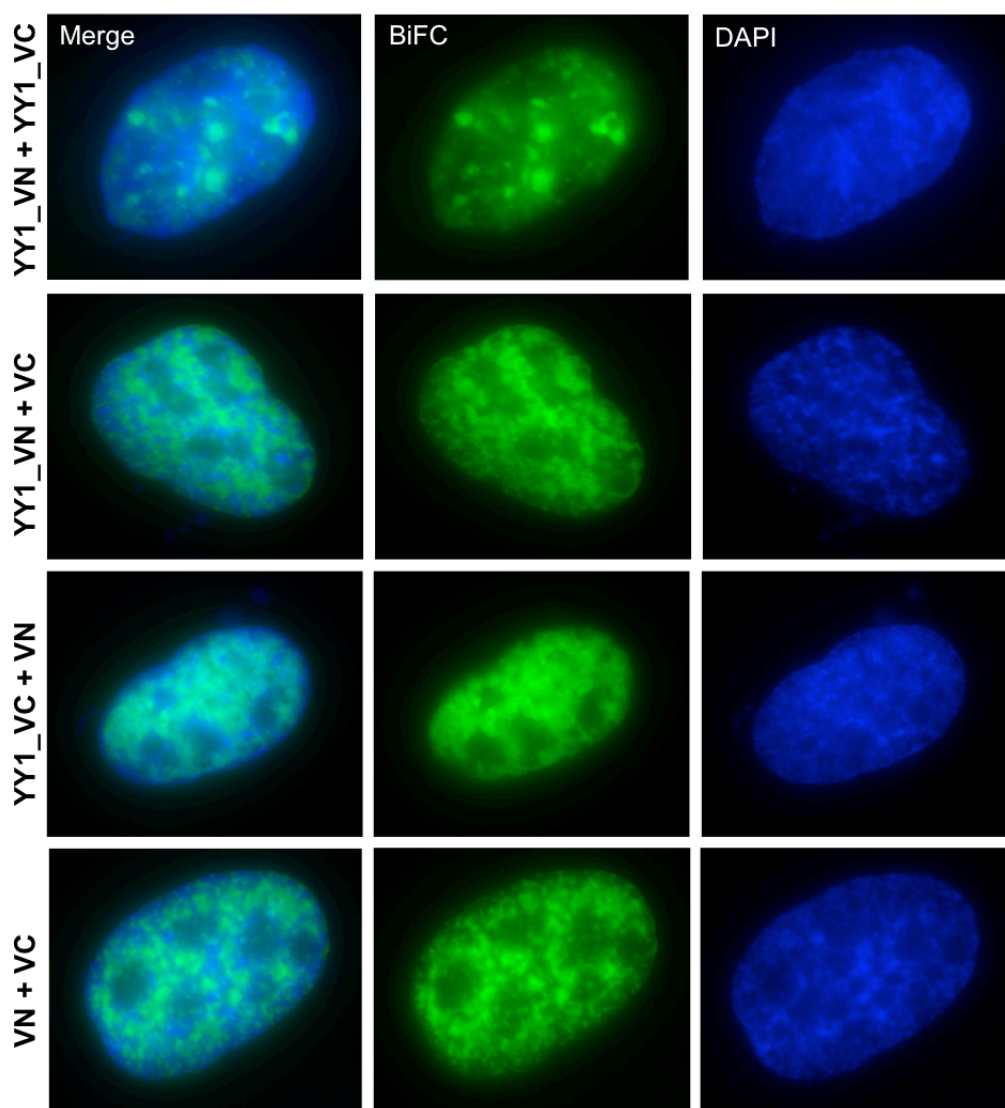


Figure 3.9 YY1 mutimerisation *in vivo* after exposure to 5Gy γ -IR.

U2OS cells transiently co-transfected with plasmids expressing the fusion proteins as in Figure 3.2A were exposed to 5Gy of γ -IR and analysed by fluorescence microscopy. Co-transfection of YY1-VN with VC or YY1-VC with VN displayed no difference in pan-nuclear fluorescence compared with cells co-transfected with the empty vectors (VC and VN). Only cells co-transfected with both YY1 fusion constructs (YY1-VN and YY1-VC) exhibited distinct foci present in the nuclei.

I next conducted additional experiments to determine whether this multimerisation was specific for damage. To this end, I first stained for γ H2AX in cells expressing YY1-BiFC foci to determine whether these foci were co-localized with sites of damage. No such co-localization was observed (Figure 3.10), although cells were allowed to recover for approximately 2 h prior to fixation, providing sufficient time for proteins to localize to the damage sites. Therefore, I subsequently utilised laser micro-irradiation to induce damage, because this method allows greater precision in monitoring recruitment (Figure 3.11). These experiments revealed that YY1 foci were not localized to the damage sites. In combination with the previous results, these observations led to the conclusion that YY1 represents a constitutively multimeric protein but that this multimerisation is not specific to its role in DSB repair.

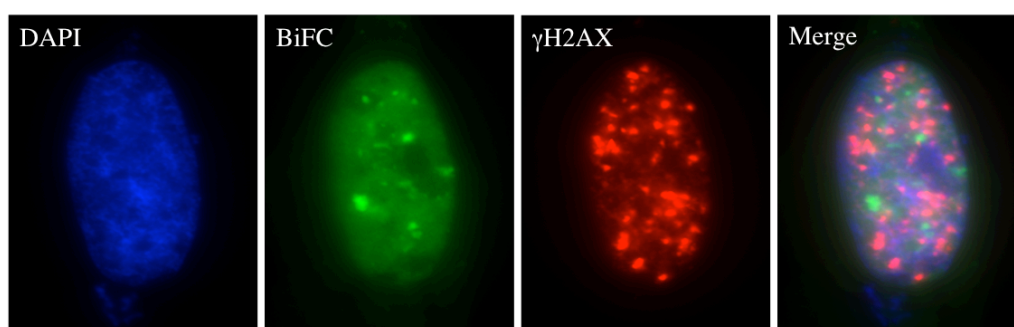


Figure 3. 10 Lack of YY1-BiFC foci co-localization with γ H2AX foci.

U2OS cells were co-transfected with YY1-VN and YY1-VC, irradiated with 5Gy of γ -IR, left to recover for 2 h, fixed with 4% PFA, and stained with anti- γ H2AX antibody. Stained cells were analysed by a fluorescence microscope.

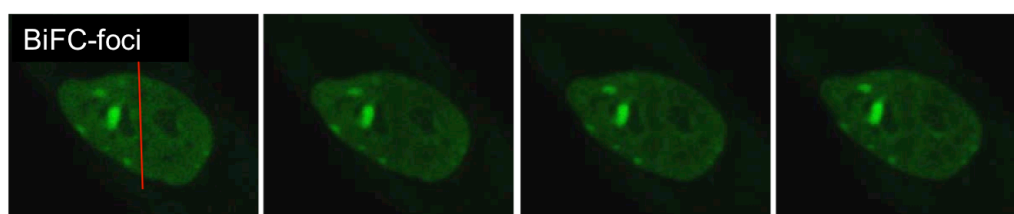


Figure 3. 11 Laser micro-irradiation treatment of U2OS cells co-transfected with YY1-VN and YY1-VC. The red line indicates the laser path.

To address the possible function of YY1 as a component of a branch-migration enzyme, it was necessary to determine whether the oligomeric YY1 associates with RUVBL2 *in vivo*. To address this issue, I again utilised the BiFC assay. Specifically, I cloned RUVBL2 into a BiFC vector that encoded the C-terminal domain of Venus (Figure 3.12A), as confirmed by sequencing of the resultant plasmid by GATC Biotech. U2OS cells were transfected with both YY1_VN and RUVBL2_VC, and the transfectants were subjected to the same conditions described previously (see section 3.2.1). Although large BiFC foci were observed in the positive control (YY1_VN+YY1_VC) as previously described as well as a pan-nuclear fluorescence in the negative control (transfected with empty vectors VN+VC) (Figure 3.12B), no foci nor fluorescence signal of any kind were detected in cells transfected with YY1_VN and RUVBL2_VC (Figure 3.12B), suggesting that these proteins might not associate physically. However, as previously described, a negative finding from this assay does not conclusively rule out the possibility of YY1 and RUVBL2 interaction. Additionally, the *in vitro* interaction of YY1 and RUVBL1-RUVBL2 (Figure 3.5) and the *in vivo* co-operative function of YY1 and RUVBL2 (Figures 3.6 and 3.8) support the possibility the observed result (Figure 3.12B) is due to a technical limitation of this assay.

To summarize, the results presented above demonstrate that YY1 forms a multimer *in vivo* regardless of its function in HR. Although a physical association of YY1 and RUVBL2 *in vivo* could not be confirmed, the HR foci data indicate that the functions of these proteins are similar. Notably, this similarity might be due to their activities as components of the INO80 complex rather than as a homolog of the bacterial branch-migration enzyme RuvA.

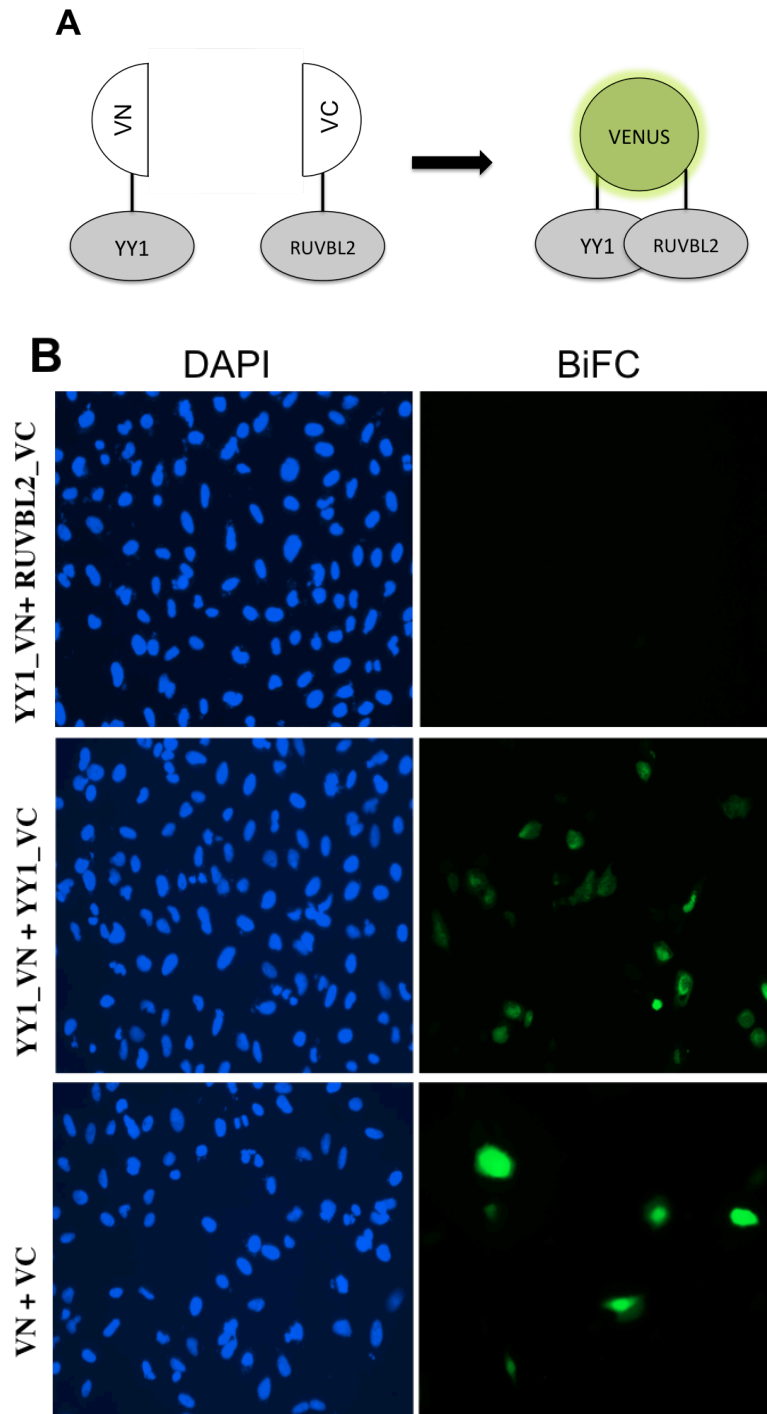


Figure 3. 12 *In vivo* association between YY1 and RUVBL2 was not detected.

(A) Schematic illustrating the cloning strategy used, wherein the coding sequences of YY1 and RUVBL2 were cloned into the N-terminal (YY1_VN) and the C-terminal (RUVBL2_VC) domains of Venus, respectively. (B) U2OS cells transiently co-transfected with plasmids expressing the fusions in A were analysed by fluorescence microscopy. Co-transfection of YY1-VN with YY1-VC was used as a positive control, whereas co-transfection with the two empty vectors VC+VN was used as a negative control. Cells co-transfected with YY1-VN and RUVBL2-VC failed to express any fluorescence compared to either the positive control exhibiting BiFC foci, or the negative control displaying pan-nuclear fluorescence. Images were taken using the EVOS® FL microscope, scale bars = 250 μ m.

3.3 Discussion

This chapter aimed to characterize the biochemical features and the function of the human YY1 protein *in vitro* and *in vivo*. We showed that human YY1 exists as multimers *in vitro* and *in vivo* and we provide a deeper characterization of its architecture. In addition, we demonstrated that YY1 associates with the RUVBL1-RUVBL2 *in vitro* and *in vivo* and that this association is essential to promote its binding to different DNAs and to perform its function in HR to potentially promote RAD51 filament formation. However, we have insufficient evidence to determine whether YY1 is a human homolog to the bacterial RuvA protein.

3.3.1 Human YY1 is a multimeric protein

Our findings confirmed the previously reported multimerisation feature of human YY1 (Wu et al., 2007). More precisely, the biochemical and structural characterisation of purified His-YY1 and Strep-II-YY1 revealed that human YY1 assembles as dimers that can associate into larger oligomeric complexes. Furthermore, we also provided *in vivo* evidence for the multimerisation of human YY1 (see sections 3.2.1 & 3.2.2). Although the crystal structure of YY1 revealed in 1997 provided essential information about its C₂H₂-type zinc-finger motifs that regulate its transcriptional activity, little was known regarding the structure of the YY1 oligomeric form. Here, we characterized the structural organization of the YY1 oligomers for the first time using EM (see section 3.2.2). Previously, two type of RuvA-DNA complexes have been reported: 1) complex I, wherein a single tetramer binds to one side of the open junction structure, and 2) complex II, consisting of two tetramers that together form octomeric RuvA, wherein the two tetramers sandwich the HJ DNA in the centre and form the octomer (Yamada et al.,

2004). This corresponds with our results, which suggest that the human YY1 consists of two dimers, each built up of oligomers that might contain 2 or 4 identical subunits according to the SEC data (López-Perrote et al., 2014). Despite the fact that we could not confirm the exact number of these oligomers, the overall structure of complex A (Figure 3.3) obtained by EM showed a very similar architecture to the tetrameric bacterial RuvA protein structure that was established by Mayanagi et al. (2008) as part of the RuvA-RuvB/HJ-DNA complex (Figure 3.13). The analysed structure of complex A revealed a square-shaped molecule with a low-density region at its centre (Figure 3.3A); this region might indicate the location where the single tetramer binds to one side of the open junction. In comparison, complex B was revealed as an elongated structure that is approximately double the size of complex A, and might represent the octomeric form of YY1 similar to RuvA complex II. Although it is highly likely that this similarity in the structure reflects homogeneity between the human YY1 and the bacterial RuvA, more evidence is required to confirm this conjecture. For example, it might be necessary to characterise the structure of the whole complex, i.e., the YY1-RUVBL1-RUVBL2/HJ-DNA complex, by EM to confirm that this complex represents the human homolog of the bacterial HJ branch-migration enzyme, similar to the one established by Mayanagi et al. (2008), i.e., the RuvA-RuvB/HJ-DNA complex.

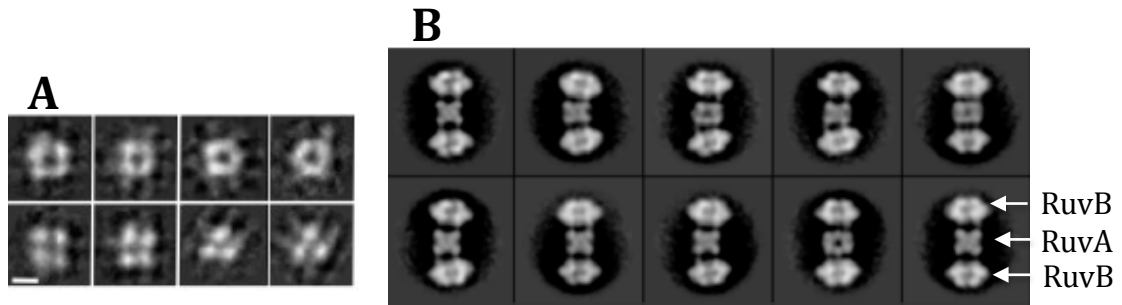


Figure 3.13 Comparison between the structure of YY1 complex A and tetrameric RuvA.

(A) 2D reference-free averages of complex A of His-YY1 show a typical square shape (from López-Perrote et al., 2014). (B) Electron microscopic images of the RuvA/RuvB/Holliday junction DNA complex. The tetrameric RuvA in the centre is tethered to RuvB hexameric rings on either side (from Mayanagi et al., 2008).

3.3.2 YY1 association with RUVBL1-RUVBL2 enhances its ability to bind several types of DNA

The C-terminal region of the YY1 protein contains C_2H_2 type zinc finger motifs that characterize its function as a transcription factor, as these motifs are capable of binding to a consensus DNA sequence [5'-(C/g/a)(G/t)(C/t/a)CATN(T/a)(T/g/c)-3'] found at the promoters of genes (Houbaviy et al., 1996). Previous work using DNA substrates containing the consensus sequence (Wu et al., 2007), however, only showed the ability of YY1 to bind DNA in the context of its transcriptional function. Our findings, in contrast, demonstrated that the oligomeric form of YY1 is able to bind *in vitro* to dsDNA containing the consensus sequence as well as to dsDNA without the consensus sequence, HJ, and ssDNA (see section 3.2.3). This suggested that YY1 functions in a distinct pathway from its transcriptional activity by binding to DNAs in the absence of the consensus sequence. In addition, the varied binding ability was identified using the oligomeric rather than the monomeric form of YY1, potentially suggesting that the

oligomeric status of YY1 is responsible for promoting its ability to support disparate DNA binding. This assumption, however, requires further testing for confirmation.

Additionally, our collaborator showed that YY1 preferentially binds the RUVBL1-RUVBL2 complex through interacting with RUVBL1 rather than RUVBL2 (see section 3.2.3). This is partially in agreement with a previous study that reported a direct interaction between YY1 and each of RUVBL1 and RUVBL2 (Wu et al., 2007). Our collaborator, however, were unable to identify such an interaction with RUVBL2 even in reaction with higher protein concentrations (López-Perrote et al., 2014). One possible explanation is that YY1 might interact with the RUVBL1-RUVBL2 complex through direct interaction with only the RUVBL1 protein. However, the finding of Wu et al. (2007) that YY1 interacts *in vitro* with RUVBL2 does not support this prediction. Therefore, RUVBL2 might also interact with YY1 albeit with lower affinity than observed for YY1-RUVBL1, being below the level of detection in the conditions used by our collaborator. Alternately, the oligomeric form utilized by our collaborator might not allow the detection of such an interaction *in vitro*. Therefore, parallel experiments using both forms of YY1; i.e, monomeric and oligomeric forms, might help to resolve this discrepancy.

Notably, regardless of the precise state of the interaction between YY1 and RUVBL1 and RUVBL2, the presence of RUVBL1-RUVBL2 as a whole complex positively shifted the affinity of YY1 towards binding all types of DNA. Previously, it has been reported that YY1 in its role as a transcription factor is able to direct the transcription initiation of the P5 promoter by first assembling the YY1-DNA complex, which then facilitates the recruitment of transcription factor IIB (TFIIB) to form a more stable complex; the YY1-TFIIB-DNA complex in turn recruits pol II to the promoter (Usheva

& Shenk, 1996). In similar manner, the YY1-DNA complexes formed by YY1 oligomers binding to various types of DNA might then target the RUVBL1-RUVBL2 complex to form a functional YY1-RUVBL1-RUVBL2-DNA complex, which in turn might either function as an independent complex or facilitate further recruitment of other proteins/complexes such as the INO80 complex or DNA repair proteins. In comparison, in fission yeast the recruitment of the Ino80 complex to a target gene is mediated by interaction with Iec1, which contains zinc finger motifs similar to those of YY1 (Hogan et al., 2010). Thus, validation of this predicted model appears to be a worthy topic of future studies.

3.3.3 YY1 co-operates with RUVBL2 to promote HR

It has been reported that YY1 functions during HR as part of the INO80 complex, potentially through binding HJs and promoting their branch migration (Wu et al., 2007). The finding by our collaborator that RUVBL1-RUVBL2 enhanced the ability of YY1 to bind HJ *in vitro* (López-Perrote et al., 2014) supports the potential role for the YY1-RUVBL1-RUVBL2 complex in HR. However, we found that depleting the respective subunits yielded no impact on DSB repair as measured by the number of γ H2AX foci as a marker for DSBs even after 8 h of recovery (Figure 3.6B). These findings, on the other hand, do not necessarily rule out a potential role for YY1 and RUVBL2 in HR, as it is highly likely that cells may have chosen another pathway to repair the damage, thus leading to an unaltered DSB readout.

Previously, only two studies have focused on the involvement of INO80 in HR (Gospodinov et al., 2008, 2011); however, these yielded conflicting results, demonstrating in the first instance that RUVBL1 and RUVBL2, which are subunits of

INO80 and other chromatin-remodelling complexes such as TIP60, are required for formation of RAD51 foci. However, the authors attributed this role to TIP60 rather than INO80, based on the restoration of the defect in RAD51 foci by treatment with a histone deacetylase inhibitor (sodium butyrate), which mimics the role of TIP60 in acetylation and relaxation of chromatin. In contrast, the same authors reported in 2011 that INO80 depletion reduced HR efficiency (approximately 2-fold) and caused defects in both the recruitment of an essential repair protein, 53BP1, and in resection; however, no defect was observed in the formation of RAD51 foci. Here, it could be argued that because HR is achieved by a series of dependent steps, an upstream defect should have affected the downstream steps, especially given the observed 2-fold defect in HR level. In contrast, in our study we observed a defect in RAD51 with no obvious defect in RPA foci in the absence of RUVBL2, YY1, RUVBL2, and YY1, or of both RUVBL2 and INO80 (Figure 3.6C&D). However, this discrepancy might be attributable to differences in study design such as the choice of cell lines or the method of counting, as Gospodinov et al. (2011) counted the number of cells with foci, whereas we counted the number of foci per cell (see Figure 1.3B–D). In addition, the studies used different methods to induce DSBs (IR vs. MMC), which might also have caused the differences in the observed outcomes. Notably, we counted only G2 cells, owing to the specific involvement of HR in the repair of DSBs in heterochromatin areas (Shibata et al., 2011), wherein a role for a chromatin remodeller such as INO80 would be obvious. Finally, we also confirmed that the defect in RAD51, particularly in RUVBL2-depleted cells, is related to its activity as a member of the INO80 complex. Specifically, we showed that a double knockdown of RUVBL2 and either of two INO80 subunits, INO80 or YY1, exhibits a phenotype identical to those of the respective single knockdowns. This observation seriously challenges the claim in Gospodinov et al.

(2008) that the defects might be attributed to TIP60 rather than INO80. Furthermore, our SCE data (Figure 3.8) might suggest that the conflict between our results and those of previous reports as related to the RAD51 foci phenotype arises solely from the depletion of YY1 and RUVBL2 rather than being due to specificity to G2 cells or DSBs induced by IR, as in these experiments we induced DSBs by treating cells with MMC and counted the final outcomes of HR.

Notably, the results from a recent study by the Jackson laboratory, published subsequently to our findings (López-Perrote et al., 2014; Nishi et al., 2014), fit to some extent with our data. Therein, it was demonstrated that depletion of the INO80 complex or its YY1 or RUVBL1 subunits resulted in a mild defect in resection upon treatment with camptothecin, as reflected by a reduction in the intensity of BrdU incorporation (ssDNA) rather than the number of foci (Nishi et al., 2014). This suggests that our experimental method may have prevented us from observing such a mild defect. Additionally, the same group observed a reduction in RAD51 foci caused by the absence of YY1 and UCHL5 (a subunit of human INO80). Thus, a mild defect in resection may have caused the observed defect in the subsequent formation of RAD51 foci. If so, the question arises as to how YY1 and RUVBL1/2 may function during resection. I suggest that the following features of these proteins might be useful in developing a relevant model: 1) YY1 in its role as a transcription factor facilitates DNA strand separation during initiation (Usheva & Shenk, 1996), and 2) the ssDNA binding domain of RUVBL1 and RUVBL2 is similar to that of RPA (Matias et al., 2006). Thus, one hypothesis might be that YY1-RUVBL1-RUVBL2 may function during resection by forming the functional complex YY1-RUVBL1-RUVBL2-DNA as previously predicted (see section 3.3.2), in which YY1 binds to dsDNA (i.e., to the broken ends)

and functions to facilitate DNA strands separation. Simultaneously, the YY1-DNA might promote recruitment of RUVBL1-RUVBL2, which in turn may bind to the resultant ssDNA to stabilize the 3' overhang generated by MRN-CtIP either before or during RPA loading. In addition, the YY1-RUVBL1-RUVBL2-DNA complex might facilitate further recruitment of essential DSB repair proteins such as BRCA2. Alternately, this complex might utilize the ATPase activity of RUVBL1/2 to allow for further relaxation of the chromatin either during this step or upon HJ binding. Conversely, another possibility may be that YY1 is only involved in extensive resection by facilitating EXO1 recruitment, as it has been reported that co-depletion of YY1 and UCHL5 caused a reduction in EXO1 but not CtIP recruitment (Nishi et al., 2014). However, it is possible that the observed defect in RAD51 foci is a consequence of the mild defect in the intensity of RPA foci, or because these proteins function to promote or stabilize the RAD51 filament. To differentiate and substantiate these models, additional studies will be required.

3.3.4 Lack of *in vivo* evidence for homology between YY1, a human subunit of the INO80 complex, and RuvA, a bacterial subunit of the branch-migration enzyme

HR is an essential process that plays fundamental roles in DSB repair, resumption of stalled replication forks, or gene rearrangement in meiosis (Krejci et al., 2012). HJ is an essential final step in HR to effect efficient repair. In prokaryotes, the complex RuvAB promotes branch migration whereas the endonuclease RuvC resolves the junction (Yamada et al., 2004). X-ray structure and EM analyses of the RuvA-DNA complex demonstrated that the N-terminal domains I and II of RuvA are required for recognition of the HJ, whereas the C-terminal domain III is required to target RuvB hexameric rings

(mammalian homologs: RUVBL1-RUVBL2) on either side of RuvA (Yamada et al., 2004). As discussed above, on the one hand, our results suggest the YY1 protein as a strong candidate to represent a human homolog of bacterial RuvA based on the structure and the ability of YY1 to bind HJ and RUVBL1-RUVBL2 *in vitro*. On the other hand, our *in vivo* results, which not only showed that YY1 associates with RUVBL2 in HR as part of the INO80 complex but also that these proteins demonstrated no additive function in SCE, diminishes the possibility of such homology. This is because if YY1 is the human homolog to RuvA, its main function should be to facilitate HJ branch migration, and, consequently, a noticeable impact should be observed in the number of SCE in the absence of such a function, i.e., in the absence of YY1 and RUVBL2. In a final attempt to obtain *in vivo* evidence for homogeneity between YY1 and RuvA, we examined the response of the multimeric YY1 form to DSBs induced by IR. However, our results (see section 3.2.6), suggested that although YY1 is a multimeric protein, co-localization to sites of damage did not occur. Furthermore, we were unable to show an *in vivo* association between YY1 and RUVBL2 (Figure 3.12). Whereas we suggest that this negative finding is highly likely to represent a limitation of the BiFC method, as in some cases even bona fide interactions cannot be detected therewith (Shyu et al., 2008; Kerppola, 2008). The RUVBL1-RUVBL2 complex comprises two hexameric rings, each formed from alternating subunits (López-Perrote et al., 2012). Therefore, YY1 might only interact directly with RUVBL1 rather than RUVBL2. However, further data are needed to determine whether YY1 is the functional ortholog of RuvA.

Chapter 4.

Removal of H2AZ by INO80 promotes
homologous recombination

4.1 Introduction

INO80 is an ATPase chromatin-remodelling complex comprised of multiple subunits and belongs to the INO80 family, which defined by a characteristic insertion in the ATPase domain. The yeast Swr1 and human p400 and SRCAP proteins are also members of the INO80 family. Notably, members of this family are capable of histone exchange (Seeber et al., 2013). In particular, the exchange of histone H2AZ, a histone variant of the core histone H2A, is controlled by INO80 family proteins. In yeast, Swr1 functions as part of the SWR complex to regulate the removal of H2A and incorporation of histone H2AZ into chromatin (Krogan et al., 2003; Kobor et al., 2004; Mizuguchi et al., 2004), whereas in mammals SRCAP (Ruhl et al., 2006) and p400 (as part of TIP60) (Xu et al., 2012) are responsible for the equivalent reaction. However, the reverse reaction, i.e., removal of H2AZ and incorporation of H2A, is catalysed by INO80 in yeast (Papamichos-Chronakis et al., 2011). Conversely, no evidence has been provided to indicate that the mammalian INO80 contributes in H2AZ removal from chromatin; instead, a histone chaperone, ANP32E, has been recently found to remove H2AZ from chromatin in mammals (Mao et al., 2014; Obri et al., 2014).

Incorporation of H2AZ into damaged chromatin has been found to be critical for DSB repair in mammals (Xu et al., 2012). Upon the induction of DSBs, H2AZ accumulates at the damaged site in a similar pattern to that of γ H2AX but with less enrichment, spreading on either side of the DSBs for approximately 10–50 kb along the chromatin. Notably, the incorporation of H2AZ at DSBs by p400 (as part of TIP60) has been found to restrict resection, wherein the absence of H2AZ causes an increase in the number of RPA foci and ssDNA. Furthermore, H2AZ incorporation was shown to be critical for NHEJ repair, as its absence resulted in the loss of KU70/80 and a decrease in NHEJ

efficiency. Conversely, the inhibition of resection by silencing CtIP in H2AZ-depleted cells rescued the defects of KU70/80 recruitment and NHEJ (Xu et al., 2012). Thus, this study clearly demonstrated that H2AZ incorporation into damaged chromatin is critical for DSBs repair, specifically the NHEJ pathway. However, whether the H2AZ removal reaction is also vital for DSB repair has not yet been established.

Substantial evidence from yeast (Downs et al., 2004; Morrison et al., 2004; Van Attikum et al., 2004) and mammals (Gospodinov et al., 2008, 2011; Kashiwaba et al., 2010) has confirmed the involvement of INO80 in HR repair, although the exact mechanism affected by INO80 in this repair pathway has remained unclear. This capacity, together with the well-known function of yeast INO80 in regulating the removal of H2AZ from chromatin (Papamichos-Chronakis et al., 2011) and the established evidence for the critical role of H2AZ incorporation in DSB repair (Xu et al., 2012) led us to formulate the hypothesis that INO80 might promote HR by removing H2AZ to allow resection. To test this hypothesis, we aimed to address two main questions in this chapter; first, whether human INO80 is involved in the removal of histone H2AZ from damaged chromatin as is observed in yeast; and second, whether the removal reaction of histone H2AZ is also critical for HR (Alatwi & Downs, 2015).

4.2 Results

4.2.1 H2AZ dynamics at sites of damaged chromatin

ChIP data from human cells has revealed that H2AZ accumulates to the sites of DSBs (Xu et al., 2012). To illustrate the dynamics of the histone variant H2AZ at sites of damaged chromatin, U2OS cells were transfected with the GFP-H2AZ expression construct and laser micro-irradiation was utilised to induce damage after 24 h, followed by live cell imaging to monitor the accumulation of H2AZ at damaged DNA. H2AZ was found to accumulate at damaged sites within seconds (Figure 4.1A); however, the incorporated H2AZ was then rapidly removed from the sites of DNA damage, as indicated by the return of the fluorescence signal intensity to pre-damaged levels within approximately 3 minutes (Figure 4.1A&C).

To determine whether the mammalian INO80 is able to facilitate the removal of H2AZ from chromatin as shown for yeast INO80 (Papamichos-Chronakis et al., 2011), we attempted to monitor the accumulation of H2AZ at sites of damaged chromatin in the absence of INO80. Towards this end, INO80 was depleted in U2OS cells using siRNA; then, after 24 h, the cells were transfected with GFP-H2AZ and laser micro-irradiated the following day. Live cell imaging demonstrated that in INO80-depleted cells, H2AZ was able to accumulate normally, with no obvious differences compared to the control. However, the removal of H2AZ was significantly slower in INO80-depleted cells compared to the control (Figure 4.1B&C). This result clearly showed that the removal of H2AZ from damaged chromatin is at least partially dependent on INO80, whereas H2AZ incorporation is INO80-independent.

Next, in order to support our finding and to confirm that the observed fluorescent signal reflected an actual accumulation of H2AZ after the induction of damage by laser micro-irradiation, the behaviour of histone H2B in U2OS cells transfected with a GFP-H2B expression construct was determined using live cell imaging after applying the same conditions previously utilised for monitoring H2AZ accumulation. As can be seen in Figure 4.2, no detectable signal was observed at the sites of DNA damage, indicating that the behaviour of H2B differed from that of H2AZ.

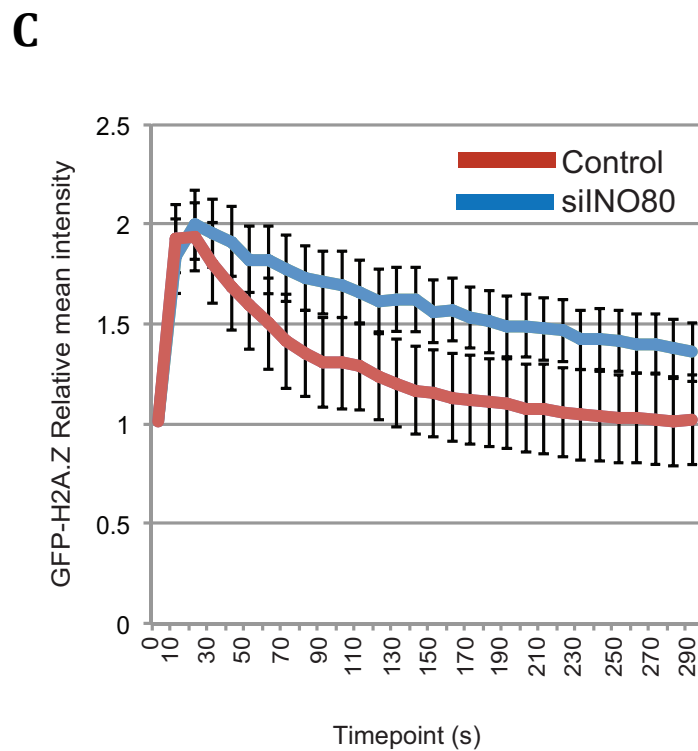
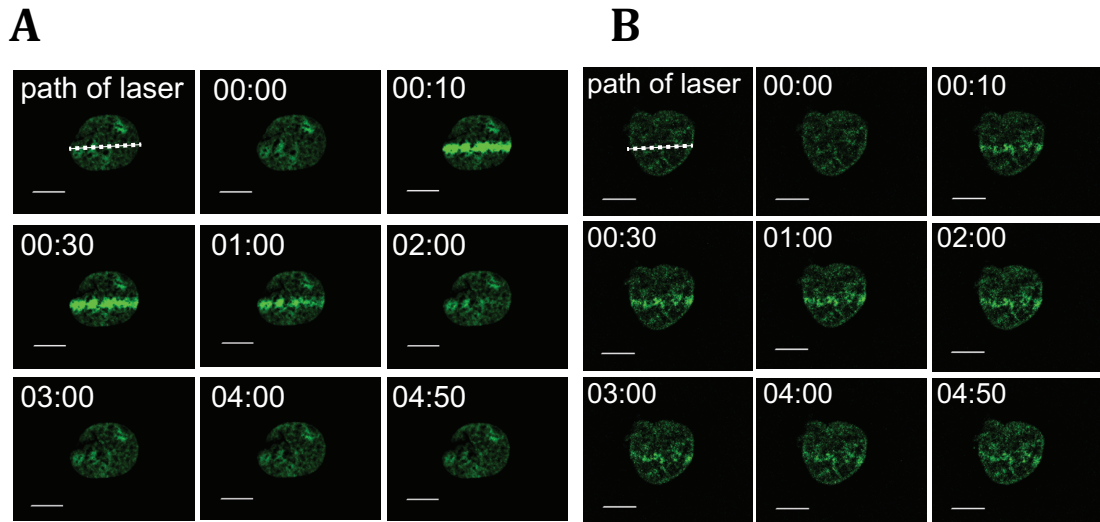


Figure 4. 1 H2AZ dynamics at sites of damaged chromatin.

(A) H2AZ is rapidly incorporated and removed from damaged DNA. (B) H2AZ dynamics at sites of damaged chromatin in siNO80 cells. In (A) & (B), U2OS cells were transfected with GFP-H2AZ, laser micro-irradiated, and captured by live cell imaging; the laser path and time points are shown. (C) Quantification of relative mean fluorescence intensity in control and siNO80 cells from three independent experiments. A minimum of 10 cells were monitored per experiment; error bars represent \pm SD. Scale bars = 10 μ m.

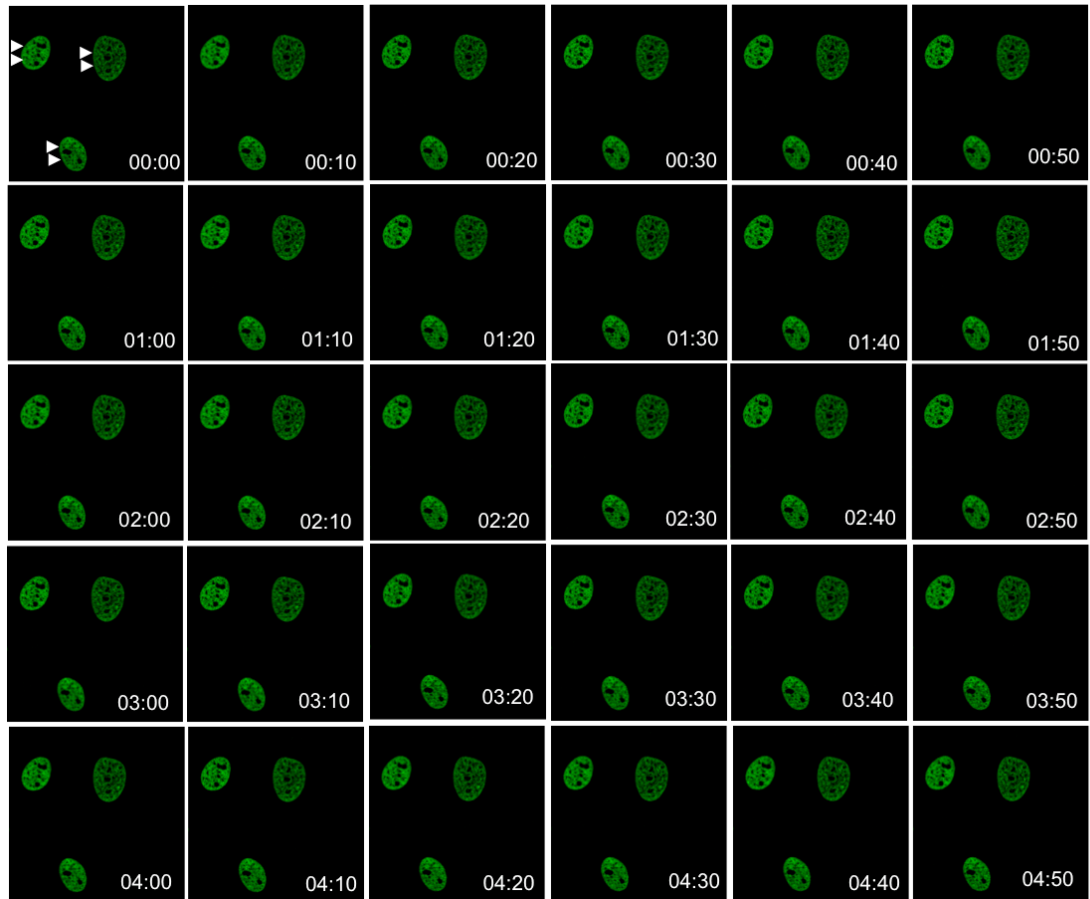


Figure 4. 2 H2B dynamics at sites of damaged chromatin.

U2OS cells transfected with GFP-H2B were laser micro-irradiated and captured by live cell imaging; time points and arrowheads indicating laser paths are shown.

4.2.2 RUVBL2, a subunit of INO80, accumulates at the sites of damaged chromatin

INO80 has been shown to accumulate at DNA DSBs by ChIP (Gospodinov et al., 2011). Here, the dynamics of the INO80 subunit RUVBL2 at damaged DNA were examined using live cell imaging, for which U2OS cells were transfected with a GFP-RUVBL2 expression construct and then laser micro-irradiated after 24 h to allow for gene expression. The accumulation of RUVBL2 at sites of damage was monitored by live cell imaging for approximately 30 minutes. As can be seen in Figure 4.3, RUVBL2 accumulated at the damaged chromatin and remained for at least 20 minutes after damage, in agreement with the previous finding by Gospodinov et al. (2011).

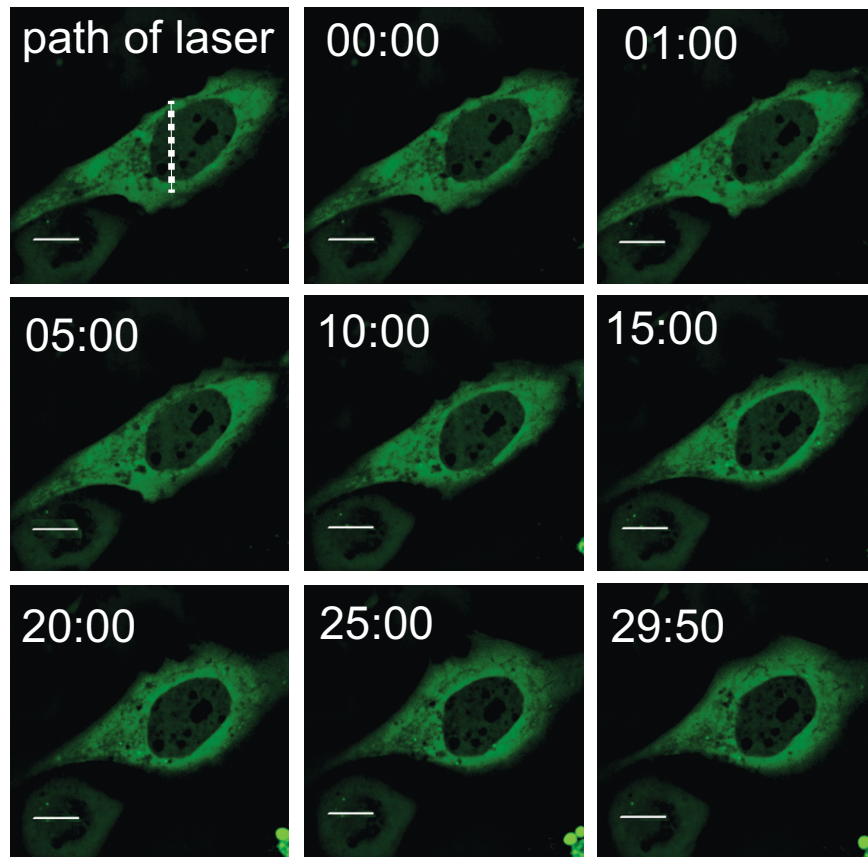
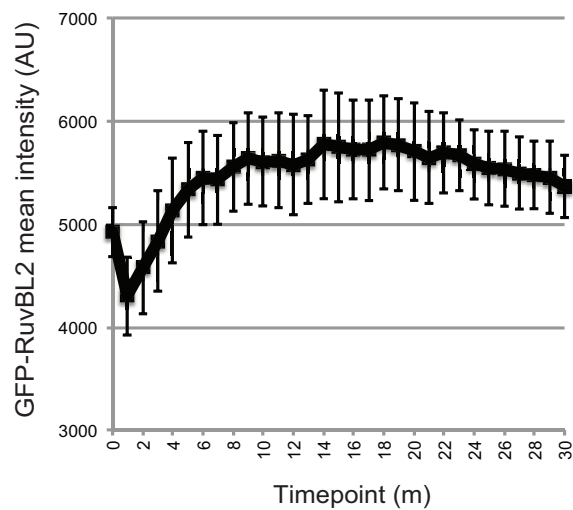
A**B**

Figure 4. 3 RUVBL2 accumulation at sites of damaged chromatin.

(A) U2OS cells transfected with GFP-RUVBL2 were subjected to laser micro-irradiation and captured by live cell imaging; the laser path and time points are shown. (B) Quantification of mean fluorescence intensity at sites of damaged DNA from three independent experiments; error bars show \pm SD. Scale bars = 10 μ m.

4.2.3 H2AZ is a barrier for resection

As mentioned in Chapter 3, we have found that the contribution of INO80 to HR in mammalian cells may occur through the promotion of RAD51 filament formation (López-Perrote et al., 2014). To investigate whether the role of mammalian INO80 in the removal of H2AZ from damaged chromatin (Figure 4.1) contributed to the HR pathway, A549 cells were transfected with siINO80, siH2AZ, or both knockdown constructs (Figure 4.4A). As previously described, these cells were then exposed to 3 Gy γ -IR to induce DSBs and fixed at 0 h (i.e., before damage) and after 2 h. Next, the cells were stained for γ H2AX, a marker for DSBs, and RPA as a readout for ssDNA formation. To restrict our analysis to G2 cells, CENP-F staining was used to mark G2 cells and only CENP-F-positive cells were counted (Figure 4.4C). In addition, to ensure that the only cells analysed were those in G2 at the time of IR, aphidicolin was added to the cells prior to IR to arrest S-phase cells and prevent them from progressing to G2 (Beucher et al., 2009; Shibata et al., 2011).

Depletion of INO80 and H2AZ did not cause any further DSBs, as no added defect in the number of γ H2AX signals was observed at 0 h, prior to the induction of DSBs by IR, compared to the control. Furthermore, cells lacking INO80 and H2AZ were not sensitive to IR, as the level of DSBs at 2 h after exposure to 3Gy γ -IR also did not differ from that of the control. At 8 h post IR, the number of γ H2AX signals decreased 2-fold, suggesting that the cells managed to repair some of the induced damage. However, the similar response between control and knocked-down cells at 8 h post IR suggested that in the absence of INO80 and H2AZ the cells were able to repair the damage by another repair pathway (Figure 4.4B).

In addition, the lack of either INO80 or H2AZ did not cause any obvious defect in the number of RPA foci prior to the induction of DSBs by IR (Figure 4.4C), indicating that the absence of these proteins *per se* did not affect resection or induce further damage to the dsDNA. Furthermore, after 2 h of inducing DSBs by IR, no obvious defect was observed on resection, i.e., the number of RPA foci, in INO80-depleted cells compared to the control (Figure 4.4C), although the depletion of H2AZ caused a significant increase in the number of RPA foci (Figure 4.4C). This result is consistent with the previous findings of Xu et al. (2012), which showed that H2AZ incorporation is required for accurate resection and that the absence of H2AZ leads to the occurrence of uncontrolled resection. Notably, the co-depletion of INO80 in cells lacking H2AZ resulted in a decrease of the number of RPA foci to a level approximating that of the control (Figure 4.4C), potentially suggesting that INO80 has a role in resection although this could not be observed directly using the current method.

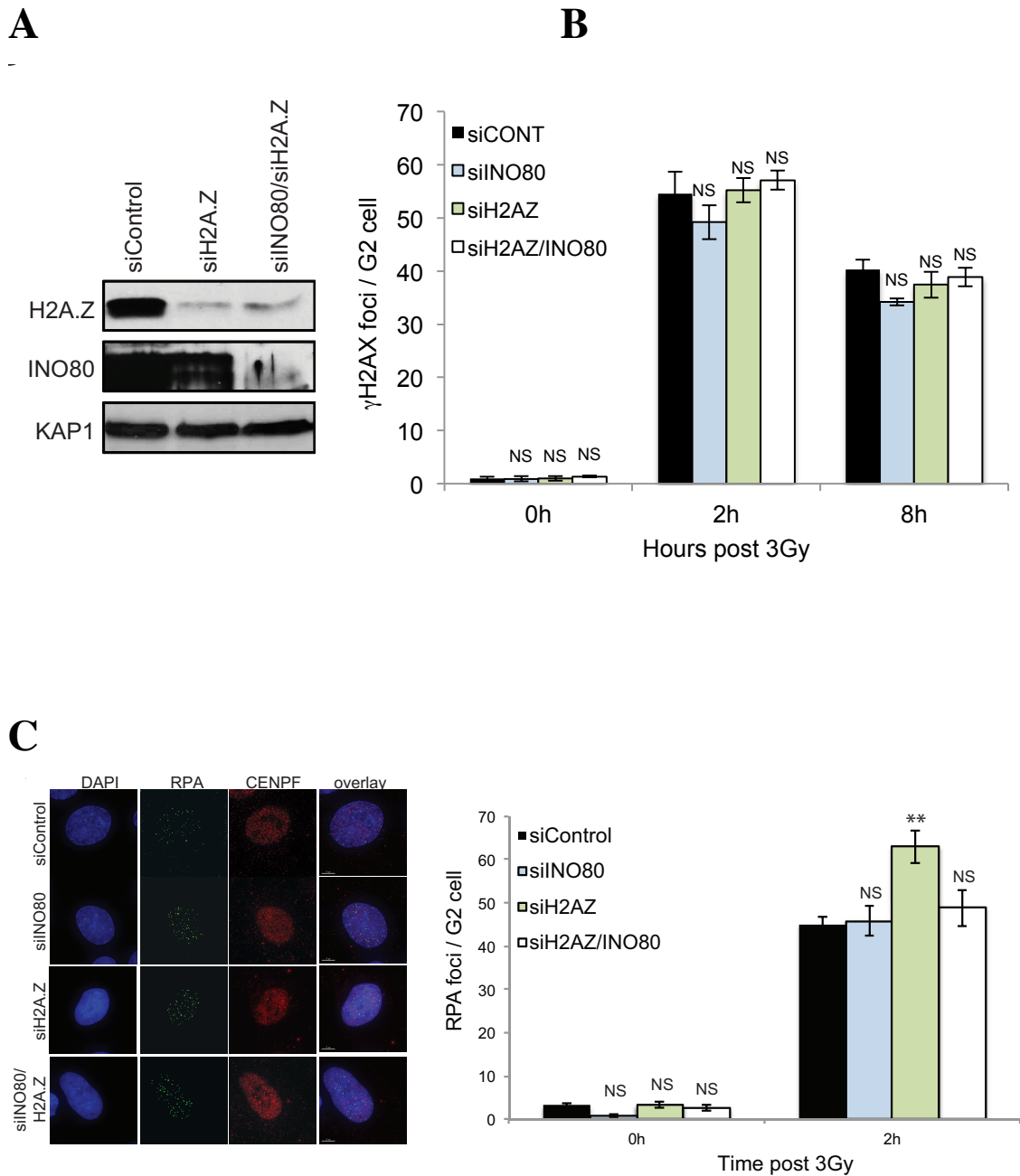


Figure 4. 4 H2AZ acts as a barrier for resection.

(A) Western blotting demonstration of the efficiency of siRNA knockdown. KAP1 was used as a loading control. (B) IR induction of γ H2AX foci in A459 cells treated with siRNAs. (C) IR induction of RPA foci in A459 cells treated with siRNAs. Left panel: representative images at 2h post exposure to 3 Gy of γ -IR, right panel: quantification of the means of foci from three independent experiments; error bars show \pm SD. P values were determined by Student's t-test, and samples were compared with control cells. $**P \leq 0.01$, N.S., not significant. Scale bars = 5 μ m.

4.2.4 Cells lacking SRCAP exhibit a resection defect

To validate the role of INO80 in resection observed by ourselves and others (Gospodinov et al., 2008, 2011), as we observed no obvious defect in its absence while others reported a defected resection phenotype, a control experiment was designed to test whether the observed resection phenotype by us represented an artefact related to the utilised methodology or was specific to the absence of INO80 and its subunits. Towards this end, SRCAP was used as a control for resection. SRCAP represents an ATPase chromatin remodeller that has been recently found to promote resection by promoting the accumulation of CtIP at DSBs (Dong et al., 2014). Accordingly, SRCAP was depleted singly and in conjunction with INO80 via siRNA in A549 cells using the method described in section 4.2.3, and followed by staining for RPA to monitor resection (Figure 4.5).

As expected, depletion of SRCAP caused a decrease in the number of RPA foci similar to that reported by Dong et al. (2014), validating this method as a means to detect resection deficits. However, the co-depletion of SRCAP and INO80 did not result in an additive defect (Figure 4.5). As depletion of INO80 alone (Figure 4.4B) also did not alter the number of observed RPA foci, this result further suggests that INO80 might not function in resection.

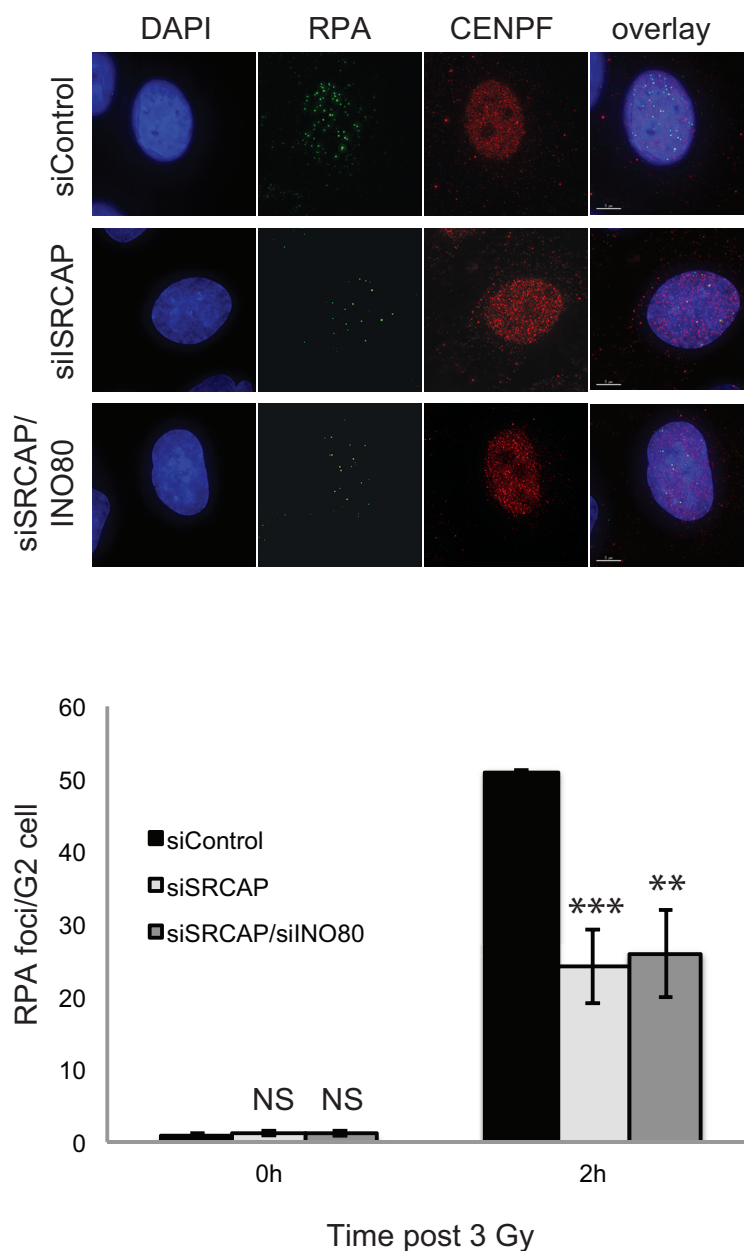


Figure 4. 5 Cells lacking SRCAP exhibit a resection defect.

IR induced RPA focus formation in A549 cells treated with siControl, siSRCAP, or siSRCAP/siINO80. Upper panel: representative images at 2h post exposure to 3 Gy of γ -IR. Lower panel: quantification of foci. Data represent the means of 3 independent assays \pm SD. P values were determined by Student's t-test, and samples were compared with control cells. *** $P = 0.0009$, ** $P = 0.002$, N.S., not significant. Scale bars = 5 μ m.

4.2.5 INO80 has a mild effect on resection

As a discrepancy existed regarding whether INO80 functions in resection that we had previously attributed to the different methodologies used to monitor resection (Discussion, Chapter 3), the results from different methods for monitoring resection were compared. To replicate the method previously used by the Jackson laboratory, which had resulted in the observation of a mild defect in resection in the absence of YY1, a subunit of human INO80 (Nishi et al., 2014), A549 cells lacking of several subunits (i.e., siINO80, siYY1, siH2AZ and siINO80/H2AZ cells) were treated with camptothecin (CPT) for 1 h and the number of cells with RPA foci was monitored. This approach allowed us to observe a modest but statistically significant defect in cells lacking either INO80 or YY1 (Figure 4.6), suggesting that INO80 may function to promote resection after the induction of DSBs, in contrast to the conclusions indicated in section 4.2.4.

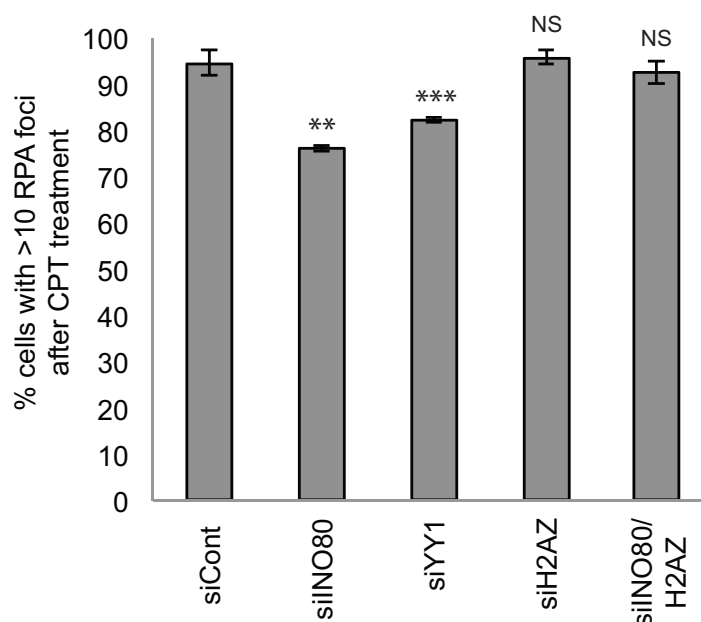


Figure 4. 6 Cells depleted for INO80 exhibit a mild defect in resection.

Quantification of RPA foci following 1 h of treatment with 1 mM camptothecin (CPT). Error bars represent \pm SD from three independent experiments. P values were determined by Student's t-test, and samples were compared with control cells. ** $P \leq 0.01$, *** $P \leq 0.001$, N.S., not significant.

4.2.6 Depletion of H2AZ rescues the RAD51 foci formation defect

Previously, we showed that the INO80 subunits YY1 and RUVBL2 promote the formation or stabilisation of RAD51 foci (López-Perrote et al., 2014). This was attributed to a component of the function of the whole complex, as co-depletion of these subunits along with the INO80 subunit resulted in no additive phenotype (Chapter 3; 3.2.4). In confirmation of these results, Figure 4.7 shows that the depletion of the INO80 subunit alone also resulted in a defect in RAD51 foci, which was similar to that observed in Chapter 3 (Figure 3.6).

However, as the aim of this chapter was to investigate the mechanism by which INO80 promotes RAD51 foci formation, it was hypothesised that the removal of H2AZ by INO80 might be a key step in this process. To test this conjecture, INO80 and H2AZ were co-depleted in A549 cells and the accumulation of RAD51 foci in G2 cells was analysed using method described previously to monitor RPA (section 4.2.3). Notably, the depletion of H2AZ in cells lacking INO80 rescued the defect in RAD51 foci formation in siINO80 cells (Figure 4.7). In addition, the loss of H2AZ alone caused a slight albeit statistically insignificant increase in the number of RAD51 foci (Figure 4.7), which might further influence the upstream increase in RPA foci observed in H2AZ-depleted cells (Figure 4.4B).

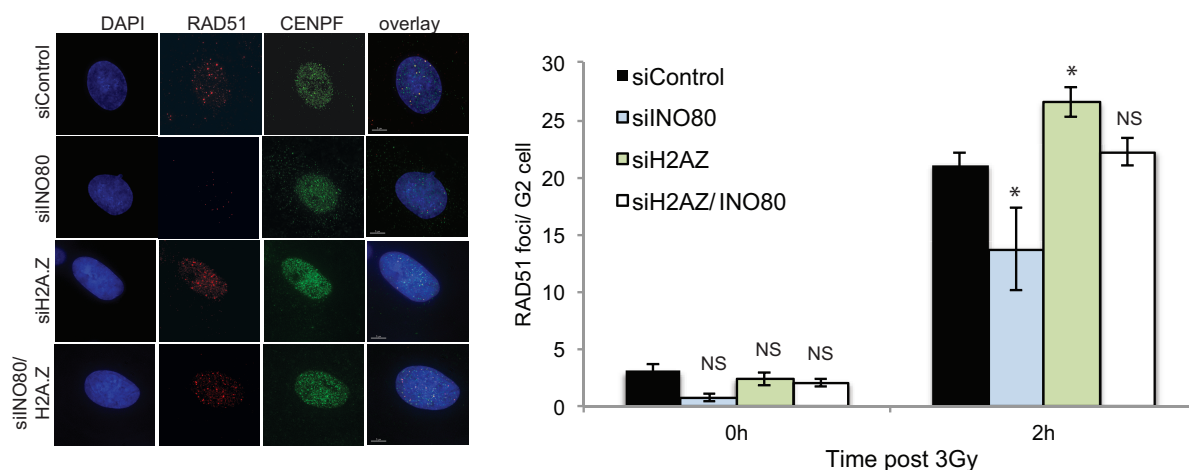


Figure 4. 7 INO80-depleted cells exhibit significant defects in RAD51 foci number that can be rescued by H2AZ depletion.

Left panel: representative images at 2h post exposure to 3 Gy of γ -IR; right panel: quantification of the means of foci from three independent experiments. Error bars show \pm SD. P values were determined by Student's t-test, and samples were compared with control cells. * $P \leq 0.05$, N.S., not significant. Scale bars = 5 μ m.

It was also noted from the SRCAP control experiment that the depletion of SRCAP resulted in a reduction in number of RAD51 foci (Figure 4.8), as had been observed previously and attributed to an upstream consequence of the defect in resection caused by the absence of SRCAP (Dong et al., 2014). However, co-depletion of INO80 and SRCAP did not result in any additive defect in the number of RAD51 foci beyond that observed upon single depletion of either subunit (Figure 4.8), suggesting that both INO80 and SRCAP might be required to promote RAD51 foci formation.

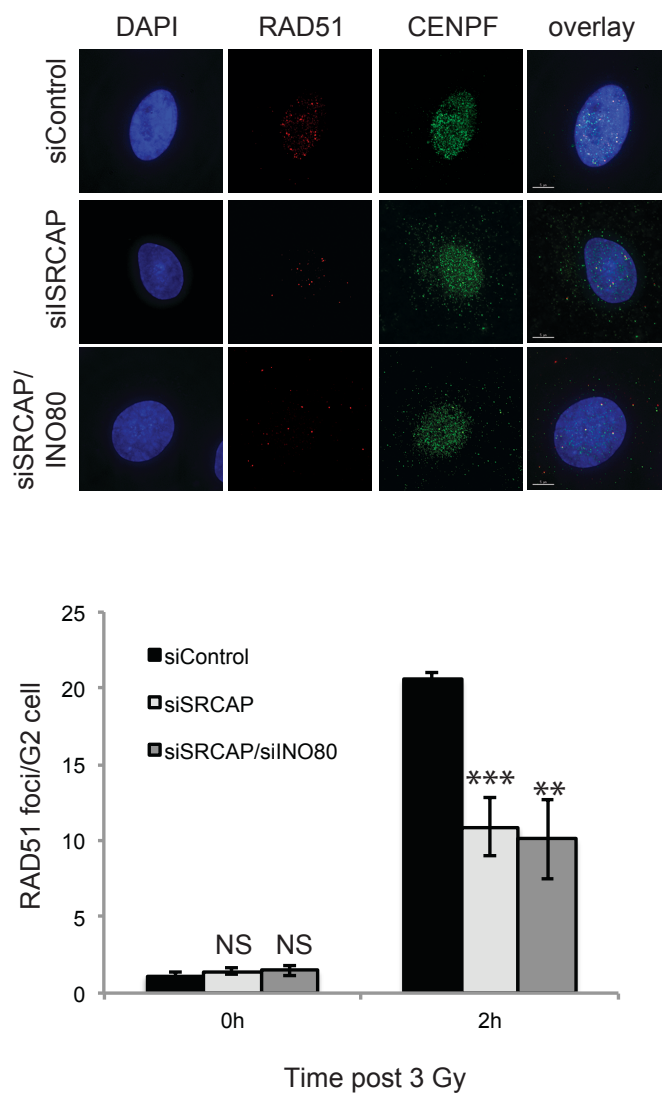


Figure 4. 8 SRCAP depletion causes a reduction in the number of RAD51 foci.

IR induced RAD51 focus formation in A549 cells treated with siControl, siSRCAP, or siSRCAP/siINO80. Upper panel: representative images at 2h post exposure to 3 Gy of γ -IR. Lower panel: quantification of foci. represent the means of 3 independent assays \pm SD. P values were determined by Student's t-test, and samples were compared with control cells. *** $P = 0.00098$, ** $P = 0.00248$, N.S., not significant. Scale bars = 5 μ m.

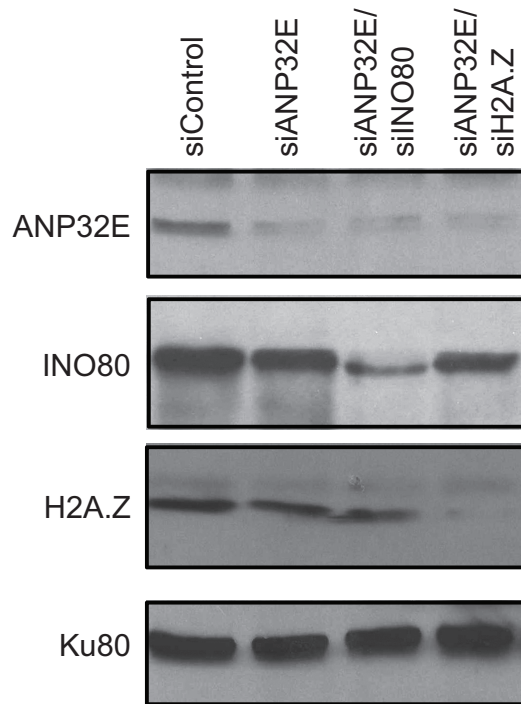
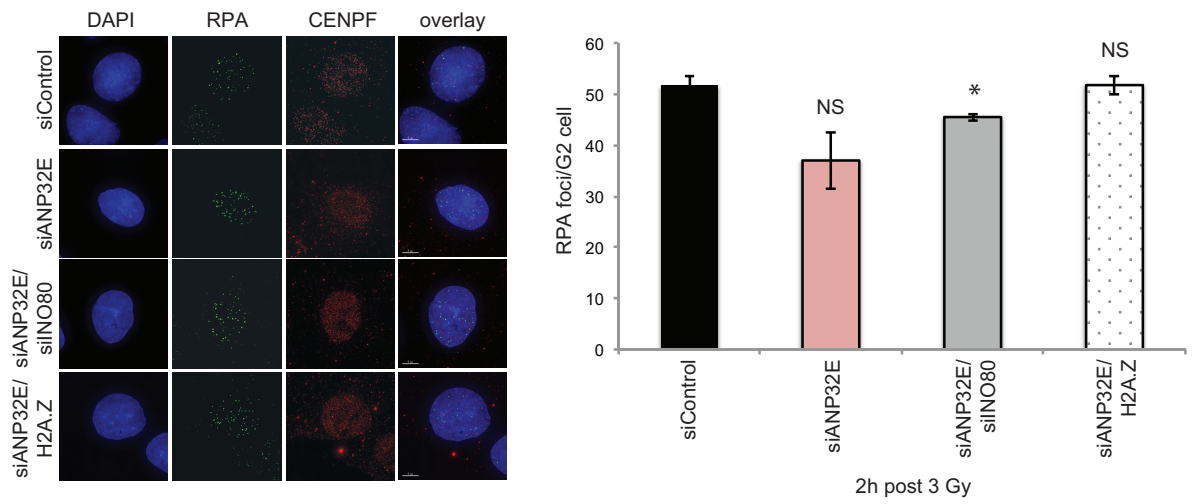
4.2.7 ANP32E works together with INO80 to remove H2AZ from chromatin

ANP32E has been identified recently as an H2AZ histone chaperone that can bind specifically to H2AZ and remove it from chromatin globally (Mao et al., 2014; Obri et al., 2014). To test whether the ANP32E is able to remove H2AZ from chromatin at DSBs in particular in similar manner to INO80, its effects on both resection and RAD51 filament formation were monitored. Specifically, siRNA was utilised to deplete ANP32E, H2AZ, or both proteins (Figure 4.9A) and RPA and RAD51 foci formation in G2 cells was monitored as previously described.

Notably, we found that the loss of ANP32E resulted in a slight albeit statistically insignificant reduction in the number of RPA foci as well as a significant reduction in the number of RAD51 foci (Figure 4.9B&C) that was similar to that observed previously following INO80 knockdown. Furthermore, H2AZ depletion in cells lacking ANP32E also rescued the defect in RAD51 (Figure 4.9C), suggesting that ANP32E functions to remove H2AZ from damaged chromatin as well as globally.

The similar phenotypes caused by INO80 and ANP32E depletion with respect to resection and RAD51 foci raised the question of the nature of the relationship between these two complexes in removing H2AZ from chromatin at DSBs. To address this issue, INO80 and ANP32E were co-depleted in A549 cells and the impact on RPA and RAD51 foci was examined (Figure 4.9A). It could be expected that if the two complexes functioned in distinct pathways to promote RAD51 foci formation, the phenotype caused by co-depletion would differ from that caused by single depletion of

either component. However, a similar phenotype was observed in each instance (Figure 4.9B&C), which suggested that INO80 works together with ANP32E to promote RAD51 foci formation by removing H2AZ from damaged chromatin.

A**B**

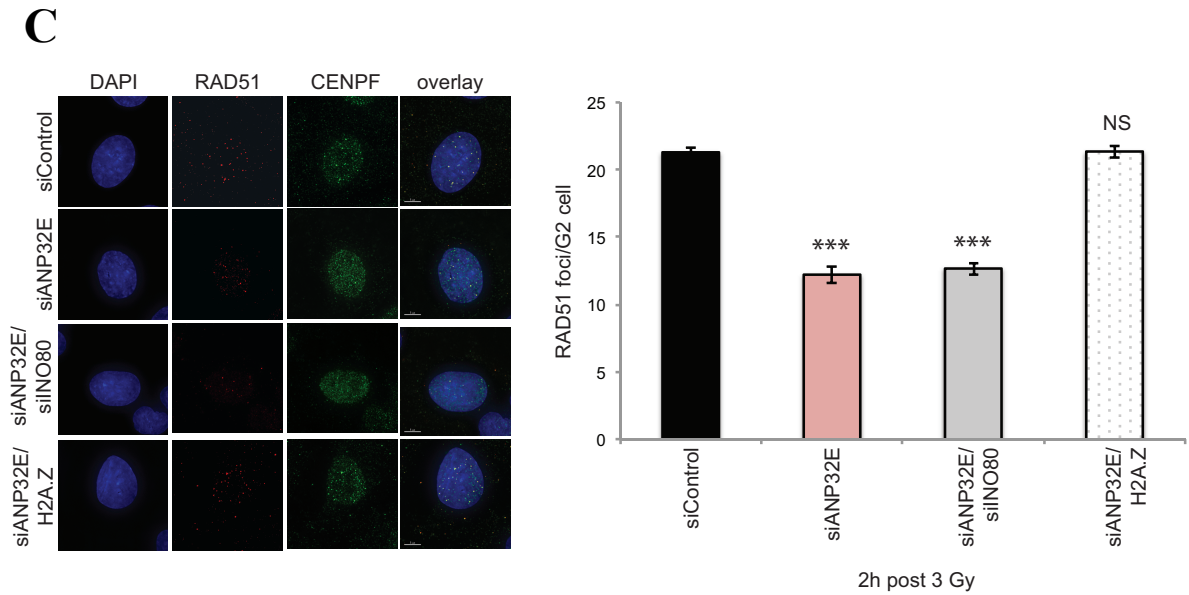


Figure 4. 9 INO80 and ANP32E work together to promote RAD51 foci formation following irradiation and their deficit can be rescued by H2AZ depletion.

(A) Western blotting showing the efficiency of siRNA knockdown. KU80 was used as a loading control. (B) IR induction of RPA foci in A459 cells treated with siRNA. Left panel: representative images at 2h post exposure to 3 Gy of γ -IR, right panel: quantification of the means of foci from three independent experiments; error bars show \pm SD. P values were determined by Student's t-test, and samples were compared with control cells. $*P \leq 0.05$; N.S., not significant. (C) IR induction of RAD51 foci in A459 cells treated with siRNA. Left panel: representative images at 2h post exposure to 3 Gy of γ -IR, right panel: quantification of the means of foci from three independent experiments; error bars show \pm SD. P values were determined by Student's t-test, and samples were compared with control cells. $***P \leq 0.001$, N.S., not significant. Scale bars = 5 μ m. (See figures 4.4 & 4.7 for siINO80 or siH2AZ data).

4.2.8 INO80 and ANP32E are required for efficient repair by HR

The observed defect in the number of RAD51 foci in cells depleted of INO80 and/or ANP32E suggested that HR was impaired in these cells. This defect, however, was minimal compared to that in cells lacking a core HR protein such as BRCA2. Therefore, the number of sister chromatid exchanges (SCEs) were monitored as a readout for the final outcome of HR, which could also provide an overview regarding the efficiency the repair pathway. Towards this end, INO80, ANP32E, H2AZ, and were co-depleted pairwise by siRNA knockdown in HeLa cells as shown in Figure 4.10. Next, these cells were labelled with BrdU and incubated with MMC for 16 h, colcemid was added to arrest the cells in mitosis followed by harvesting of the mitotic cells. To observe SCEs, chromosomes were spread and stained according to standard procedure.

Cells depleted of INO80 or ANP32E showed a reduction in the number of SCEs compared to the control cells (Figure 4.10A&B) and co-depletion of INO80 and ANP32E resulted in a similar defect as either single depletion (Figure 4.10B). Notably, the SCE defects were rescued upon H2AZ depletion in cells lacking either factor (Figure 4.10A&B), which confirms the previous finding that INO80 and ANP32E work co-operatively to remove H2AZ from damaged chromatin. However, the absence of H2AZ alone did not affect the efficiency of HR, as the number of SCEs in following H2AZ knockdown was similar to the control level (Figure 4.10A). This finding might suggest that the incorporation of H2AZ into chromatin is not important for HR although its removal is critical for repair by HR; this possibility will be discussed further in the Discussion (section 4.3) of this chapter.

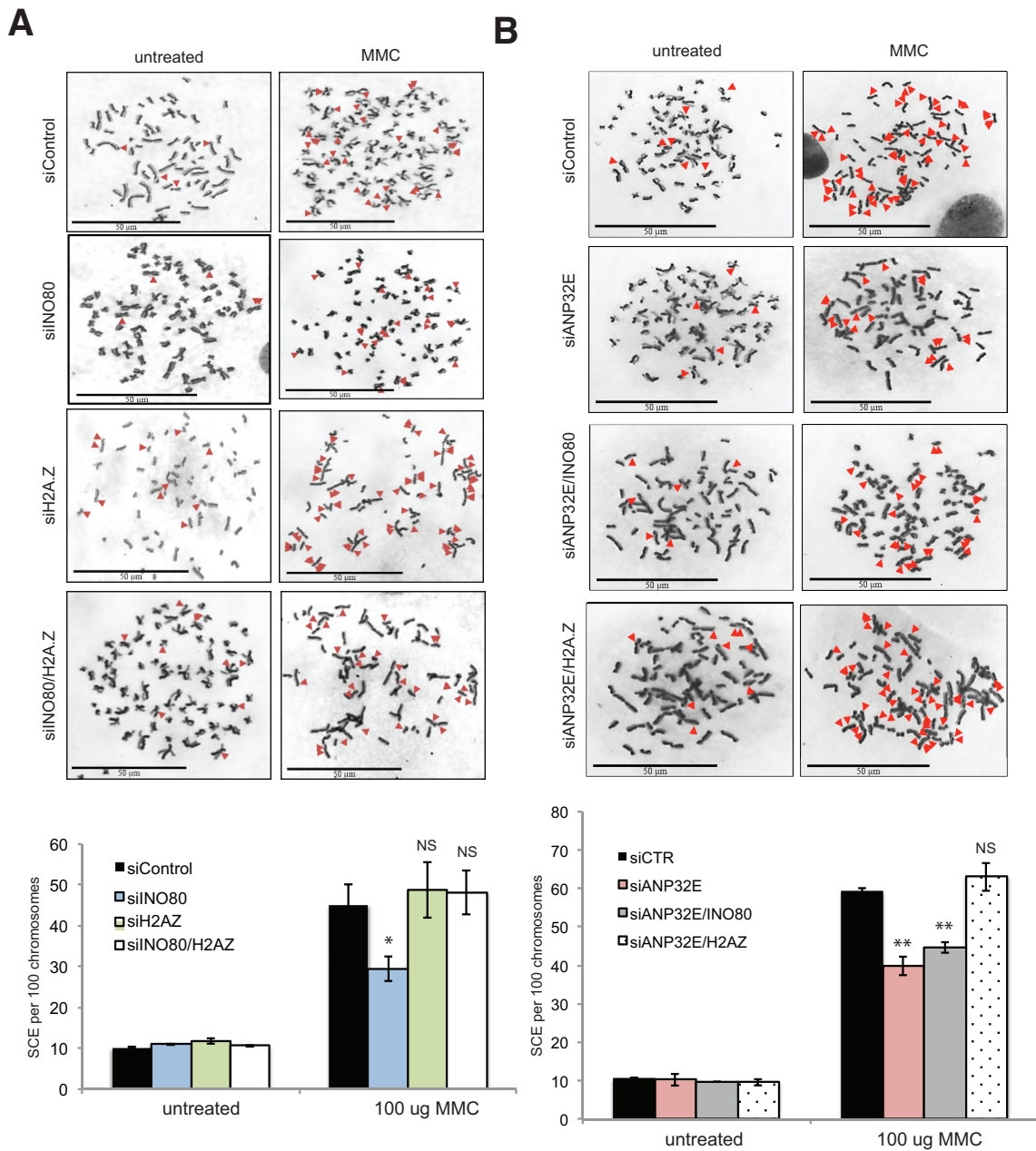


Figure 4. 10 Depletion of H2AZ rescues the SCE defect in cells depleted of INO80 or ANP32E.

Top panel in (A) & (B) Representative images of mitotic spreads in either MMC-treated or untreated HeLa cells; chromosomes were labelled with BrdU and stained with Giemsa allowing visualisation of the exchange between sister chromatids. Lower panel in (A) & (B) Quantification of the number of SCEs per 100 chromosomes in several siRNA cells. Error bars represent the means of 3 independent experiments \pm SD. P values were determined by Student's t-test, and samples were compared with control cells. * $P \leq 0.05$, ** $P \leq 0.01$, N.S., not significant.

4.3 Discussion

The aim of this chapter was to investigate the mechanism by which INO80 promotes HR. A key study from the Price laboratory showed that H2AZ plays a critical role in HR (Xu et al., 2012), suggesting that the role of INO80 in the removal of H2AZ from chromatin might be involved in regulation HR; however, this INO80 function has not previously been demonstrated in mammals. In particular, Xu et al. (2012) observed an increase in RPA and BrdU foci (denoting ssDNA) caused by the depletion of H2AZ, indicating that H2AZ restricts resection. In comparison, our results demonstrated that in the absence of INO80, the formation of RAD51 foci was defective. It was therefore hypothesised that if mammalian INO80 also functions in H2AZ removal, as has been reported in yeast (Papamichos-Chronakis et al., 2011), INO80-depleted cells should be unable to remove H2AZ, resulting in the blockage of resection and subsequent defects in the formation of RAD51 foci. Thus, if this model were correct, depletion of H2AZ in cells lacking INO80 should rescue the RAD51 foci defect (Figure 4.11). Overall, the findings of this chapter supported this hypothesis, as it was shown that H2AZ was transiently incorporated into damaged chromatin followed by its rapid removal and the removal reaction was dependent on INO80. In addition, it was found that H2AZ acted as a barrier for resection and that INO80 functioned together with ANP32E during HR to remove H2AZ to allow resection and the subsequent efficient repair by HR.

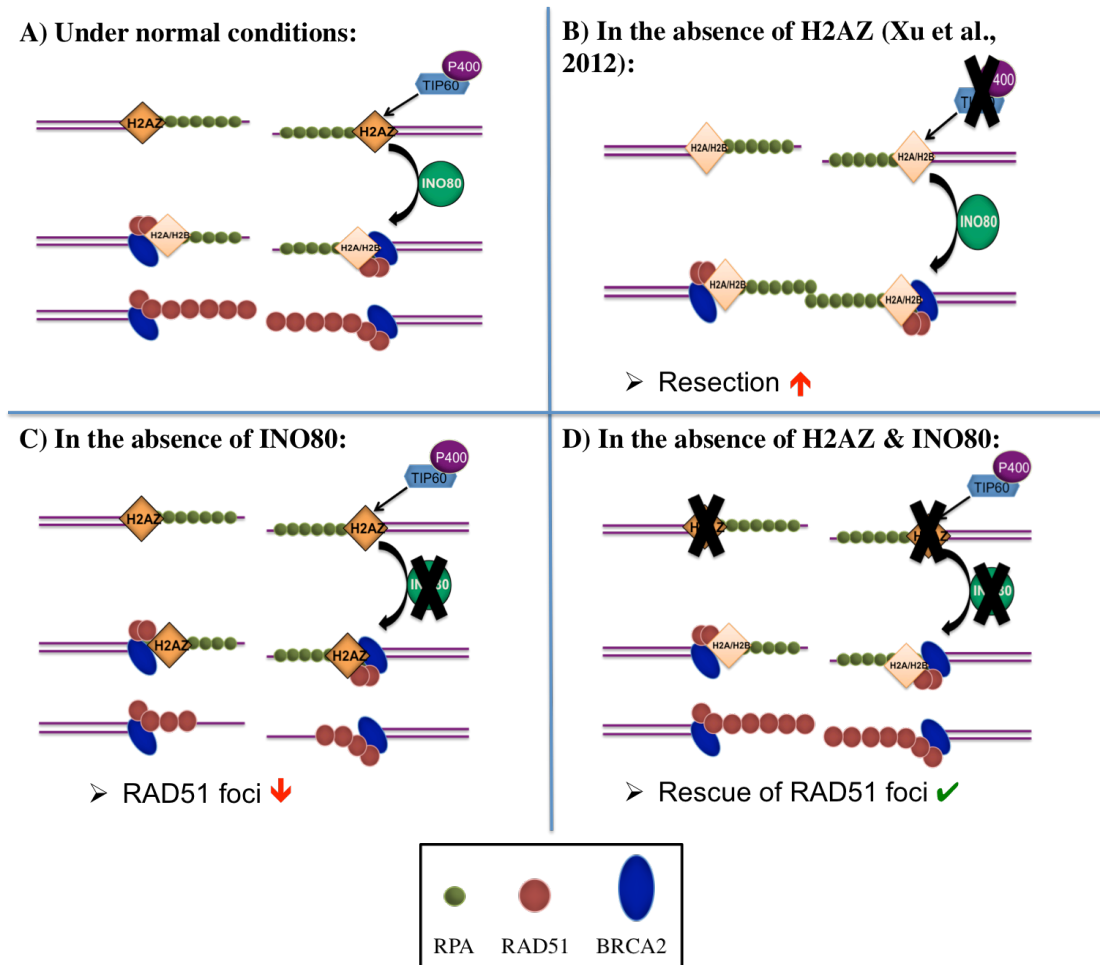


Figure 4. 11 Diagram illustrating the status of HR in four models.

(A) Normal HR: H2AZ is incorporated into chromatin by P400 and then needs to be removed by either INO80, according to yeast data (Papamichos-Chronakis et al., 2011), or ANP32E as has been shown in mammals (Mao et al., 2014; Obri et al., 2014) in order to achieve proper repair. (B) Model proposed by Xu et al. (2012), in which the absence of H2AZ causes an increase in resection. (C) Model based on the data from the current study, in which the absence of INO80 results in a decrease in RAD51 foci numbers. (D) The hypothesised model, in which H2AZ removal in INO80-depleted cells would rescue the defect in RAD51 foci formation.

4.3.1 H2AZ removal from damaged chromatin in human cells is dependent on INO80

The finding of this chapter revealed that H2AZ transiently accumulates to the sites of DNA damage. By using laser micro-irradiation and live cell imaging we provided evidence that H2AZ is incorporated into damaged chromatin within seconds and then rapidly removed within approximately 3 minutes (Figure 4.1) (Alatwi & Downs, 2015). This result is in agreement with a study that was published simultaneously with our published data, in which laser micro-irradiation in fixed cells was used to observe the accumulation of H2AZ in human cells in conjunction with an anti-H2AZ antibody (Gursoy-Yuzugullu et al., 2015). Similar to our results, they found that H2AZ accumulates to the damaged sites immediately after damage induction and that no H2AZ signals were detected in fixed samples after 10 minutes. The difference in the time required for H2AZ removal between the studies might be attributed to the distinct methodologies used; notably, sample fixation may result in a poorer representation of the actual process in cells compared to live cell imaging procedures.

Furthermore, this chapter provided the first evidence that mammalian INO80 regulates the removal of the histone variant H2AZ (Figure 4.1) (Alatwi & Downs, 2015), similar to its function in yeast (Papamichos-Chronakis et al., 2011). Specifically, laser micro-irradiation and live cell imaging data showed that in INO80-depleted cells, H2AZ was accumulated at levels similar to those of the control, whereas the removal of H2AZ was significantly slower in INO80-depleted cells (Figure 4.1). Notably, it has been shown in yeast that INO80 is required for the global removal of unacetylated H2AZ from chromatin and that the failure of H2AZ removal leads to a sensitivity towards

replication stress and DNA damage-inducing drugs (Papamichos-Chronakis et al., 2011). Furthermore, and most importantly, a histone exchange assay by Papamichos-Chronakis et al. (2011) showed that INO80 activity in yeast involves the replacement of the histone H2AZ with a core histone H2A, i.e., H2AZ is removed from the chromatin and replaced with H2A. H2A- or H2AZ-monomers were incubated with SWR1 and INO80 chromatin remodellers and H2AZ or H2A dimers, respectively, and the reactions were analysed by native PAGE and western blot. This revealed INO80's ability to replace histones, more precisely replacing H2AZ with H2A (Papamichos-Chronakis et al., 2011). However, our micro-irradiation data showed that INO80 only removed H2AZ from the damaged chromatin and we have no evidence to claim that INO80 replaces H2AZ with H2A. A likely experiment to consider in future would be to co-transfect cells with both GFP-H2AZ and mCherry-H2A. This would allow us to easily monitor the dynamics of both histones as well as INO80 activity towards them. Currently, our data only reflect the ability of INO80 in removing H2AZ from the damaged chromatin, as opposed to it being replaced with H2A.

Additionally, the dynamics of RUVBL2, a subunit of INO80, were followed using live cell imaging after damage induction by laser micro-irradiation, which demonstrated that RUVBL2 begins to accumulate at sites of damaged DNA within one minute and remains for approximately 20 minutes (Figure 4.3). Owing to a technical issue it was not possible to show the accumulation of the INO80 subunits at the damaged DNA sites; however, based on the previous data from Chapter 3 it was considered likely that INO80 functions in HR as a whole complex rather than as independent subunits, such as RUVBL2 and YY1. Furthermore, this result agreed with a previous published ChIP study, which showed that INO80 is recruited to sites of DNA damage (Kashiwaba et al.,

2010; Gospodinov et al., 2011). Therefore, our data indicated that the INO80 complex is likely recruited to damaged DNA during a period that overlaps with the removal of H2AZ from damaged chromatin.

Finally, it is worth noting that the recent report by Gursoy-Yuzugullu et al. (2015) also showed that the removal of H2AZ from damaged DNA required ANP32E. This is in agreement with another recent finding of the role for ANP32E as a histone chaperone that can bind specifically to H2AZ and effect its global removal from chromatin in mammals (Mao et al., 2014; Obri et al., 2014).

4.3.2 INO80 has a moderate role in resection

The results of this chapter showed that the depletion of INO80 did not lead to an obvious defect in resection (Figure 4.4C), which is consistent with our previous results (López-Perrote et al., 2014) but conflicts with the findings of two reports by others that investigated the role of INO80 in HR (Gospodinov et al., 2008, 2011). This discrepancy has been discussed thoroughly in Chapter 3 and was attributed to the different methodologies used (see Chapter 3, section 3.3.3). In comparison, the experiments in the present chapter utilised SRCAP, which has a critical role in resection, as a positive control (Dong et al., 2014) such that the known resection phenotype following SRCAP depletion could be detected via our method to observe resection in G2 cells following the induction of DSBs by 3 Gy of γ -IR. This both validated the used method and clarified that the observed resection phenotype related to INO80 depletion, if present, reflects only a modest function of INO80 in resection in G2 cells.

Notably, however, other groups have recently reported a moderate role for the INO80 in resection as well. For example, the Jackson group reported a mild defect in resection, observed as a reduction in the intensity of BrdU foci (ssDNA) rather than their number upon treatment with CPT, caused by depletion of INO80, YY1, or RUVBL1 (subunits of the INO80 complex) (Nishi et al., 2014). Similarly, Dong et al. (2014) reported a modest defect in resection in a stable INO80 knockout cell line, observed as a slight reduction in the percentage of cells with RPA foci upon treatment with 10 Gy IR. Accordingly, an additional method was thus also utilised in the current chapter to mimic the subtle INO80 resection phenotype, wherein resection was monitored as the percentage of cells with RPA foci upon treatment with CPT. This method allowed the observation of a modest but statistically significant defect in resection in cells depleted for either INO80 or YY1 (Figure 4.6). It should be noted, however, that the mechanism of DSB formation by CPT arises from replication stress during S phase as this chemical inhibits the nuclear enzyme DNA topoisomerase type I (topo I) (Liu et al., 2000). Therefore, the inability to observe a significant albeit mild phenotype in the G2-exclusive method might reflect a restriction of the role of INO80 in resection to S phase.

Furthermore, the results presented in this chapter confirm the critical role for H2AZ in resection, which has been reported previously by Xu et al. (2012). Specifically, the absence of H2AZ resulted in an increase in RPA foci number suggesting that H2AZ acts as a barrier for resection. Notably, Xu et al. (2012) found that the absence of H2AZ caused a loss of KU70/80 in addition to an increase in resection, whereas the inhibition of resection following CtIP depletion in H2AZ-depleted cells resulted in restoration of KU70/80 levels and NHEJ pathway function. These results indicate that the incorporation of H2AZ at DSBs is an important factor for efficient NHEJ and the loss

of the KU complex in cells lacking H2AZ might suggest that H2AZ serves as a key factor for its recruitment. In addition, the current results also showed that in cells depleted for both INO80 and H2AZ, the number of RPA foci was restored to the control level (Figure 4.4C), supporting that INO80 might play a role in resection even in G2 cells.

4.3.3 INO80 promotes RAD51 foci formation by removing H2AZ at DSB sites

It was demonstrated in Chapter 3 that INO80, including its subunits YY1 and RUVBL2, functions in HR by promoting or stabilising RAD51 foci formation. The aim of the current chapter was to investigate the mechanism underlying this function of INO80. In particular, it was found that the absence of the INO80 protein, a catalytic subunit of the INO80 complex, caused a reduction in the number of RAD51 foci similar to that observed previously in cells lacking YY1, RUVBL2, or both INO80 and RUVBL2. This confirmed the previous assertion that INO80 acts as a whole complex to promote repair by HR. Conversely, the significant defect in RAD51 foci is unlikely to represent a direct consequence of the modest defect in resection, suggesting that INO80 has an additional function in promoting RAD51 foci formation. One possibility is that the INO80 complex is involved in either the recruitment or expression of the key repair protein BRCA2. In particular, a very recent study has shown that INO80 and YY1 regulate the expression of the BRCA2- and CDKN1A-interacting protein (BCCIP) (Su et al., 2016). BCCIP α and β interact directly through their N-terminal regions with BRCA2 (amino acids 2883 to 3053) and have been shown to interact with RAD51 as well (Lu et al., 2005). Notably, these interactions were found to be critical for HR as silencing BCCIP α and/or β by shRNA resulted in a significant reduction of IR-induced

RAD51 foci (Lu et al., 2005). Thus, INO80 might regulate repair via HR through the regulation of BCCIP expression.

Alternatively, the complete rescue of the defect in RAD51 foci formation upon H2AZ depletion in cells lacking INO80 (Figure 4.7) suggests an additional possibility for INO80 function, confirming the assumption that INO80 functions in HR by removing H2AZ from damaged chromatin to allow efficient repair. In other words, the RAD51 foci defect in cells lacking INO80 is consequent to resection blockage caused by the failure to remove H2AZ from damaged chromatin in the absence of INO80. Notably, the rescue phenotype in cells co-depleted of both INO80 and H2AZ, which indicates that H2AZ needs to be removed to permit the accurate loading of RAD51 at focal sites, further supports this model.

4.3.4 INO80 work co-operatively with ANP32E to promote HR by removing H2AZ from damaged chromatin

ANP32E has been recently identified as a mammalian H2AZ histone chaperone that can bind and remove H2AZ from chromatin. ANP32E recognises and binds to H2AZ through an interaction between its C-terminal acidic region and the α C helix of H2AZ (T103 and I104) (Mao et al., 2014; Obri et al., 2014) and disruption of this H2AZ region inhibits their interaction (Gursoy-Yuzugullu et al., 2015). These H2AZ residues are conserved in H2A although with the inclusion of an extra glycine residue; notably, the insertion of a similar glycine residue in H2AZ also abolishes the interaction with ANP32E (Mao et al., 2014; Obri et al., 2014). An aim of the current chapter was to examine the impact of this function of ANP32E at DSBs. It was found that ANP32E works co-operatively with INO80 to promote RAD51 foci formation by removing

H2AZ from damaged chromatin (Figure 4.9), expanding on the finding of Gursoy-Yuzugullu et al. (2015) that ANP32E is required for the removal of H2AZ at DSBs. However, this result raises several additional questions, including the role of INO80 in the H2AZ removal reaction considering the established binding of ANP32E, and whether INO80 or ANP32E is dependent on the other for recruitment, binding, or function.

4.3.5 Efficient HR requires the removal of H2AZ by INO80 and ANP32E

The SCE data from the current study showed that efficient HR requires the involvement of both INO80 and ANP32E. The defect in the number of SCEs in the absence of INO80 and/or ANP32E mimics that observed in the number of RAD51 foci; therefore, it is highly likely that the SCE deficit is consequent to an upstream defect in RAD51 foci formation. Furthermore, this finding suggests that the main role for INO80 and ANP32E is to remove H2AZ from damaged chromatin to allow the efficient loading of RAD51 at its focal sites.

Additionally, this data also indicated that the incorporation of H2AZ is not required for HR, although its removal is critical, as the absence of H2AZ alone resulted in the establishment of levels of SCE similar to those of the control. However, in the absence of INO80 or ANP32E, under which conditions H2AZ cannot be removed, a significant reduction in the number of SCEs was observed (Figure 4.10). According to Xu et al. (2012), the incorporation of H2AZ is critical for repair by NHEJ, as the depletion of H2AZ leads to the abolishment of KU70/80 recruitment at sites of damaged DNA and a significant reduction in the level of NHEJ. Notably, the γ H2AX data presented herein

indicated that after 8 h of DSB induction by IR, cells subjected to knockdown of INO80, H2AZ, or both managed to repair the damage to the level of the control, suggesting that these cells incorporated a different repair pathway to repair DSBs, such as either NHEJ or Alt-NHEJ. As the KU complex is lost in H2AZ-depleted cells and the NHEJ pathway is defective, cells would thus be required to utilise the Alt-NHEJ pathway to repair DSBs. This was confirmed through the observation of efficient repair by Alt-NHEJ in cells lacking H2AZ, approximating the level of repair observed in control cells (Xu et al., 2012).

In summary, once DSBs occur, H2AZ is incorporated into damaged chromatin within seconds (Alatwi & Downs, 2015), facilitating H4 acetylation and leading to a weakening of the histone interactions within nucleosomes by interrupting the interaction between H2A and H4, thus resulting in a relaxed, open chromatin configuration (Xu et al., 2012). This chromatin relaxation is important to promote KU70/80 complex recruitment to sites of DSBs and to facilitate NHEJ (Xu et al., 2012). However, H2AZ then needs to be removed shortly thereafter by both INO80 and ANP32E to allow accurate loading for the establishment of RAD51 foci and, eventually, efficient HR (Alatwi & Downs, 2015).

Chapter 5.

Role of INO80 in chromosomal stability

5.1 Introduction

Chromosomal instability (CIN) represents one of the main causes of genomic instability and describes a dynamic state wherein cells continuously gain or lose whole chromosomes or chromosomal fragments. CIN has been strongly associated with several types of cancer, such as breast, lung and colon cancers (McGranahan et al., 2012). Appropriate chromosomal segregation is reliant upon the functional and structural accuracy of the centromere, a fundamental component of each chromosome (Verdaasdonk & Bloom, 2011; Bloom, 2014). In turn, H2AZ, a histone variant of the core histone H2A, has been shown to comprise one of the critical factors for maintaining centromere structure. Specifically, H2AZ-containing nucleosomes function as a boundary between euchromatin and heterochromatin (Meneghini et al., 2003). Loss of H2AZ results in the loss of centromere silencing owing to impaired regulation of CENP-C expression, a centromere protein required for centromere silencing (Hou et al., 2010; Greaves et al., 2007).

In a previous publication, our laboratory was the first to identify a role for the INO80 complex in chromosome segregation in budding yeast (Chambers et al., 2012). In the study, yeast strains lacking either Ise6 or Ino80 were found to be defective for chromosome segregation owing to the enrichment of H2AZ in pericentric chromatin. The authors had also shown that H2AZ overexpression or down-regulation accelerates or prevents the development of polyploidy, respectively (Chambers et al., 2012). Polyploidy and chromosomal structural abnormality, including chromosome and chromatid breaks, have been shown by others to occur subsequent to loss of YY1, a human subunit of INO80, as well (Wu et al., 2007). Finally, Cao et al. (2015) have recently found that the depletion of INO80 by siRNA resulted in an increase in the

number of cells with more than two centrosomes per nucleus, aberrant cytokinesis, and multipolar spindle formation. Together, these different lines of evidence indicate the association of INO80 with chromosomal stability.

The experiments in this chapter were based on our finding from Chapter 4 that INO80 plays a role in the removal of H2AZ from chromatin in mammals (Alatwi & Downs, 2015) and the observation that H2AZ constitutes a major component of human centromeres (Greaves et al., 2007), which have been shown to be vital for the fidelity of chromosome segregation in yeast (Chambers et al., 2012). Therefore, we hypothesised that the loss of INO80 might result in structural centromeric defects owing to the local enrichment of H2AZ, eventually leading to chromosomal instability. Accordingly, we aimed to address whether human INO80 contributes to the maintenance of faithful chromosome segregation, and if so, whether it might be suitable for use as a therapeutic target for CIN+ tumours, which may not be able to tolerate further perturbations to chromosome segregation pathways.

5.2 Results

5.2.1 Depletion of INO80 results in an increase in the number of micronuclei (MN) in CIN+ cells

MN formation constitutes one of the well-established biomarkers for chromosomal instability. MN formation can be initiated from acentric chromosome fragments, acentric chromatid fragments, or whole chromosomes that failed to attach properly to the spindle microtubule (Fenech et al., 2011). Therefore, we utilised MN to test whether the absence of INO80 would lead to or increase chromosomal instability. INO80 was depleted by siRNA-mediated knockdown in the CIN+ cell line U2OS and in the CIN- cell line BR1-hTERT (a human fibroblast line that is genomically stable). Karyotype analysis of U2OS cells confirmed that this cell line is aneuploid, carrying approximately 65–70 chromosomes and exhibiting both numerical and structural CIN (Janssen and Medema, 2012); thus, it has been classified as a CIN+ cell line. After two rounds of INO80 knockdown, the cells were allowed to grow for 24 h before they were stained with DAPI (Figure 5.1).

The percentage of MN was found to be higher in the CIN+ (U2OS) control compared to the CIN- cell line, further confirming that U2OS represents a CIN+ cell line (Figure 5.1). While not statistically significant, depletion of INO80 in U2OS cells led to an increase in the percentage of MN of almost 2-fold compared to the MN percentage in the control U2OS cells, suggesting that INO80 may be important to prevent further CIN (Figure 5.1). Notably, the absence of INO80 also slightly increased the percentage of MN in the CIN- cell line as well; however, the MN percentage in the CIN- cell line was still low compared to that in the CIN+ cells (Figure 5.1).

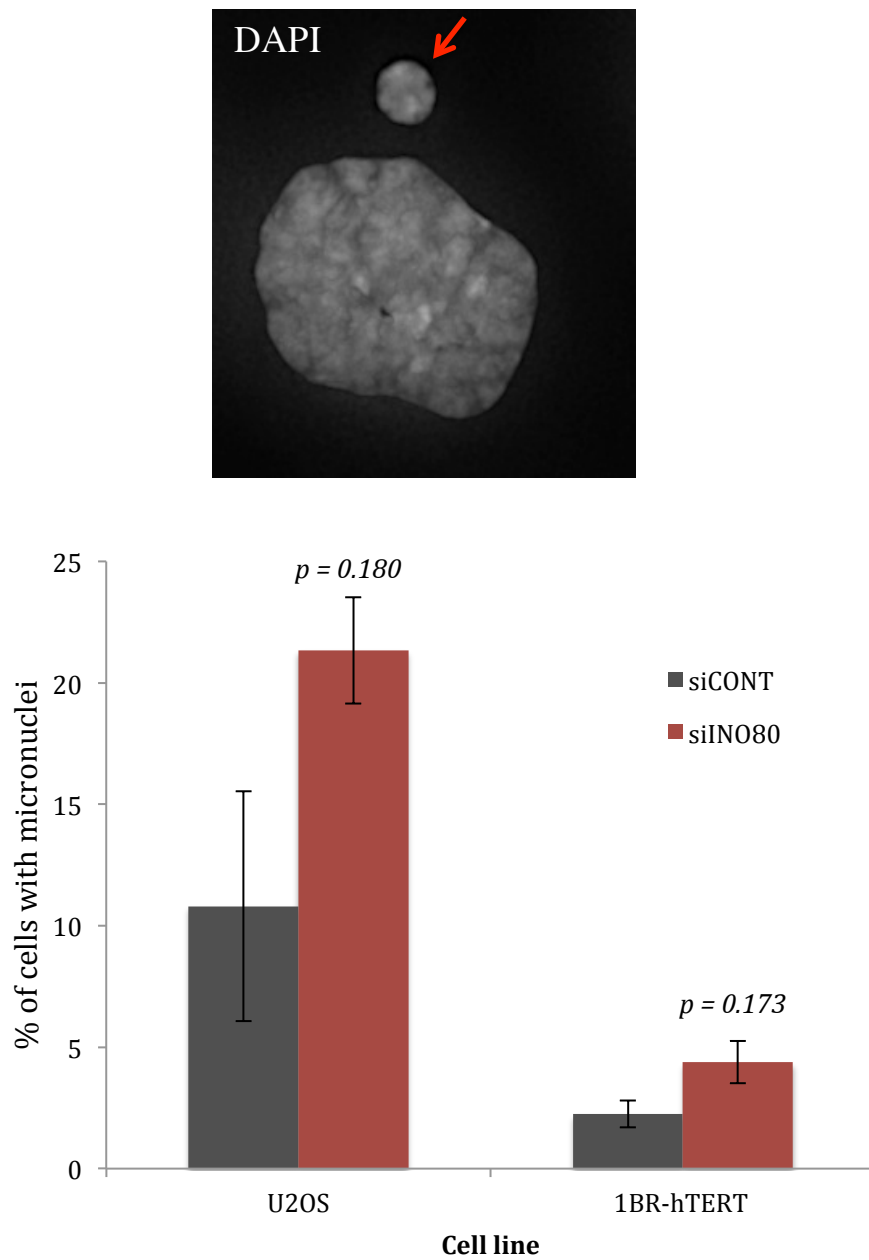


Figure 5. 1 Depletion of INO80 results in an increase in the number of micronuclei in CIN+ cells.

Top panel: representative image showing cells with micronuclei in the U2OS cell line; the arrow indicates a micronucleus. Lower panel: quantification of the percentage of cells with micronuclei in the control (CONT) and siINO80 cells in the different cell lines. Error bars represent \pm SD of duplicate experiments. P values were determined by Student's t-test, and samples were compared with control cells.

5.2.2 Depletion of INO80 causes a defect in structural CIN rather than numerical CIN in U2OS cells

To further investigate the role of INO80 in CIN, next we monitored the mitosis aberrations in U2OS cells. INO80 was again depleted and the cells subsequently allowed to grow for 24 h. Then, the cells were fixed with 4% PFA and stained with DAPI. The experiment initially was designed to monitor anaphase bridges, which represent another biomarker for CIN that can originate when a dicentric chromosome becomes pulled to opposite poles; such dicentric chromosomes can be generated from either a misrepair of chromosome breaks or telomere to telomere end fusions (Fenech et al., 2011). Anaphase bridges may also result from a failure in resolving the linkage between sister chromatids, i.e., failure in resolving cohesion or decatanation via top II (Fenech et al., 2011; Tanaka & Hirota, 2016). However, other breakages were also observed in U2OS cells, such as uncompleted bridges and acentric or lagging chromosomes. Therefore, all types of breakages were included as representing defects in mitosis (Figure 5.2). Notably, the percentage of cells with aberrant mitosis was substantially higher in INO80-depleted U2OS cells compared to the control. This suggests that the INO80 complex plays an important role in ensuring the fidelity of mitosis (Figure 5.2). Furthermore, in both control and siINO80-treated 1BR-hTERT cells, few mitotic aberrations of any kind could be observed, which might be due to the high genomic stability manifested by these cells.

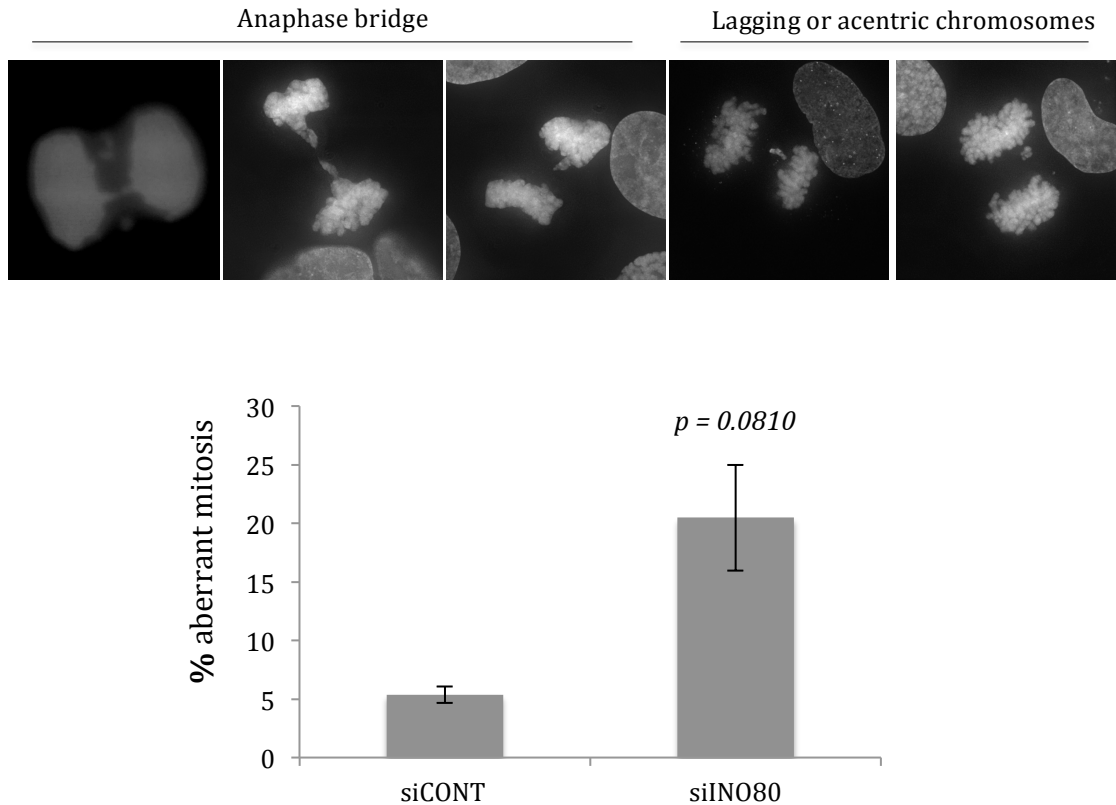


Figure 5. 2 Depletion of INO80 causes a defect in structural CIN in U2OS cells.

Top panel: representative images of the observed mitotic aberrations. Lower panel: quantification of the percentage of mitotic aberrations in U2OS cells. Error bars represent \pm SD of duplicate experiments. P value was determined by Student's t-test, and samples were compared with control cells.

Next, we determined whether the absence of INO80 caused an increase in aneuploidy within U2OS cells. Aneuploidy or chromosomal number was determined by counting the centromere number. Centromeres were labelled by staining with a CENP-A antibody, which allows the visualisation and straightforward counting of centromeres (Figure 5.3). Although U2OS constitutes an aneuploid cell line and the average number of chromosomes in these cells is approximately 65–70 (Janssen and Medema, 2011), a further change in chromosome number would be expected following the depletion of INO80. However, no difference was observed in the number of chromosomes between INO80-depleted cells and the control (Figure 5.3). This finding might suggest that the absence of INO80 caused a structural rather than numerical CIN in U2OS cells.

Alternatively, additional rounds of cell division might be necessary to see significant changes in the population. Unfortunately, due to the transient nature of siRNA depletion, this is not easily testable in our system. We note that owing to the low number of mitotic 1BR-hTERT cells obtained, no data was generated from this cell line.

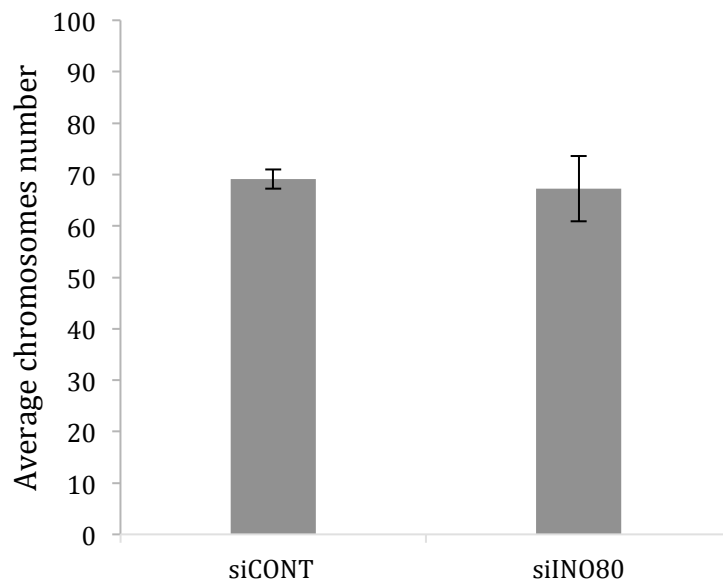
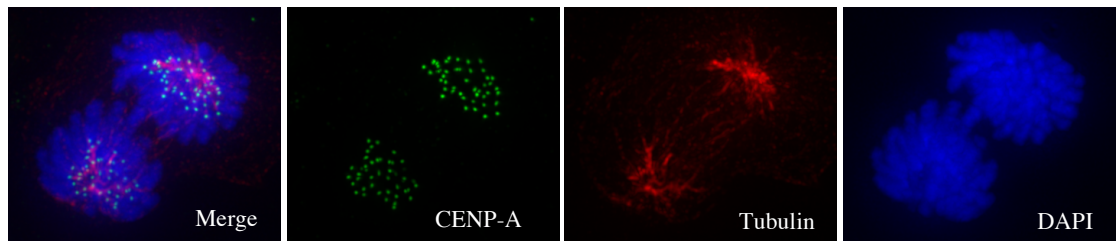


Figure 5. 3 Depletion of INO80 does not affect the number of chromosomes in U2OS cells.

Top panel: representative images showing chromosome segregation in anaphase cells. Lower panel: quantification of the average number of chromosomes in U2OS cells. Error bars \pm SD of duplicate experiments.

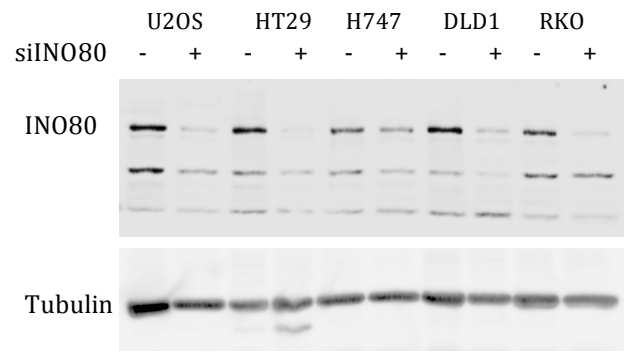
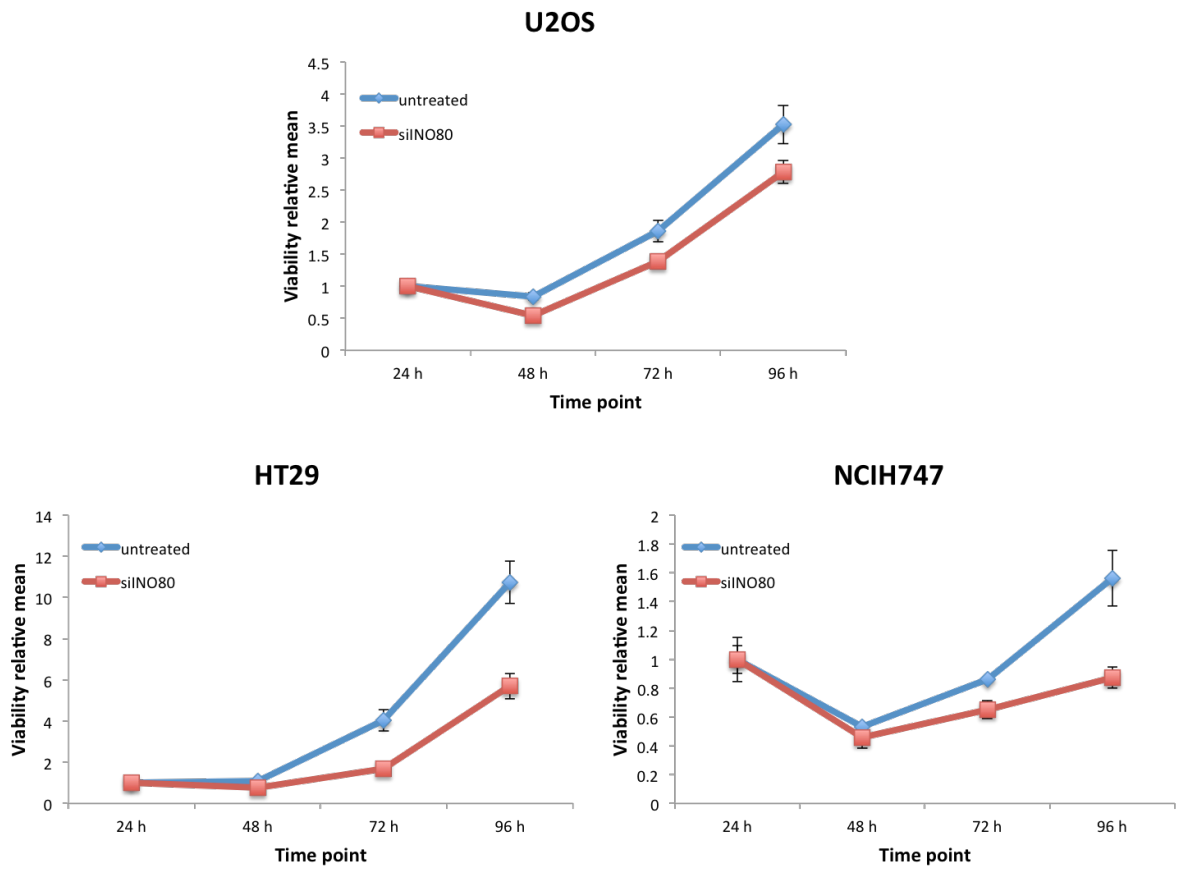
5.2.3 Loss of INO80 causes cell death in CIN+ cells

Together, the previous data from yeast (Chambers et al., 2012) and humans (Chapter 4; Alatwi & Downs, 2015) respectively suggest that the loss of INO80 causes chromosome segregation errors owing to aberrant pericentric H2AZ enrichment and that H2AZ removal is partially dependent on the presence of INO80 in response to DNA damage. As our findings in U2OS cells further suggested that INO80 plays a role in chromosomal stability, we next examined whether the loss of INO80 in CIN+ cells led to any lethal effect on their growth. To this end, colorectal cancer cell lines were utilised in addition to the CIN+ cell line U2OS (Tanno et al., 2015) as they have been intensively analysed and classified as representing CIN+ and CIN- cell lines (Burrell et al., 2013). INO80 was depleted as previously described via siRNA in CIN+ cells (U2OS, HT29, and NCIH747) and CIN- cells (DLD1 and RKO) (Figure 5.4A). The cells were then seeded into 96-well plates, to which CellTiter-Blue reagent was added and cell viability was measured at the required time point using a microplate reader.

Theoretically, if the INO80 complex functions in maintaining chromosomal stability, a reduction in cell viability in CIN+ cells might be expected as these cells would experience further increase in CIN in the absence of INO80 and thus their viability would be severely challenged. In support of this, depletion of INO80 caused an increase in cell death in CIN+ cell lines compared to the control (untreated cells) (Figure 5.4B). Notably, the cell death was more obvious beginning at 48 h in all CIN+ cell lines; therefore, this might represent the point at which the cells reach the peak of H2AZ enrichment. Subsequently, a higher degree of defective HR and larger number structurally defective centromeres would likely occur, negatively impacting viability. It

is also possible that H2AZ mislocalisation may impact on transcriptional regulation of essential genes.

However, DLD1 CIN⁻ cell line, no difference was observed in cell viability between untreated and siINO80-transfected cells. This may suggest that INO80 is required when cells experience CIN and therefore could be used to target CIN⁺ tumours. Conversely, RKO cells, which had been classified as a CIN⁻ cell line according to the Burrell et al. (2013) study, showed a phenotype similar to that observed for CIN⁺ cells. This led us to further investigate the CIN state of this cell line, as described in the next section (5.4).

A**B**

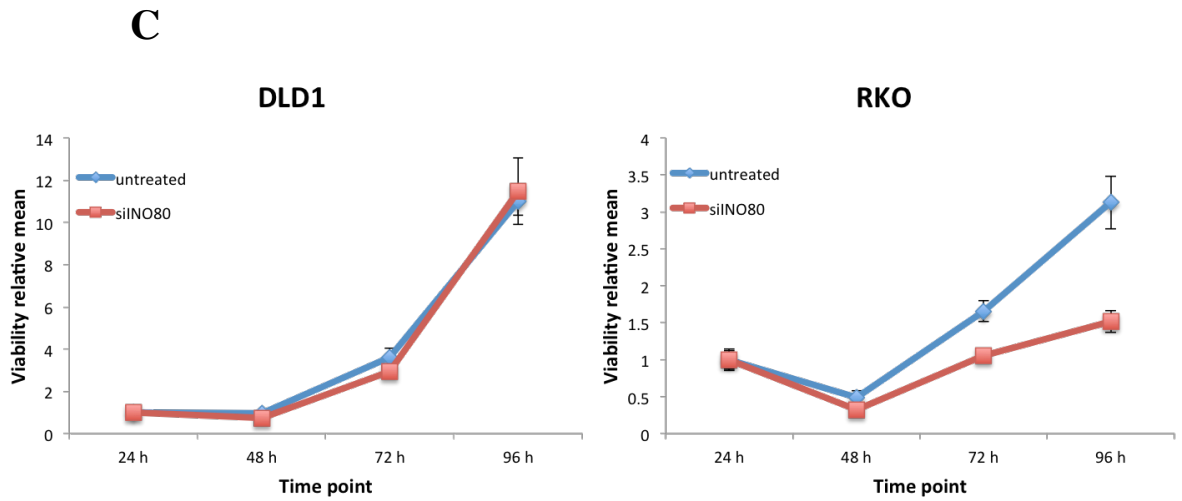


Figure 5. 4 Loss of INO80 causes cells lethality in CIN+ cells.

(A) Western blot performed 24 h after the second round of siINO80 transfection in the indicated cell lines; tubulin was used as a loading control. (B) Cell viability in CIN+ cell lines (U2OS, HT29, and NCIH747) and (C) in CIN- cell lines (DLD1 and RKO) in untreated and siINO80-transfected cells at the indicated time points. Viability values reflect the means relative to measurement at 24 h. Each experiment was performed in triplicated wells; error bars represent \pm SD from three independent experiments.

5.2.4 RKO cells are sensitive to the loss of INO80

Based on the Burrell et al. (2013) classification RKO constitutes a CIN⁻ cell line; however, it exhibited a similar phenotype to that of CIN⁺ cell lines in response to INO80 depletion as measured by the cell viability assay (Figure 5.4B&C). Therefore, we checked the chromosomal stability state for this cell line by monitoring MN and anaphase bridges as described in sections 5.2.1 & 5.2.2.

Previously, Burrell et al. (2013) reported an approximate rate of 18% anaphase segregation errors for RKO cells, which was considered to fall within the range of the CIN⁻ cell lines compared to a mean of 38% for the CIN⁺ cell lines (Burrell et al., 2013). In comparison, in the present study only approximately 6% of RKO cells were found to be MN positive although approximately 19% of cells exhibited anaphase bridges (Figure 5.5), in agreement with their classification as a CIN⁻ cell line as determined by Burrell et al. (2013). However, depletion of INO80 in these cells increased the percentage of cells with MN to approximately 14% and 40% of anaphase cells exhibited bridges (Figure 5.5), suggesting that INO80 plays a vital role in maintaining chromosomal stability in this cell line. Notably, we determined that the HR pathway is defective in RKO cells as BRCA1 and BRCA2 were found to be mutated in this cell line according to the COSMIC Cell Line Project database; specifically, substitution missense and frameshift deletion mutations were identified in these genes, respectively (Wellcome Trust Sanger Institute, 2016). This additional deficit may provide clues regarding the importance of INO80 for this cell line; further discussion on this topic is provided at the end of section 5.3.1.

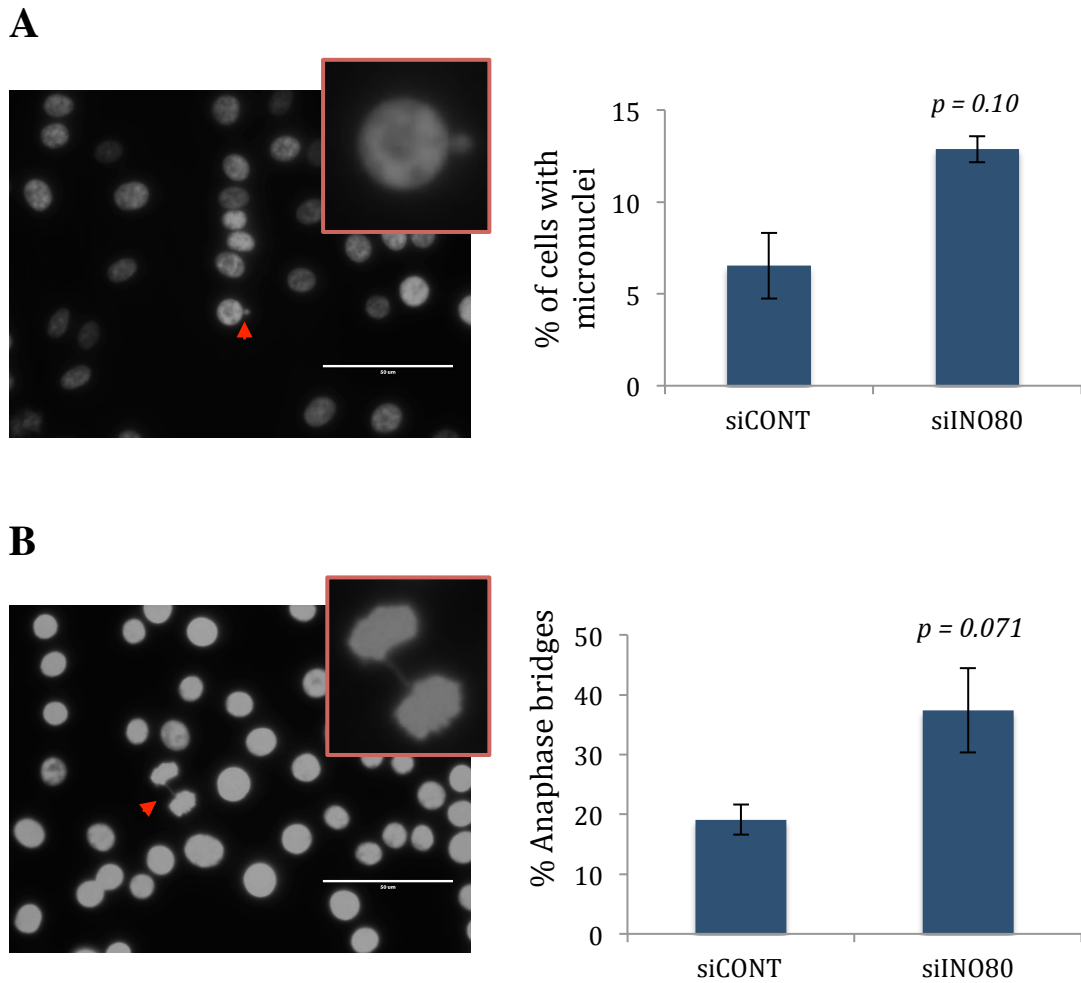


Figure 5. 5 RKO is sensitive to INO80 loss.

(A) Right panel: representative image of MN in RKO cells; left panel: quantification of the percentage of control and siINO80 RKO cells with micronuclei (red arrowhead). (B) Right panel: representative image of an anaphase bridge in RKO cells; left panel: quantification of the percentage of control and siINO80 RKO cells with anaphase bridges (red arrowhead). Error bars represent \pm SD from three independent experiments. P values were determined by Student's t-test, and samples were compared with control cells.

5.3 Discussion

This chapter aimed to investigate the role of INO80 in chromosomal stability within human cells and to ascertain the potential for using such a chromatin remodeller in targeting CIN+ tumours. Our results showed that the depletion of INO80 caused an increase in CIN, which was observed as an increase in the percentages of micronuclei and mitotic aberrations. Furthermore, we found that the depletion of INO80 increased cell death in CIN+ cells.

5.3.1 INO80 is likely to be required for chromosomal stability

Our results confirmed the previously reported role of INO80 in maintaining chromosomal stability (Wu et al., 2007; Chambers et al., 2012; Kracker et al., 2014; Cao et al., 2015). In particular, here we showed that INO80 is probably required for preventing or moderating CIN, as its depletion caused an increase in the percentages of MN and mitotic aberrations. This might indicate a primary role for INO80 in maintaining chromosomal stability and mitotic fidelity. Furthermore, as MN may arise from chromosomal structural or attachment errors in mitosis (Fenech et al., 2011) and the observed aberrant mitoses included anaphase bridges and acentric or lagging chromosomes in siINO80-U2OS cells, the enrichment of these features suggested that INO80 may be important for preventing such mitotic structural and attachment errors. Similarly, it has been reported that the depletion of BAF180, a subunit of the BPAF chromatin remodelling complex, also caused an increase in the percentages of MN and aberrant mitosis in U2OS and BR1-hTERT cells (Brownlee et al., 2014). However, whereas our result from U2OS cells showed that no further aneuploidy was caused by the depletion of INO80 (Figure 5.3), the depletion of BAF180 resulted in aneuploidy

consequent to a subsequent defect in cohesion (Brownlee et al., 2014). This discrepancy might be due to the method used to monitor aneuploidy in our study, in particular as the premature separation of sister chromatids and an increase in chromosome breaks have been reported as a result of down-regulation of INO80 in CH12-F3 cells, a lymphoma cell line (Kracker et al., 2015). Therefore, a metaphase spread method should be used in future research to provide a precise number of chromosomes and monitor any premature separation of sister chromatids.

Notably, a role for INO80 in chromosomal stability in mammals has been reported in other studies. For example, it has been shown that loss of YY1, a subunit of INO80, causes polyploidy and chromosomal abnormalities including chromosome and chromatid breaks and triradial or quadriradial chromosomes. This phenotype was linked to the role of YY1 in DNA repair (Wu et al., 2007). Furthermore, Cao et al. (2015) reported an increase in the number of cells with large nuclei, cells with more than two centrosomes, aberrant cytokinesis, and multipolar spindle formation caused by the depletion of INO80. The authors also observed high expression of p21 in siINO80 cells, thus attributing these phenotypes to the role of INO80 as a negative regulator of p21 (Cao et al., 2015). In addition, polyploidy was observed in yeast strains lacking the INO80 subunits Ino80 or Ies6 consequent to H2AZ enrichment at pericentric chromatin (Chambers et al., 2012). Taken together, these findings indicate that INO80 represents a fundamental player in maintaining chromosomal stability and mitotic fidelity. They also indicate a high probability that the multiple functions of INO80 including its roles in DNA repair, negative regulation of p21 expression, and eviction of H2AZ from chromatin work in concert to generate CIN.

Although the means by which deficient HR may lead to CIN are not clear, an earlier study has shown that mild or severe defects in RAD51, i.e., leading to deficient HR, could cause incomplete separation during anaphase, whereas only severe defects would lead to a multipolar anaphase state and cell death (Laulier et al., 2011). This differential outcome might explain the cell death that was observed in the CIN⁻ colorectal cell line, RKO (Figure 5.4), in which we found that HR was defective owing to mutations in the key repair proteins BRCA1 and BRCA2, which could be considered to represent a severe defect. Therefore, the additional absence of INO80 yielded a phenotype similar to that of CIN⁺ cell lines (Figure 5.4). However, our preferred model to explain the overall function for INO80 in maintaining chromosomal stability relies upon its role as a chromatin remodeller to remove H2AZ from chromatin. Specifically, in the absence of INO80, H2AZ would accumulate to high levels at centromeres, impairing their function; in conjunction with an upstream defect in HR, these deficits would eventually lead to an increase in CIN. This model will be tested by the Downs laboratory in subsequent experiments. We note that it is also possible that all of the described functions of INO80 could also be attributed to a role in the maintenance of mitosis fidelity.

5.3.2 INO80 constitutes a proposed therapeutic target for CIN⁺ tumours

CIN represents one of the hallmark features that are found in most cancers at an advanced level and in almost all solid tumours such as colon, lung, and cervical tumours (Tanaka & Hirota, 2016). Recently, several therapeutic strategies have been developed to target mitosis or, more precisely, CIN⁺ tumours to suppress cancer by inducing mitotic arrest and eventually apoptotic cell death, such as the use of a microtubule

stabiliser and targeting mitotic checkpoints. However, the challenges related to controlling the dose of these drugs to allow the disruption of mitosis in tumour cells but not in normal cells has limited the use of these strategies to cure cancer in patients (Tanaka & Hirota, 2016). Notably, however, it has been found that suppressing CIN in colorectal tumour cell lines by increasing the microtubule assembly rate accelerates tumour growth in these cells (Ertych et al., 2014). This led to the conjecture that increasing CIN beyond the lethal level might induce cell death. In support of this model, Zasadil et al. (2016) have recently found that an increase in CIN level was able to inhibit tumour cell growth but did not suppress its initiation (Zasadil et al., 2016). This observation provides a new therapeutic option by which to preferentially reduce cancer cells; however, the main challenge to this strategy lies in identifying the molecular target.

In the current study, we have taken advantage of the role of INO80 in maintaining chromosomal stability (see 5.3.1) to test its suitability as a therapeutic target that could increase the CIN rate and ultimately kill CIN⁺ tumour cells. Our viability assay data showed that the absence of INO80 increased cell death in CIN⁺ tumour cells, whereas this outcome was not observed in the CIN⁻ cell line DLD1 (Figure 5.4). This led us to propose INO80 as a promising therapeutic target that might be utilised to increase CIN to a lethal level and eventually suppress CIN⁺ tumour growth. These results may be further improved in the future by expanding the panel of tested cell lines (both CIN⁺ and CIN⁻ cells), as our experiments originally included additional colorectal cell lines (CIN⁺: HT55 & T84; CIN⁻: GP2D) that were not subjected to full testing because of difficulties in their culture. Furthermore, subsequent studies to ascertain whether targeting INO80 might increase CIN⁺ cell sensitivity towards chemotherapeutic drugs;

e.g., the microtubule stabilisers taxane or paclitaxel, might help to reduce the required dose concentration of these agents to a level that would increase their efficiency in suppressing tumour growth without affecting healthy cells.

Chapter 6.

Discussion

The work outlined in this thesis provides a novel characterization of the structure and biochemical features of YY1, a human subunit of INO80, which also reveal its ability to form multimers *in vivo* and *in vitro* and to bind several types of DNA (Chapter 3). Furthermore, this study demonstrates a novel mechanism of how human INO80 promotes HR repair through its ability to remove H2AZ from damaged chromatin. In addition, it provides the first evidence related to the dynamics of H2AZ on damaged chromatin in human cells. Specifically, H2AZ is incorporated within seconds onto induced damage and then rapidly removed, and the removal reaction is partially dependent on INO80 (Chapter 4). Moreover, this work confirms the role of INO80 in the maintenance of chromosomal stability during mitosis and shows that the loss of INO80 is lethal for CIN+ tumour cell lines; thus leading to the proposal of INO80 as a therapeutic target for CIN+ tumour cells (Chapter 5).

A major challenge lies in understanding how ATPase chromatin-remodelling complexes manipulate the highly compact chromatin structure by effectively evicting, exchanging, or sliding histones or nucleosomes along the DNA. Our finding in Chapter 3 expands our understanding of how human INO80 efficiently interacts with the DNA through a direct association between YY1-RUVBL1/2 and DNA. The established structure of YY1 and its multimerisation feature may also assist in understanding how the INO80 complex performs its remodelling activity. The establishment of the “embryonic” structure of yeast INO80 by Tosi et al. (2013) and the identification of all of the crosslinks between INO80 subunits and nucleosomes has advanced the field by explaining the manner in which INO80 achieves some of its remodelling activities. It has been suggested that INO80 can form a flexible cradle between its head, neck, and body regions that can accommodate and embrace the nucleosome. It is envisioned that

nucleosomal DNA binds to the head, neck, and body, whereas the flexible foot region attaches to histones at both sides of the nucleosome. It has also been suggested that the large conformational change in INO80 might facilitate the open nucleosome conformation, in which H2A-H2B dimers are moderately disassociated from the H3-H4 tetramer, and that this could subsequently enable the histone-exchange activity of the INO80 complex (Tosi et al., 2013). Notably, the head of INO80 is formed from Rvb1/2, whereas the body consists of the N-terminal domain and metazoan subunits that contribute to high-affinity DNA or nucleosome recognition (Tosi et al., 2013). Chen et al. (2011) further showed that YY1 recruitment is dependent on the HSA domain in humans, the latter of which, according to Tosi et al. (2013), together with its dependent subunits form the foot of the embryonic INO80. In contrast, Wu et al. (2007) found that the recruitment of YY1 is dependent on the N-terminal domain and the middle segment of mammalian INO80. Our result from Chapter 3, however, suggested that YY1 is likely to be located within the body of INO80 as it indicated that YY1 directly interacted with the RUVBL1/2 complex and this interaction increased the affinity towards binding several types of DNA. Therefore, it is possible that the YY1 functions to loosen the interaction between DNA and the nucleosomes, thus for example facilitating nucleosomes sliding.

In addition, mislocalized unacetylated H2AZ represents a source of genome instability, as in yeast the failure in removing unacetylated H2AZ by INO80 resulted in a sensitivity to replication stress and DNA damage-inducing drugs (Papamichos-Chronakis et al., 2011). Furthermore, overexpression of H2AZ has been found in several types of cancer including breast as well as sporadic colorectal and bladder cancers (Monteiro et al., 2014). Our finding in Chapter 4 extends our understanding of

the dynamic state of H2AZ in human cells, in which H2AZ is transiently and immediately incorporated into damaged chromatin and then rapidly removed. Our finding also provides novel evidence regarding the dependency of H2AZ removal on INO80 in human cells (Alatwi & Downs, 2015); moreover, this removal reaction has been shown by others to require ANP32E as well (Gursory-Yuzugullu et al., 2015). This identified mechanism will likely be of assistance in future studies investigating the regulation of H2AZ enrichment.

With respect to DSB repair, however, the removal of H2AZ from damaged chromatin by both INO80 and ANP32E comprises the fundamental mechanism to ensure the fidelity of HR. In this situation, failure in removing H2AZ from damaged chromatin constitutes a barrier for resection, which leads to the inefficient loading of RAD51 foci and ultimately defective HR (Alatwi & Downs, 2015). The Price group showed that the incorporation of H2AZ at damaged sites is required for H4 acetylation, which eventually leads to open and relaxed chromatin consequent to the destabilisation of histone-histone and histone-DNA interactions (Xu et al., 2012). Subsequently, the same group has recently reported that it is the removal of H2AZ that is required for H4 acetylation, suggesting that the binding of ANP32E to H2AZ may free the H4 tail and promote its acetylation, which in turn will ultimately relax the chromatin (Gursory-Yuzugullu et al., 2015). Based on this finding, they hypothesized that the transient incorporation of H2AZ at sites of DNA damage may temporarily ‘heterochromatinise’ and stabilize the damaged chromatin to allow time for the cell to prepare the chromatin for repair, whereas the subsequent removal of H2AZ may lead to relaxed chromatin at the site where resection occurs (Gursory-Yuzugullu et al., 2015). In either case, the presence of H2AZ results in the DNA at DSBs being inaccessible until the H2AZ is

removed, which according to their data requires approximately 10 minutes via ANP32E. In contrast, repair is known to be an immediate process as upon inducing DSBs γ H2AX is rapidly formed to initiate the repair and facilitate the recruitment of repair proteins (see 1.3.3.2). Therefore, our favoured model is that the deposition of H2AZ instead promotes the formation of open and relaxed chromatin allowing accessibility to the damage sites by repair proteins, whereupon H2AZ removal is required to allow for resection and ultimately efficient HR.

Finally, recent studies have shed light on the role of INO80 in chromosomal stability and the fidelity of mitosis. In yeast, Ino80 regulates chromosomal stability through its role in regulating H2AZ removal, as H2AZ enrichment in the pericentric chromatin leads to aneuploidy (Chambers et al., 2012). In comparison, in human cells INO80 was found to function in mitosis through negatively controlling the expression of the tumour suppressor p21. In particular, loss of INO80 increased p21 expression, resulting in a significant increase in the number of cells with more than two centrosomes per nucleus, aberrant cytokinesis, and multipolar spindle formation (Cao et al., 2015). Our results in Chapter 5 confirm the role of INO80 in the maintenance of chromosomal stability. Furthermore, they demonstrated that the loss of INO80 induced cell death in CIN+ cell lines, which led us to propose that INO80 may be utilised to therapeutically target CIN+ tumour cells. Notably, INO80 was recently found to interact with BAP1, a tumour suppressor that also stabilizes INO80 during DNA replication in normal cells; accordingly, INO80 is downregulated in BAP1-defective cancer cells through its destabilization (Lee et al., 2014). Furthermore, very recent studies have found that INO80 is highly expressed in cervical cancer cells (Hu et al., 2016), non-small cell lung cancer (Zhang et al., 2016), and melanoma (Zhou et al., 2016). Hu et al. (2016) also

demonstrated that INO80 regulates the expression of Nanog, a transcription factor associated with the self-renewal and pluripotency of embryonic stem cells and which was found to be activated in cervical cancer cells. INO80 knockdown in these cells arrested cells in G0/G1 phase and suppressed tumour growth (Hu et al., 2016). In lung cancer cells (Zhang et al., 2016) and melanoma (Zhou et al., 2016), INO80 has been found to promote oncogenic transcription. Conversely, INO80 silencing inhibits tumour proliferation *in vitro* and tumour growth in mice (Zhang et al., 2016; Zhou et al., 2016). Taken together, these various lines of evidence strongly indicate a critical role for INO80 in guarding genome stability and selectively inhibiting the tumour growth of several types of cancers.

References

Abbott, D.W., Ivanova, V.S., Wang, X., Bonner, W.M., Ausió, J. (2001). Characterization of the Stability and Folding of H2A.Z Chromatin Particles IMPLICATIONS FOR TRANSCRIPTIONAL ACTIVATION. *J. Biol. Chem.* 276, 41945–41949.

Ahnesorg P., Smith P. & Jackson S.P. (2006). XLF interacts with the XRCC4-DNA ligase IV complex to promote DNA nonhomologous end-joining. *Cell* 124, 301–313.

Alatwi, H.E., Downs, J.A. (2015). Removal of H2A.Z by INO80 promotes homologous recombination. *EMBO rep* 16, 986–994.

Altaf, M., Auger, A., Covic, M., Côté, J. (2009). Connection between histone H2A variants and chromatin remodeling complexes This paper is one of a selection of papers published in this Special Issue, entitled CSBMCB's 51st Annual Meeting – Epigenetics and Chromatin Dynamics, and has undergone the Journal's usual peer review process. *Biochem. Cell Biol.* 87, 35–50.

Bakkenist, C.J., Kastan, M.B. (2003). DNA damage activates ATM through intermolecular autophosphorylation and dimer dissociation. *Nature* 421, 499–506.

Bannister, A.J., Zegerman, P., Partridge, J.F., Miska, E.A., Thomas, J.O., Allshire, R.C., Kouzarides, T. (2001). Selective recognition of methylated lysine 9 on histone H3 by

the HP1 chromo domain. *Nature* 410, 120–124.

Barski, A., Cuddapah, S., Cui, K., Roh, T.-Y., Schones, D.E., Wang, Z., Wei, G., Chepelev, I., Zhao, K. (2007). High-Resolution Profiling of Histone Methylations in the Human Genome. *Cell* 129, 823–837.

Basnet, H., Su, X.B., Tan, Y., Meisenhelder, J., Merkurjev, D., Ohgi, K.A., Hunter, T., Pillus, L., Rosenfeld, M.G. (2014). Tyrosine phosphorylation of histone H2A by CK2 regulates transcriptional elongation. *Nature* 516, 267–271.

Bergmann, J.H., Rodríguez, M.G., Martins, N.M.C., Kimura, H., Kelly, D.A., Masumoto, H., Larionov, V., Jansen, L.E.T., Earnshaw, W.C. (2011). Epigenetic engineering shows H3K4me2 is required for HJURP targeting and CENP-A assembly on a synthetic human kinetochore. *EMBO J.* 30, 328–340.

Beucher A., Birraux J., Tchouandong L., Barton O., Shibata A., Conrad S., Goodarzi A.A., Krempler A., Jeggo P.A. & Löbrich M. (2009). ATM and Artemis promote homologous recombination of radiation-induced DNA double-strand breaks in G2. *EMBO J.* 28, 3413–3427.

Bhaumik, S.R., Smith, E., Shilatifard, A. (2007). Covalent modifications of histones during development and disease pathogenesis. *Nat Struct Mol Biol* 14, 1008–1016.

Billon, P., Côté, J. (2012). Precise deposition of histone H2A.Z in chromatin for genome expression and maintenance. *Biochimica et Biophysica Acta (BBA) - Gene*

Regulatory Mechanisms, Histone chaperones and Chromatin Assembly 1819, 290–302.

Binda, O., Sevilla, A., LeRoy, G., Lemischka, I.R., Garcia, B.A., Richard, S. (2013). SETD6 monomethylates H2AZ on lysine 7 and is required for the maintenance of embryonic stem cell self-renewal. *Epigenetics* 8, 177–183.

Black, B.E., Jansen, L.E.T., Maddox, P.S., Foltz, D.R., Desai, A.B., Shah, J.V., Cleveland, D.W. (2007). Centromere Identity Maintained by Nucleosomes Assembled with Histone H3 Containing the CENP-A Targeting Domain. *Molecular Cell* 25, 309–322.

Bloom, K.S. (2014). Centromeric Heterochromatin: The Primordial Segregation Machine. *Annual Review of Genetics* 48, 457–484.

Bošković, A., Bender, A., Gall, L., Ziegler-Birling, C., Beaujean, N., Torres-Padilla, M.-E. (2012). Analysis of active chromatin modifications in early mammalian embryos reveals uncoupling of H2A.Z acetylation and H3K36 trimethylation from embryonic genome activation. *Epigenetics* 7, 747–757.

Boyarchuk, E., Filipescu, D., Vassias, I., Cantaloube, S., Almouzni, G. (2014). Pericentric heterochromatin state during the cell cycle controls the histone variant composition of centromeres. *J Cell Sci* jcs.14, 81–89.

Boyne, M.T., Pesavento, J.J., Mizzen, C.A., Kelleher, N.L. (2006). Precise Characterization of Human Histones in the H2A Gene Family by Top Down Mass

Spectrometry. *J. Proteome Res.* 5, 248–253.

Brownlee, P.M., Meisenberg, C., Downs, J.A. (2014). The SWI/SNF chromatin remodelling complex: Its role in maintaining genome stability and preventing tumorigenesis. *DNA Repair, Cutting-edge Perspectives in Genomic Maintenance* 32, 127–133.

Burrell, R.A., McClelland, S.E., Endesfelder, D., Groth, P., Weller, M.-C., Shaikh, N., Domingo, E., Kanu, N., Dewhurst, S.M., Gronroos, E., Chew, S.K., Rowan, A.J., Schenk, A., Sheffer, M., Howell, M., Kschischo, M., Behrens, A., Helleday, T., Bartek, J., Tomlinson, I.P., Swanton, C. (2013). Replication stress links structural and numerical cancer chromosomal instability. *Nature* 494, 492–496.

Cao, L., Ding, J., Dong, L., Zhao, J., Su, J., Wang, L., Sui, Y., Zhao, T., Wang, F., Jin, J., Cai, Y. (2015). Negative Regulation of p21 Waf1/Cip1 by Human INO80 Chromatin Remodeling Complex Is Implicated in Cell Cycle Phase G2/M Arrest and Abnormal Chromosome Stability. *PLOS ONE* 10, e0137411.

Carr, A.M., Dorrington, S.M., Hindley, J., Phear, G.A., Aves, S.J., and Nurse, P. (1994). Analysis of a histone H2A variant from fission yeast: evidence for a role in chromosome stability. *Mol. Gen. Genet.* 245, 628–635.

Ceccaldi, R., Rondinelli, B., D'Andrea, A.D. (2016). Repair Pathway Choices and Consequences at the Double-Strand Break. *Trends in Cell Biology, Special Issue: Quality Control* 26, 52–64.

Chambers, A. L. & Downs, J. A. (2012). The RSC and INO80 chromatin-remodeling complexes in DNA double-strand break repair. *Prog Mol Biol Transl Sci* 110, 229–61.

Chambers, A. L., Ormerod, G., Durley, S. C., Sing, T. L., Brown, G. W., Kent, N. A. & Downs, J. A. (2012). The INO80 chromatin remodeling complex prevents polyploidy and maintains normal chromatin structure at centromeres. *Genes Dev* 26, 2590–603.

Chapman, J. R., Taylor, M. R. & Boulton, S. J. (2012). Playing the end game: DNA double-strand break repair pathway choice. *Molecular Cell* 47, 497–510.

Cheeseman, I.M., Desai, A. (2008). Molecular architecture of the kinetochore–microtubule interface. *Nat Rev Mol Cell Biol* 9, 33–46.

Chen, L., Cai, Y., Jin, J., Florens, L., Swanson, S.K., Washburn, M.P., Conaway, J.W., Conaway, R.C. (2011). Subunit Organization of the Human INO80 Chromatin Remodeling Complex AN EVOLUTIONARILY CONSERVED CORE COMPLEX CATALYZES ATP-DEPENDENT NUCLEOSOME REMODELING. *J. Biol. Chem.* 286, 11283–11289.

Chen, M. and Shen, X. (2010). The INO80 chromatin remodeling complex. *Handbook of Cell Signaling*. Elsevier.

Clapier, C.R., Cairns, B.R. (2009). The Biology of Chromatin Remodeling Complexes. *Annual Review of Biochemistry* 78, 273–304.

Clarkson, M. J., Wells, J. R., Gibson, F., Saint, R. & Tremethick, D. J. (1999). Regions of variant histone His2AvD required for *Drosophila* development. *Nature* 399, 694–697.

Conaway, R. C. & Conaway, J. W. (2009). The INO80 chromatin remodeling complex in transcription, replication and repair. *Trends Biochem Sci* 34, 71–7.

Costantini S., Woodbine L., Andreoli L., Jeggo P.A. & Vindigni A. (2007). Interaction of the Ku heterodimer with the DNA ligase IV/Xrcc4 complex and its regulation by DNA-PK. *DNA Repair (Amst.)* 6, 712–722.

Dalvai, M., Fleury, L., Bellucci, L., Kocanova, S., Bystricky, K. (2013). TIP48/Reptin and H2A.Z Requirement for Initiating Chromatin Remodeling in Estrogen-Activated Transcription. *PLOS Genet* 9, e1003387.

Dennehey, B.K., Tyler, J. (2014). Histone Chaperones in the Assembly and Disassembly of Chromatin, in: Workman, J.L., Abmayr, S.M. (Eds.), *Fundamentals of Chromatin*. Springer New York, pp. 29–67.

Dong, S., Han, J., Chen, H., Liu, T., Huen, M.S.Y., Yang, Y., Guo, C., Huang, J. (2014). The human SRCAP chromatin remodeling complex promotes DNA-end resection. *Curr. Biol.* 24, 2097–2110.

Downs, J. A., Allard, S., Jobin-Robitaille, O., Javaheri, A., Auger, A., Bouchard, N., Kron, S. J., Jackson, S. P. & Cote, J. (2004). Binding of chromatin-modifying activities to phosphorylated histone H2A at DNA damage sites. *Molecular Cell* 16, 979–90.

Dunican, D., McWilliam, P., Tighe, O., Parle-McDermott, A. and Croke, D. (2002). Gene expression differences between the microsatellite instability (MIN) and chromosomal instability (CIN) phenotypes in colorectal cancer revealed by high density cDNA array hybridization. *Oncogene*, 21, 3253–3257.

Earnshaw, W.C., Honda, B.M., Laskey, R.A., Thomas, J.O., (1980). Assembly of nucleosomes: the reaction involving *X. laevis* nucleoplasmin. *Cell* 21, 373–383.

Ebbert, R., Birkmann, A. & Schuller, H. J. (1999). The product of the SNF2/SWI2 paralogue INO80 of *Saccharomyces cerevisiae* required for efficient expression of various yeast structural genes is part of a high-molecular-weight protein complex. *Mol Microbiol* 32, 741–51.

Ertych, N., Stolz, A., Stenzinger, A., Weichert, W., Kaulfuß, S., Burfeind, P., Aigner, A., Wordeman, L., Bastians, H. (2014). Increased microtubule assembly rates influence chromosomal instability in colorectal cancer cells. *Nat Cell Biol* 16, 779–791.

Faast, R., Thonglairoam, V., Schulz, T.C., Beall, J., Wells, J.R.E., Taylor, H., Matthaei, K., Rathjen, P.D., Tremethick, D.J., Lyons, I. (2001). Histone variant H2A.Z is required for early mammalian development. *Current Biology* 11, 1183–1187.

Fan, J.Y., Rangasamy, D., Luger, K., Tremethick, D.J. (2004). H2A.Z Alters the Nucleosome Surface to Promote HP1 α -Mediated Chromatin Fiber Folding. *Molecular Cell* 16, 655–661.

Fanning, E., Klimovich, V., Nager, A.R. (2006). A dynamic model for replication protein A (RPA) function in DNA processing pathways. *Nucleic Acids Res.* 34, 4126–4137.

Fenech, M., Kirsch-Volders, M., Natarajan, A.T., Surralles, J., Crott, J.W., Parry, J., Norppa, H., Eastmond, D.A., Tucker, J.D., Thomas, P. (2011). Molecular mechanisms of micronucleus, nucleoplasmic bridge and nuclear bud formation in mammalian and human cells. *Mutagenesis* 26, 125–132.

Fenn, S., Breitsprecher, D., Gerhold, C.B., Witte, G., Faix, J., and Hopfner, K.P. (2011). Structural biochemistry of nuclear actin-related proteins 4 and 8 reveals their interaction with actin. *EMBO J.* 30, 2153–2166.

Filippakopoulos, P., Picaud, S., Mangos, M., Keates, T., Lambert, J.-P., Barsyte-Lovejoy, D., Felletar, I., Volkmer, R., Müller, S., Pawson, T., Gingras, A.-C., Arrowsmith, C.H., Knapp, S. (2012). Histone Recognition and Large-Scale Structural Analysis of the Human Bromodomain Family. *Cell* 149, 214–231.

Filippo, J.S., Sung, P., Klein, H. (2008). Mechanism of Eukaryotic Homologous Recombination. *Annual Review of Biochemistry* 77, 229–257.

Fischle, W., Tseng, B.S., Dormann, H.L., Ueberheide, B.M., Garcia, B.A., Shabanowitz, J., Hunt, D.F., Funabiki, H., Allis, C.D. (2005). Regulation of HP1–chromatin binding by histone H3 methylation and phosphorylation. *Nature* 438, 1116–1122.

Fischle, W., Wang, Y., Jacobs, S.A., Kim, Y., Allis, C.D., Khorasanizadeh, S. (2003). Molecular basis for the discrimination of repressive methyl-lysine marks in histone H3 by Polycomb and HP1 chromodomains. *Genes Dev.* 17, 1870–1881.

Flaus A., Martin D.M., Barton G.J., Owen-Hughes T. (2006). Identification of multiple distinct Snf2 subfamilies with conserved structural motifs. *Nucleic Acids Res* 34, 2887–2905.

Foltz, D.R., Jansen, L.E.T., Bailey, A.O., Yates III, J.R., Bassett, E.A., Wood, S., Black, B.E., Cleveland, D.W. (2009). Centromere-Specific Assembly of CENP-A Nucleosomes Is Mediated by HJURP. *Cell* 137, 472–484.

Fraga, M.F., Ballestar, E., Villar-Garea, A., Boix-Chornet, M., Espada, J., Schotta, G., Bonaldi, T., Haydon, C., Ropero, S., Petrie, K., Iyer, N.G., Pérez-Rosado, A., Calvo, E., Lopez, J.A., Cano, A., Calasanz, M.J., Colomer, D., Piris, M.Á., Ahn, N., Imhof, A., Caldas, C., Jenuwein, T., Esteller, M. (2005). Loss of acetylation at Lys16 and trimethylation at Lys20 of histone H4 is a common hallmark of human cancer. *Nat Genet* 37, 391–400.

Fujita, Y., Hayashi, T., Kiyomitsu, T., Toyoda, Y., Kokubu, A., Obuse, C., Yanagida,

M. (2007). Priming of Centromere for CENP-A Recruitment by Human hMis18 α , hMis18 β , and M18BP1. *Developmental Cell* 12, 17–30.

Fujiwara, Y., Mayanagi, K., Morikawa, K. (2008). Functional significance of octameric RuvA for a branch migration complex from *Thermus thermophilus*. *Biochemical and Biophysical Research Communications* 366, 426–431.

Galvani, A., Courbeyrette, R., Agez, M., Ochsenbein, F., Mann, C., Thuret, J.-Y. (2008). In Vivo Study of the Nucleosome Assembly Functions of ASF1 Histone Chaperones in Human Cells. *Mol. Cell. Biol.* 28, 3672–3685.

Gerhold, C.B., Winkler, D.D., Lakomek, K., Seifert, F.U., Fenn, S., Kessler, B., Witte, G., Luger, K., and Hopfner, K.P. (2012). Structure of Actin-related protein 8 and its contribution to nucleosome binding. *Nucleic Acids Res.* 40, 11036–11046.

Gordon, S., Akopyan, G., Garban, H., Bonavida, B. (2005). Transcription factor YY1: structure, function, and therapeutic implications in cancer biology. *Oncogene* 25, 1125–1142.

Gorynia, S., Bandejas, T.M., Pinho, F.G., McVey, C.E., Vornhein, C., Round, A., Svergun, D.I., Donner, P., Matias, P.M., and Carrondo, M.A. (2011). Structural and functional insights into a dodecameric molecular machine – the RuvBL1/RuvBL2 complex. *J. Struct. Biol.* 176, 279–291.

Gospodinov, A., Tsaneva, I. & Anachkova, B. (2009). RAD51 foci formation in response to DNA damage is modulated by TIP49. *Int J Biochem Cell Biol* 41, 925–33.

Gospodinov, A., Vaissiere, T., Krastev, D. B., Legube, G., Anachkova, B. & Herceg, Z. (2011). Mammalian Ino80 mediates double-strand break repair through its role in DNA end strand resection. *Mol Cell Biol* 31, 4735–45.

Gottlieb T.M. & Jackson S.P. (1993). The DNA-dependent protein kinase: requirement for DNA ends and association with Ku antigen. *Cell* 72, 131–142.

Greaves, I.K., Rangasamy, D., Ridgway, P., Tremethick, D.J. (2007). H2A.Z Contributes to the Unique 3D Structure of the Centromere. *Proceedings of the National Academy of Sciences of the United States of America* 104, 525–530.

Gursoy-Yuzugullu, O., Ayrapetov, M.K., Price, B.D. (2015). Histone chaperone Anp32e removes H2A.Z from DNA double-strand breaks and promotes nucleosome reorganization and DNA repair. *PNAS* 112, 7507–7512.

Heitz, E. (1928). Das Heterochromatin der Moose. I. *Jahrb f wissensch Bot.* 69, 762–818.

Henikoff, S., Ahmad, K. (2005). Assembly of Variant Histones into Chromatin. *Annual Review of Cell and Developmental Biology* 21, 133–153.

Hirota, T., Lipp, J.J., Toh, B.-H., Peters, J.-M. (2005). Histone H3 serine 10 phosphorylation by Aurora B causes HP1 dissociation from heterochromatin. *Nature*

438, 1176–1180.

Hogan, C.J., Aligianni, S., Durand-Dubief, M., Persson, J., Will, W.R., Webster, J., Wheeler, L., Mathews, C.K., Elderkin, S., Oxley, D., Ekwall, K., Varga-Weisz, P.D. (2010). Fission yeast Iec1-ino80-mediated nucleosome eviction regulates nucleotide and phosphate metabolism. *Mol. Cell. Biol.* 30, 657–674.

Hou, H., Wang, Y., Kallgren, S.P., Thompson, J., Yates, J.R., Jia, S. (2010). Histone Variant H2A.Z Regulates Centromere Silencing and Chromosome Segregation in Fission Yeast. *J. Biol. Chem.* 285, 1909–1918.

Houbaviy, H.B., Usheva, A., Shenk, T., Burley, S.K. (1996). Cocystal structure of YY1 bound to the adeno-associated virus P5 initiator. *Proc. Natl. Acad. Sci. U.S.A.* 93, 13577–13582.

Hu, J., Liu, J., Chen, A., Lyu, J., Ai, G., Zeng, Q., Sun, Y., Chen, C., Wang, J., Qiu, J., Wu, Y., Cheng, J., Shi, X., Song, L. (2016). Ino80 promotes cervical cancer tumorigenesis by activating Nanog expression. *Oncotarget*.

Huertas P. & Jackson S.P. (2009). Human CtIP mediates cell cycle control of DNA end resection and double strand break repair. *J. Biol. Chem.* 284, 9558–9565.

Huisinga, K., Brower-Toland, B. and Elgin, S. (2006). The contradictory definitions of heterochromatin: transcription and silencing. *Cromosoma* 115, 110–122.

Iliakis, G., Murmann, T., Soni, A. (2015). Alternative end-joining repair pathways are the ultimate backup for abrogated classical non-homologous end-joining and homologous recombination repair: Implications for the formation of chromosome translocations. *Mutation Research/Genetic Toxicology and Environmental Mutagenesis, Insights into formation and consequences of chromosome aberrations: Report on the 11th International Symposium on Chromosomal Aberrations (ISCA 11), Rhodes, Greece, September 12-14, 2014* 793, 166–175.

Jackson, J.D., Gorovsky, M.A. (2000). Histone H2A.Z has a conserved function that is distinct from that of the major H2A sequence variants. *Nucleic Acids Res* 28, 3811–3816.

Jackson, S.P., and Bartek, J. (2009). The DNA-damage response in human biology and disease. *Nature* 461, 1071–1078.

Janssen, A., Medema, R.H. (2011). Mitosis as an anti-cancer target. *Oncogene* 30, 2799–2809.

Jeggo, P.A., Downs, J.A. (2014). Roles of chromatin remodellers in DNA double strand break repair. *Experimental Cell Research, DNA DAMAGE AND REPAIR* 329, 69–77.

Jeong, K.W., Kim, K., Situ, A.J., Ulmer, T.S., An, W., Stallcup, M.R. (2011). Recognition of enhancer element-specific histone methylation by TIP60 in transcriptional activation. *Nat Struct Mol Biol* 18, 1358–1365.

Jiang, X., Xu, Y., Price, B.D. (2010). Acetylation of H2AX on lysine 36 plays a key role in the DNA double-strand break repair pathway. *FEBS Lett.* 584, 2926–2930.

Kakarougkas, A., Ismail, A., Klement, K., Goodarzi, A.A., Conrad, S., Freire, R., Shibata, A., Lobrich, M., Jeggo, P.A. (2013). Opposing roles for 53BP1 during homologous recombination. *Nucleic Acids Res.* 41, 9719–9731.

Kalocsay, M., Hiller, N.J., Jentsch, S. (2009). Chromosome-wide Rad51 Spreading and SUMO-H2A.Z-Dependent Chromosome Fixation in Response to a Persistent DNA Double-Strand Break. *Molecular Cell* 33, 335–343.

Kashiwaba, S., Kitahashi, K., Watanabe, T., Onoda, F., Ohtsu, M. & Murakami, Y. (2010). The mammalian INO80 complex is recruited to DNA damage sites in an ARP8 dependent manner. *Biochem Biophys Res Commun* 402, 619–25.

Kennedy, R.D., and D'Andrea, A.D. (2006). DNA repair pathways in clinical practice: lessons from pediatric cancer susceptibility syndromes. *J. Clin. Oncol.* 24, 3799–3808.

Kerppola, T.K. (2008). BIMOLECULAR FLUORESCENCE COMPLEMENTATION (BiFC) ANALYSIS AS A PROBE OF PROTEIN INTERACTIONS IN LIVING CELLS. *Annu Rev Biophys* 37, 465–487.

Kitayama, K., Kamo, M., Oma, Y., Matsuda, R., Uchida, T., Ikura, T., Tashiro, S., Ohyama, T., Winsor, B., Harata, M. (2009). The human actin-related protein hArap5:

nucleo-cytoplasmic shuttling and involvement in DNA repair. *Exp Cell Res* 315, 206–217.

Klopf E., Paskova L., Sole C., Mas G., Petryshyn A., Posas F., et al. (2009). Cooperation between the INO80 complex and histone chaperones determines adaptation of stress gene transcription in the yeast *Saccharomyces cerevisiae*. *Mol Cell Biol* 29, 4994–5007.

Kobor, M.S., Venkatasubrahmanyam, S., Meneghini, M.D., Gin, J.W., Jennings, J.L., Link, A.J., Madhani, H.D., and Rine, J. (2004). A protein complex containing the conserved Swi2/Snf2-related ATPase Swr1p deposits histone variant H2A.Z into euchromatin. *PLoS Biol.* 2, E131.

Kouzarides, T. (2007). Chromatin modifications and their function. *Cell* 128, 693–705.

Kracker, S., Di Virgilio, M., Schwartzenuber, J., Cuenin, C., Forveille, M., Deau, M.-C., McBride, K.M., Majewski, J., Gazumyan, A., Seneviratne, S., Grimbacher, B., Kutukculer, N., Herceg, Z., Cavazzana, M., Jabado, N., Nussenzweig, M.C., Fischer, A., Durandy, A. (2015). An inherited immunoglobulin class-switch recombination deficiency associated with a defect in the INO80 chromatin remodeling complex. *J. Allergy Clin. Immunol.* 135, 998–1007.e6.

Krejci, L., Altmannova, V., Spirek, M. & Zhao, X. (2012). Homologous recombination and its regulation. *Nucleic Acids Res*, 40, 5795–818.

Krogan, N.J., Keogh, M.C., Datta, N., Sawa, C., Ryan, O.W., Ding, H., Haw, R.A.,

Pootoolal, J., Tong, A., Canadien, V., et al. (2003). A Snf2 family ATPase complex required for recruitment of the histone H2A variant Htz1. *Mol. Cell* 12, 1565–1576.

Kruhlak, M.J., Celeste, A., Dellaire, G., Fernandez-Capetillo, O., Müller, W.G., McNally, J.G., Bazett-Jones, D.P., Nussenzweig, A. (2006). Changes in chromatin structure and mobility in living cells at sites of DNA double-strand breaks. *J Cell Biol* 172, 823–834.

Kuo, A.J., Song, J., Cheung, P., Ishibe-Murakami, S., Yamazoe, S., Chen, J.K., Patel, D.J., Gozani, O. (2012). The BAH domain of ORC1 links H4K20me2 to DNA replication licensing and Meier-Gorlin syndrome. *Nature* 484, 115–119.

Kurihara, T., Hori, M., Takeda, H., Inoue, M., Yoneda, Y. (1996). Partial purification and characterization of a protein kinase that is activated by nuclear localization signal peptides. *FEBS Letters* 380, 241–245.

Laskey RA, Honda BM, Mills AD, Finch JT (1978). Nucleosomes are assembled by an acidic protein which binds histones and transfers them to DNA. *Nature* 275(5679), 416–420.

Laulier, C., Cheng, A., Stark, J.M. (2011). The relative efficiency of homology-directed repair has distinct effects on proper anaphase chromosome separation. *Nucl. Acids Res.* 39, 5935–5944.

Lavin, M.F. (2008). Ataxia-telangiectasia: from a rare disorder to a paradigm for cell

signalling and cancer. *Nat. Rev. Mol. Cell Biol.* 9, 759–769.

Lee, H.-S., Lee, S.-A., Hur, S.-K., Seo, J.-W., Kwon, J. (2014). Stabilization and targeting of INO80 to replication forks by BAP1 during normal DNA synthesis. *Nat Commun* 5, 5128.

Lee, H.-S., Park, J.-H., Kim, S.-J., Kwon, S.-J., Kwon, J. (2010). A cooperative activation loop among SWI/SNF, γ -H2AX and H3 acetylation for DNA double-strand break repair. *EMBO J* 29, 1434–1445.

Lewin, B., Krebs, J., Kilpatrick, S.T., Goldstein, E.S. (2011). *Lewin's GENES X*. Jones & Bartlett Learning.

Li, B., Pattenden, S.G., Lee, D., Gutiérrez, J., Chen, J., Seidel, C., Gerton, J., Workman, J.L. (2005). Preferential occupancy of histone variant H2AZ at inactive promoters influences local histone modifications and chromatin remodeling. *Proc Natl Acad Sci U S A* 102, 18385–18390.

Li, X., Corsa, C.A.S., Pan, P.W., Wu, L., Ferguson, D., Yu, X., Min, J., Dou, Y. (2010). MOF and H4 K16 acetylation play important roles in DNA damage repair by modulating recruitment of DNA damage repair protein Mdc1. *Mol. Cell. Biol.* 30, 5335–5347.

Liu J., Doty T., Gibson B. & Heyer W-D. (2010). Human BRCA2 protein promotes RAD51 filament formation on RPA-covered single-stranded DNA. *Nat. Struct. Mol.*

Biol. 17, 1260–1262.

Liu, L.F., Desai, S.D., Li, T.-K., Mao, Y., Sun, M., Sim, S.-P. (2000). Mechanism of Action of Camptothecin. *Annals of the New York Academy of Sciences* 922, 1–10.

López-Perrote, A., Alatwi, H.E., Torreira, E., Ismail, A., Ayora, S., Downs, J.A., Llorca, O. (2014). Structure of Yin Yang 1 Oligomers that Cooperate with RuvBL1-RuvBL2 ATPases. *J. Biol. Chem.* jbc.M114.567040.

López-Perrote, A., Muñoz-Hernández, H., Gil, D., Llorca, O. (2012). Conformational transitions regulate the exposure of a DNA-binding domain in the RuvBL1–RuvBL2 complex. *Nucleic Acids Res* 40, 11086–11099.

Lorentz A., Heim L., Schmidt H. (1992). The switching gene *swi6* affects recombination and gene expression in the mating-type region of *Schizosaccharomyces pombe*. *Mol Gen Genet* 233, 436–442.

Losada, A. (2014). Cohesin in cancer: chromosome segregation and beyond. *Nat Rev Cancer* 14, 389–393.

Lou, Z., Minter-Dykhouse, K., Franco, S., Gostissa, M., Rivera, M.A., Celeste, A., Manis, J.P., van Deursen, J., Nussenzweig, A., Paull, T.T., et al. (2006). MDC1 maintains genomic stability by participating in the amplification of ATM-dependent DNA damage signals. *Mol. Cell* 21, 187–200.

Lu, H., Guo, X., Meng, X., Liu, J., Allen, C., Wray, J., Nickoloff, J.A., Shen, Z. (2005). The BRCA2-Interacting Protein BCCIP Functions in RAD51 and BRCA2 Focus Formation and Homologous Recombinational Repair. *Mol. Cell. Biol.* 25, 1949–1957.

Luger, K. (2001). Nucleosomes: Structure and Function, in: eLS. John Wiley & Sons, Ltd.

Luger, K., Dechassa, M.L., Tremethick, D.J. (2012). New insights into nucleosome and chromatin structure: an ordered state or a disordered affair? *Nat Rev Mol Cell Biol* 13, 436–447.

Luk, E., Ranjan, A., FitzGerald, P.C., Mizuguchi, G., Huang, Y., Wei, D., Wu, C. (2010). Stepwise Histone Replacement by SWR1 Requires Dual Activation with Histone H2A.Z and Canonical Nucleosome. *Cell* 143, 725–736.

Ma Y., Pannicke U., Schwarz K. & Lieber M.R. (2002). Hairpin opening and overhang processing by an Artemis/DNA-dependent protein kinase complex in nonhomologous end joining and V(D)J recombination. *Cell* 108, 781–794.

Maeshima, K., Imai, R., Tamura, S. and Nozaki, N. (2014). Chromatin as dynamic 10-nm fibers. *Chromosoma* 123, 225–237.

Mao, Z., Pan, L., Wang, W., Sun, J., Shan, S., Dong, O., Liang, X., Dai, L., Ding, X., Chen, S., Zhang, Z., Zhu, B. and Zhou, Z. (2014). Anp32e, a higher eukaryotic histone chaperone directs preferential recognition for H2A.Z. *Cell Research* 24, 389–399.

Matias, P.M., Gorynia, S., Donner, P., Carrondo, M.A. (2006). Crystal Structure of the Human AAA+ Protein RuvBL1. *J. Biol. Chem.* 281, 38918–38929.

Mayanagi, K., Fujiwara, Y., Miyata, T., Morikawa, K. (2008). Electron microscopic single particle analysis of a tetrameric RuvA/RuvB/Holliday junction DNA complex. *Biochemical and Biophysical Research Communications* 365, 273–278.

McGranahan, N., Burrell, R.A., Endesfelder, D., Novelli, M.R., Swanton, C. (2012). Cancer chromosomal instability: therapeutic and diagnostic challenges. *EMBO reports* 13, 528–538.

Meneghini, M.D., Wu, M., Madhani, H.D. (2003). Conserved Histone Variant H2A.Z Protects Euchromatin from the Ectopic Spread of Silent Heterochromatin. *Cell* 112, 725–736.

Millar, C.B., Xu, F., Zhang, K., Grunstein, M. (2006). Acetylation of H2AZ Lys 14 is associated with genome-wide gene activity in yeast. *Genes Dev* 20, 711–722.

Mimitou, E.P., Symington, L.S. (2009). DNA end resection: Many nucleases make light work. *DNA Repair, Checkpoint response to DNA damage* 8, 983–995.

Mimitou, E.P., Symington, L.S. (2011). DNA end resection--unraveling the tail. *DNA Repair (Amst.)* 10, 344–348.

Mimori T. & Hardin J.A. (1986). Mechanism of interaction between Ku protein and DNA. *J. Biol. Chem.* 261, 10375–10379.

Min, J., Tian, Y., Xiao, Y., Wu, L., Li, L. and Chang, S. (2013). The mINO80 chromatin remodeling complex is required for efficient telomere replication and maintenance of genome stability. *Cell Research* 23, 1396–1413.

Mizuguchi, G., Shen, X., Landry, J., Wu, W.H., Sen, S., and Wu, C. (2004). ATPdriven exchange of histone H2AZ variant catalyzed by SWR1 chromatin remodeling complex. *Science* 303, 343–348.

Monteiro, F.L., Baptista, T., Amado, F., Vitorino, R., Jerónimo, C., Helguero, L.A. (2014). Expression and functionality of histone H2A variants in cancer. *Oncotarget* 5, 3428–3443.

Morrison, A. J., Highland, J., Krogan, N. J., Arbel-Eden, A., Greenblatt, J. F., Haber, J. E., Shen, X. (2004). INO80 and γ -H2AX interaction links ATP-dependent chromatin remodeling to DNA damage repair. *Cell* 119, 767–775.

Morrison, A.J., Kim, J.-A., Person, M.D., Highland, J., Xiao, J., Wehr, T.S., Hensley, S., Bao, Y., Shen, J., Collins, S.R., Weissman, J.S., Delrow, J., Krogan, N.J., Haber, J.E., Shen, X. (2007). Mec1/Tel1 Phosphorylation of the INO80 Chromatin Remodeling Complex Influences DNA Damage Checkpoint Responses. *Cell* 130, 499–511.

Murr, R., Loizou, J.I., Yang, Y.-G., Cuenin, C., Li, H., Wang, Z.-Q., Herceg, Z. (2006).

Histone acetylation by Trrap-Tip60 modulates loading of repair proteins and repair of DNA double-strand breaks. *Nat. Cell Biol.* 8, 91–99.

Murray, J. M., Stiff, T. & Jeggo, P. A. (2012). DNA double-strand break repair within heterochromatic regions. *Biochem Soc Trans* 40, 173–8.

Musselman, C.A., Lalonde, M.-E., Côté, J., Kutateladze, T.G. (2012). Perceiving the epigenetic landscape through histone readers. *Nat Struct Mol Biol* 19, 1218–1227.

Nano, N., Houry, W.A. (2013). Chaperone-like activity of the AAA+ proteins Rvb1 and Rvb2 in the assembly of various complexes. *Philos Trans R Soc Lond B Biol Sci* 368.

Nishi, R., Wijnhoven, P., le Sage, C., Tjeertes, J., Galanty, Y., Forment, J.V., Clague, M.J., Urbé, S., Jackson, S.P. (2014). Systematic characterization of deubiquitylating enzymes for roles in maintaining genome integrity. *Nat Cell Biol* 16, 1016–1026.

Obri, A., Ouarrhni, K., Papin, C., Diebold, M., Padmanabhan, K., Marek, M., Stoll, I., Roy, L., Reilly, P., Mak, T., Dimitrov, S., Romier, C. & Hamiche, A. (2014). ANP32E is a histone chaperone that removes H2A.Z from chromatin. *Nature* 505, 648–653.

Ogiwara, H., Ui, A., Otsuka, A., Satoh, H., Yokomi, I., Nakajima, S., Yasui, A., Yokota, J., Kohno, T. (2011). Histone acetylation by CBP and p300 at double-strand break sites facilitates SWI/SNF chromatin remodeling and the recruitment of non-homologous end joining factors. *Oncogene* 30, 2135–2146.

Olins A.L., Olins D.E. (1974). Spheroid chromatin units (v bodies). *Science* 183, 330–332.

Papamichos-Chronakis, M., Krebs, J.E., Peterson, C.L. (2006). Interplay between Ino80 and Swr1 chromatin remodeling enzymes regulates cell cycle checkpoint adaptation in response to DNA damage. *Genes Dev.* 20, 2437–2449.

Papamichos-Chronakis, M., Watanabe, S., Rando, O.J., Peterson, C.L. (2011). Global regulation of H2A.Z localization by the INO80 chromatin remodeling enzyme is essential for genome integrity. *Cell* 144, 200–213.

Papin, C., Humbert, O., Kalashnikova, A., Eckert, K., Morera, S., Kas, E. & Grigoriev, M. (2010). 3'- to 5' DNA unwinding by TIP49b proteins. *FEBS J*, 277, 2705–14.

Park EJ, Hur SK, Kwon J. (2010). Human INO80 chromatin-remodelling complex contributes to DNA double-strand break repair via the expression of Rad54B and XRCC3 genes. *Biochem J*, 431, 179–87.

Park, Y.-J., Dyer, P.N., Tremethick, D.J., Luger, K. (2004). A New Fluorescence Resonance Energy Transfer Approach Demonstrates That the Histone Variant H2AZ Stabilizes the Histone Octamer within the Nucleosome. *J. Biol. Chem.* 279, 24274–24282.

Price, B.D., D'Andrea, A.D. (2013). Chromatin Remodeling at DNA Double-Strand Breaks. *Cell* 152, 1344–1354.

Qiu, Y., Liu, L., Zhao, C., Han, C., Li, F., Zhang, J., Wang, Y., Li, G., Mei, Y., Wu, M.,

Wu, J., Shi, Y. (2012). Combinatorial readout of unmodified H3R2 and acetylated H3K14 by the tandem PHD finger of MOZ reveals a regulatory mechanism for HOXA9 transcription. *Genes Dev.* 26, 1376–1391.

Radman-Livaja, M., Rando, O.J. (2010). Nucleosome positioning: How is it established, and why does it matter? *Developmental Biology, Special Section: Gene Expression and Development* 339, 258–266.

Raisner, R.M., Hartley, P.D., Meneghini, M.D., Bao, M.Z., Liu, C.L., Schreiber, S.L., Rando, O.J., Madhani, H.D. (2005). Histone Variant H2A.Z Marks the 5' Ends of Both Active and Inactive Genes in Euchromatin. *Cell* 123, 233–248.

Rogakou, E.P., Pilch, D.R., Orr, A.H., Ivanova, V.S., and Bonner, W.M. (1998). DNA double-stranded breaks induce histone H2AX phosphorylation on serine 139. *J. Biol. Chem.* 273, 5858–5868.

Rosa, J.L. da, Holik, J., Green, E.M., Rando, O.J., Kaufman, P.D. (2011). Overlapping Regulation of CenH3 Localization and Histone H3 Turnover by CAF-1 and HIR Proteins in *Saccharomyces cerevisiae*. *Genetics* 187, 9–19.

Roy, R., Chun, J. & Powell, S. N. (2012). BRCA1 and BRCA2: different roles in a common pathway of genome protection. *Nat Rev Cancer* 12, 68–78.

Saksouk, N., Simboeck, E., Déjardin, J., (2015). Constitutive heterochromatin formation and transcription in mammals. *Epigenetics & Chromatin* 8, 3.

Sarcinella, E., Zuzarte, P.C., Lau, P.N.I., Draker, R., Cheung, P. (2007). Monoubiquitylation of H2A.Z Distinguishes Its Association with Euchromatin or Facultative Heterochromatin. *Mol Cell Biol* 27, 6457–6468.

Sarma, K., Reinberg, D. (2005). Histone variants meet their match. *Nat Rev Mol Cell Biol* 6, 139–149.

Schlissel, M. S. (2002). Does artemis end the hunt for the hairpin-opening activity in V(D)J recombination? *Cell* 109, 1–4.

Schneider, R., Bannister, A.J., Myers, F.A., Thorne, A.W., Crane-Robinson, C., Kouzarides, T. (2004). Histone H3 lysine 4 methylation patterns in higher eukaryotic genes. *Nat Cell Biol* 6, 73–77.

Seeber, A., Dion, V., Gasser, S.M. (2013). Checkpoint kinases and the INO80 nucleosome remodeling complex enhance global chromatin mobility in response to DNA damage. *Genes Dev.* 27, 1999–2008.

Sevilla, A., Binda, O. (2014). Post-translational modifications of the histone variant h2az. *Stem Cell Research* 12, 289–295.

Sharma, G.G., So, S., Gupta, A., Kumar, R., Cayrou, C., Avvakumov, N., Bhadra, U., Pandita, R.K., Porteus, M.H., Chen, D.J., Cote, J., Pandita, T.K. (2010). MOF and histone H4 acetylation at lysine 16 are critical for DNA damage response and double-

strand break repair. *Mol. Cell. Biol.* 30, 3582–3595.

Shen X., Mizuguchi G., Hamich A., Wu C. A. (2000). chromatin remodeling complex involved in transcription and DNA processing. *Nature* 406, 541–4.

Shen X., Ranallo R., Choi E., Wu C. (2003). Involvement of actin-related proteins in ATP-dependent chromatin remodeling. *Mol Cell* 12, 147–55.

Shi, X., Hong, T., Walter, K.L., Ewalt, M., Michishita, E., Hung, T., Carney, D., Peña, P., Lan, F., Kaadige, M.R., Lacoste, N., Cayrou, C., Davrazou, F., Saha, A., Cairns, B.R., Ayer, D.E., Kutateladze, T.G., Shi, Y., Côté, J., Chua, K.F., Gozani, O. (2006). ING2 PHD domain links histone H3 lysine 4 methylation to active gene repression. *Nature* 442, 96–99.

Shibata A., Conrad S., Birraux J., Geuting V., Barton O., Ismail A., Kakarougkas A., Meek K., Taucher-Scholz G., Löbrich M. & Jeggo P.A. (2011). Factors determining DNA double-strand break repair pathway choice in G2 phase. *EMBO J.* 30, 1079–1092.

Shimada, K., Oma, Y., Schleker, T., Kugou, K., Ohta, K., Harata, M., Gasser, S.M., (2008). Ino80 Chromatin Remodeling Complex Promotes Recovery of Stalled Replication Forks. *Current Biology* 18, 566–575.

Shogren-Knaak, M., Ishii, H., Sun, J.-M., Pazin, M.J., Davie, J.R., Peterson, C.L. (2006). Histone H4-K16 acetylation controls chromatin structure and protein interactions. *Science* 311, 844–847.

- Shyu, Y.J., Hiatt, S.M., Duren, H.M., Ellis, R.E., Kerppola, T.K., Hu, C.D. (2008). Visualization of protein interactions in living *Caenorhabditis elegans* using bimolecular fluorescence complementation analysis. *Nat Protoc* 3, 588–596.
- Smeenk, G., Attikum, H. van. (2013). The Chromatin Response to DNA Breaks: Leaving a Mark on Genome Integrity. *Annual Review of Biochemistry* 82, 55–80.
- Smeenk, G., Mailand, N. (2016). Writers, Readers, and Erasers of Histone Ubiquitylation in DNA Double-Strand Break Repair. *Front Genet* 7.
- Smerdon, M.J. (1991). DNA repair and the role of chromatin structure. *Curr. Opin. Cell Biol.* 3, 422–428.
- Strahl, B.D., Allis, C.D. (2000). The language of covalent histone modifications. *Nature* 403, 41–45.
- Struhl, K., Segal, E. (2013). Determinants of nucleosome positioning. *Nat Struct Mol Biol* 20, 267–273.
- Stucki, M., Clapperton, J.A., Mohammad, D., Yaffe, M.B., Smerdon, S.J., Jackson, S.P. (2005). MDC1 Directly Binds Phosphorylated Histone H2AX to Regulate Cellular Responses to DNA Double-Strand Breaks. *Cell* 123, 1213–1226.
- Su, J., Sui, Y., Ding, J., Li, F., Shen, S., Yang, Y., Lu, Z., Wang, F., Cao, L., Liu, X.,

Jin, J., Cai, Y. (2016). Human INO80/YY1 chromatin remodeling complex transcriptionally regulates the BRCA2- and CDKN1A-interacting protein (BCCIP) in cells. *Protein Cell* 1–12.

Sullivan, M., Morgan, D.O. (2007). Finishing mitosis, one step at a time. *Nat Rev Mol Cell Biol* 8, 894–903.

Suto, R.K., Clarkson, M.J., Tremethick, D.J., Luger, K. (2000). Crystal structure of a nucleosome core particle containing the variant histone H2A.Z. *Nat Struct Mol Biol* 7, 1121–1124.

Svetelis, A., Gévry, N., Gilles Grondin, G. and Gaudreau, L. (2010). H2A.Z overexpression promotes cellular proliferation of breast cancer cells. *Cell Cycle* 9:2, 364–370.

Talbert, P.B., Henikoff, S. (2010). Histone variants — ancient wrap artists of the epigenome. *Nat Rev Mol Cell Biol* 11, 264–275.

Tanaka, K., Hirota, T. (2016). Chromosomal instability: A common feature and a therapeutic target of cancer. *Biochimica et Biophysica Acta (BBA) - Reviews on Cancer* 1866, 64–75.

Tosi, A., Haas, C., Herzog, F., Gilmozzi, A., Berninghausen, O., Ungewickell, C., Gerhold, C.B., Lakomek, K., Aebersold, R., Beckmann, R., Hopfner, K.-P. (2013). Structure and subunit topology of the INO80 chromatin remodeler and its nucleosome

complex. *Cell* 154, 1207–1219.

Tsukuda T., Fleming A.B., Nikoloff J.A., Osley M.A. (2005). Chromatin remodelling at a DNA doublestrand break site in *Saccharomyces cerevisiae*. *Nature* 438, 379–83.

Tsukuda, T., Lo, Y. C., Krishna, S., Sterk, R., Osley, M. A. & Nikoloff, J. A. (2009). INO80-dependent chromatin remodeling regulates early and late stages of mitotic homologous recombination. *DNA Repair (Amst)* 8, 360_9.

Udugama M., Sabri A., Bartholomew B. (2011). The INO80 ATP-dependent chromatin remodeling complex is a nucleosome spacing factor. *Mol Cell Biol* 31, 662–73.

Usheva, A., Shenk, T. (1996). YY1 transcriptional initiator: Protein interactions and association with a DNA site containing unpaired strands. *PNAS* 93, 13571–13576.

Van Attikum, H., Fritsch, O., Hohn, B. & Gasser, S. M. (2004). Recruitment of the INO80 complex by H2A phosphorylation links ATP-dependent chromatin remodeling with DNA double-strand break repair. *Cell* 119, 777–88.

Vassileva, I., Yanakieva, I., Peycheva, M., Gospodinov, A., Anachkova, B. (2014). The mammalian INO80 chromatin remodeling complex is required for replication stress recovery. *Nucleic Acids Res.* 42, 9074–9086.

Venkatesh, S., Workman, J.L. (2015). Histone exchange, chromatin structure and the regulation of transcription. *Nat Rev Mol Cell Biol* 16, 178–189.

Verdaasdonk, J.S., Bloom, K. (2011). Centromeres: unique chromatin structures that drive chromosome segregation. *Nat Rev Mol Cell Biol* 12, 320–332.

Vermeulen, M., Mulder, K.W., Denissov, S., Pijnappel, W.W.M.P., Schaik, F.M.A. van, Varier, R.A., Baltissen, M.P.A., Stunnenberg, H.G., Mann, M., Timmers, H.T.M. (2007). Selective Anchoring of TFIID to Nucleosomes by Trimethylation of Histone H3 Lysine 4. *Cell* 131, 58–69.

Vorobiev, S., Strokopytov, B., Drubin, D.G., Frieden, C., Ono, S., Condeelis, J., Rubenstein, P.A., and Almo, S.C. (2003). The structure of nonvertebrate actin: implications for the ATP hydrolytic mechanism. *Proc. Natl. Acad. Sci. USA*, 100, 5760–5765.

Wellcome Trust Sanger Institute, Genome Research Limited (2016). COSMIC Cell Line Project. Available at: http://cancer.sanger.ac.uk/cell_lines/sample/overview?id=909698 (Accessed: 5 November 2016).

Wieland, G., Orthaus, S., Ohndorf, S., Diekmann, S., Hemmerich, P. (2004). Functional Complementation of Human Centromere Protein A (CENP-A) by Cse4p from *Saccharomyces cerevisiae*. *Mol. Cell. Biol.* 24, 6620–6630.

Wilson, C., H.J. Bellen, and W.J. Gehring. (1990). Position effects on eukaryotic gene expression. *Annu Rev Cell Biol* 6, 679–714.

Windhofer, F., Wu, W., Wang, M., Singh, S.K., Saha, J., Rosidi, B., Iliakis, G. (2007). Marked Dependence on Growth State of Backup Pathways of NHEJ. *International Journal of Radiation Oncology • Biology • Physics* 68, 1462–1470.

Wu, S., Shi, Y., Mulligan, P., Gay, F., Landry, J., Liu, H., Lu, J., Qi, H.H., Wang, W., Nickoloff, J.A., Wu, C., Shi, Y. (2007). A YY1–INO80 complex regulates genomic stability through homologous recombination–based repair. *Nat Struct Mol Biol* 14, 1165–1172.

Xu, Y., Ayrapetov, M.K., Xu, C., Gursoy-Yuzugullu, O., Hu, Y., Price, B.D. (2012). Histone H2A.Z Controls a Critical Chromatin Remodeling Step Required for DNA Double-Strand Break Repair. *Molecular Cell* 48, 723–733.

Yamada, K., Ariyoshi, M., Morikawa, K. (2004). Three-dimensional structural views of branch migration and resolution in DNA homologous recombination. *Current Opinion in Structural Biology* 14, 130–137.

Yang, Y., Lu, Y., Espejo, A., Wu, J., Xu, W., Liang, S., Bedford, M.T. (2010). TDRD3 is an Effector Molecule for Arginine Methylated Histone Marks. *Mol Cell* 40, 1016–1023.

Yun, M.H., Hiom, K. (2009). CtIP-BRCA1 modulates the choice of DNA double-strand-break repair pathway throughout the cell cycle. *Nature* 459, 460–463.

Zasadil, L.M., Britigan, E.M.C., Ryan, S.D., Kaur, C., Guckenberger, D.J., Beebe, D.J., Moser, A.R., Weaver, B.A. (2016). High rates of chromosome missegregation suppress tumor progression but do not inhibit tumor initiation. *Mol. Biol. Cell* 27, 1981–1989.

Zeng, L., Zhang, Q., Li, S., Plotnikov, A.N., Walsh, M.J., Zhou, M.-M. (2010). Mechanism and Regulation of Acetylated Histone Binding by the Tandem PHD Finger of DPF3b. *Nature* 466, 258–262.

Zhang, H., Roberts, D.N., Cairns, B.R. (2005). Genome-Wide Dynamics of Htz1, a Histone H2A Variant that Poises Repressed/Basal Promoters for Activation through Histone Loss. *Cell* 123, 219–231.

Zhang, S., Zhou, B., Wang, L., Li, P., Bennett, B.D., Snyder, R., Garantziotis, S., Fargo, D.C., Cox, A.D., Chen, L., Hu, G. (2016). INO80 is required for oncogenic transcription and tumor growth in non-small cell lung cancer. *Oncogene*.

Zhou, B., Wang, L., Zhang, S., Bennett, B.D., He, F., Zhang, Y., Xiong, C., Han, L., Diao, L., Li, P., Fargo, D.C., Cox, A.D., Hu, G. (2016). INO80 governs superenhancer-mediated oncogenic transcription and tumor growth in melanoma. *Genes Dev.* 30, 1440–1453.

Zhou, Z., Feng, H., Zhou, B.-R., Ghirlando, R., Hu, K., Zwolak, A., Miller Jenkins, L.M., Xiao, H., Tjandra, N., Wu, C., Bai, Y. (2011). Structural basis for recognition of centromere histone variant CenH3 by the chaperone Scm3. *Nature* 472, 234–237.

Zlatanova, J., Thakar, A. (2008). H2A.Z: View from the Top. *Structure* 16, 166–179.

Zucchi, I., Mento, E., Kuznetsov, V.A., Scotti, M., Valsecchi, V., Simionati, B., Vicinanza, E., Valle, G., Pilotti, S., Reinbold, R., Vezzoni, P., Albertini, A., Dulbecco, R. (2004). Gene expression profiles of epithelial cells microscopically isolated from a breast-invasive ductal carcinoma and a nodal metastasis. *Proc Natl Acad Sci U S A* 101, 18147–18152.

Appendix

Structure of Yin Yang 1 Oligomers That Cooperate with RuvBL1-RuvBL2 ATPases*

Received for publication, March 19, 2014, and in revised form, May 22, 2014. Published, JBC Papers in Press, July 2, 2014, DOI 10.1074/jbc.M114.567040

Andrés López-Perrote[‡], Hanan E. Alatwi[§], Eva Torreira[‡], Amani Ismail[§], Silvia Ayora[¶], Jessica A. Downs^{§1}, and Oscar Llorca^{‡2}

From the [‡]Centro de Investigaciones Biológicas, Consejo Superior de Investigaciones Científicas, Ramiro de Maetzu 9, 28040 Madrid, Spain, [§]Genome Damage and Stability Centre, University of Sussex, Science Park Road, Falmer, Brighton BN1 9RQ, United Kingdom, and [¶]Centro Nacional de Biotecnología, Consejo Superior de Investigaciones Científicas, Darwin 3, 28049 Madrid, Spain

Background: Oligomerization of transcription factor YY1 is not well understood.

Results: YY1 assembles homo-oligomers that bind DNAs without the consensus sequence, whose structure is studied by electron microscopy.

Conclusion: RuvBL1-RuvBL2 enhances YY1 binding to DNAs without the consensus sequence for the transcription factor.

Significance: YY1-RuvBL1-RuvBL2 complexes could contribute to functions beyond transcription, and we find this occurs during homologous recombination.

Yin Yang 1 (YY1) is a transcription factor regulating proliferation and differentiation and is involved in cancer development. Oligomers of recombinant YY1 have been observed before, but their structure and DNA binding properties are not well understood. Here we find that YY1 assembles several homo-oligomeric species built from the association of a bell-shaped dimer, a process we characterized by electron microscopy. Moreover, we find that YY1 self-association also occurs *in vivo* using bimolecular fluorescence complementation. Unexpectedly, these oligomers recognize several DNA substrates without the consensus sequence for YY1 *in vitro*, and DNA binding is enhanced in the presence of RuvBL1-RuvBL2, two essential AAA+ ATPases. YY1 oligomers bind RuvBL1-RuvBL2 hetero-oligomeric complexes, but YY1 interacts preferentially with RuvBL1. Collectively, these findings suggest that YY1-RuvBL1-RuvBL2 complexes could contribute to functions beyond transcription, and we show that YY1 and the ATPase activity of RuvBL2 are required for RAD51 foci formation during homologous recombination.

Yin Yang 1 (YY1)³ is a polycomb group transcription factor that regulates important cellular events through activation or repression of transcription. YY1 is ubiquitously expressed in many tissues and participates in replication, differentiation, proliferation, embryogenesis, and development (1–4). YY1 overexpression in some tumors correlates with recurrences and

bad prognosis, and YY1 has been proposed as a marker for cancer progression (5). Interestingly, recent reports have broadened the spectrum of processes regulated by YY1 such as silencing of retro-elements in embryonic cells (6), regulation of long noncoding RNAs (7), inactivation of the X chromosome in the females of mammals (4), and a direct role in V(D)J recombination during early B-cell development (8).

Human YY1 is a 414-amino acid protein with a predicted molecular mass of 44 kDa and highly conserved in eukaryotes (sequence identity between human and mouse >98%) (1) (Fig. 1A). Putative structural and functional homologs in *Schizosaccharomyces pombe* (Iec1) (9) and *Drosophila melanogaster* (PHO (pleiohomeotic) and PHOL (pleiohomeotic-like)) (10) have been studied. YY1 hallmark is four C₂H₂-type zinc finger motifs located at its C terminus (residues 298–397), responsible for the sequence-specific recognition of a consensus DNA sequence (5'-(C/g/a)(G/t)(C/t/a)CATN(T/a)(T/g/c)-3', where the uppercase letters indicate the preferred base for each position) being the most frequent ACAT and CCAT. This C-terminal region harbors part of the transcriptional repression activity of YY1. The co-crystal structure of residues 293–414 bound to the adeno-associated virus P5 promoter showed the four zinc fingers interacting with the DNA major groove. The structure revealed that the interaction with the consensus sequence is defined by specific contacts between YY1 side chains and bases of the DNA (11). Less is known about other segments of the protein. The N terminus has been implicated in transcriptional activation, whereas residues 170–201 participate in transcriptional repression (12, 13). Residues 201–226 form the REPO (recruitment of polycomb) domain, involved in polycomb group repression (14).

There is evidence that YY1 is important for maintaining genome stability (15), but this could in part work through its role as a transcriptional regulator of genes involved in DNA damage responses (16, 17). Yet YY1 could also have a direct role in DNA damage responses as it has been shown that YY1-INO80 complexes may function in DNA repair by homologous recombination (HR) (15). INO80 is a multisubunit chromatin-

* This work was supported by the Spanish Government (SAF2011-22988 (to O. L.), BES-2009-014133 (to A. L.-P.), BFU2012-39879-C02-02 (to S. A.)) and by Cancer Research UK (CEA-C7905 (to J. A. D.)).

¹ To whom correspondence should be addressed. Tel.: 44-1273-678-369; E-mail: J.A.Downs@sussex.ac.uk.

² To whom correspondence should be addressed. Tel.: 34-91-837-31-12 (ext. 4446); E-mail: ollorca@cib.csic.es.

³ The abbreviations used are: YY1, Yin Yang 1; HR, homologous recombination; HJ, Holliday junction; SEC, size exclusion chromatography; RCT, random conical tilt; RPA, replication protein A; WB, Western blot; IF, immunofluorescence; BiFC, bimolecular fluorescence complementation; IR, ionizing radiation; Gata3, GATA-binding protein 3; Gy, gray; nt, nucleotide; H2AX, histone 2AX; CENPF, centromere protein F.

remodeling complex that includes, in addition to YY1 and the Ino80 catalytic subunit, RuvBL1 and RuvBL2 (18, 19), two closely related (65% sequence similarity) AAA+ (ATPases associated with diverse cellular activities) proteins (20, 21). They share homology with RuvB, the prokaryotic helicase involved in Holliday junction (HJ) resolution during HR. RuvB assembles as hexameric rings, and its DNA-dependent ATPase activity provides the energy for branch migration (22). RuvBL1 and RuvBL2 are essential in multiple processes including transcription, DNA repair, and nonsense-mediated mRNA decay, and their overexpression is associated with tumorigenesis (20, 21).

X-ray crystallography (23–25) and electron microscopy (EM) (26–28) revealed that RuvBL1 and RuvBL2 are organized in three domains. Domain I (DI) and III (DIII) comprise the catalytic ATPase core, responsible for the oligomerization in homo-hexameric rings with a central channel. RuvBL1 and RuvBL2 also assemble hetero-oligomers with alternating RuvBL1 and RuvBL2 subunits (23–25). DII is a unique insertion connected to the ATPase core, resembling an OB-fold, and recombinant DII domains of RuvBL1 interact with ssDNA, dsDNA, and ssRNA *in vitro* (23–25). Using cryo-EM we recently solved the structure of human RuvBL1-RuvBL2 complexes assembled as hetero-dodecamers composed of two hexameric rings interacting back-to-back (27). These dodecamers co-existed in two different conformations whose functional significance is still unclear. RuvBL1 and RuvBL2 interact with YY1 *in vitro* (15), but these complexes have not been characterized in detail.

Although there is evidence that YY1 can oligomerize *in vitro* (15), little is currently known about the structure or DNA binding activity of these oligomeric complexes. Moreover, it is not known if YY1 forms oligomers *in vivo*. Here we have analyzed the assembly of YY1 using EM, and we determine the low resolution architecture of these YY1 oligomers, providing new structural information on full-length YY1. In addition, we also provide evidence of YY1 self-association *in vivo*. Interestingly, we find that YY1 oligomers bind to several DNA substrates without the consensus sequence for YY1 as a transcription factor. These oligomers also bind to RuvBL1-RuvBL2 ATPases *in vitro*, and we find that RuvBL1-RuvBL2 enhances DNA binding by YY1. These findings help explain some unconventional functions ascribed to YY1 recently that could hardly be understood only on the basis of its function as a transcription factor. We explore one of these, and we show that, consistent with previous results (15), YY1 and RuvBL1-RuvBL2 cooperate during DNA repair, but in addition our results indicate these proteins are required for the correct assembly of RAD51 filaments and that this function is dependent on RuvBL2 ATPase activity.

EXPERIMENTAL PROCEDURES

Expression and Purification of Recombinant Proteins—His-YY1 was expressed using *Escherichia coli* Origami (DE3) cells, and induction was performed by the addition of 0.5 mM isopropyl 1-thio- β -D-galactopyranoside (final concentration) at 37 °C for 3 h. For Strep-II-YY1, BL21 (DE3) cells were used, and induction was carried out by the addition of 0.1 mM isopropyl 1-thio- β -D-galactopyranoside (final concentration) at 28 °C for

4 h. In both cases the medium was supplemented with 0.1 mM ZnCl₂ (final concentration) at the time of induction, and cell lysis was performed by sonication in 100 mM Na₂HPO₄/NaH₂PO₄, 300 mM NaCl, 0.1 mM ZnCl₂ containing a mixture of proteases inhibitors (Roche Applied Science). His-YY1 was purified by affinity chromatography using a HisTrap HP column (GE Healthcare) equilibrated in 100 mM Na₂HPO₄/NaH₂PO₄, 300 mM NaCl, 50 mM imidazole, 0.1 mM ZnCl₂ followed by a cationic exchange Mini S PC 3.2/3 (GE Healthcare) column. Purified His-YY1 was dialyzed against 50 mM Tris-HCl, pH 7.4, 200 mM NaCl, 10% (v/v) glycerol, 0.1 mM ZnCl₂ overnight and stored at –80 °C. Strep-II-YY1 was purified in one step using a StrepTrap HP column (GE Healthcare) equilibrated in 50 mM Tris-HCl, pH 7.4, 500 mM NaCl, 10% (v/v) glycerol, 0.1 mM ZnCl₂, and eluted using 2.5 mM D-desthiobiotin in the same buffer. Purified Strep-II-YY1 was dialyzed in the same buffer as His-YY1 and stored at –80 °C. In all cases, size exclusion chromatography (SEC) was used as a final step of purification using a BioSep-SEC-S4000 (Phenomenex) or a Superdex 200 PC 3.2/30 column (GE Healthcare) equilibrated in 50 mM Tris-HCl, pH 7.4, 200 mM NaCl, 10% (v/v) glycerol, 0.1 mM ZnCl₂.

His-RuvBL1 and His-RuvBL2 were expressed in BL21 (DE3) cells by induction with 0.1 mM isopropyl 1-thio- β -D-galactopyranoside (final concentration) at 28 °C for 4 h. They were purified by affinity chromatography using a HisTrap HP column (GE Healthcare) equilibrated in 50 mM Tris-HCl, pH 7.4, 300 mM NaCl, 10% (v/v) glycerol, 20 mM imidazole and eluted using a gradient of 20–500 mM imidazole. Fractions containing the proteins were pooled and dialyzed overnight at 4 °C in 25 mM Tris-HCl, pH 7.4, 250 mM NaCl. In the indicated cases, SEC was performed using a Superdex 200 PC 3.2/30 (GE Healthcare) or Superdex 200 10/300 GL (GE Healthcare) column equilibrated in 50 mM Tris-HCl, pH 7.4, 250 mM NaCl, 10% (v/v) glycerol. His-RuvBL1-RuvBL2 and RuvBL1-RuvBL2 were produced as described (27).

Affinity Purification of YY1-RuvBL1-RuvBL2 Complexes—Recombinant Strep-II-YY1 was used to test interactions with His-RuvBL1, His-RuvBL2, His-RuvBL1-RuvBL2, and RuvBL1-RuvBL2 proteins *in vitro*. Pulldown assays were performed by incubation of purified Strep-II-YY1 with a 2-fold molar excess of the purified partner (His-RuvBL1, His-RuvBL2, His-RuvBL1-RuvBL2, or RuvBL1-RuvBL2) in 50 mM Tris-HCl, pH 7.4, 500 mM NaCl, 10% (v/v) glycerol, 0.1 mM ZnCl₂ for 20 min on ice followed by the addition of StrepTactin High Performance Resin (GE Healthcare) and further incubation for 30 min at 4 °C with agitation. After 3 washes with the reaction buffer, proteins retained in the resin were eluted with 50 mM Tris-HCl, pH 7.4, 500 mM NaCl, 10% (v/v) glycerol, 0.1 mM ZnCl₂, 2.5 mM D-desthiobiotin. All purification steps were monitored by SDS-PAGE, and protein detection was carried out using Oriole® Fluorescent Gel Stain (Bio-Rad) or silver staining.

Glutaraldehyde Cross-linking—Purified His-YY1 (0.1 μ g/ μ l) was dialyzed in 100 mM Na₂HPO₄/NaH₂PO₄, 300 mM NaCl, 0.1 mM ZnCl₂ for 3 h, and 13.5 μ l of the protein were cross-linked in 15- μ l reactions on ice using glutaraldehyde 0.005% (v/v) (final concentration) for 30 min. The reactions were stopped using 192 mM Tris-glycine (final concentration). Samples were

YY1 Oligomers That Bind RuvBL1-RuvBL2

analyzed by SDS-PAGE and Western blotting using the anti-YY1 antibody.

GraFix—Affinity-purified Strep-II-YY1 (10 μM) was stabilized in a discontinuous glycerol/glutaraldehyde gradient by the GraFix method (29). 100 μl of the sample were applied on the top of the tube. As a control, sample was also applied into a similar glycerol gradient without the cross-linking agent. Samples were centrifuged at 30,000 rpm, 4 $^{\circ}\text{C}$ for 18 h (rotor SW 55 Ti). After centrifugation, fractions were collected, and reactions stopped by the addition of 192 mM Tris-Glycine (final concentration).

Electron Microscopy and Image Processing—A few microli- ters of each of the samples analyzed were deposited on carbon-coated grids immediately after elution from the SEC column and stained using 2% (w/v) uranyl acetate. All observations were performed in a JEOL 1230 transmission electron microscope operated at 100 kV. Images were collected using a low-dose protocol and a 4k x 4k TVIPS CMOS detector under control of the EM-TOOLS software (TVIPS). Final magnification of the CMOS micrographs was 68222.5 \times . Contrast transfer function for each micrograph was estimated using CTFFIND3 (30) and corrected using BSOFT (31) before selecting particles. Particles were boxed and extracted from the micrographs using e2boxer in EMAN2 (32). 16362 particles for complex A and 52713 particles for complex B were boxed and classified using reference-free methods in EMAN (33), EMAN2 (32), and XMIPP (34). Particles were binned at 4.56 $\text{\AA}/\text{pixel}$ before further processing. *Ab initio* structures for each experiment were obtained by the random conical tilt (RCT) method (35) using XMIPP (34). RCT was applied on those molecule images classified as belonging to the same view of the oligomer and using the images of these same molecules after tilting the specimen holder by 45 $^{\circ}$. The resulting volumes were then used as templates for angular refinement using EMAN (33). The rotational symmetry of the YY1 complexes was determined by calculating the power rotational spectra of sections of the RCT structures generated using SPIDER (36) along the longitudinal axis of the complex, as implemented in XMIPP (34), as well as for the reference-free two-dimensional averages. Refinement was performed without assuming any symmetry, but after some rounds of refinement 2-fold rotational symmetry was imposed and refined further until convergence. The hand selected was that provided by the RCT structure. The resolution of the structure (20 \AA) was estimated using Fourier shell correlation (FSC) and a 0.5 correlation coefficient. We verified that the bias of the template used for angular refinement did not affect convergence significantly. For this, we refined the same dataset from four independent templates and imposing 2-fold symmetry. Images were refined from: (i) a RCT structure; (ii) a structure obtained using the common lines method as implemented in the *startAny* command from EMAN (33); (iii) a model generated using the *startcsym* program from EMAN (33), searching for particles with the best 2-fold rotational symmetry, which are the defined as top views, and for particles with the best mirror symmetry and poor 2-fold symmetry, defined as sided views; class averages from each group and the 2-fold symmetry were used to generate a three-dimensional model; (iv) a model was generated using *e2initialmodel.py* in EMAN2 (32), where a ran-

dom featureless blob model is used to seed a refinement using reference-free class averages. All structures were filtered according to the estimated resolution and rendered using UCSF Chimera (37).

DNA Substrates—DNAs were made by annealing combinations of oligonucleotides (Table 1). In each case one of the oligonucleotides was labeled at the 5'-end by polynucleotide kinase with [γ - ^{32}P]ATP before annealing. Holliday junction J3, which has 40-bp arms, was made from oligonucleotides J3-1 to J3-4, the duplex dsDNA_no_sp_1 (not containing the consensus sequence) from J3-2 and J3-5, and dsDNA_sp_1 (containing the consensus sequence) from 43-1 and 43-2. The 80-nt ssDNA substrate used was labeled J3-2 oligonucleotide. Holliday junction HJ_25 (with 25-bp arms) was made from oligonucleotides HJ_1 to HJ_4. Annealing was performed in 100 mM phosphate buffer, pH 7.5, with the appropriate combinations of oligonucleotides, mixing one radiolabeled oligonucleotide with cold complementary oligonucleotides in a 1:2 ratio. The annealed products were resolved on an 8% non-denaturing polyacrylamide gel. The bands containing the annealed substrates were purified as described in Zecchi *et al.* (38). DNA concentration was calculated by scintillation counting. DNA substrates labeled with Cy5 (Sigma) at the 5'-end were annealed as described for the γ - ^{32}P -labeled substrates. Holliday junction HJ_25_sp was made from oligonucleotides HJ_12 and HJ_34_1 and HJ_25_no_sp from HJ_12 and HJ_34_2. dsDNA containing (dsDNA_sp_2) or not (dsDNA_no_sp_2) the consensus sequence for YY1 were made from oligonucleotides DS_1 and DS_2, and DS_3 and DS_4, respectively.

Electrophoretic Mobility Shift Assays (EMSA)—Binding of YY1 and RuvBL1-RuvBL2 to DNA was analyzed through EMSA using different radiolabeled DNA substrates (0.3 nM). Reactions were performed in 50 mM Tris-HCl, pH 7.5, 0.05 mg/ml BSA, 60 mM NaCl, 10% (v/v) glycerol, 1 mM MgCl₂, 0.1 mM ZnCl₂, 1 mM DTT for 30 min at 37 $^{\circ}\text{C}$. Complexes were separated by 8 or 6% native-PAGE in Tris borate-EDTA 0.5 \times at 4 $^{\circ}\text{C}$. Gels were run at 200 V for 3 h and dried before autoradiography and phosphorimaging. Apparent binding constants were determined as the protein concentration resulting in half binding to a DNA substrate at 0.3 nM by EMSA. The exact value of the half-binding point was determined from interpolation on a Hill plot. Binding constants are the average values obtained from at least three independent experiments (the results given stand within a 10% standard error).

For the supershift experiments, reactions were carried out in the same conditions as those for the binding assays, but after incubation at 37 $^{\circ}\text{C}$ for 30 min, the indicated amounts of anti-YY1 antibody or PBS 1 \times as a control was added to reactions and further incubated for 15 min at 37 $^{\circ}\text{C}$. Samples were separated under the same conditions as those described before for the binding assays. Binding of YY1 fractions from the SEC to Cy5-labeled DNA (10 nM) substrates was also analyzed through EMSA. Reactions were carried out on ice for 30 min in buffer 50 mM Tris-HCl, pH 7.4, 150 mM NaCl, 10% (v/v) glycerol, 10 mM MgCl₂, 0.1 mM ZnCl₂. Complexes were solved on 6% native-PAGE gels in Tris borate-EDTA 0.5 \times at 4 $^{\circ}\text{C}$. Fluorescence of the DNA was detected with a Fujifilm FLA-3000 equipment. Native-PAGE gels were transferred to PVDF membranes, and

protein was detected by Western blot with the anti-YY1 antibody.

Cell Culture and Irradiation—A549 and U2OS cells were cultured in Eagle's minimum essential medium (MEM) or DMEM (Invitrogen), respectively, supplemented with 10% FCS, L-glutamine, penicillin, and streptomycin (Invitrogen) at 37 °C in a humidified 95% air and 5% CO₂ atmosphere. Cells were irradiated by exposure to a ¹³⁷Cs source.

Small Interfering RNA (siRNA) Knockdown Conditions and Antibodies—siRNA-mediated knockdown was achieved using HiPerFect Transfection Reagent (Qiagen) following the manufacturer's instructions. siRNA duplexes were transfected into 4 × 10⁵ of logarithmically growing cells per condition. Cells were harvested 24 h later, retransfected with siRNA, and then seeded and grown for 48 h. The primary antibodies used were: γH2AX (Millipore) at 1:800 for IF, replication protein A (RPA; Millipore) at 1:100 for IF, RAD51 (Santa Cruz Biotechnology) at 1:200 for IF, CENPF (Abcam) at 1:1000 for IF, YY1 (H-414, Santa Cruz Biotechnology) at 1:1000 for WB, RuvBL2 (Abcam) at 1:5000 for WB, and KAP-1 (Abcam) at 1:1000 for WB. Anti-YY1 antibody (H-10 X, Santa Cruz Biotechnologies) for super-shift experiments was used. The secondary antibodies used were: FITC (Sigma) at 1:100 for IF, Cy3 (Sigma) at 1:200 for IF, AlexaFluor 488/555/350 (Invitrogen) at 1:400 for IF, goat anti-rabbit HRP at 1:10,000 for WB, rabbit anti-mouse HRP at 1:2,000 for WB. Anti-His-HRP conjugated antibody (Sigma) was used at 1:10,000 for WB.

Bimolecular Fluorescence Complementation (BiFC)—1.5 × 10⁵ of U2OS cells were co-transfected with 0.25 μg of VN173- and VC155-derived plasmids using a NanoJuice Transfection Reagent kit (Novagen). 24 h post-transfection cells were fixed with 3% (w/v) paraformaldehyde, permeabilized with 0.5% Triton X-100, and mounted with Vectashield containing 4',6-diamidino-2-phenylindole (DAPI; Vector Laboratories Ltd). Slides were analyzed and imaged using an Applied Precision® Delta Vision® RT Olympus IX70 deconvolution microscope.

Immunofluorescence—Cells plated on coverslips were fixed for 10 min with fixative (2% (w/v) paraformaldehyde, 3% (w/v) sucrose, 1× PBS) and permeabilized for 3 min with 0.2% Triton X-100 in PBS. When staining for RPA/RAD51 in cells not transfected with plasmid, pre-extraction was performed by treatment with 0.2% Triton X-100 in PBS for 0.5–1 min before paraformaldehyde fixation. Cells were rinsed with PBS and incubated with primary antibody diluted in PBS + 2% (w/v) BSA for 1 h at room temperature. Cells were washed 3 times, incubated with secondary antibody (diluted in PBS + 2% (w/v) BSA) for 30 min at room temperature in the dark, incubated with DAPI for 10 min, and washed 3 times with PBS. Slides were mounted using Vectashield and visualized/analyzed using a Nikon-e400 microscope and imaged using an Applied Precision® Delta Vision® RT Olympus IX70 deconvolution microscope and softWoRx® Suite software. For γH2AX, RPA, and RAD51 foci quantification, a minimum of 30 cells were scored blindly per experiment, and error bars represent the S.D. between three experiments.

Plasmids and Constructs for in Vivo Studies—The BiFC plasmids pBiFC-VN173 (encoding the N-terminal region of Venus; Addgene no. 22010) and pBiFC-VC155 (encoding the C-termi-

nal region of Venus; Addgene no. 22011) were obtained from Chang-Deng Hu (via Addgene (49)). The coding region of YY1 was amplified from the YY1 cDNA (Source BioScience) and cloned into the BiFC plasmids to create pYY1-VN and pYY1-VC. The RuvBL2 complete human ORF cDNA (accession number NM_006666) was purchased from Origene as GFP-tagged transfection-ready DNA. To generate siRNA-resistant RuvBL2 expression constructs, the following nucleotides were mutated: 451 G to A, 460 A to T, 466 A to T using QuikChange site-directed mutagenesis (Stratagene). The GFP-RuvBL2^{K83A} ATPase mutant construct was generated using QuikChange site-directed mutagenesis (Stratagene) on the siRNA-resistant template.

RESULTS

YY1 Assembles Two Distinct Oligomeric Species—Human full-length His-tagged YY1 (His-YY1) was expressed in bacteria and purified to homogeneity (Fig. 1B) for structural and biochemical studies. His-YY1 migrated with the apparent mobility of a larger protein (~65–68 kDa) due to its amino acid composition (39). We analyzed the functionality of the recombinant protein by testing the ability of His-YY1 to bind DNA using synthetic 4-way DNA substrates (HJ) by EMSA (Fig. 1C). His-YY1 bound two types of HJ with arms of 40 bp (Fig. 1C, left panel) and 25 bp (Fig. 1C, right panel). The shifted band was specifically super-shifted with an anti-YY1 antibody unable to shift DNA complexes of the RecU resolvase used as a control (not shown). There were several His-YY1 DNA complexes, suggesting the binding of multiple monomers to each DNA molecule and opening the possibility of YY1 oligomerization (15).

Confirming the work by Wu *et al.* (15), we found that His-YY1 behaved as an oligomer in a SEC (Fig. 1D), but in addition we observed that His-YY1 migrated as two distinct species, an ~100–150-kDa complex (named as complex A) and a larger oligomer of about 200–300 kDa (complex B). Complex A could correspond to a 2- or 3-mer according to the calibration of the column using molecular weight standards (Fig. 1D), and this complex appeared as square-shaped molecules compatible with an oligomer by EM (Fig. 1E). Complex B appeared at the microscope as an elongated molecule with roughly double length than complex A (Fig. 1E). Some larger species were also detected eluting from the column (Fig. 1D), but they appeared as aggregates in the electron microscope (Fig. 1E, inset). Oligomerization was also detected by analyzing the electrophoretic mobility of His-YY1 after a mild cross-linking using glutaraldehyde, which showed the presence of multimers containing several subunits migrating as dimers and also larger oligomers (Fig. 1F). Several lines of evidence revealed that complex B was assembled by the oligomerization of complex A, as the ratio between complex B and A in SEC was dependent on the input sample concentration. When fractions from the SEC corresponding to complex B were re-injected in the same column, a peak containing His-YY1 that migrates as complex A and containing square-shaped molecules was detected (Fig. 1G). This was interpreted as resulting from the disassembling of the larger species, suggesting an equilibrium between the two oligomers.

YY1 Oligomers That Bind RuvBL1-RuvBL2

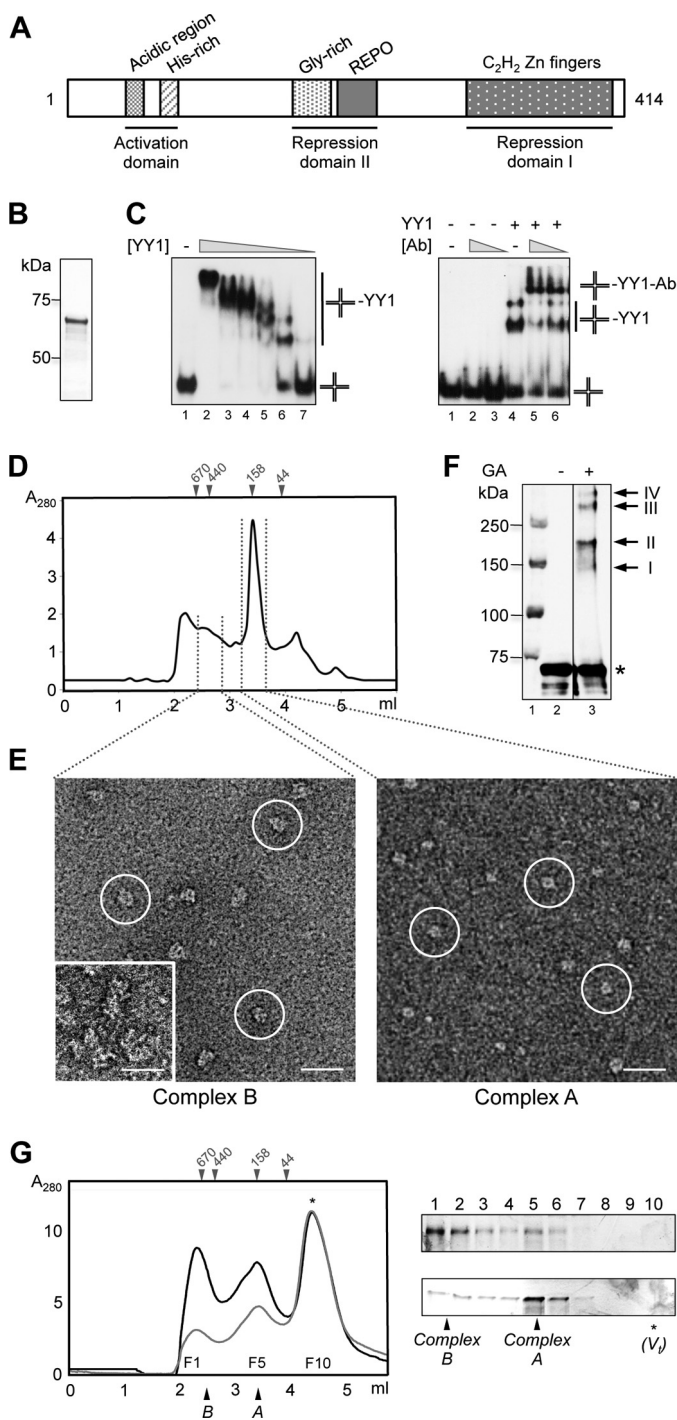


FIGURE 1. Purification and characterization of human YY1. *A*, scheme of human YY1 primary sequence. Relevant domains and motifs are indicated. *B*, SimplyBlue (Invitrogen) staining SDS-PAGE of purified His-YY1. *C*, *left panel*, His-YY1 was incubated with a synthetic HJ DNA (described as J3 under “Experimental Procedures”), and reactions were resolved by 6% non-denaturing PAGE. 0.3 nM of HJ (J3) was titrated with increasing amounts of YY1 (lanes 2–7, 1920, 960, 480, 240, 120, and 60 nM, respectively). *Right panel*, antibody super shift experiments demonstrated the specificity of the interaction. *Lane 1*, HJ probe alone (described as HJ_25_no_sp under “Experimental Procedures”); *lanes 2 and 3*, 2 and 1 μ g of anti-YY1 antibody (Ab) alone, respectively; *lane 4*, YY1 protein alone (100 nM); *lanes 5 and 6*, incubation of YY1 protein (100 nM) with 2 and 1 μ g of anti-YY1 antibody, respectively. Positions of unbound HJ probe, YY1-HJ, and YY1-HJ-antibody shifted-bands are indicated. *D*, SEC of purified His-YY1 in a BioSep-SEC-S4000 (Phenomenex) column. The column was calibrated with molecular weight standards (GE Healthcare), and the elution volume for some of the standards is shown on the top of the chromatogram. *E*, different fractions from the SEC in *D* were observed in the electron microscope, and fields from representative electron micrographs are shown. Typical molecule images are highlighted within circles. The inset in the left panel shows a view of aggregates found to elute first from the SEC column. The scale bar represents 250 Å. *F*, Western blot with an anti-YY1 antibody of His-YY1 after cross-linking with glutaraldehyde (GA); *lane 1*, molecular weight standards (Bio-Rad); *lane 2*, control without GA; *lane 3*, 30 min of incubation with GA. His-YY1 monomer migrates as a 70-kDa protein in SDS-PAGE (labeled as *). Cross-linked bands, with a relative molecular weight multiples of the YY1 monomer, are labeled with arrows. *G*, SEC of His-YY1 was as in *D* (black line). The peak fraction corresponding to complex B was re-injected (gray line) in the same column, and the fractions (F1 to F10) of both experiments were analyzed by silver-stained SDS-PAGE. The top panel corresponds to fractions from the black line and bottom panel for the gray line chromatography, respectively. Positions of the YY1 complexes A and B as well as molecular weight standards (GE Healthcare) used for column calibration are indicated. Total volume of the column (V_t) is indicated by an asterisk (*).

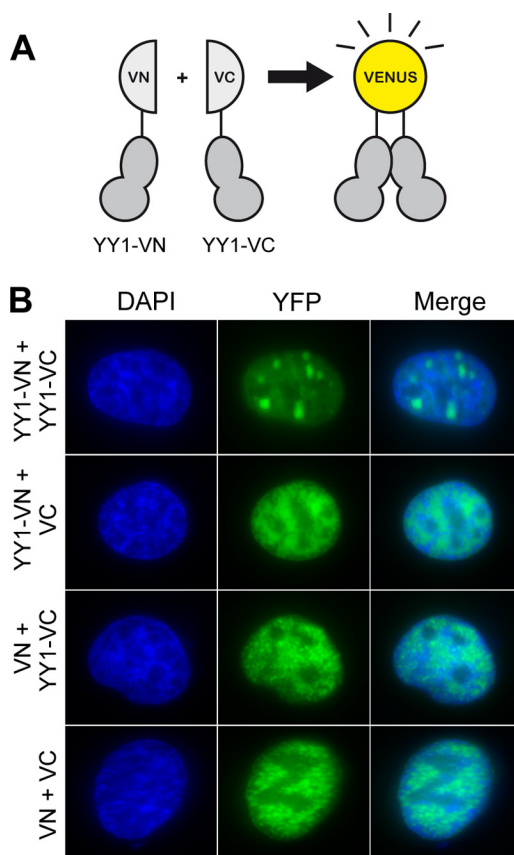


FIGURE 2. YY1 multimerizes *in vivo*. *A*, scheme of the expression constructs used in BiFC experiments. The coding sequence of YY1 was fused to either the N-terminal (YY1-VN) or C-terminal (YY1-VC) domain of Venus. *B*, U2OS cells transiently co-transfected with plasmids expressing the fusions in *A* were analyzed by microscopy. Co-transfection of YY1-VN with VC or YY1-VC with VN displayed no difference in pan-nuclear fluorescence compared with cells co-transfected with the empty vectors (VC and VN). Only cells co-transfected with both YY1 fusion constructs (YY1-VN and YY1-VC) had distinct foci present in the nuclei.

YY1 Forms Multimers *in Vivo*—Whether the oligomerization of YY1 found for the recombinant protein also occurs *in vivo* is unknown. Thus we used BiFC to detect YY1 self-association *in vivo*. We created two YY1 fusion constructs with complementary fragments (VN or VC) of the YFP fluorescent reporter protein Venus (Fig. 2*A*). Fluorescence occurs when the complementary fragments of Venus are in close proximity, providing readout of protein-protein interactions *in vivo*. We co-trans-

fered the complementary fragments of YY1 with the complementary fragments of Venus. *in vivo* self-association of YY1 was detected by BiFC. We created two YY1 fusion constructs with complementary fragments (VN or VC) of the YFP fluorescent reporter protein Venus (Fig. 2*A*). Fluorescence occurs when the complementary fragments of Venus are in close proximity, providing readout of protein-protein interactions *in vivo*. We co-trans-

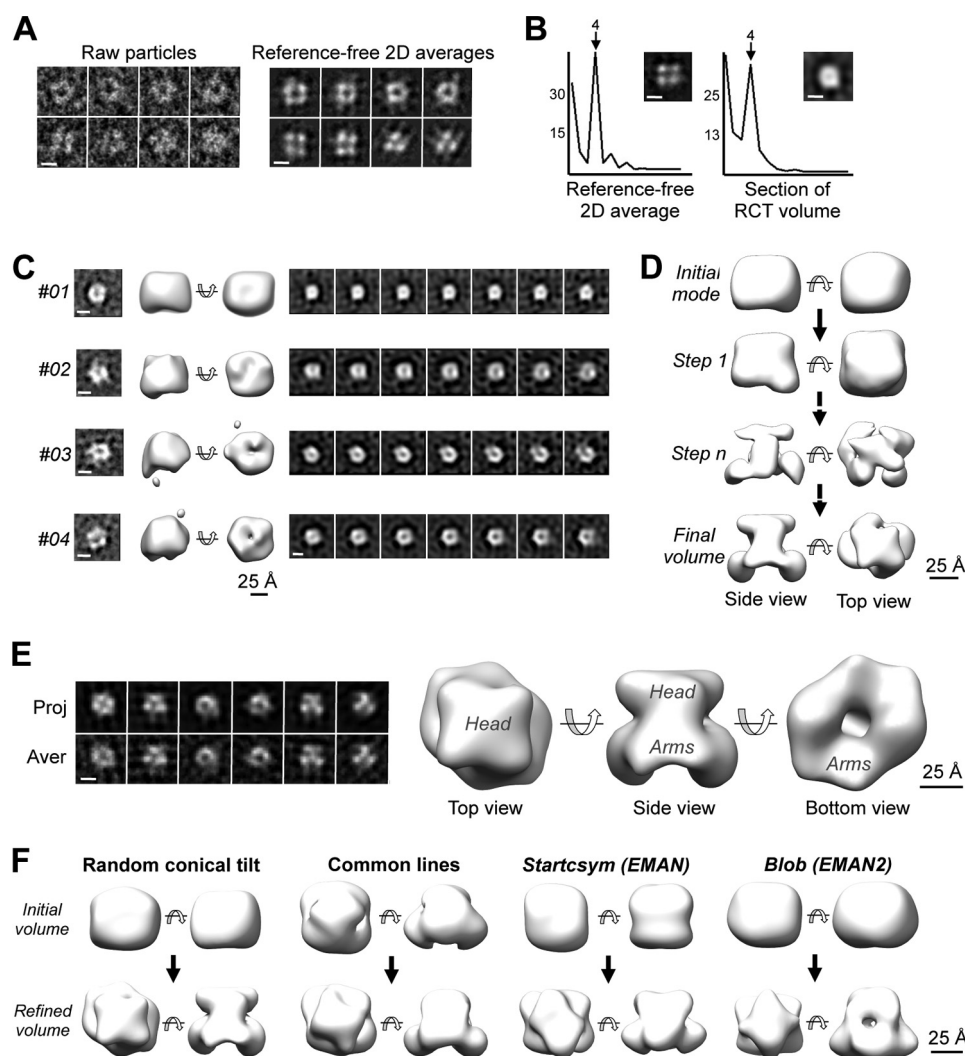


FIGURE 3. Structure of the human YY1 dimer. *A*, single molecule images and two-dimensional reference-free averages of complex A of His-YY1 show a typical square shape. The scale bar represents 5 nm. *B*, *left panel*, analysis of the rotational power spectra of a representative reference-free two-dimensional (2D) average of YY1. *Right panel*, rotational power spectra of sections along the longitudinal axis of the YY1 RCT structure. One representative section is displayed that revealed a strong component with 4-fold symmetry compatible with a dimeric or tetrameric complex. Scale bars represent 5 nm. *C*, four representative *ab initio* low resolution structures of YY1 complex A obtained by the RCT method. Two-dimensional reference-free averages used for each three-dimensional reconstruction are shown in the *left panels* and sections of each of the models (*right panels*). The scale bar represents 25 Å. *D*, angular refinement of YY1 dimer (complex A). Initial refinement was performed without imposing any symmetry (*steps 1 and n*) using the RCT model #01 shown in *C* as the initial template, and after convergence, c2 rotational symmetry was imposed and further refined (*Final volume*). Volumes are shown rendered at a threshold representing around 75% of the protein mass for visualization of structural features. The scale bar represents 25 Å. *E*, three-dimensional structure of the YY1 dimer (complex A) obtained after angular refinement. The scale bar represents 25 Å. Characteristic regions of the complex, defined as head and arm, are labeled. The *left panel* shows the comparison of the computational projections (*Proj.*) of the refined volume with the averages (*Aver.*) of the single molecule images assigned to each orientation. The scale bar represents 5 nm. *F*, angular refinement of YY1 complex A using several initial volumes as templates to discard a significant model bias. Refinement was performed applying 2-fold rotational symmetry and using as templates: a random conical tilt structure, a reconstruction obtained by common lines, or using the Startcsym command in EMAN (33) and a featureless blob using methods defined in EMAN2 (32). In all cases refinements converged to very similar structures (*Refined volume*). The scale bar represents 25 Å.

ected cells with the YY1-VN and YY1-VC fusion constructs. As controls, cells were transfected with YY1-VN in combination with the VC empty vector (YY1-VN and VC), YY1-VC with the VN empty vector (VN and YY1-VC), or the two empty vectors (VN and VC). In all of the control cells, we saw pan-nuclear fluorescence. However, when the YY1 constructs were co-transfected, we saw distinct foci present in the cells (Fig. 2*B*), suggesting that YY1 forms multimers *in vivo*.

YY1 Assembles a Bell-shaped Core Dimer—To further understand the structure of the YY1 multimers, an homogenous preparation of complex A from the peak fraction of a SEC experiment was observed by EM, revealing a square-shaped

molecule with approximate dimensions of 60×50 Å, a low density region at its center (Fig. 3*A*), and a clear maximum in 4-fold rotational power spectra compatible with the oligomerization of 2 or 4 identical YY1 subunits (Fig. 3*B*, *left panel*). Several low resolution *ab initio* structures of YY1 complex A were obtained for homogenous sub-classes using the RCT method (Fig. 3*C*, four representative RCT structures are shown). Sections along the longitudinal axis of these *ab initio* structures revealed a square shape (Fig. 3*C*), with a 4-fold maximum in the rotational power spectra (Fig. 3*B*, *right panel*). Given that the SEC experiment suggested that YY1 oligomers are either 2- or 3-mers but never 4-mers, the

YY1 Oligomers That Bind RuvBL1-RuvBL2

images in the electron microscope suggested the assembly of an YY1 dimer.

Dimerization of YY1 was further supported by solving the structure of these oligomers using 16,362 images obtained in the electron microscope (Fig. 3E). First, a three-dimensional reconstruction of YY1 was obtained by image processing methods and using an *ab initio* RCT structure as the initial template (*model #01* in Fig. 3C) for refinement and applying no symmetry constrains (Fig. 3E). The estimated molecular mass of this non-symmetrized reconstruction, defined by the number of voxels occupied by the reconstruction and assuming an average density for proteins, was ~100 kDa, which only matched a dimeric species. Then, 2-fold symmetry was applied to obtain the structure of YY1 complex A at 20 Å resolution (Fig. 3E). The structure of the YY1 revealed two regions (Fig. 3E). The top region (“head”) was compact and displayed a square shape and was therefore responsible for the strong component of 4-fold symmetry detected in the averages (Fig. 3B). The bottom region (the “arms”) was slightly elongated and fitted better to 2-fold symmetry. To rule out a significant bias of the initial template during image processing, we confirmed that the data converged to very similar reconstructions when using several initial models obtained by distinct methods: RCT, common lines, use of rotational symmetry, and a featureless blob (see “Experimental Procedures” for details) (Fig. 3F).

YY1 Multimerizes by the Association of Dimers—The structural characterization of YY1 complex B was first addressed by concentrating His-YY1 to enrich the complex, but this resulted in its aggregation. We then produced an N-terminal Strep-II-tagged version (Strep-II-YY1) that yielded a major peak composed of abundant complex B in SEC (Fig. 4A). Strep-II-YY1 behaved as a discrete high molecular weight band in SDS-PAGE after stabilization with a mild concentration of glutaraldehyde using the GraFix method (29) (Fig. 4B), clearly indicative of a defined oligomeric species. Images of Strep-II-YY1 complex B revealed an elongated molecule (Fig. 4C), and similar images were obtained for the complex after GraFix (not shown) and for His-YY1 complex B (Fig. 4D). A minor percentage of Strep-II-YY1 complex A co-existed in the same micrographs (20% of the data set) (Fig. 4C), and *ab initio* RCT structures for each complex were obtained by the RCT method to deal with this heterogeneity. Complex B (80% of the data set) appeared as elongated structures of roughly 100 Å in length, approximately double in size than the dimers (Fig. 4E). We were unable to refine these structures to higher resolutions despite rigorous attempts. Major difficulties were found to assign each molecule image to a certain conformation as well as the ambiguities to define the axis of rotational symmetry. Nonetheless, the two-dimensional averages of the complexes and their RCT structures suggested that these were distinct oligomeric species assembled by the association of dimers, and several models could be possible (Fig. 4F).

YY1 Oligomers Can Bind DNA with and without the Consensus Sequence—Zinc finger motifs of YY1 define its function as a transcription factor by recognizing a consensus DNA sequence. We verified that Strep-II-YY1 oligomeric fractions obtained by SEC (Fig. 5A) recognize a short dsDNA (20-bp) and 4-way HJ,

containing a consensus sequence (CCAT) by EMSA (Fig. 5, B and C, Table 1). Unexpectedly, we found that YY1 oligomers could also bind a 25-bp dsDNA without a consensus sequence (although with less affinity than the dsDNA with the consensus sequence) and a HJ without a consensus sequence (Fig. 5, B–E), suggesting these oligomers could have acquired new DNA binding properties. The DNA mobility shifts observed correlated with YY1 present in the fractions as revealed when the native gels were analyzed by Western blot with an anti-YY1 antibody (Fig. 5, B–E, bottom panels). Maximum binding was detected for the peak fraction enriched in YY1 oligomers, mainly complex B. These results revealed that YY1 can bind DNA after oligomerization, and remarkably these oligomers seem to have the potential to recognize some DNA substrates even when lacking the consensus sequence.

RuvBL1-RuvBL2 Interacts with YY1 and Enhances DNA Binding—YY1 has been shown to bind RuvBL1 and RuvBL2 (18, 19), and thus we decided to analyze if the oligomeric forms of YY1 also interacted with these ATPases and how this could affect DNA binding. RuvBL1 and RuvBL2 assemble homo-hexameric rings on their own, whereas its co-expression results in a mixture of hetero-hexameric and dodecameric complexes that are believed to be functional forms of these ATPases in the cell (23–25). We purified His-RuvBL1, His-RuvBL2, and His-RuvBL1-RuvBL2 complexes and also RuvBL1-RuvBL2 where the tag was removed (27) (Fig. 6A), and the oligomeric state of each sample was characterized by SEC (Fig. 6B). Purified His-RuvBL1 was resolved as a mixture of oligomers and free subunits, whereas His-RuvBL2 did not oligomerize under our experimental conditions. On the other hand, His-RuvBL1-RuvBL2 and RuvBL1-RuvBL2 formed hetero-oligomeric complexes with an approximate 1:1 ratio that we interpreted as hexamers and dodecamers based on previous information (27). We found that Strep-II-YY1 interacted with His-RuvBL1 but not His-RuvBL2 under our experimental conditions after pulling down the Strep-II tag and eluting the retained His-RuvBL1 or His-RuvBL2 with D-desthiobiotin (Fig. 6C, lanes 3 and 5). Similar experiments performed using purified His-RuvBL1 hexamers or monomers retrieved identical results (not shown), indicating that Strep-II-YY1 interacts with these two forms of His-RuvBL1. Also, we observed that RuvBL1-RuvBL2 (either containing or not the His tag) was also eluted in complex with Strep-II-YY1 (Fig. 6D; note that His-RuvBL1 and RuvBL1 run differently on SDS-PAGE).

We analyzed how the interaction between YY1 and RuvBL1-RuvBL2 affected DNA binding by EMSA, and we focused on two dsDNAs, one containing and another one missing the consensus sequence for YY1 (Fig. 7), and compared its binding affinity to the binding to a HJ DNA without a consensus sequence. We first measured the affinity of each protein for these forms of DNA and included also ssDNA in our analysis (Fig. 7A, Table 2). The interaction of YY1 with both dsDNAs mainly revealed two types of complexes, a single band of shifted DNA and a complex migrating at the gel well at high protein concentrations (Fig. 7A, left panel). YY1 bound 4–5 times better to the dsDNA containing the consensus sequence, but the difference in binding affinity between the specific DNA and HJ DNA was only 2–3 times (Table 2). Binding to ssDNA was also

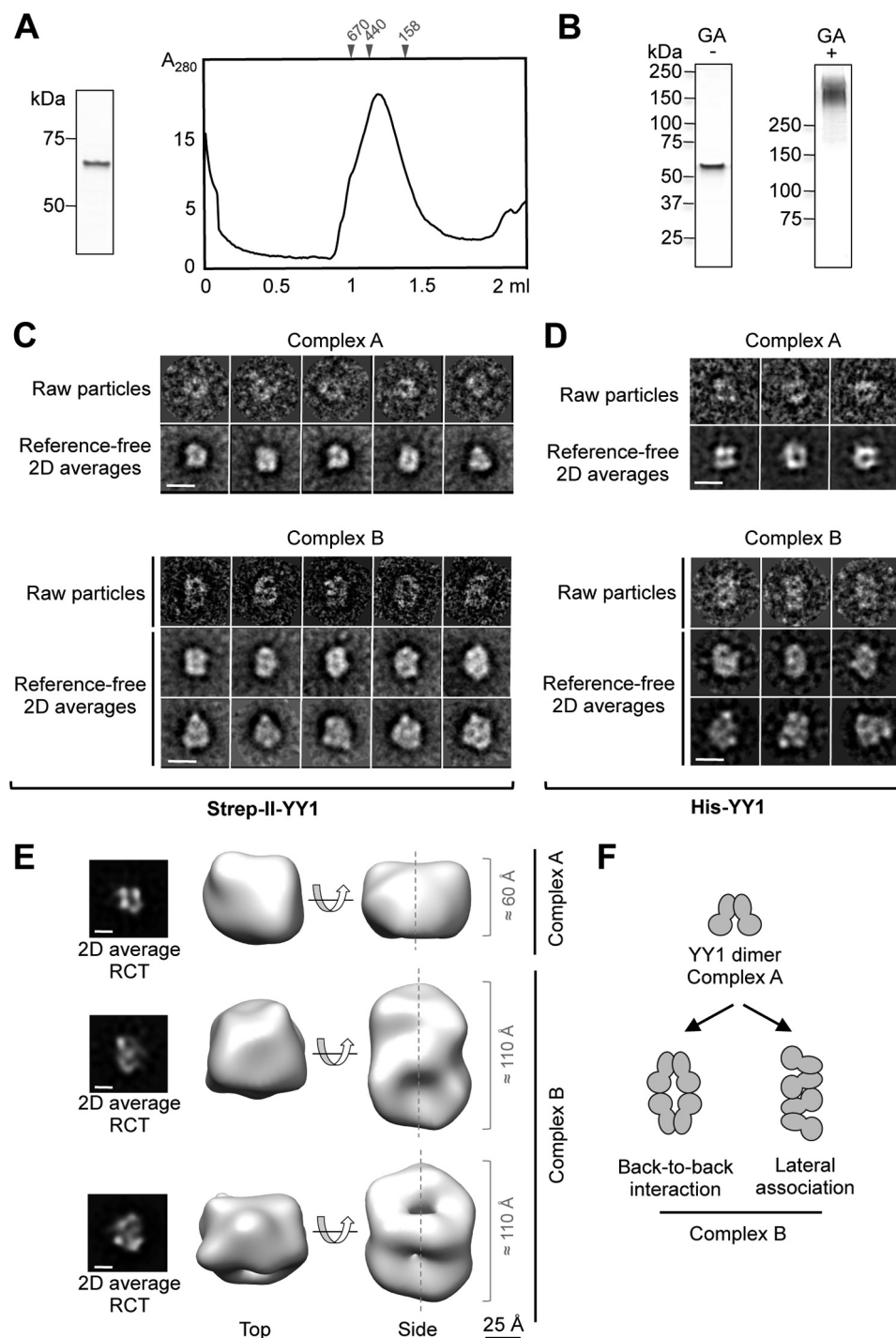


FIGURE 4. YY1 multimerizes in larger complexes by the association of YY1 dimers. *A*, purification of Strep-II-YY1. *Left panel*, SDS-PAGE and SimplyBlue (Invitrogen) staining of purified Strep-II-YY1. *Right panel*, SEC of Strep-II-YY1 using a Superdex 200 PC 3.2/30 (GE Healthcare) column. Molecular weight standards (GE Healthcare) used for column calibration are indicated on the top of the chromatogram. *B*, silver staining SDS-PAGE of the Strep-II-YY1 protein purified and stabilized by the GraFix method in a glycerol/glutaraldehyde (GA) gradient (left panel) and in a glycerol gradient (right panel). *C*, selected raw molecule images and reference-free averages of Strep-II-YY1 (complexes A and B). The scale bar represents 10 nm. *2D averages*, two dimensional averages. *D*, raw molecule images and reference-free averages of His-YY1 (complexes A and B). Images for both samples (His- and Strep-II-tagged YY1) were similar. The scale bar represents 10 nm. *E*, representative RCT structures obtained from images and averages of Strep-II-YY1. The peak from the SEC contained a mixture of complexes A and B. The scale bar represents 25 Å. The two-dimensional averages of the images used for each RCT reconstructions are shown in the left panels. The scale bar represents 5 nm. *F*, hypothetical models for the association of YY1. Two potential ways of association of YY1 dimers into larger oligomers, based on the two-dimensional averages and the RCT structures of complexes A and B, are proposed.

observed. The analysis of the binding of RuvBL1-RuvBL2 to DNA showed that the preferred substrate was HJ (J3) followed by the 80-nt ssDNA (Fig. 7*A*, right panel; Table 2). RuvBL1-RuvBL2 bound DNA forming several complexes. Interestingly,

when RuvBL1-RuvBL2 and YY1 were incubated together in the presence of a dsDNA with or without the consensus sequence, we observed that the top bands corresponding to DNA shifted by YY1 were enhanced significantly (Fig. 7*B*, compare lane 6 for

YY1 Oligomers That Bind RuvBL1-RuvBL2

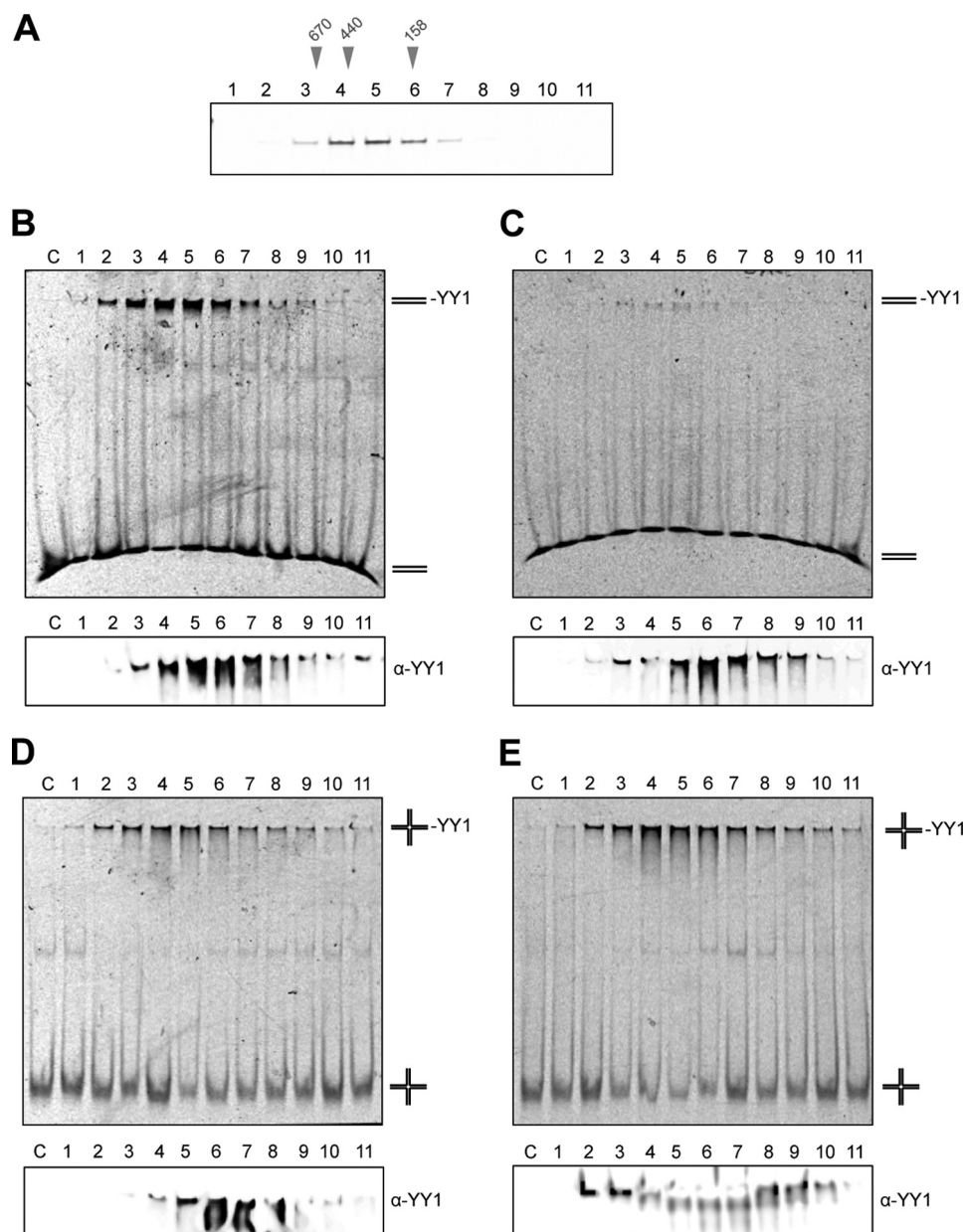


FIGURE 5. YY1 oligomers recognize DNA with and without the consensus sequence. *A*, purified Strep-II-YY1 was fractionated as in Fig. 4*A* and analyzed by SDS-PAGE and silver-staining. Molecular weight markers used for SEC calibration are indicated *above the gel*. *B*, EMSA using the fractions from the SEC experiment shown in *A* and a dsDNA containing the consensus sequence for YY1 (CCAT) (described as dsDNA_sp_2 under “Experimental Procedures”). *C*, EMSA as in *B* but using a dsDNA that does not contain the consensus sequence (described as dsDNA_no_sp_2 under “Experimental Procedures”). *D*, EMSA as in *B* but using a synthetic 4-way HJ containing the consensus sequence for YY1 (CCAT) (described as HJ_25_sp under “Experimental Procedures”). *E*, EMSA as in *D* but using a synthetic 4-way HJ that does not contain the consensus sequence (described as HJ_25_no_sp under “Experimental Procedures”). Lanes labeled as C (*B–E*) show the nucleic acid in each case in the absence of protein. The *bottom panels (B–E)* show the same gels, run for longer, and where the presence of YY1 in the shifted DNA was detected by Western blot with an anti-YY1 antibody (α -YY1).

YY1 alone with lanes 7–9 for YY1 incubated with RuvBL1-RuvBL2). Experiments were done at a YY1 concentration that resulted in <10% of DNA shifted in the absence of RuvBL1-RuvBL2, and at the highest RuvBL1-RuvBL2 concentration used (700 nM), a 5-fold increase in the amount of YY1 complexes with the consensus sequence and a 7-fold for YY1 complexes with dsDNA without the consensus sequence was observed. Similar effects were found for ssDNA (Fig. 7*C*) and a HJ (Fig. 7*D*). Control experiments were performed where the different DNA substrates were incubated with YY1 and an excess of BSA to demonstrate that the enhancement in binding

is not due to a “protein concentration” stabilizing effect (data not shown).

Taken together, these results are a strong indication that YY1 and RuvBL1-RuvBL2 can form a complex with increased affinity for DNA. Interestingly, these effects are found to occur also when the DNA does not contain the consensus sequence for YY1.

*YY1 and RuvBL1-RuvBL2 Cooperate in Vivo to Promote RAD51 Foci Formation during Homologous Recombination—*YY1 functions in HR as part of the INO80 complex (containing RuvBL1 and RuvBL2 subunits), and although the mechanism for this is unknown, it has been suggested that it could occur

TABLE 1
Sequences of oligonucleotides used for constructing several DNA substrates

Name	Sequence 5'-3'	5'-Label
J3-1	CGCAAGCGACAGGAACCTCGAGAAGCTTCCGGTAGCAGCCTGAGCGGTGGTGAATTCCTCGAGGTTCTCTGTCGCTTGCG	γ - ³² P
J3-2	CGCAAGCGACAGGAACCTCGAGGAATTCACCACCCGCTCAACTCACTGCAGCTAGACTCGAGGTTCTCTGTCGCTTGCG	
J3-3	CGCAAGCGACAGGAACCTCGAGTCTAGACTGCAGTTGAGTCCCTGCTAGGACGGATCCCTCGAGGTTCTCTGTCGCTTGCG	
J3-4	CGCAAGCGACAGGAACCTCGAGGGATCCGTCCTAGCAAGGGGCTGTACCAGGAAGCTTCTCGAGGTTCTCTGTCGCTTGCG	
J3-5	CGCAAGCGACAGGAACCTCGAGTCTAGACTGCAGTTGAGTTGAGCGGTGGTGAATTCCTCGAGGTTCTCTGTCGCTTGCG	γ - ³² P
43-1	ACAGGAATTCCTCGAGGCGCCATTTTGTGCTGTCTAGAGACT	
43-2	AGTCTCTAGACAGCACAAAATGGCGCCTCGAGGAATTCCTGT	γ - ³² P
HJ_1	GACGCTGCCGAATTCCTGGCGTTAGGAGATACCGATAAGCTTCGGCTTAA	
HJ_2	CTTAAGCCGAAGCTTATCGGTATCTTGCTTACGACGCTAGCAAGTGATC	Cy5
HJ_3	TGATCACTTGCTAGCGTCGTAAGCAGCTCGTGTCTAGAGACATCGA	
HJ_4	ATCGATGTCTCTAGACAGCAGGACCTAACGCCAGAATTCGGCAGCGT	
HJ_12	GACGCTGCCGAATTCCTGGCGTTAGGAGATACCGATAAGCTTCGGCTTAAATTTCTTAAGCCGAAGCTTATCGGTATCTTGCG	
HJ_34_1	TGATCACTTGCTAGCGTCGTAAGCAGCTCGTGTCTAGAGACATCGATTTATCGATGTCTCTAGACAGCAGGACCCCT	Cy5
HJ_34_2	AACGCCAGAATTCGGCAGCGT	
DS_1	AGGGTCTCCATTTTGAAGCG	Cy5
DS_2	CGCTTCAAATGGAGACCCT	
DS_3	CTGAAGGGGGGCTATAAAAGGGGGT	
DS_4	ACCCCTTTTATAGCCCCCTTCAG	

through the recognition of Holliday junction-like structures (15). Our findings showing that the interaction of YY1 and RuvBL1-RuvBL2 enhances binding to ssDNA and dsDNA prompted us to further define their role during HR. We explored if these proteins cooperate at several stages of the HR process where HJ substrates are not available and also the requirement of catalytic activity of the RuvBL1-RuvBL2 ATPases. To investigate this, we transfected cells with siRNA targeting YY1 and examined them after treatment with ionizing radiation (IR) (Fig. 8). HR is restricted to the S and G₂ phases of the cell cycle in mammalian cells, so we immunostained for CENPF to identify G₂ phase cells and then measured the accumulation of DNA damage response factors into IR induced foci. We found that the number of phosphorylated H2AX (γ H2AX)-containing foci at the 2-h time point was unaffected by depletion of YY1 (Fig. 8A), suggesting that the initial detection and signaling of the DNA breaks are unaltered. At 8 h after treatment, the BRCA2 (breast cancer type 2 susceptibility protein)-depleted cells, which are HR-defective, showed a modest increase in foci at this time point (Fig. 8A).

After recognition, DNA breaks are resected to leave 3' ssDNA overhangs that are bound by RPA. Subsequent to resection, BRCA2 mediates the replacement of RPA with RAD51 filaments on the ssDNA overhang, and the RAD51 filament performs the homology search and strand invasion steps (40). When we examined RPA foci formation in G₂ cells, we found no difference in the number of foci in the cells depleted for YY1 when compared with control cells (Fig. 8B). Whereas it is possible that the extent of resection is affected, this result suggests that there is no defect in the number of resected DNA breaks in these cells. Cells depleted for BRCA2 show normal γ H2AX and RPA foci but defective RAD51 foci after IR (Fig. 8, B and C). Similar to loss of BRCA2, we found that there were significantly fewer RAD51 foci in the YY1 and RuvBL2 depleted cells, although the severity of the defect was not as pronounced as in the BRCA2-depleted cells (Fig. 8C). Notably, we found that depletion of RuvBL2 recapitulated HR defects after YY1 depletion. Specifically, the numbers of γ H2AX and RPA foci were largely unaffected by depletion of RuvBL2, but the number of

RAD51 foci was reduced to similar levels as those observed in YY1-depleted cells (Fig. 8).

These results showed that depletion of YY1 or RuvBL2 resulted in comparable HR defects, suggesting that YY1 and RuvBL2 could cooperate to promote or stabilize RAD51 filament formation. To investigate whether this was the case, we analyzed the formation of γ H2AX, RPA, and RAD51 foci in G₂ cells following IR exposure after depletion of YY1, RuvBL2, or both (Fig. 9A). If these subunits were functioning at separate steps during HR, we would predict an increase in unrepaired breaks when they are co-depleted, leading to an increase in γ H2AX foci. Furthermore, if YY1 and RuvBL2 were promoting or stabilizing RAD51 foci formation via distinct mechanisms, depletion of both proteins would result in a greater defect in RAD51 foci relative to cells with depletion of a single subunit. However, we found that both γ H2AX and RAD51 foci formations were similar in cells depleted of both proteins to cells depleted of either individual subunits (Fig. 9B), indicating that these genes function on the same pathway to promote HR.

We made use of a point mutation within the Walker A motif of RuvBL2 that impairs ATP binding but does not disrupt its folding (41) to determine whether the ATPase activity of RuvBL2 is required for the observed effect on RAD51 foci formation after IR exposure. To do this we generated a siRNA-resistant GFP-tagged RuvBL2 expression construct and then introduced the K83A point mutation into this construct (Fig. 9C). We then transfected the wild type and mutant constructs (along with a GFP control) alongside siRNA directed against RuvBL2 and analyzed γ H2AX and RAD51 foci formation in GFP-positive G₂ cells. We found that the wild type construct was able to complement the RAD51 foci formation defect of the RuvBL2-depleted cells, whereas the mutant construct was not able to complement the defect (Fig. 9D), indicating that the ATPase activity of RuvBL2 is required during this step of HR. All these data suggest that the epistatic function of YY1 and RuvBL1-RuvBL2 during HR requires the catalytic activity of these ATPases, at least in the case of RuvBL2.

YY1 Oligomers That Bind RuvBL1-RuvBL2

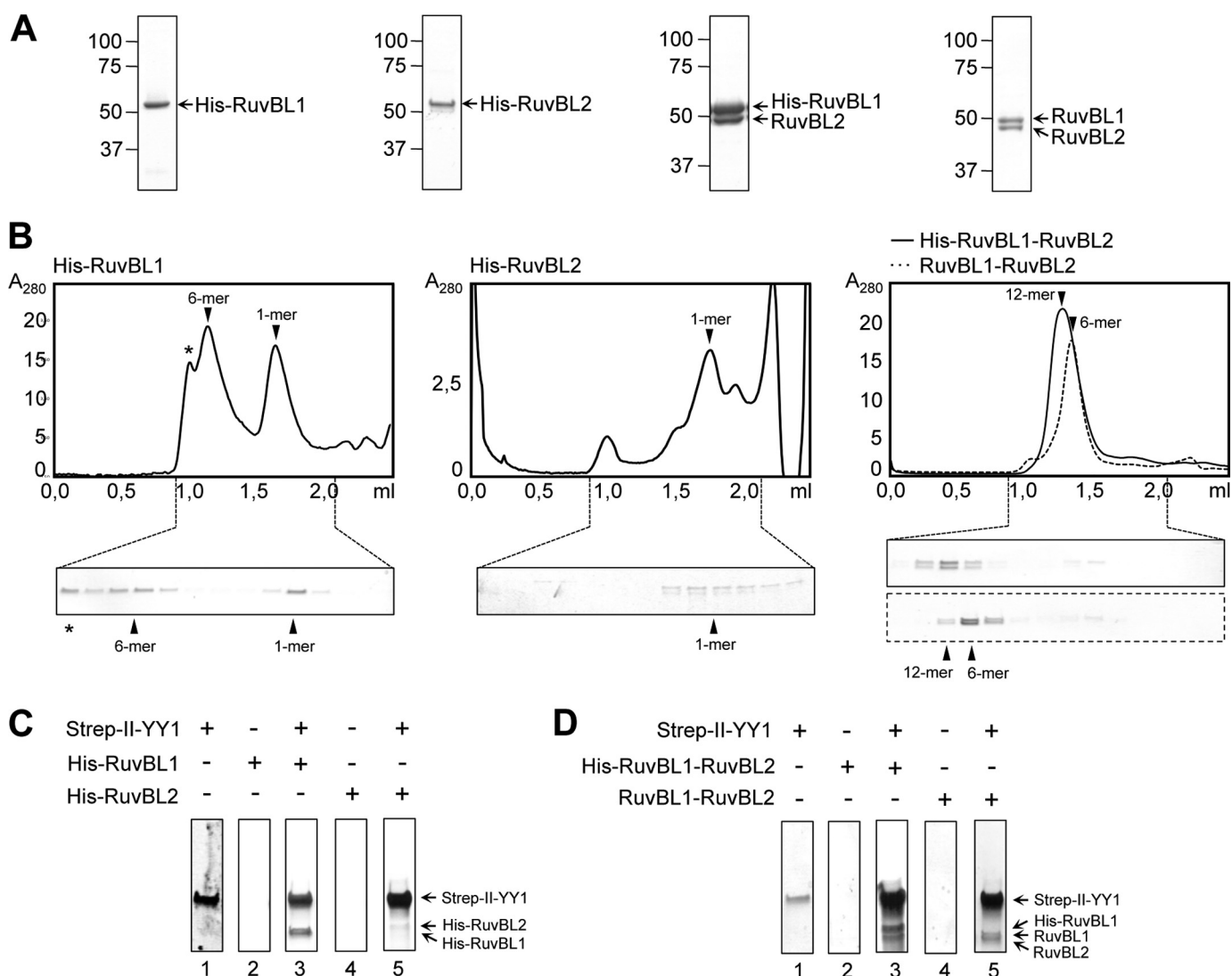


FIGURE 6. Analysis of the interaction of purified YY1 with RuvBL1 and RuvBL2. *A*, SDS-PAGE and SimplyBlue (Invitrogen) staining of purified His-RuvBL1, His-RuvBL2, His-RuvBL1-RuvBL2, and RuvBL1-RuvBL2. *B*, chromatograms and SDS-PAGE analysis of the fractions from a SEC of His-RuvBL1, His-RuvBL2, and His-RuvBL1-RuvBL2 (solid line) and RuvBL1-RuvBL2 (dash line) using a Superdex 200 PC 3.2/30 (GE Healthcare) column. Proteins were stained using SimplyBlue (Invitrogen) (His-RuvBL1, His-RuvBL1-RuvBL2, and RuvBL1-RuvBL2) or by silver staining (His-RuvBL2). The positions for the different oligomeric species (12-mer, dodecamer; 6-mer, hexamer; 1-mer, monomer) are indicated in each case and were determined by comparison with molecular weight standards. The asterisk (*) in the case of His-RuvBL1 SEC indicates a peak of aggregated material as observed by EM. *C*, pull-down experiments of Strep-II-YY1 and His-RuvBL1 or His-RuvBL2. Strep-II-YY1 was incubated without (lane 1) or with His-RuvBL1 (lane 3) or His-RuvBL2 (lane 5) and affinity purified using the Strep-II-tag present in YY1. As a control, His-RuvBL1 (lane 2) or His-RuvBL2 (lane 4) was purified in the same conditions but in the absence of YY1. *D*, pull-down experiments of Strep-II-YY1 and His-RuvBL1-RuvBL2 or RuvBL1-RuvBL2. Strep-II-YY1 was incubated without (lane 1) or with His-RuvBL1-RuvBL2 (lane 3) or RuvBL1-RuvBL2 (lane 5) and affinity-purified as in *A*. As a control, His-RuvBL1-RuvBL2 (lane 2) or RuvBL1-RuvBL2 (lane 4) was pull down in the same conditions as those before but in the absence of YY1.

DISCUSSION

Recombinant YY1 was previously shown to behave as an oligomer in SEC and glutaraldehyde cross-linking experiments (15). Our structural characterization of the transcription factor YY1 not only confirms those results using His-YY1 and Strep-II-YY1, but in addition it offers a deeper understanding of the architecture of these oligomers. We determine that YY1 assembles as dimers that can associate into larger oligomeric complexes, and we characterize the structural organization of these oligomers using EM. Moreover, we show that the self-association of YY1 also occurs *in vivo*. The most characteristic structural feature for the transcription factor YY1 is the C-terminal C₂H₂-type zinc finger motifs (11). Although the main function

of these motifs is to interact with nucleic acids, they have been also implicated in protein-protein interactions, including in some cases homo-dimerization (42–44). One example is Ikaros, a protein containing six C₂H₂-type zinc fingers, four of which are involved in DNA binding and the two C-terminal fingers are responsible for the assembly of a homodimer (45). Thus, it is conceivable that YY1 could use, at least in part, these multifunctional zinc fingers to homo-dimerize. Interestingly, dimerization of Ikaros dramatically increased its affinity for DNA, and a similar effect could be taking place in the case of YY1 (see below).

YY1 zinc finger motifs are responsible for specifically binding to a consensus DNA sequence (5'-(C/g/a)(G/t)(C/t/a)-

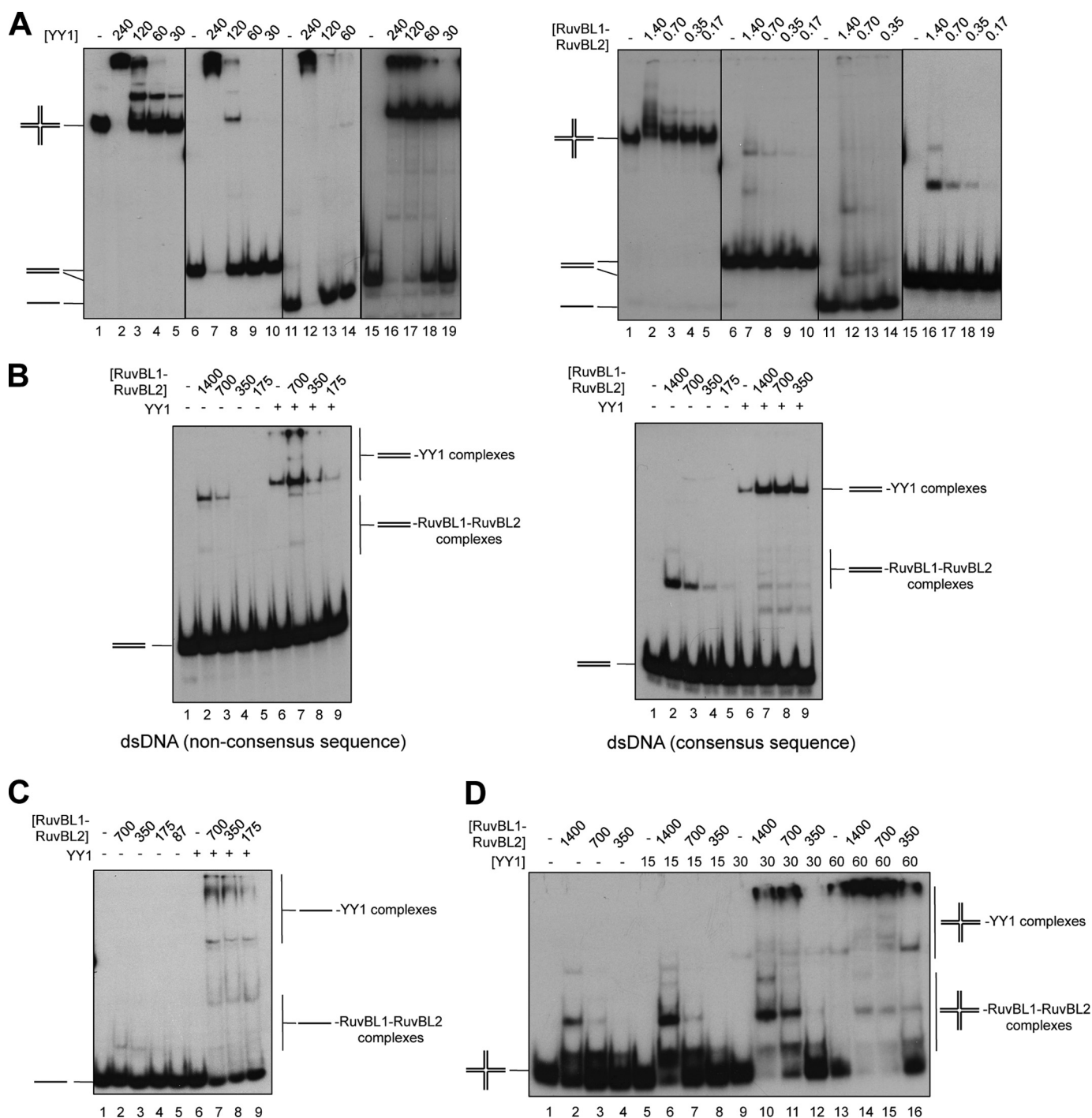


FIGURE 7. YY1 and RuvBL1-RuvBL2 cooperate in DNA binding. *A, left panel*, EMSA assays showing binding of Strep-II-YY1 to several DNA substrates (described under "Experimental Procedures") and represented as a schematic in each gel. Binding reactions contained 0, 240, 120, 60, or 30 nM protein and 0.3 nM DNA species: HJ (J3) (lanes 1–5), dsDNA non-consensus sequence (dsDNA_no_sp_1) (lanes 6–10), 80-nt ssDNA (lanes 11–14), and dsDNA consensus sequence (dsDNA_sp_1) (lanes 15–19). *Right panel*, EMSA assays showing binding of His-RuvBL1-RuvBL2 to the same DNA substrates. Binding reactions contained 0, 1.4, 0.7, 0.35, or 0.17 μ M protein and 0.3 nM DNA species: HJ (J3) (lanes 1–5), dsDNA non-consensus sequence (dsDNA_no_sp_1) (lanes 6–10), 80-nt ssDNA (lanes 11–14), and dsDNA consensus sequence dsDNA_sp_1) (lanes 15–19). Reactions were performed as described under "Experimental Procedures," and protein-DNA complexes were visualized by 6% PAGE and autoradiography. *B*, RuvBL1-RuvBL2 enhances the binding of YY1 to dsDNA either containing (*right panel*, dsDNA_sp_1) or not the consensus sequence (*left panel*, dsDNA_no_sp_1). Reactions assembled on ice contained combinations of a decreasing concentration of His-RuvBL1-RuvBL2 (1.4, 0.7, 0.35 or 0.17 μ M) and a fixed concentration of Strep-II-YY1 (120 nM in the *left panel* and 15 nM in the *right panel*). After DNA addition (0.3 nM), samples were incubated for 30 min at 37 °C before electrophoresis. *C*, YY1 and RuvBL1-RuvBL2 also cooperate in ssDNA binding. Shown is a similar experiment as *B* but using a 80-nt ssDNA (0.3 nM) (lanes 1–9). His-RuvBL1-RuvBL2 concentrations were varied as indicated from 700 to 87 nM, and the fixed concentration of Strep-II-YY1 used was 120 nM. *D*, EMSA of the enhancement in binding of Strep-II-YY1 to HJ (J3) (0.3 nM) in the presence of the indicated concentrations His-RuvBL1-RuvBL2 (concentrations are expressed in nM).

YY1 Oligomers That Bind RuvBL1-RuvBL2

CATN(T/a)(T/g/c)-3') found at the promoters of target genes (11). DNA binding by the oligomeric forms of YY1 is not well characterized, and the work by Wu *et al.* (15) used nucleic acid

TABLE 2
DNA binding affinities of YY1 and RuvBL1-RuvBL2

DNA	$K_{d \text{ app}}^a$ YY1	$K_{d \text{ app}}$ RuvBL1-RuvBL2
	<i>nM</i>	μM
dsDNA_sp_1	40	$>2^b$
dsDNA_no_sp_1	170	$>2^b$
80-nt ssDNA	180	1.8
Holliday junction J3	90	1

^a The apparent binding constant ($K_{d \text{ app}}$) for each substrate was determined from a compilation of at least three separate gel shift experiments, each with a dilution series of protein and a DNA substrate concentration fixed at 0.3 nM.

^b The $K_{d \text{ app}}$ for this substrate is estimated, because at the maximal protein concentration tested (2 μM) $<25\%$ of the DNA was retained.

substrates with a consensus sequence for YY1, where it could be difficult to identify interactions with DNA distinct to those as a transcription factor. In this context, one significant new finding of our study is that these oligomers can interact with several DNAs that do not contain the consensus sequence, at least *in vitro*. This is consistent with the finding that YY1 binds to RNA during inactivation of one X chromosome in mammalian females independent of a consensus motif (4). What could be the molecular/structural basis for these unconventional interactions between YY1 and nucleic acids? C_2H_2 -type zinc finger domains can bind, in addition to DNA, to several nucleic acids such as ssRNA, dsRNA, and DNA-RNA hetero-duplexes (44), although the structural basis for these properties are poorly

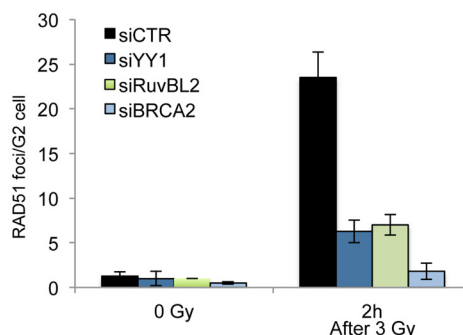
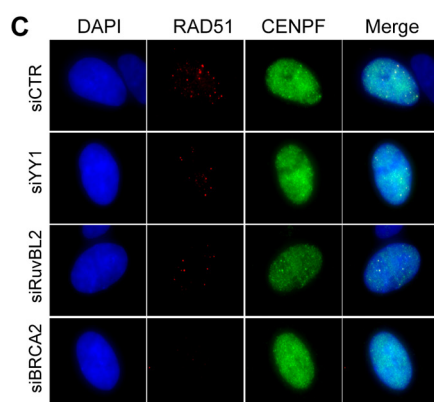
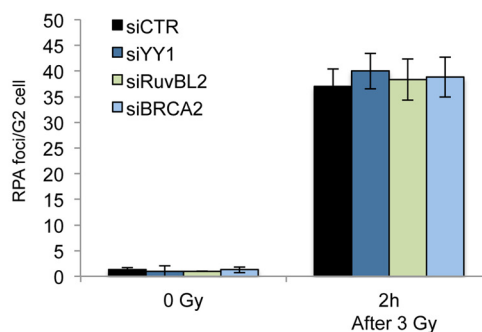
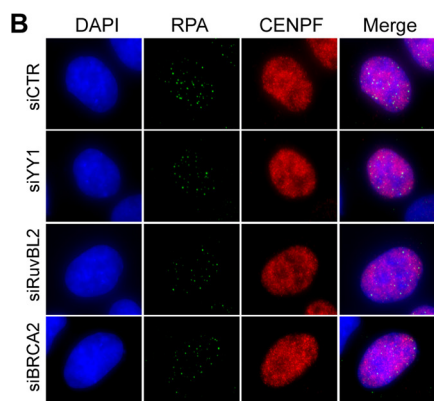
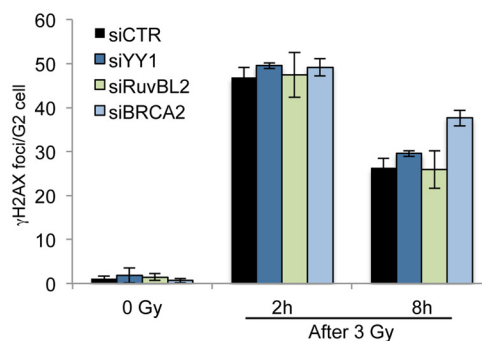
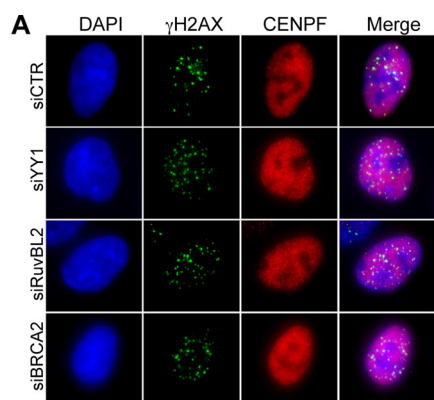


FIGURE 8. YY1 and RuvBL2 function during G₂ to promote RAD51 foci formation, but not γH2AX or RPA foci, after exposure to IR. A, A549 cells were transfected with scrambled siRNA (siCTR) or siRNA directed against YY1, RuvBL2, or BRCA2, irradiated (3 Gy) and harvested 2 or 8 h later and immunostained for γH2AX and CENPF (to identify G₂ phase cells). Average γH2AX foci per G₂ cell were quantified (right panel). B, cells transfected as in A were irradiated (3 Gy), harvested after 2 h, and immunostained for RPA and CENPF. Average RPA foci per G₂ cell were quantified (right panel). C, cells transfected as in A were immunostained for RAD51 and CENPF, and average RAD51 foci per G₂ cell were quantified (right panel). All data (A–C) are the means of >3 experiments; error bars, S.D.

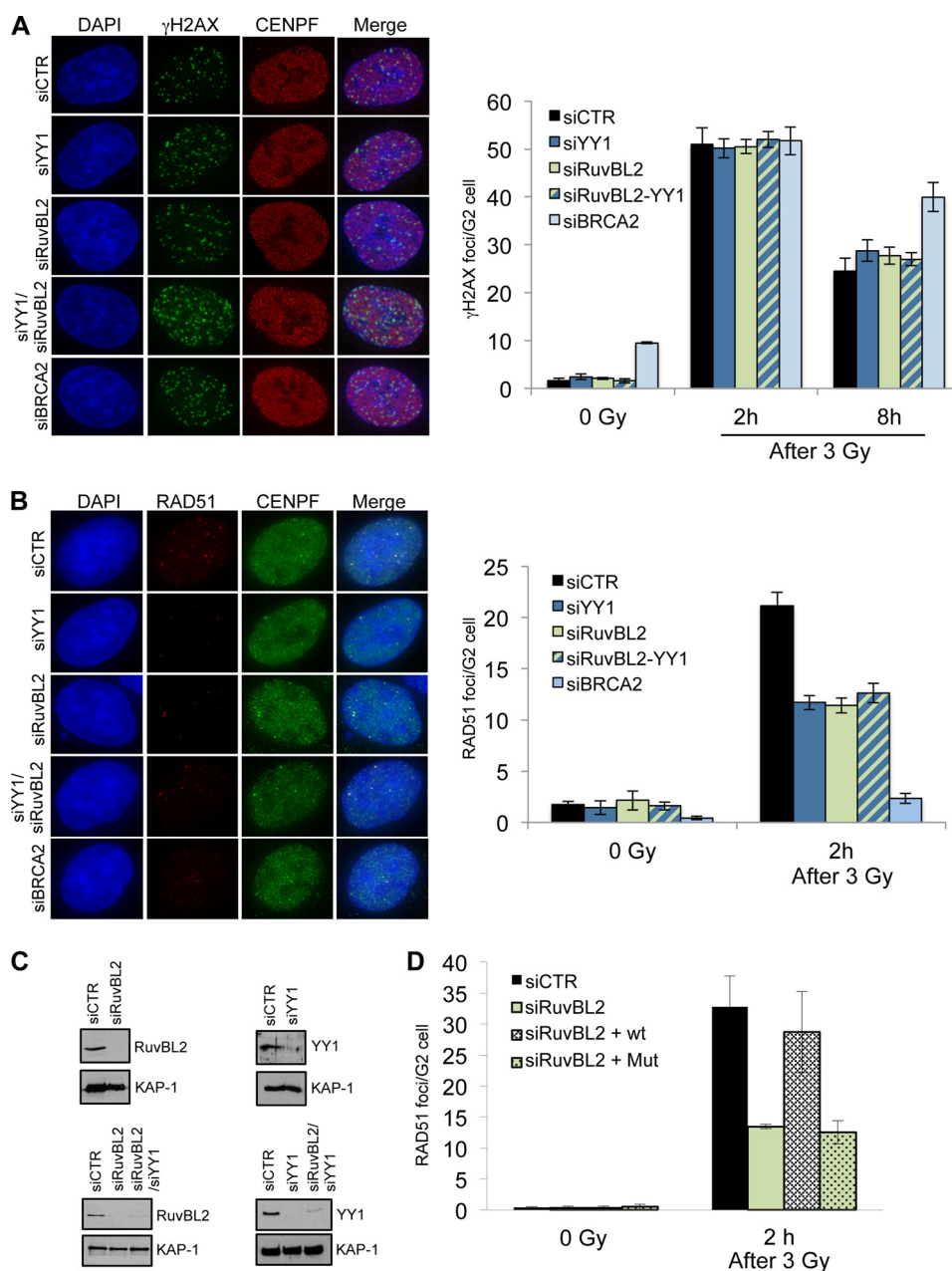


FIGURE 9. RuvBL2 cooperates with YY1 to promote RAD51 foci formation, and the ATPase activity of RuvBL2 is required for this activity. *A*, A549 cells were transfected with scrambled siRNA (siCTR) or siRNAs directed against YY1, RuvBL2, or BRCA2, as indicated, irradiated (3 Gy), harvested 2 or 8 h later, and immunostained for γ H2AX and CENPF (to identify G₂ phase cells). Average γ H2AX foci per G₂ cell were quantified (right panel). *B*, cells treated as in *A* were immunostained for RAD51 and CENPF, and average RAD51 foci per G₂ cell were quantified (right panel). All data (*A* and *B*) are the mean of >3 experiments; error bars, S.D. *C*, top, Western blot analysis of whole cell extracts prepared from A549 cells transfected with the indicated siRNA. Bottom, Western blot analysis of whole cell extracts prepared from A549 cells transfected with single or double siRNA constructs as indicated. Anti-KAP1 is shown as a loading control. *D*, U2OS cells transfected with siRNA directed against RuvBL2 and either GFP, GFP-RuvBL2, or GFP-RuvBL2-K83A were irradiated (3 Gy), harvested, and immunostained for RAD51 and CENPF. Average RAD51 foci per GFP positive G₂ cell were quantified and are presented as the means of three experiments; error bars, S.D.

understood. One hypothesis might be that the oligomerization of YY1 could expand its properties to bind DNA, RNA, and/or other proteins by the combination of zinc fingers motifs from several monomers. This opens the possibility that, when in the form of larger oligomers and/or as part of larger complexes, YY1 could contribute to functions unrelated to those of a transcription factor. Interestingly, recent reports describe roles of YY1 in distinct functions such as proviral silencing in embryonic cells (6), the regulation of the expression of long non-coding RNAs during myogenesis (7), and in V(D)J somatic

rearrangement of Ig loci during B-cell development by a mechanism that involves long distance DNA interactions (46).

One of these unconventional functions is the link between YY1 and DNA repair (15, 47). We predict that the functions of YY1 in DNA repair should be independent of the recognition of specific sequences, and our results indicate that YY1 has the potential to do so. We corroborate that YY1 functions in HR, but in addition, our data suggest that defects in HR observed in the absence of YY1 may be due to, at least in part, an inability to efficiently promote formation or stabilization of the RAD51 filament.

YY1 Oligomers That Bind RuvBL1-RuvBL2

A direct interaction of YY1 with RuvBL1 and RuvBL2 has been previously described (15). These AAA+ ATPases are implicated in several cellular processes as part of large macromolecular assemblies, such as INO80, SWR1, TIP60, and R2TP complexes, among others (20, 21). Despite both proteins being essential, not much is known about their mechanism of action, and the functional significance of the several oligomeric forms of RuvBL1 and RuvBL2 is still unclear (20, 21). We tested the interaction of YY1 with the RuvBL1 and RuvBL2 ATPases, showing that this interaction takes place also with purified YY1 oligomers. In addition, we observed that YY1 binds RuvBL1-RuvBL2 complexes, but YY1 interacts preferentially with RuvBL1, and it associates to RuvBL2 mostly when this is in complex with RuvBL1. We cannot rule out that RuvBL2 could bind YY1 at higher concentrations.

Unexpectedly, we found that when YY1 and RuvBL1-RuvBL2 are incubated together with several DNA substrates, they interact with the nucleic acids with enhanced affinity compared with each protein on their own, and this effect is especially relevant when considering those DNAs without a consensus sequence. YY1 forms a complex with DNA that is detected as a lower migrating band in EMSA experiments, and the abundance of this complex is enhanced 7-fold in the presence of RuvBL1-RuvBL2. These results suggest that YY1 and RuvBL1-RuvBL2 cooperate to enhance binding to DNA. Similar findings have been recently described for another transcription factor, GATA-binding protein 3 (Gata3), which controls differentiation of T cells (48). Gata3 forms a complex with RuvBL2, and it was proposed that the interaction promoted the DNA binding activity of Gata3.

Thus, the interaction of YY1 with RuvBL1 and RuvBL2 either alone or as part of a larger complex could represent a mechanism to modify the functionality of this transcription factor. The molecular/structural bases for this remain to be explored, but RuvBL1-RuvBL2 contains two regions with the potential to bind nucleic acids. Domain II shows a structure reminiscent of RPA, and recombinant DII domains from RuvBL1 in isolation bind ssRNA, ssDNA and dsDNA (24). Similar to other AAA+ family members, RuvBL1 and RuvBL2 assemble hexameric complexes with a central channel that could potentially bind ssDNA (24), although this has not been demonstrated experimentally. YY1 could cooperate with any of these two potential DNA binding sites in RuvBL1-RuvBL2 to enhance the affinity for nucleic acids, somehow mimicking the behavior of the bacterial homolog RuvB, which has poor DNA binding itself and needs to interact with RuvA to bind DNA structures (22). The mechanism of how exactly YY1, RuvBL1, and RuvBL2 proteins cooperate to promote steps during HR and/or other cellular events needs to be further explored. Here we provide evidence suggesting an important role of the RuvBL1-RuvBL2 ATPases in enhancing the DNA binding properties of YY1, which could be directly linked to the regulation of different cellular processes, including transcription and DNA repair.

Acknowledgments—We thank Andreas Kakarougkas (Sussex) and Martín Alcorlo (Centro de Investigaciones Biológicas, Consejo Superior de Investigaciones Científicas) for technical assistance.

REFERENCES

1. Gordon, S., Akopyan, G., Garban, H., and Bonavida, B. (2006) Transcription factor YY1: structure, function, and therapeutic implications in cancer biology. *Oncogene* **25**, 1125–1142
2. Calame, K., and Atchison, M. (2007) YY1 helps to bring loose ends together. *Genes Dev.* **21**, 1145–1152
3. He, Y., and Casaccia-Bonnel, P. (2008) The Yin and Yang of YY1 in the nervous system. *J. Neurochem.* **106**, 1493–1502
4. Jeon, Y., and Lee, J. T. (2011) YY1 tethers Xist RNA to the inactive X nucleation center. *Cell* **146**, 119–133
5. Nicholson, S., Whitehouse, H., Naidoo, K., and Byers, R. J. (2011) Yin Yang 1 in human cancer. *Crit. Rev. Oncog.* **16**, 245–260
6. Schlesinger, S., Lee, A. H., Wang, G. Z., Green, L., and Goff, S. P. (2013) Proviral silencing in embryonic cells is regulated by Yin Yang 1. *Cell Rep.* **4**, 50–58
7. Lu, L., Sun, K., Chen, X., Zhao, Y., Wang, L., Zhou, L., Sun, H., and Wang, H. (2013) Genome-wide survey by ChIP-seq reveals YY1 regulation of lincRNAs in skeletal myogenesis. *EMBO J.* **32**, 2575–2588
8. Liu, H., Schmidt-Supprian, M., Shi, Y., Hobeika, E., Barteneva, N., Jumaa, H., Pelanda, R., Reth, M., Skok, J., and Rajewsky, K. (2007) Yin Yang 1 is a critical regulator of B-cell development. *Genes Dev.* **21**, 1179–1189
9. Hogan, C. J., Aligianni, S., Durand-Dubief, M., Persson, J., Will, W. R., Webster, J., Wheeler, L., Mathews, C. K., Elderkin, S., Oxley, D., Ekwall, K., and Varga-Weisz, P. D. (2010) Fission yeast Iec1-ino80-mediated nucleosome eviction regulates nucleotide and phosphate metabolism. *Mol. Cell Biol.* **30**, 657–674
10. Brown, J. L., Fritsch, C., Mueller, J., and Kassis, J. A. (2003) The *Drosophila* pho-like gene encodes a YY1-related DNA binding protein that is redundant with pleiohomeotic in homeotic gene silencing. *Development* **130**, 285–294
11. Houbavii, H. B., Usheva, A., Shenk, T., and Burley, S. K. (1996) Cocrystal structure of YY1 bound to the adeno-associated virus P5 initiator. *Proc. Natl. Acad. Sci. U.S.A.* **93**, 13577–13582
12. Lewis, B. A., Tullis, G., Seto, E., Horikoshi, N., Weinmann, R., and Shenk, T. (1995) Adenovirus E1A proteins interact with the cellular YY1 transcription factor. *J. Virol.* **69**, 1628–1636
13. Yang, W. M., Inouye, C., Zeng, Y., Bearss, D., and Seto, E. (1996) Transcriptional repression by YY1 is mediated by interaction with a mammalian homolog of the yeast global regulator RPD3. *Proc. Natl. Acad. Sci. U.S.A.* **93**, 12845–12850
14. Wilkinson, F. H., Park, K., and Atchison, M. L. (2006) Polycomb recruitment to DNA *in vivo* by the YY1 REPO domain. *Proc. Natl. Acad. Sci. U.S.A.* **103**, 19296–19301
15. Wu, S., Shi, Y., Mulligan, P., Gay, F., Landry, J., Liu, H., Lu, J., Qi, H. H., Wang, W., Nickoloff, J. A., and Wu, C. (2007) A YY1-INO80 complex regulates genomic stability through homologous recombination-based repair. *Nat. Struct. Mol. Biol.* **14**, 1165–1172
16. Doetsch, M., Gluch, A., Poznanovi, G., Bode, J., and Vidakovi, M. (2012) YY1-binding sites provide central switch functions in the PARP-1 gene expression network. *PLoS ONE* **7**, e44125
17. Ishii, H., Hulett, M. D., Li, J. M., Santiago, F. S., Parish, C. R., and Khachigian, L. M. (2012) Yin Yang-1 inhibits tumor cell growth and inhibits p21WAF1/Cip1 complex formation with cdk4 and cyclin D1. *Int. J. Oncol.* **40**, 1575–1580
18. Bao, Y., and Shen, X. (2011) SnapShot: chromatin remodeling: INO80 and SWR1. *Cell* **144**, 158–158.e152
19. Chen, L., Cai, Y., Jin, J., Florens, L., Swanson, S. K., Washburn, M. P., Conaway, J. W., and Conaway, R. C. (2011) Subunit organization of the human INO80 chromatin remodeling complex: an evolutionarily conserved core complex catalyzes ATP-dependent nucleosome remodeling. *J. Biol. Chem.* **286**, 11283–11289
20. Nano, N., and Houry, W. A. (2013) Chaperone-like activity of the AAA+ proteins Rvb1 and Rvb2 in the assembly of various complexes. *Philos. Trans R Soc. Lond. B. Biol. Sci.* **368**, 20110399
21. Rosenbaum, J., Baek, S. H., Dutta, A., Houry, W. A., Huber, O., Hupp, T. R., and Matias, P. M. (2013) The emergence of the conserved AAA+ ATPases Pontin and Reptin on the signaling landscape. *Sci. Signal.* **6**, mr1

22. Yamada, K., Miyata, T., Tsuchiya, D., Oyama, T., Fujiwara, Y., Ohnishi, T., Iwasaki, H., Shinagawa, H., Ariyoshi, M., Mayanagi, K., and Morikawa, K. (2002) Crystal structure of the RuvA-RuvB complex: a structural basis for the Holliday junction migrating motor machinery. *Mol. Cell* **10**, 671–681
23. Gorynia, S., Bandejas, T. M., Pinho, F. G., McVey, C. E., Vornheim, C., Round, A., Svergun, D. I., Donner, P., Matias, P. M., and Carrondo, M. A. (2011) Structural and functional insights into a dodecameric molecular machine: the RuvBL1/RuvBL2 complex. *J. Struct. Biol.* **176**, 279–291
24. Matias, P. M., Gorynia, S., Donner, P., and Carrondo, M. A. (2006) Crystal structure of the human AAA+ protein RuvBL1. *J. Biol. Chem.* **281**, 38918–38929
25. Petukhov, M., Dagkessamanskaja, A., Bommer, M., Barrett, T., Tsaneva, I., Yakimov, A., Quéval, R., Shvetsov, A., Khodorkovskiy, M., Käs, E., and Grigoriev, M. (2012) Large-scale conformational flexibility determines the properties of AAA+ TIP49 ATPases. *Structure* **20**, 1321–1331
26. Cheung, K. L., Huen, J., Houry, W. A., and Ortega, J. (2010) Comparison of the multiple oligomeric structures observed for the Rvb1 and Rvb2 proteins. *Biochem. Cell Biol.* **88**, 77–88
27. López-Perrote, A., Muñoz-Hernández, H., Gil, D., and Llorca, O. (2012) Conformational transitions regulate the exposure of a DNA-binding domain in the RuvBL1-RuvBL2 complex. *Nucleic Acids Res.* **40**, 11086–11099
28. Torreira, E., Jha, S., López-Blanco, J. R., Arias-Palomo, E., Chacón, P., Cañas, C., Ayora, S., Dutta, A., and Llorca, O. (2008) Architecture of the pontin/reptin complex, essential in the assembly of several macromolecular complexes. *Structure* **16**, 1511–1520
29. Kastner, B., Fischer, N., Golas, M. M., Sander, B., Dube, P., Boehringer, D., Hartmuth, K., Deckert, J., Hauer, F., Wolf, E., Uchtenhagen, H., Urlaub, H., Herzog, F., Peters, J. M., Poerschke, D., Lüthmann, R., and Stark, H. (2008) GraFix: sample preparation for single-particle electron cryomicroscopy. *Nat. Methods* **5**, 53–55
30. Mindell, J. A., and Grigorieff, N. (2003) Accurate determination of local defocus and specimen tilt in electron microscopy. *J. Struct. Biol.* **142**, 334–347
31. Heymann, J. B., and Belnap, D. M. (2007) Bsoft: image processing and molecular modeling for electron microscopy. *J. Struct. Biol.* **157**, 3–18
32. Tang, G., Peng, L., Baldwin, P. R., Mann, D. S., Jiang, W., Rees, I., and Ludtke, S. J. (2007) EMAN2: an extensible image processing suite for electron microscopy. *J. Struct. Biol.* **157**, 38–46
33. Ludtke, S. J., Baldwin, P. R., and Chiu, W. (1999) EMAN: semiautomated software for high-resolution single-particle reconstructions. *J. Struct. Biol.* **128**, 82–97
34. Scheres, S. H., Núñez-Ramírez, R., Sorzano, C. O., Carazo, J. M., and Marabini, R. (2008) Image processing for electron microscopy single-particle analysis using XMIPP. *Nat. Protoc.* **3**, 977–990
35. Radermacher, M., Wagenknecht, T., Verschoor, A., and Frank, J. (1987) Three-dimensional reconstruction from a single-exposure, random conical tilt series applied to the 50S ribosomal subunit of *Escherichia coli*. *J. Microsc.* **146**, 113–136
36. Shaikh, T. R., Gao, H., Baxter, W. T., Asturias, F. J., Boisset, N., Leith, A., and Frank, J. (2008) SPIDER image processing for single-particle reconstruction of biological macromolecules from electron micrographs. *Nat. Protoc.* **3**, 1941–1974
37. Goddard, T. D., Huang, C. C., and Ferrin, T. E. (2007) Visualizing density maps with UCSF Chimera. *J. Struct. Biol.* **157**, 281–287
38. Zecchi, L., Lo Piano, A., Suzuki, Y., Cañas, C., Takeyasu, K., and Ayora, S. (2012) Characterization of the Holliday junction resolving enzyme encoded by the *Bacillus subtilis* bacteriophage SPP1. *PLoS ONE* **7**, e48440
39. Shi, Y., Lee, J. S., and Galvin, K. M. (1997) Everything you have ever wanted to know about Yin Yang 1. *Biochim Biophys. Acta* **1332**, F49–F66
40. Thompson, L. H. (2012) Recognition, signaling, and repair of DNA double-strand breaks produced by ionizing radiation in mammalian cells: the molecular choreography. *Mutat Res.* **751**, 158–246
41. Maslon, M. M., Hrstka, R., Vojtesek, B., and Hupp, T. R. (2010) A divergent substrate-binding loop within the pro-oncogenic protein anterior gradient-2 forms a docking site for Reptin. *J. Mol. Biol.* **404**, 418–438
42. Brayer, K. J., Kulshreshtha, S., and Segal, D. J. (2008) The protein-binding potential of C2H2 zinc finger domains. *Cell Biochem. Biophys.* **51**, 9–19
43. Brayer, K. J., and Segal, D. J. (2008) Keep your fingers off my DNA: protein-protein interactions mediated by C2H2 zinc finger domains. *Cell Biochem. Biophys.* **50**, 111–131
44. Iuchi, S. (2001) Three classes of C2H2 zinc finger proteins. *Cell. Mol. Life Sci.* **58**, 625–635
45. Sun, L., Liu, A., and Georgopoulos, K. (1996) Zinc finger-mediated protein interactions modulate Ikaros activity, a molecular control of lymphocyte development. *EMBO J.* **15**, 5358–5369
46. Atchison, M. L. (2014) Function of YY1 in long-distance DNA interactions. *Front Immunol.* **5**, 45
47. Jiang, Y., Wang, X., Bao, S., Guo, R., Johnson, D. G., Shen, X., and Li, L. (2010) INO80 chromatin remodeling complex promotes the removal of UV lesions by the nucleotide excision repair pathway. *Proc. Natl. Acad. Sci. U.S.A.* **107**, 17274–17279
48. Hosokawa, H., Tanaka, T., Kato, M., Shinoda, K., Tohyama, H., Hanazawa, A., Tamaki, Y., Hirahara, K., Yagi, R., Sakikawa, I., Morita, A., Nagira, M., Poyurovsky, M. V., Suzuki, Y., Motohashi, S., and Nakayama, T. (2013) Gata3/Ruvbl2 complex regulates T helper 2 cell proliferation via repression of Cdkn2c expression. *Proc. Natl. Acad. Sci. U.S.A.* **110**, 18626–18631
49. Shyu, Y. J., Suarez, C. D., and Hu, C. D. (2008) Visualization of ternary complexes in living cells by using a BiFC-based FRET assay. *Nat. Protoc.* **3**, 1693–1702

Structure of Yin Yang 1 Oligomers That Cooperate with RuvBL1-RuvBL2 ATPases

Andrés López-Perrote, Hanan E. Alatwi, Eva Torreira, Amani Ismail, Silvia Ayora,
Jessica A. Downs and Oscar Llorca

J. Biol. Chem. 2014, 289:22614-22629.

doi: 10.1074/jbc.M114.567040 originally published online July 2, 2014

Access the most updated version of this article at doi: [10.1074/jbc.M114.567040](https://doi.org/10.1074/jbc.M114.567040)

Alerts:

- [When this article is cited](#)
- [When a correction for this article is posted](#)

[Click here](#) to choose from all of JBC's e-mail alerts

This article cites 49 references, 16 of which can be accessed free at <http://www.jbc.org/content/289/33/22614.full.html#ref-list-1>



Removal of H2A.Z by INO80 promotes homologous recombination

Hanan E Alatwi & Jessica A Downs*

Abstract

The mammalian INO80 remodelling complex facilitates homologous recombination (HR), but the mechanism by which it does this is unclear. Budding yeast INO80 can remove H2A.Z/H2B dimers from chromatin and replace them with H2A/H2B dimers. H2A.Z is actively incorporated at sites of damage in mammalian cells, raising the possibility that H2A.Z may need to be subsequently removed for resolution of repair. Here, we show that H2A.Z in human cells is indeed rapidly removed from chromatin flanking DNA damage by INO80. We also report that the histone chaperone ANP32E, which is implicated in removing H2AZ from chromatin, similarly promotes HR and appears to work on the same pathway as INO80 in these assays. Importantly, we demonstrate that the HR defect in cells depleted of INO80 or ANP32E can be rescued by H2A.Z co-depletion, suggesting that H2A.Z removal from chromatin is the primary function of INO80 and ANP32E in promoting homologous recombination.

Keywords ANP32E; chromatin; H2A.Z; homologous recombination; INO80

Subject Categories DNA Replication, Repair & Recombination; Chromatin, Epigenetics, Genomics & Functional Genomics

DOI 10.15252/embr.201540330 | Received 5 March 2015 | Revised 9 June 2015 | Accepted 10 June 2015 | Published online 3 July 2015

EMBO Reports (2015) 16: 986–994

Introduction

The INO80 family of chromatin remodelling enzymes is defined by an insertion in the ATPase domain and, in addition to INO80, includes yeast Swr1 and human p400 and SRCAP. Evidence suggests that members of this family are capable of histone exchange reactions (for review, see [1]). Swr1, as part of the SWR complex, removes H2A/H2B dimers and replaces them with H2A.Z/H2B [2,3]. Mammalian SRCAP and p400 (as part of TIP60) are related to yeast SWR and perform the same function [4,5]. The budding yeast INO80 complex has been shown to catalyse the reverse reaction and replace H2A.Z/H2B dimers with H2A/H2B [6]. In mammalian cells, the histone chaperone ANP32E has been shown to remove H2A.Z from chromatin [7,8], but it has not been investigated whether mammalian INO80 contributes to this activity.

INO80 has been widely implicated in homologous recombination [9–20]. There is evidence in both yeast and mammalian cells that INO80 functions to promote resection [9,15,18,19], and although the defect in mammalian cells depleted of INO80 is relatively mild, this may be sufficient to impair efficient HR.

Recently, incorporation of H2A.Z by TIP60 at damaged chromatin was found to restrict resection [5]. In the absence of H2A.Z, recruitment of the non-homologous end-joining (NHEJ) complex Ku70/Ku80 to DNA breaks is impaired, and this appeared to be a consequence of unrestricted resection [5]. Taken together, these data raise the possibility that INO80 may promote HR by removing H2A.Z to allow resection. We investigated this possibility and found that H2A.Z is incorporated and then very rapidly removed from chromatin following DNA damage. We found that the removal of H2A.Z from chromatin is dependent on INO80. Notably, while the depletion of H2A.Z does lead to increased RPA foci, consistent with a role in preventing unrestricted resection, we find that the depletion of INO80 has only marginal effects on resection. Instead, we find that cells are unable to efficiently replace RPA with RAD51, and consequently, the formation of sister chromatid exchanges is impaired in the absence of INO80. These data suggest that H2A.Z removal performs an additional function during HR that is separated from regulating resection. We also investigated the potential role of ANP32E in mediating HR and found that its depletion results in a similar defect as loss of INO80, and they appear to function together in mediating HR. Strikingly, we find that the co-depletion of H2A.Z and either INO80 or ANP32E fully rescues the defects in RAD51 foci and SCE formation of siINO80 or siANP32E cells, suggesting that the primary function of INO80 and ANP32E in promoting HR is the removal of H2A.Z from damaged chromatin.

Results and Discussion

H2A.Z dynamics at damaged chromatin

To investigate the possibility that H2A.Z is removed from chromatin subsequent to its incorporation after DNA damage, we introduced a GFP-tagged expression construct into cells. Using live cell imaging, we monitored H2A.Z accumulation at DNA damage sites induced by laser micro-irradiation. Consistent with previous findings [5], we found that H2A.Z is incorporated after damage (Fig 1A). Strikingly,

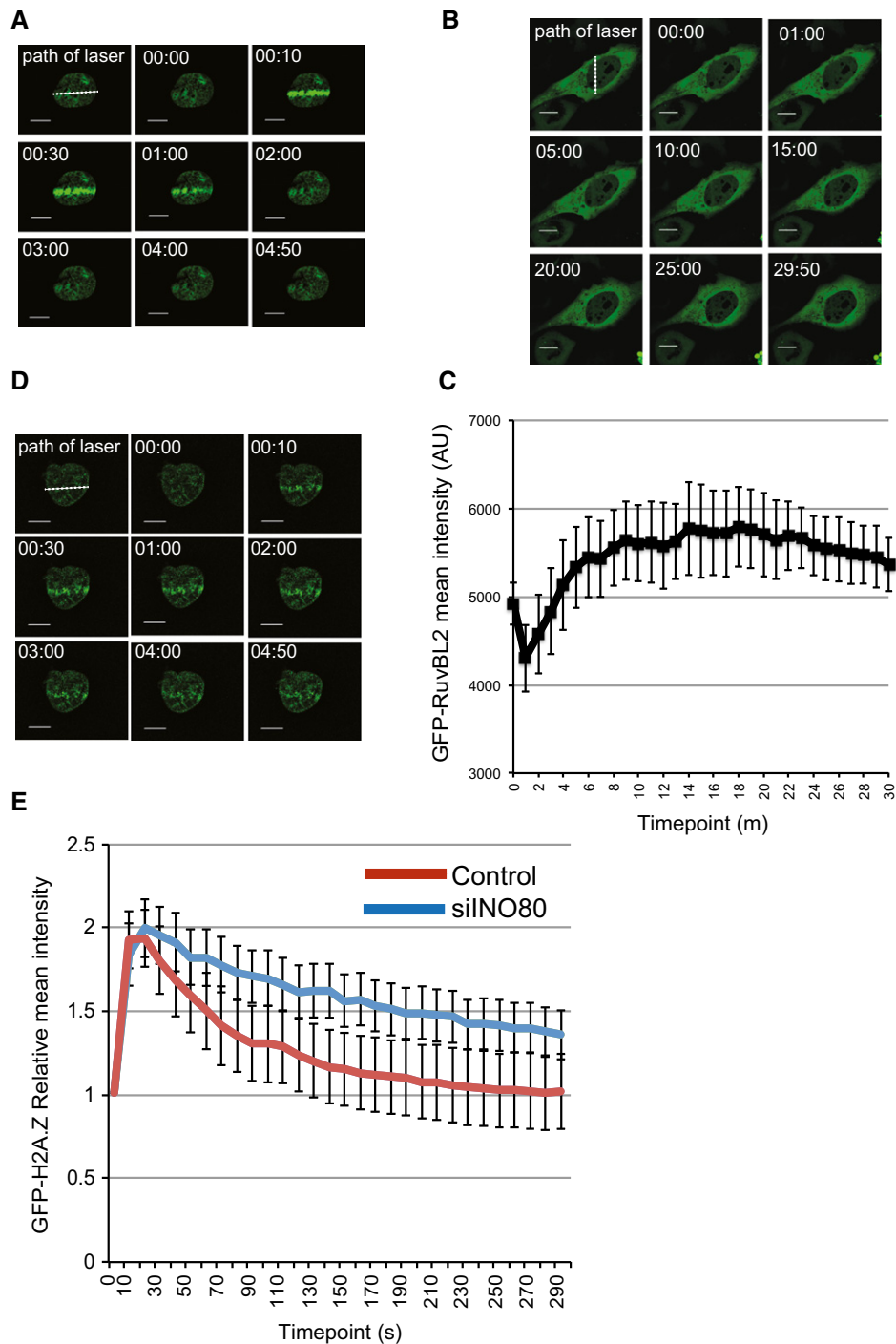


Figure 1. H2A.Z dynamics at damaged chromatin.

A H2A.Z is rapidly incorporated and removed from chromatin in the vicinity of damaged DNA. U2OS cells transfected with GFP-H2A.Z were laser micro-irradiated and monitored by live cell imaging. Representative images taken at indicated time points are shown.

B The RuvBL2 subunit of INO80 accumulates at sites of damaged DNA. U2OS cells transfected with EGFP-RuvBL2 were laser micro-irradiated and monitored by live cell imaging. Representative images taken at indicated time points are shown.

C Quantification of mean fluorescence intensity at sites of micro-irradiation \pm SE ($n = 3$).

D Removal of H2A.Z from chromatin in the vicinity of damaged DNA is at least partly dependent on INO80. USOS cells treated with siINO80 were transfected with GFP-H2A.Z, laser micro-irradiated and monitored by live cell imaging. Representative images taken at indicated time points are shown.

E Quantification of relative mean fluorescence intensity \pm SD at sites of micro-irradiation in control (U2OS; $n = 3$) and siINO80 cells ($n = 3$) in a minimum of 10 cells per experiment.

Data information: Scale bars represent 10 μ m.

we found that it is subsequently very rapidly removed from chromatin, with signal intensity returning to pre-damage levels within 3 min (Fig 1A and E). This is distinct from the behaviour of GFP-tagged core histone H2B, which we find shows no detectable patterns of movement under these conditions (Fig EV1A). This result suggests that H2A.Z is actively removed from damaged chromatin after it is incorporated.

While budding yeast INO80 is capable of removing H2A.Z from chromatin and replacing it with H2A [6], this has not been investigated for mammalian INO80. INO80 has previously been shown to accumulate at DNA DSBs when analysed using chromatin immunoprecipitation [15]. We analysed the dynamics of the RuvBL2 subunit of INO80, and in agreement with the ChIP data [15], we find that it accumulates in chromatin in proximity to damage induced by laser micro-irradiation, but then remains in the vicinity of damaged chromatin until at least 15 min after damage (Figs 1B, C and EV1B).

To determine whether H2A.Z removal following damage is dependent on INO80, we analysed GFP-H2A.Z dynamics after depleting INO80 (siINO80). We found that the accumulation of H2A.Z in laser-irradiated chromatin is unaffected by depletion of INO80. In contrast, the removal of accumulated H2A.Z in damaged chromatin is significantly slower in cells depleted of INO80 when compared with control cells (Fig 1D and E), indicating that INO80 contributes to the removal of H2A.Z from chromatin in mammalian cells.

INO80 facilitates multiple steps during HR

There is evidence that INO80 contributes to HR in mammalian cells. In order to investigate the contribution of INO80 and H2A.Z to this pathway, we restricted our analyses to G2 cells using CENP-F, whose expression is limited to late S and G2 phases of the cell cycle [21], as a marker. There is evidence that the resection step of HR is defective in mammalian cells lacking INO80 [15,18]. We therefore monitored the appearance of RPA foci following irradiation as a readout of single-stranded DNA formation. We did not detect a difference in the number of RPA foci in cells treated with siINO80 when compared with control cells (Fig 2A). In contrast, and consistent with a previous report [22], we find that the depletion of SRCAP has an obvious impact on the number of IR-induced RPA foci (Fig EV2). The absence of an obvious defect in RPA foci formation is consistent with our previous work investigating the YY1 and RuvBL2 subunits of INO80 [17], but is apparently at odds with other reports [15,18]. We considered that one possibility for the discrepancy between these findings is the different methodologies and conditions used to monitor resection. We therefore used a different

approach and monitored the number of cells with RPA foci following treatment with camptothecin (CPT), and, in doing so, found a modest but statistically significant defect in cells treated with siRNA targeting either the INO80 or YY1 subunits of the INO80 complex (Fig 2D), suggesting that INO80 does function to promote resection following DNA double strand breaks.

We next monitored the accumulation of RAD51 foci following irradiation and found a more substantial defect in INO80-depleted cells (Fig 2B). It seems unlikely that this is entirely a consequence of the minor resection defect in siINO80 cells, and it therefore suggests that INO80 has an additional function in promoting RAD51 foci formation during HR.

Depletion of H2A.Z rescues the RAD51 foci formation defect of cells depleted of ANP32E and INO80

We hypothesised that the removal of H2A.Z from damaged chromatin by INO80 may be an important aspect of the ability of INO80 to promote RAD51 foci formation. To test this, we co-depleted H2A.Z and INO80 (Fig 2C) and analysed the accumulation of RPA and RAD51 foci following DNA damage. We found that, while the depletion of H2A.Z alone had no detectable effect, the depletion of H2A.Z rescued the defect in RAD51 foci accumulation in siINO80 cells (Fig 2B). Using the assay in which we can uncover defect in RPA foci formation in siINO80 cells, we find that the depletion of H2A.Z also rescues this defect (Fig 2D). Loss of H2A.Z alone results in a greater number of RPA foci following irradiation (Fig 2A), consistent with a previous report showing that H2A.Z is a barrier to resection [5]. Interestingly, the number of RPA foci appears to be reduced when INO80 is also depleted back to wild-type levels (Fig 2A), suggesting there may be crosstalk between the resection machinery and INO80.

Very recently, the histone chaperone ANP32E was shown to remove H2A.Z from chromatin in mammalian cells, both globally [7,8] and from chromatin at sites of damage [23]. We were therefore interested in understanding whether ANP32E might contribute to HR in a similar manner to INO80. We depleted ANP32E and monitored RPA and RAD51 foci formation as previously, and we found that loss of ANP32E results in a similar defect in RAD51 foci formation following irradiation as we find with the depletion of INO80 (Fig 3B). Notably, the depletion of both ANP32E and INO80 results in no further defects in RAD51 foci accumulation following irradiation (Fig 3A–C), suggesting that they are working together to facilitate this step in HR. Most importantly, the co-depletion of H2A.Z in cells lacking ANP32E rescues the defects in foci formation of the siANP32E cells (Fig 3B and C).

Figure 2. Cells lacking INO80 have a modest resection defect and a more significant defect in RAD51 foci accumulation, and these defects are rescued by depletion of H2A.Z.

- A IR induced RPA focus formation in A549 cells treated with siControl, siINO80, siH2A.Z or siINO80/siH2A.Z. Left hand panel: representative images. Right hand panel: quantification of foci.
 B IR induced RAD51 foci formation in A549 cells treated with siControl, siINO80, siH2A.Z or siINO80/siH2A.Z. Left hand panel: representative images. Right hand panel: quantification of foci.
 C Western blot analysis showing efficiency of siRNA depletion. KAP1 is used as a loading control.
 D Quantification of RPA foci following 1 h of treatment with camptothecin (CPT).

Data information: Scale bars represent 5 μ m. Data represent the mean of 4 (A, B) or 3 (D) independent assays \pm SD. NS, not significant; * $P \leq 0.05$; ** $P \leq 0.01$; *** $P \leq 0.001$ by Student's t-test.

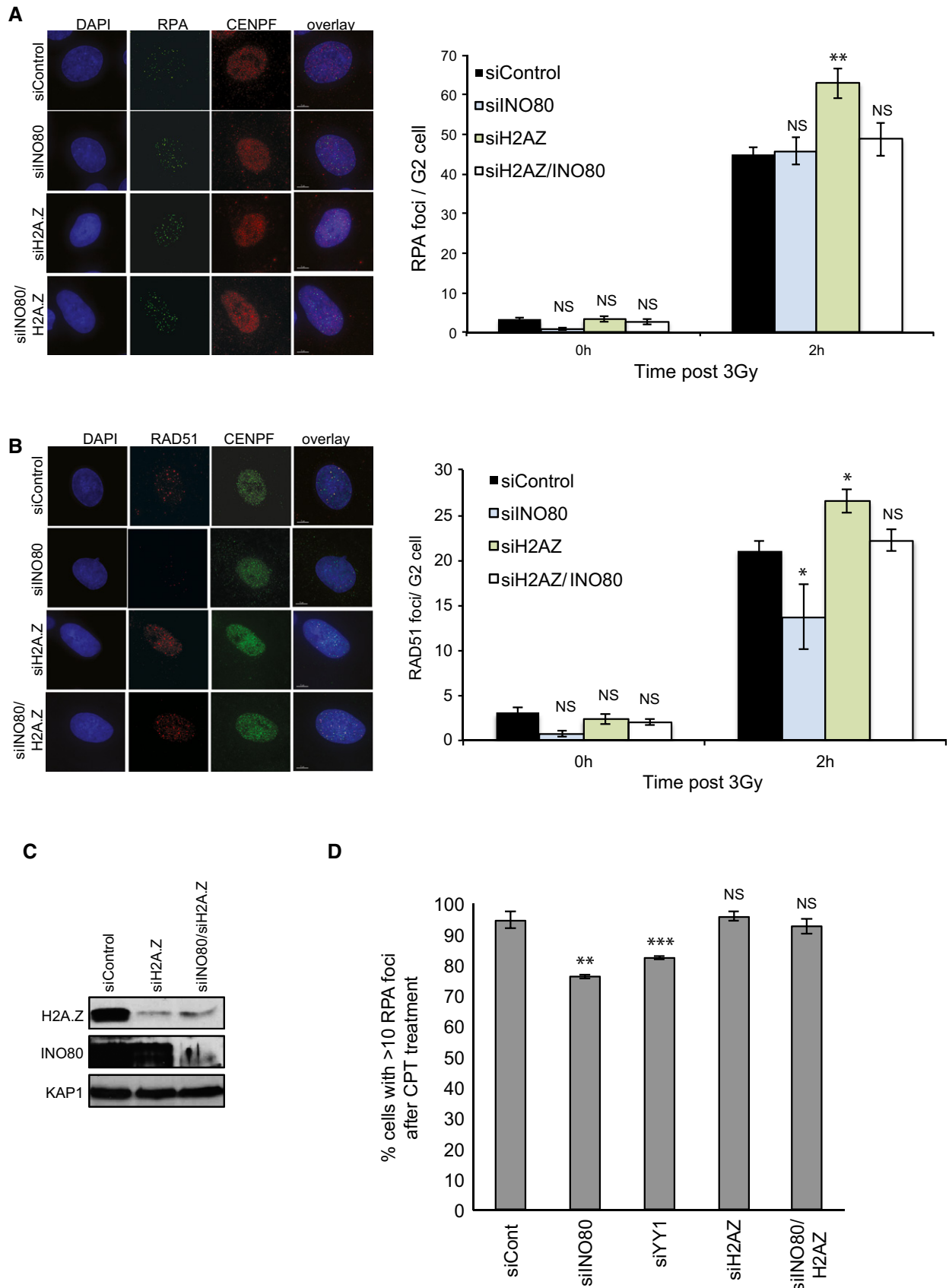


Figure 2.

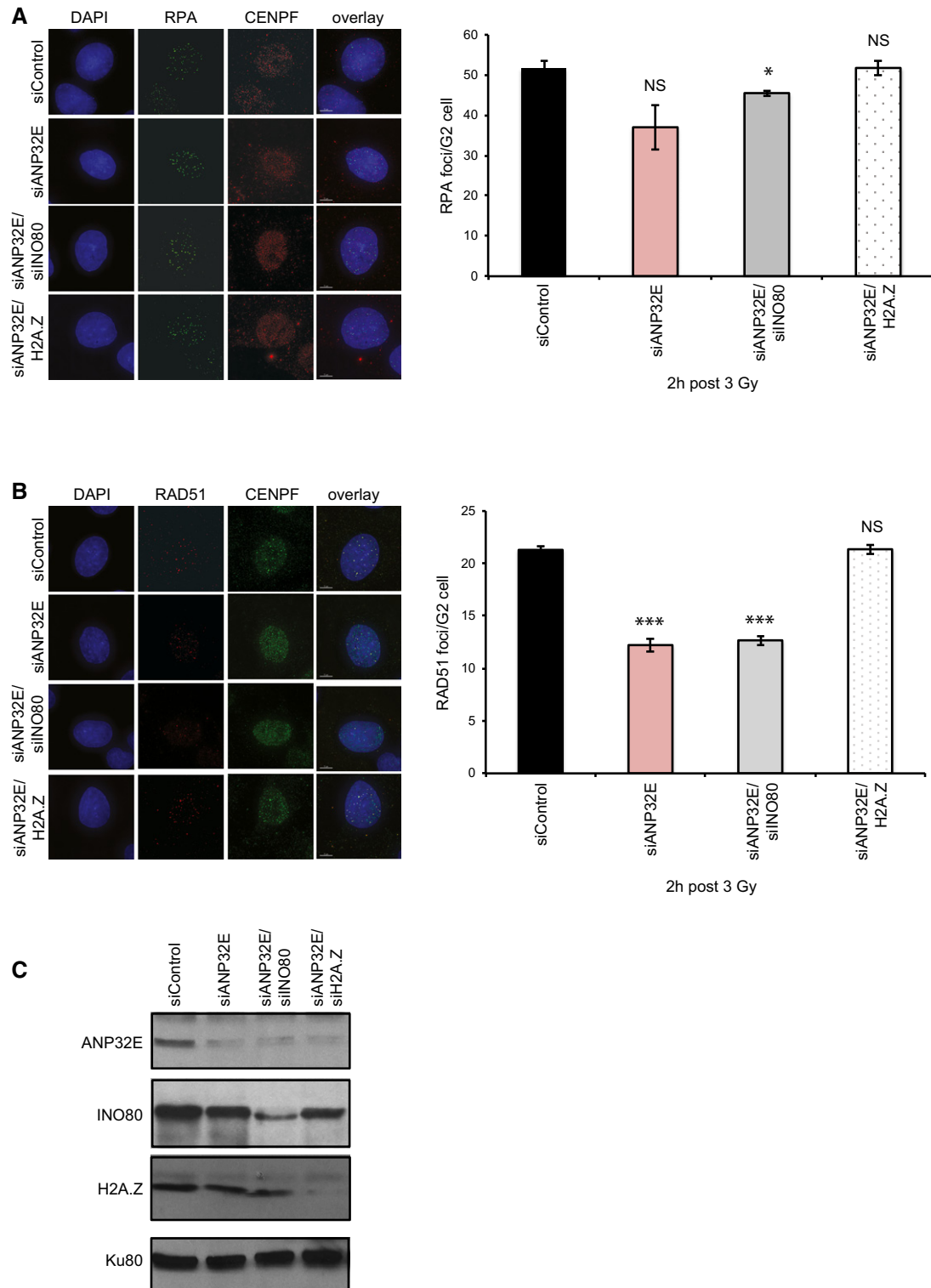


Figure 3. INO80 and ANP32E work together to promote RAD51 foci formation following irradiation, which is rescued by the depletion of H2A.Z.

A IR induced RPA focus formation in A549 cells treated with siControl, siANP32E, siANP32E/siINO80 or siANP32E/siH2A.Z. Left hand panel: representative images. Right hand panel: mean number of foci \pm SD.

B IR induced RAD51 focus formation in A549 cells treated with siControl, siANP32E, siANP32E/siINO80 or siANP32E/siH2A.Z. Left hand panel: representative images. Right hand panel: mean number of foci \pm SD.

C Western blot analysis showing efficiency of siRNA depletion. Ku80 is used as a loading control.

Data information: Scale bars represent 5 μ m. All data (A, B) are from a minimum of 3 independent assays. NS, not significant; * $P \leq 0.05$; *** $P \leq 0.001$ by Student's t-test.

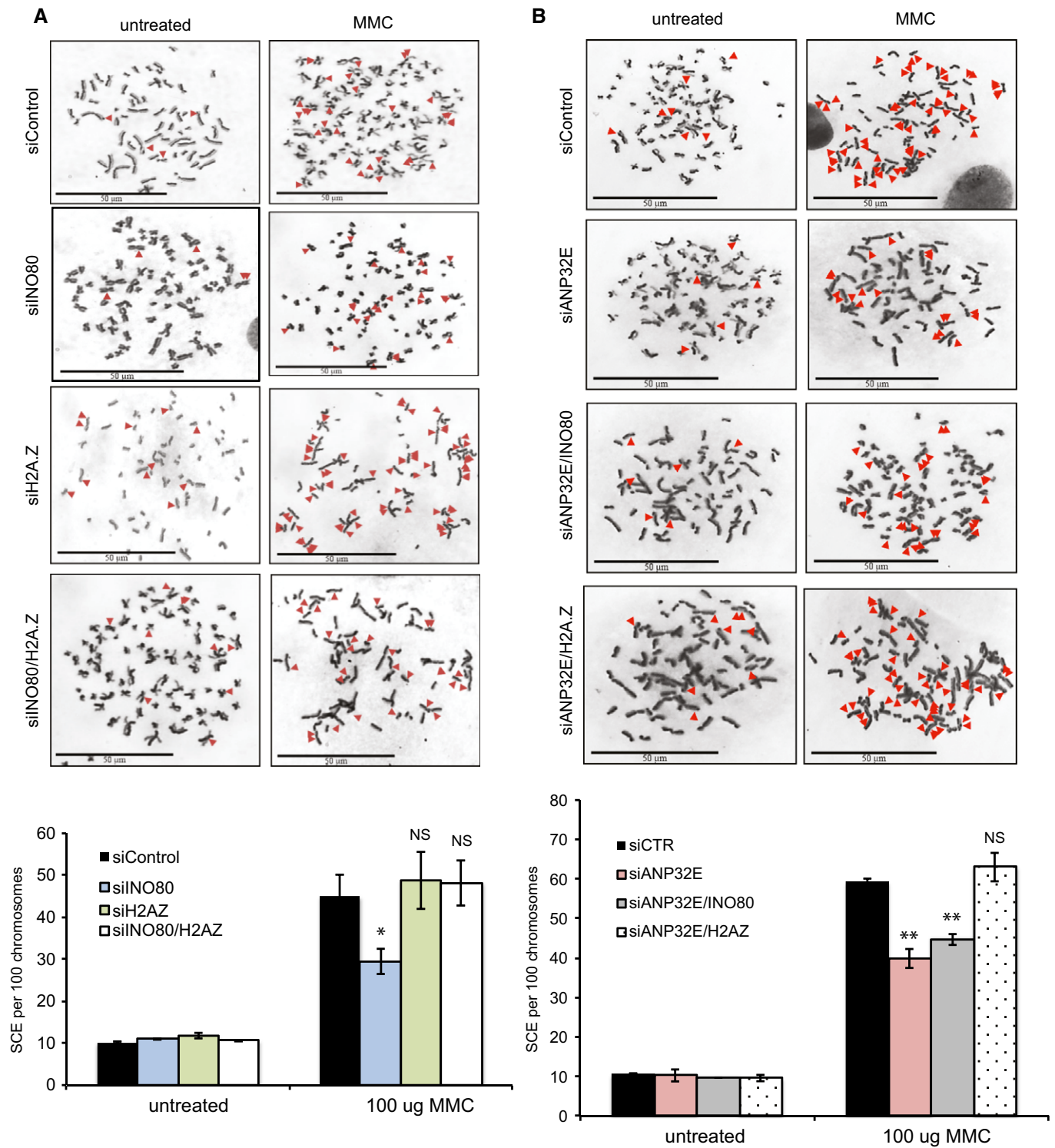


Figure 4. Wild-type levels of sister chromatid exchanges (SCEs) are dependent on H2A.Z removal by INO80 and ANP32E.

A SCEs were monitored in HeLa cells treated with siControl, siINO80, siH2A.Z or siINO80/siH2A.Z following treatment with mitomycin C (MMC). The reduction in SCEs in cells lacking INO80 is rescued by the co-depletion of H2A.Z. Upper panel: representative images. Lower panel: mean number of SCEs \pm SD. SCEs were scored in at least 1,000 chromosomes from three independent experiments.

B SCEs were monitored in HeLa cells treated with siControl, siANP32E, siANP32E/siINO80 or siANP32E/siH2A.Z. There is no further reduction in SCEs in cells depleted of both ANP32E and INO80 when compared with ANP32E alone. As with siINO80, the reduction in SCEs in cells lacking ANP32E can be rescued by the co-depletion of H2A.Z. Upper panel: representative images. Lower panel: mean number of foci \pm SD.

Data information: Scale bars represent 50 μ m. All data are from a minimum of 3 independent assays. NS, not significant; * $P \leq 0.05$; ** $P \leq 0.01$ by Student's *t*-test.

Depletion of H2A.Z rescues the sister chromatid exchange (SCE) defect of cells depleted of ANP32E and INO80

The reduction in RAD51 foci formation in cells lacking INO80 or ANP32E suggests that HR is impaired in these cells. However, the reduction is modest when compared with cells lacking core HR proteins, such as BRCA2. We therefore monitored sister chromatid exchanges (SCEs) as a measure of HR completion. To do this, we treated cells with mitomycin C (MMC) because this results in a very substantial increase in SCEs, giving us the best possibility of detecting defects in the pathway. Additionally, unlike IR, MMC-induced lesions are repaired predominantly by HR.

We found that cells lacking either INO80 or ANP32E show reduced numbers of SCEs when compared with control cells (Fig 4A and B). Depletion of H2A.Z alone had no detectable effect on SCE numbers after MMC treatment (Fig 4A). Similar to our results monitoring RAD51 foci formation, we found that the co-depletion of H2A.Z rescued the defects in SCEs in cells lacking either INO80 or ANP32E (Fig 4A and B). In addition, the depletion of both INO80 and ANP32E yielded similar levels of SCEs to cells lacking either INO80 or ANP32E (Fig 4B), suggesting, as above, that they are working together to facilitate HR.

Collectively our data suggest that H2A.Z is removed from chromatin after DNA damage by ANP32E and INO80, and this removal—either from the chromatin flanking the DSB, or from the sister chromatid, or both—is required for HR. Very recently, Price and colleagues also found that H2A.Z is removed from chromatin at sites of DNA damage in an ANP32E-dependent manner [23]. Interestingly, they found that failure to remove H2A.Z from chromatin in the vicinity of damage results in reduced Ku70/Ku80 binding, which impairs NHEJ activity. Loss of H2A.Z leads to similar impairment of Ku70/Ku80 binding and NHEJ activity [5] and is consistent with a model in which the coupled incorporation and removal of H2A.Z is required to prevent promiscuous resection and promote NHEJ. While INO80 has been implicated in mediating resection, our data suggest that this is a minor role and that it has a greater impact on facilitating HR at a step downstream of resection. Taken together with the data from the Price laboratory, we speculate that H2A.Z removal has multiple roles in DSB responses. As we were restricting our analyses to late S and G2 cells, one intriguing possibility is that H2A.Z dynamics are used differentially throughout the cell cycle to promote distinct steps in both major DSB repair pathways. Importantly, if H2A.Z is not deposited into chromatin in the vicinity of DNA damage in the first place, then INO80 and ANP32E are no longer required for wild-type levels of RAD51 foci or SCE formation in these assays, indicating that the removal of H2A.Z from chromatin in the vicinity of DNA damage is their primary function in HR.

Materials and Methods

Cell culture and irradiation

A549, HeLa or U2OS cells were cultured in MEM or DMEM (Gibco), respectively, supplemented with 10% FCS, L-glutamine, penicillin and streptomycin (Gibco) at 37°C in a humidified 95% air and 5% CO₂ atmosphere. Cells were irradiated by exposure to a ¹³⁷Cs source.

Small interfering RNA (siRNA) knockdown conditions

siRNA-mediated knockdown was achieved using HiPerFect Transfection Reagent (Qiagen) following the manufacturer's instructions. siRNA duplexes (Dharmacon SMARTpool) were transfected into 4×10^5 of logarithmically growing cells per condition. Cells were harvested 24 h later, retransfected with siRNA and were then seeded and grown for 48 h. The siRNA oligonucleotide used for ANP32E was 5'-CGGCUUCCAGCUUAAAUA-3' (Dharmacon).

Antibodies

The primary antibodies used were as follows: γ H2AX (Upstate Technology; 05-636) at 1:800 for IF, RPA (Merck Millipore; LS-C38952) at 1:100 for IF, RAD51 (Santa Cruz Biotechnology; SC-8349) at 1:200 and CENP-F (Abcam; ab108483) for IF, INO80 (Abcam; ab118787, and Bethyl; A303-371A) at 1:2,000 for WB, H2A.Z (Cell Signaling Technology; 2718S) at 1:1,000 for WB, ANP32E (Sigma-Aldrich; SAB2100124) at 1:1,000 for WB, KAP1 (Abcam; ab22553) at 1:1,000 for WB and KU80 (Abcam; ab33242) at 1:1,000 for WB.

The secondary antibodies used were as follows: FITC (Sigma-Aldrich; F0257) at 1:100 for IF, Cy3 (Sigma-Aldrich; C2306) at 1:200 for IF, AlexaFluor 488 (Invitrogen; A21206) at 1:400 for IF, Goat Anti-Rabbit Immunoglobulin/HRP (Dako; P0449) at 1:2,000 for WB, Rabbit Anti-Mouse Immunoglobulins/HRP (Dako; P044801-2) at 1:2,000 for WB.

Immunofluorescence

A549 cells plated on glass slides were fixed for 10 min with fixative (2% (w/v) PFA, 3% (w/v) sucrose, 1 \times PBS) and permeabilised for 3 min with 0.2% Triton X-100 in PBS. When staining for RPA/RAD51, pre-extraction was performed by treatment with 0.2% Triton X-100 in PBS for 0.5–1 min prior to PFA fixation. Cells were rinsed with PBS and incubated with primary antibody diluted in PBS + 2% (w/v) BSA for 1 h at room temperature (RT). Cells were washed three times, incubated with secondary antibody (diluted in PBS + 2% (w/v) BSA) for 30 min at RT in the dark, incubated with 4',6-diamidino-2-phenylindole (DAPI) for 10 min and washed three times with PBS. Slides were mounted using Vectashield and visualised/analysed using a Nikon-e400 microscope and imaged using an Applied Precision[®] Delta Vision[®] RT Olympus IX70 deconvolution microscope and softWoRx[®] Suite software. For γ H2AX, RPA, and RAD51 foci quantification, a minimum of 30 cells per experiment was scored blindly and error bars represent the SD between three experiments.

For analysis in Fig 2D, cells were treated for 1 h with 1 mM camptothecin (CPT; Sigma-Aldrich) and left to recover for 1 h. Recovered cells were then stained, and γ H2AX-positive cells were scored as above in a minimum of 100 cells per experiment.

Sister chromatid exchange (SCE) assay

Analysis of SCEs was carried out as described previously [24]. Briefly, HeLa cells were grown for 48 h in BrdU and treated with 100 μ g mitomycin C (MMC) for 16 h; then, 10 μ g/ml colcemid was added for 2 h to collect cells in mitosis. SCEs were scored in at least 1,000 chromosomes from three independent experiments.

Laser micro-irradiation

Exponentially growing human U2OS cells were plated onto 35-mm glass-bottom dishes (MatTek) and transfected with the pTGF β -H2AZ construct, pEGFP-RUVBL2 (Origene) or pEGFP-H2B using Nano-Juice according to the manufacturer's protocol. The cells were allowed to express the construct for 24 h and were then incubated with 10 μ g/ml Hoechst 3458 for 30 min at 37°C before irradiation. The microscope system used was an Intelligent Imaging Innovations spinning disc confocal with a Yokogawa CSU-X1 on an Olympus IX-71. GFP-positive cells were irradiated with 405-nm ultraviolet laser set at power of 7:1,000 for either H2AZ or H2B and at 30:1,000 for RUVBL2 and channelled through a 60 \times objective. Images were captured at 10-s intervals following laser damage for a total time of 5 min for H2AZ or H2B and 30 min for RUVBL2. Images generated were acquired on a Photometrics Evolve 512 \times 512 EMCCD using Slidebook 6 software. In protein recruitment experiments, signal intensity was quantified along the laser path, using Slidebook 6 software, in a minimum of 10 cells and error bars represent the SD between three independent experiments.

Expanded View for this article is available online:

<http://embor.embopress.org>

Acknowledgements

This work was supported by Cancer Research UK (C7905/A16417) and the Ministry of Higher Education—Saudi Arabia. We thank Cornelia Meisenberg for experimental assistance, Brendan Price for sharing unpublished data, and Penny Jeggo, Alessandro Bianchi and members of the Downs laboratory for suggestions and helpful discussions.

Author contributions

HA and JAD designed the experiments and analysed the data; HA carried out all experiments and statistical analyses; and JAD wrote the manuscript.

Conflict of interest

The authors declare that they have no conflict of interest.

References

- Watanabe S, Peterson CL (2010) The INO80 family of chromatin-remodeling enzymes: regulators of histone variant dynamics. *Cold Spring Harb Symp Quant Biol* 75: 35–42
- Mizuguchi G, Shen X, Landry J, Wu WH, Sen S, Wu C (2004) ATP-driven exchange of histone H2AZ variant catalyzed by SWR1 chromatin remodeling complex. *Science* 303: 343–348
- Kobor MS, Venkatasubrahmanyam S, Meneghini MD, Gin JW, Jennings JL, Link AJ, Madhani HD, Rine J (2004) A protein complex containing the conserved Swi2/Snf2-related ATPase Swr1p deposits histone variant H2AZ into euchromatin. *PLoS Biol* 2: 1–13
- Ruhl DD, Jin J, Cai Y, Swanson S, Florens L, Washburn MP, Conaway RC, Conaway JW, Chrivia JC (2006) Purification of a human SRCAP complex that remodels chromatin by incorporating the histone variant H2AZ into nucleosomes. *Biochemistry* 45: 5671–5677
- Xu Y, Ayrapetov MK, Xu C, Gursoy-Yuzugullu O, Hu Y, Price BD (2012) Histone H2AZ controls a critical chromatin remodeling step required for DNA double-strand break repair. *Mol Cell* 48: 723–733
- Papamichos-Chronakis M, Watanabe S, Rando OJ, Peterson CL (2011) Global regulation of H2AZ localization by the INO80 chromatin-remodeling enzyme is essential for genome integrity. *Cell* 144: 200–213
- Mao Z, Pan L, Wang W, Sun J, Shan S, Dong Q, Liang X, Dai L, Ding X, Chen S *et al* (2014) Anp32e, a higher eukaryotic histone chaperone directs preferential recognition for H2AZ. *Cell Res* 24: 389–399
- Obri A, Ouararhni K, Papin C, Diebold ML, Padmanabhan K, Marek M, Stoll I, Roy L, Reilly PT, Mak TW *et al* (2014) ANP32E is a histone chaperone that removes H2AZ from chromatin. *Nature* 505: 648–653
- van Attikum H, Fritsch O, Gasser SM (2007) Distinct roles for SWR1 and INO80 chromatin remodeling complexes at chromosomal double-strand breaks. *EMBO J* 26: 4113–4125
- Fritsch O, Benvenuto G, Bowler C, Molinier J, Hohn B (2004) The INO80 protein controls homologous recombination in *Arabidopsis thaliana*. *Mol Cell* 16: 479–485
- Tsukuda T, Fleming AB, Nickoloff JA, Osley MA (2005) Chromatin remodeling at a DNA double-strand break site in *Saccharomyces cerevisiae*. *Nature* 438: 379–383
- Kawashima S, Ogiwara H, Tada S, Harata M, Wintersberger U, Enomoto T, Seki M (2007) The INO80 complex is required for damage-induced recombination. *Biochem Biophys Res Commun* 355: 835–841
- Wu S, Shi Y, Mulligan P, Gay F, Landry J, Liu H, Lu J, Qi HH, Wang W, Nickoloff JA (2007) A YY1-INO80 complex regulates genomic stability through homologous recombination-based repair. *Nat Struct Mol Biol* 14: 1165–1172
- Tsukuda T, Lo YC, Krishna S, Sterk R, Osley MA, Nickoloff JA (2009) INO80-dependent chromatin remodeling regulates early and late stages of mitotic homologous recombination. *DNA Repair (Amst)* 8: 360–369
- Gospodinov A, Vaissiere T, Krastev DB, Legube G, Anachkova B, Herceg Z (2011) Mammalian Ino80 mediates double-strand break repair through its role in DNA end strand resection. *Mol Cell Biol* 31: 4735–4745
- Neumann FR, Dion V, Gehlen LR, Tsai-Pflugfelder M, Schmid R, Taddei A, Gasser SM (2012) Targeted INO80 enhances subnuclear chromatin movement and ectopic homologous recombination. *Genes Dev* 26: 369–383
- Lopez-Perrote A, Alatwi HE, Torreira E, Ismail A, Ayora S, Downs JA, Llorca O (2014) Structure of Yin Yang 1 Oligomers that Cooperate with RuvBL1-RuvBL2 ATPases. *J Biol Chem* 289: 22614–22629
- Nishi R, Wijnhoven P, leSage C, Tjeertes J, Galanty Y, Forment JV, Clague MJ, Urbe S, Jackson SP (2014) Systematic characterization of deubiquitylating enzymes for roles in maintaining genome integrity. *Nat Cell Biol* 16: 1016–1026, 1–8
- van Attikum H, Fritsch O, Hohn B, Gasser SM (2004) Recruitment of the INO80 complex by H2A phosphorylation links ATP-dependent chromatin remodeling with DNA double-strand break repair. *Cell* 119: 777–788
- Morrison AJ, Highland J, Krogan NJ, Arbel-Eden A, Greenblatt JF, Haber JE, Shen X (2004) INO80 and g-H2AX interaction links ATP-dependent chromatin remodeling to DNA damage repair. *Cell* 119: 767–775

21. Liao H, Winkfein RJ, Mack G, Rattner JB, Yen TJ (1995) CENP-F is a protein of the nuclear matrix that assembles onto kinetochores at late G2 and is rapidly degraded after mitosis. *J Cell Biol* 130: 507–518
22. Dong S, Han J, Chen H, Liu T, Huen MS, Yang Y, Guo C, Huang J (2014) The human SRCAP chromatin remodeling complex promotes DNA-end resection. *Curr Biol* 24: 2097–2110
23. Gursoy-Yuzugullu O, Ayrapetov MK, Price BD (2015) Histone chaperone Anp32e removes H2A.Z from DNA double-strand breaks and promotes nucleosome reorganization and DNA repair. *Proc Natl Acad Sci USA* 112: 7507–7512
24. Beucher A, Birraux J, Tchouandong L, Barton O, Shibata A, Conrad S, Goodarzi AA, Krempler A, Jeggo PA, Löbrich M (2009) ATM and Artemis promote homologous recombination of radiation-induced DNA double-strand breaks in G2. *EMBO J* 28: 3413–3427



License: This is an open access article under the terms of the Creative Commons Attribution 4.0 License, which permits use, distribution and reproduction in any medium, provided the original work is properly cited.